Mid-America Earthquake Center

MODELING OF HYSTERETIC BEHAVIOR OF BEAM-COLUMN CONNECTIONS BASED ON SELF-LEARNING SIMULATION

by

Gun Jin Yun, Jamshid Ghaboussi and Amr S. Elnashai

Department of Civil and Environmental Engineering
University of Illinois at Urbana-Champaign
Urbana, Illinois

August 2007

Amr S. Elnashai, Ph.D., Director

ABSTRACT

Current AISC-LRFD code requires that the moment-rotation characteristics of connections be known. Moreover, it requires that these characteristics be incorporated in the analysis and member design under factored loads (AISC, 2001). Conventional modeling approaches to improve the prediction of cyclic behavior starts with a choice of a phenomenological model followed by calibration of the model parameters. However, not only is the improvement limited due to inherent limitations of this approach, but also test results indicate a large variability in load-carrying capacity under earthquake loading.

In this research, a new neural network (NN) based cyclic material model is applied to inelastic hysteretic behavior of connections. In the proposed model, two energy-based internal variables are introduced to expedite the learning of hysteretic behavior of materials or structural components. The model has significant advantages over conventional models in that it can handle complex behavior due to local buckling and tearing of connecting elements. Moreover, its numerical implementation is more efficient than the conventional models since it does not need an interaction equation and a plastic potential. A new approach based on a self-learning simulation algorithm is used to characterize the hysteretic behavior of the connections from structural tests. The proposed approach is verified by applying it to both synthetic and experimental examples. For its practical application in semi-rigid connections, design variables are included as inputs to the model through a physical principle based module. The extended model also gives reasonable predictions under earthquake loads even when it is presented with new geometrical properties and loading scenario as well.

ACKNOWLEDGEMENTS

The authors would like to express sincere appreciation to Professor Billie F. Spencer, Professor Yi-Kwei Wen, Professor Youssef Hashash and Dr. SungMoon Jung for their valuable suggestions. Although not directly involved in this research, the authors would also like to express special thanks to Professor William J. Hall, former Oversight Committee Chair of SAC Steel Project, for his great help.

TABLE OF CONTENTS

LIST OF TABLES

LIST OF FIGURES

CHAPTER 1 INTRODUCTION

1.1 Problem Description and Motivation

One essential philosophy of seismic provisions in modern building codes is to make structures behave in a ductile manner under earthquakes without collapse. In the case of steel moment-frame buildings, the nonlinear behavior of beam-column connections significantly affects the dynamic response under earthquakes since connection regions are one of the primary sources of hysteretic damping. Because of lack of understanding the actual nonlinear hysteretic behavior of welded-flange-bolted-web connection under earthquakes, significant economic losses occurred as a result of many brittle connection failures in the 1994 Northridge earthquake even though it was following basic seismic provisions of the building codes. Since then, many other ductile connection types have been researched through experiments. Therefore, accurate and reliable characterization of the behavior of various connection types is very important both in the seismic design and life-time safety of steel moment-frame buildings. Evidently, current AISC-LRFD code requires that the moment-rotation characteristics of connections be known and these characteristics be incorporated in analysis and member design under factored loads (AISC 2001).

Since the behavior of the connections under earthquakes can be very much different from that under monotonic loading, its load-carrying capacity under severe earthquake loading should be ensured to meet seismic provisions of the building codes. The basic requirement in seismic design of connections is a balanced stiffness-strength-ductility capacity of connections. From a design point of view, the ductility and deformational

capacity are major interests and it is noteworthy that they are functions of yield mechanisms and critical failure modes of the connection. Therefore, reliable predictions of the resistance of the yield mechanism and failure mode are required. The ductile connection performance can be assured by having lower resistance of a yield mechanism than that of any critical brittle failure mode. According to extensive experimental research on various connection types so far, many different yield mechanisms and failure modes under cyclic loading are possible even for the same connection type. This occurs because the cyclic behavior of the connection depends on its detailed geometric properties, variations in construction quality and proximity between yield mechanisms and critical failure modes. Moreover, there are various topological connection types used in practice; welded-flange-bolted-web connection; extended-end-plate connection; T-stub connection; double-flange-angle connection; connections with reduced beam section, and so on.

Over the past several decades, there have been numerous research efforts on new or improved connections by experiments and comparisons with analytical models for behavior of connections. However, experiments on some of the connection types were conducted under monotonic loading. Using simple concepts of load path, equilibrium and simple mechanics, many equations to define yield mechanisms and failure/yield moments were suggested and validated with experimental results. They, however, can be used only for design purposes. To characterize the cyclic behavior of connections and implement it in structural analysis programs, the connection behavior is frequently modeled with simplified analytical models such as bilinear and tri-linear models (FEMA-355F 2000). Of course, there are highly sophisticated models for accurately representing the complex

inelastic behavior of connections such as multi-linear or nonlinear model accounting for stiffness and strength degradation as well as pinching effect during its cyclic loop. However, not only do they have limitations in accuracy due to their inherent assumptions and simplifications but also they are highly dependent on the given connections tested. Moreover, careful calibrations of the experimental results are required before using them. Furthermore, the modeling of interactions between connecting elements and other complex behavior such as local buckling and tearing of components is still challenging and remains unresolved with existing phenomenological models. Considering the fact that there has been no standard and systematic procedure for developing phenomenological models from experimental data, variations of the models are inevitable. It is worthwhile to mention that modeling errors can lead to inaccurate predictions of the connection stiffness during cyclic response and result in significant error in seismic performance evaluations of steel moment-frame buildings by existing analytical or phenomenological connections models.

In summary, the motivations of this research are to overcome those limitations of conventional phenomenological models for characterizing the inelastic hysteretic behavior of connections and to provide new and direct modeling approach to inelastic hysteretic behavior of connections from experimental data.

1.2 Information-based Cyclic Material Modeling

Neural Networks (NN) have been applied in material modeling instead of phenomenological models. Potential applications of the NN approach in material modeling were first suggested by Ghaboussi et al. (Ghaboussi, et al. 1991) and it has been

extensively researched for various applications such as modeling of soil material (Hashash, et al. 2003), metal plasticity and time-dependent behavior of concrete materials (Jung and Ghaboussi 2006). A unique advantage of NN based constitutive models is that they are trained to learn the material behavior directly from experimental stress-strain data. If the training data contains sufficient information, then the trained NN can learn the material behavior and function as a constitutive model in computational mechanics. However, the usual modeling of the material behavior with NN requires the results of comprehensive material tests that may not always be available, and in some case not possible. To facilitate the use of the NN based material model, an auto-progressive training algorithm was proposed by Ghaboussi, et al. (Ghaboussi, et al. 1998a). The latter can perform on-line training of the NN based material model through the incorporation of experimental measurements with conventional incremental-iterative nonlinear finite element analysis.

For capturing the path-dependent material behavior, several past states of stresses and strains along the equilibrium path are used as inputs in conventional NN based models. Total or incremental stresses and strains were used in the NN based material models. However, difficulties are frequently encountered when the NN based model is requested to learn complex cyclic material behavior in multi-dimensional stress space. Modeling of cyclic behavior of structural components and materials is very important in predicting the response of structures subjected to earthquake loading. Even though the NN has been extensively used for material modeling, they have been limited to monotonic behavior and one-dimensional problems in the case of cyclic behavior. However, the potential of the NN based model is immense so it can be applied to

complex cyclic material behavior. To open up practical applications of the NN based material model to many engineering problems, a new robust cyclic material model using the learning capabilities of the NN is suggested as one of the objectives in this report.

1.3 Objectives and Research Significance

The objectives of this report are 1) Development of a new NN based cyclic material model for inelastic hysteretic behavior of steel beam-column connections (the NN based cyclic material model for application to steel beam-column connections are named as NN based connection model or simply NN based model later); 2) Development of a self-learning simulation framework that can enable development of the NN based connection model directly from local and global structural testing; 3) Development of a generalized hybrid NN (GHNN) based inelastic hysteretic model that includes design variables. The distinct advantage of the GHNN based model is that it can be reasonably responsive to changes in design variables as well as loading scenarios. It is a first-ever design-based dynamic hysteretic model for steel beam-column connections.

Since there has been no general hysteretic model for structural components or materials within a phenomenological-based framework, the development of the new NN based cyclic material model is expected to lead to significant applications to many practical problems in earthquake engineering. Even with the conventional NN based material model, difficulties have been encountered when they are expected to learn complex cyclic material behavior under load reversing conditions. Therefore, the first objective in this report is development of a new NN based cyclic material model and its application to steel beam-column connections. The new NN based connection models

shows viable and promising performance in representing complex cyclic behavior of connections even in earthquake type loading. However, experimental data are not always available, for example, in the form of rotational cyclic behavior of connections. In order to facilitate the use of the NN based connection model, a new self-learning simulation framework is developed for obtaining the NN based connection model directly from large or small-scale structural tests. The framework is developed in conjunction with three-dimensional finite element analysis with geometrical nonlinearity. Moreover, the significant impact of the proposed GHNN based model is that the optimal seismic performance objective of structures can be obtained since the model includes a set of design variables for each connection type and the model can be reasonably responsive to the variation of design variables and loading scenarios. There have been many experimental investigations in the earthquake engineering community, but these were mainly limited to understanding yield mechanisms and failure modes of new designs. There has been no systematic approach in connecting experimental data to computational modeling processes. Significance of the research in this report is establishments of the strong connections between experimental and computational research through the self-learning simulation framework and opening-up of potential applications of the NN based connection model for practical design purposes.

1.4 Organization of the Report

This report is presented in 7 Chapters. In Chapter 1, current problems and limitations in modeling of the cyclic behavior of beam-column connections are explained and the benefits from using an information-based modeling approach are also discussed. It is

followed by primary objectives of the report and their significances. In the Chapter 2, features of the cyclic behavior of connections are explained based on the abundance of experimental observations. For each connection type, the yield mechanisms observed from experiments are described and the primary factors that influence the capacity of connections are discussed. This is followed by a series of literature reviews on the modeling methods of cyclic behavior of connections ranging from phenomenological approach to three-dimensional finite element analysis approach. In particular, the component-based modeling approach incorporated with NN based cyclic material model is highlighted. In Chapter 3, a novel NN based cyclic material model is proposed with a series of numerical examples from one-dimensional through multi-dimensional problems. In Chapter 4, the proposed model is applied to steel beam-column connections. For the purpose of the applications, a nonlinear finite element program using three-dimensional beam-column element with geometric nonlinearity is developed employing lumped inelasticity. A new simulation method of frame structures with NN based plastic hinges is proposed. In Chapter 5, a new self-learning simulation framework for determining the inelastic hysteretic model for connections from experiments are developed and then it is tested with a series of examples using both synthetic and experimental data. Towards extensive applications of the proposed model to daily practical applications, a generalized hybrid NN (GHNN) based inelastic hysteretic model for connections is proposed in Chapter 6. The generalized features of the model are demonstrated with extended-end-plate and top-and-seat-angle-with-double-web-angle connections under cyclic and earthquake loading. Finally, conclusions are made and recommended future research is introduced in Chapter 7.

CHAPTER 2 MODELING OF INELASTIC CYCLIC BEHAVIOR OF STEEL BEAM-COLUMN CONNECTIONS

2.1 Introduction

In this chapter, cyclic behavior of steel beam-column connections is discussed focusing on their seismic performances and analytical modeling approaches. Accurate modeling of the cyclic behavior of connections is very important in evaluation of seismic performances and design of steel moment-frame buildings. After the 1994 Northridge earthquake, many experiments on steel beam-column connections were carried out to improve the seismic performance of fully welded beam-column connections and to suggest new connection types with improved seismic resistance. Observations from the past experiments on various connection types, their cyclic behavior, and yielding/failure mechanisms will be briefly reviewed in the following section.

2.2 Cyclic Behavior of Steel Beam-Column Connections

Since the 1994 Northridge earthquake, extensive research on seismic response and performance of various connection types has been carried out. The large variations in the load-carrying capacity observed in the experiments are likely due to many different yield mechanisms and failure modes. As such, large variations in strength and ductility can lead to difficulties in modeling of the cyclic behavior. Particularly, plastic engagement of connecting components significantly affects the cyclic behavior of connections. Therefore, distinguishing between energy-dissipative and non-energy-dissipative

components is important in designing connections aimed at earlier development of ductile mechanisms than brittle mechanisms (Plumier 1994). It is also important to give sufficient over-strength factor to the components that are likely to show brittle failure mechanisms. The non-energy-dissipative mechanisms for each connection type under cyclic loading conditions are summarized in Table 2.1.

In the case of welded-flange-bolted-web connections, the cyclic behavior is much more stable than the earlier bolted connections. Its stable cyclic behavior is illustrated in Figure 2.1. The stable energy dissipation is mostly provided by the inelastic deformations in the shear panel zones and in the welds between beam and column flanges. Their contributions to the total energy dissipation can be controlled by a supplementary column web plate. In the case of extended-end-plate connections, flexural deformations of the end plate and axial deformations of the bolts contribute to the energy dissipation under cyclic loading. Particularly, it has been observed in the past experiments that the more the bolts contribute to the energy-dissipation, the more hysteretic pinching is amplified. As shown in Figure 2.2(a), the ductility is very low after the bolts have failed. If the end plate is stiffened, it can ensure yielding of the beam and lead to very good energy dissipation capacity as shown in Figure 2.2(c). Therefore, thickness of the end plate and the column flange and diameter of the bolts are very important design parameters for the extended-end-plate connection. In the case of top-and-seat-angle connections, flexural deformations of the column flange and the angles are primary sources of the energy dissipation under cyclic loading. As the thickness of the angles increases, the flexural deformation of the column flanges increases. In the case of bolted-shear-tab connections,

the cyclic behavior could be non-symmetric due to preloading effect of the gravity loads and contact between beam flange and column face as illustrated in Figure 2.3.

Table 2.1 Various Connection Types and Their Brittle Failure Mechanisms under Cyclic Loading

Number	Connection Type	Non-energy-dissipative mechanism	Classification
(1)	Welded-flange-bolted-web connection	a. Local buckling of column web b. Fracture of weld	Pre-Northridge
(2)	Welded-flange-bolted-web connection with improved welding	a. Local buckling of column web b. Fracture of weld	Post-Northridge
(3)	Welded-flange-bolted-web connection with improved weld access hole	a. Local buckling of column web b. Fracture of weld	Post-Northridge
(4)	Extended-end-plate connection	a. Fracture of bolts in tension	Post-Northridge
(5)	Bolted-flange-plate connection	a. Fracture of weld b. Fracture of bolts in shear	Post-Northridge
(6)	T-stub connection	a. Shear fracture of bolts b. Tensile fracture of bolts	Post-Northridge
(7)	Double-flange-angle connection	a. Fracture of bolts in shear	Post-Northridge
(8)	Web-angle connection	a. Fracture of weld b. Shear fracture of bolts c. Tensile fracture of bolts	Post-Northridge
(9)	Reduced-beam-section connection	a. Lateral torsional buckling b. Fracture of weld	Post-Northridge
(10)	Composite-partially-restrained connection	?	Post-Northridge
(11)	Connection with friction and damping	?	Post-Northridge
(12)	Connection with self-centering capability	?	Post-Northridge

Note) Any premature local buckling of plates should be avoided for all connections

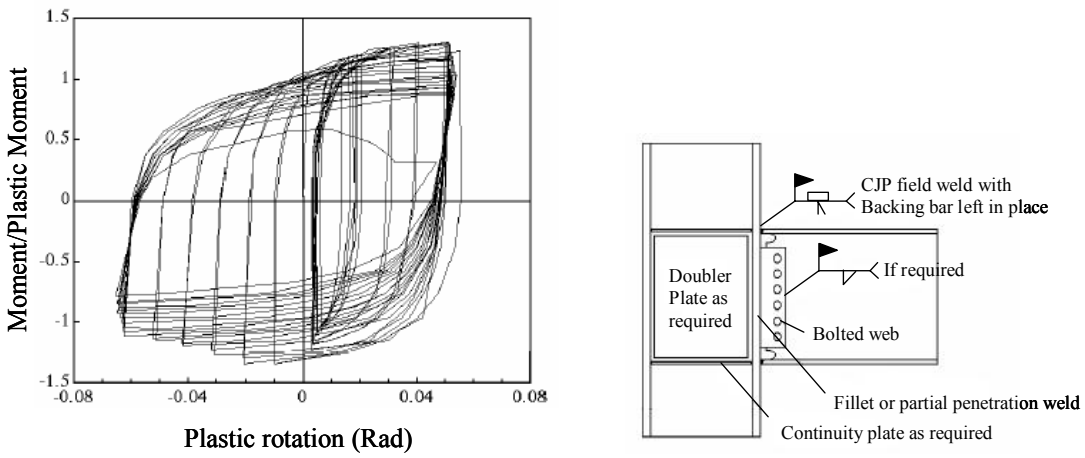

Figure 2.1 Moment-Rotation Cyclic Behavior of Welded-Flange-Bolted-Web Connection (FEMA-355D 2000)

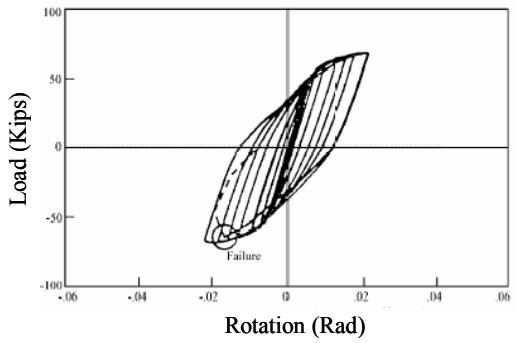

(a) Fracture in Bolt

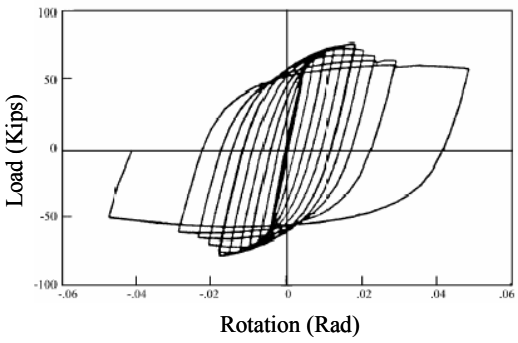

(b) Plastic Deformation in End-Plate

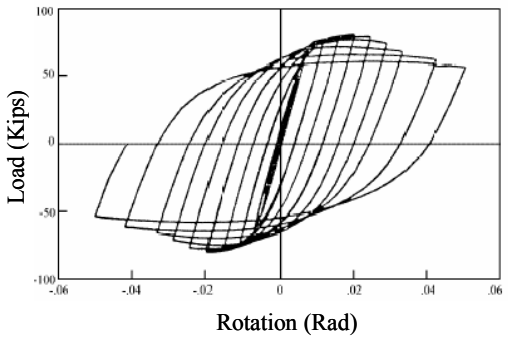

(c) Plastic Deformation in Beam (Stiffened End Plate)

Figure 2.2 Cyclic Behavior of Extended-End-Plate Connection (FEMA-355D 2000)

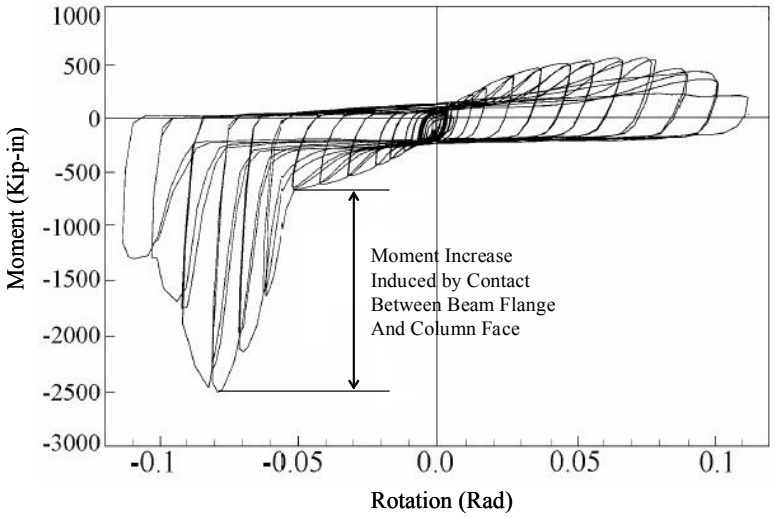

Figure 2.3 Moment-Rotation Curve for Bolted-Shear-Tab Connection (FEMA-355D 2000)

In summary, because of the topological complexity of connections and a large number of possible yield mechanisms, the cyclic behavior can vary significantly even within the same connection type. Development sequences of the yield mechanisms can also affect the rotational capacity of connections because of the interaction between the

components. Mainly for this reason, there are difficulties in modeling of the cyclic behavior of the connections.

2.3 Modeling Approaches of Cyclic Behavior of Steel Beam-Column Connections

There are four different approaches to model the cyclic behavior of beam-column connections; 1) Phenomenological modeling; 2) Mechanical modeling; 3) Refined three-dimensional finite element modeling and 4) Neural network (NN) based modeling approach. In this section, the existing modeling approaches are briefly reviewed and a neural network based modeling approach combined with mechanical model is introduced in more detail.

2.3.1 Phenomenological Models

The phenomenological models are mainly based on curve-fitting techniques whereby a simple mathematical expression reproduces the experimental data with some curve-fitting constants. The constants are calibrated by the experimental data. The advantage of the phenomenological model is that once the constants are determined, the moment-rotation relationship can be explicitly expressed and used in ordinary structural analysis for design purposes. There is wide-spectrum of phenomenological models with varying degrees of complexity. Some examples of these models are: Richard-Abbott model (Richard and Abbott 1975), the power model, the Chen-Lui exponential model (Lui and Chen 1986) and the bounding-line model (Albermani, et al. 1994).

In order to trace the cyclic behavior of connections, the static monotonic moment-rotation can be used following three types of methods; independent hardening method, kinematic hardening method and bounding surface method. The independent hardening method can not consider the deterioration of connection properties such as initial stiffness and the initial yield moment. In the case of bounding surface method, Masing rule is used to trace the reversals resulting from unloading and reloading by directly following a nonlinear curve. If a static monotonic curve is defined as follow.

$$f(M, q_c) = 0 \tag{2-1}$$

then the unloading and reloading curve can be assumed by the following equation.

$$f\left(\frac{M - M^*}{2}, \frac{q - q^*}{2}\right) = 0 \tag{2-2}$$

Where (M*, θ*) are the point at which the load reversal occurs. The tangent stiffness corresponding to loading is expressed as follow.

$$K_{tan} = \frac{dM}{dq} = g(M, q) \tag{2-3}$$

The tangent stiffness corresponding to unloading and reloading is expressed as follow.

$$K_{tan} = \frac{dM}{dq} = g\left(\frac{M - M^*}{2}, \frac{q - q^*}{2}\right) \tag{2-4}$$

Numerous studies have also been conducted to predict the experimentally observed cyclic behavior of various beam-column connection types. Although the phenomenological models can be generally used for all kinds of connections under dynamic loadings, it can not consider stiffness and strength degradations and pinching in cyclic behaviors. It is noteworthy that there has not been a generally accepted phenomenological model for the complex cyclic behavior of all the steel beam-column connections.

2.3.1.1 Advanced Phenomenological Models

There is a relatively simple phenomenological model that represents the moment-rotation relationship of semi-rigid connections (Bernuzzi, et al. 1996). The model is based on a bilinear representation of semi-cycle by introducing the four different stiffness values. This model was applied to a flush end-plate connection subjected to cyclic loadings.

In order to investigate the seismic responses of steel moment-frame buildings with connection failures, a smooth connection-fracture hysteresis model based on Bouc-Wen model was developed (Wang and Wen 2000). An asymmetric model is combined with a slip-lock element in serial mode to represent pinching and slip in cyclic behaviors of steel beam-column connections. Even though the modified Bouc-Wen model can reproduce any test result, many parameters relating to the shape of hysteresis before and after fractures should be determined prior to its application.

In 2000, a hysteretic connection element was proposed by Deng et al. (Deng, et al. 2000). The stiffness and strength degradation and pinching of cyclic curves were expressed in terms of damage state variables. It was implemented in a computer program, DRAIN-3DX with piece-wise linear cyclic relationships following an automatic event definition algorithm. However, since the damage model is dependent on a particular loading history, more experiments on any specific connection type needs to be done for further applications.

In the following section, two most widely used non-pinching cyclic connection models are described. These models are used for the purpose of verifications of a

proposed model in this report. They are; Ramberg-Osgood model (Ang and Morris 1984) and Frye-Morris' model (Frye and Morris 1975).

2.3.1.2 Standardized Ramberg-Osgood Model

The Ramberg-Osgood model was originally developed for modeling non-linear stress-strain relationships (Ramberg and Osgood 1943). In 1984, it was standardized by Ang and Morris (Ang and Morris 1984) for its application in steel beam-column connections. The moment-rotation relationship is expressed as follow;

$$\frac{q}{q_0} = \frac{|PM|}{PM_0}\left[1 + \frac{|PM|^{n-1}}{PM_0}\right] ; \; K_i = \frac{M_0}{q_0} \tag{2-5}$$

where M_0 and θ_0 are the moment and rotation that define a crossing point A in Figure 2.4; P is a dimensionless parameter dependent on the connection type and geometry; n is a parameter defining the steepness of the curve. The parameter P is expressed as follows.

$$P = \prod_{j=1}^{m} q_j^{a_j} \tag{2-6}$$

Where q_j is value of the j-th size parameter; a_j is a dimensionless exponent that indicates the effect of the j-th size parameter on the curve and m is the number of size parameters for a given connection type. P and n values are tabulated for each connection type in (Ang and Morris 1984). For its application in modeling the cyclic behavior of connections, the rotational tangent stiffness can be obtained by taking the derivative of equation (2-5). The tangent stiffness in unloading and reloading curve is illustrated in Figure 2.4.

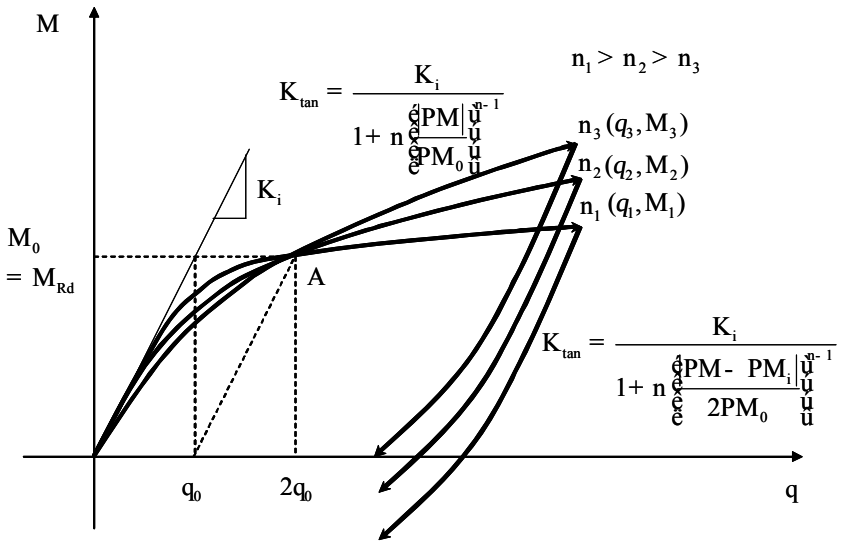

Figure 2.4 Standardized Ramberg-Osgood Model for Connections

2.3.1.3 Frye and Morris' Polynomial Model

In 1975, Frye and Morris proposed an empirical model whereby the rotation is expressed by an odd-power polynomial function of moment and other curve-fitting parameters (Frye and Morris 1975). They fitted curves to the available experimental results of connections subjected to monotonic loadings.

$$q = C_1(PM) + C_2(PM)^3 + C_3(PM)^5 \qquad (2\text{-}7)$$

Where M and θ are the moment and rotation, respectively; C_1, C_2 and C_3 are curve-fitting parameters; P is a standardized parameter which is a function of the important geometrical parameters such as connecting member size and plate thickness, etc. The parameter P is expressed as follows.

$$P = \prod_{j=1}^{m} q_j^{a_j} \qquad (2\text{-}8)$$

Where q_j is the value of the j-th size parameter; a_j is dimensionless exponent that indicates the effect of the j-th size parameter on the curve and m is the number of size parameters for a given connection type. The standardized connection moment-rotation functions are tabulated in Table 2.2. Taking the derivative of equation (2-7) with respect to the rotation (θ), the tangent stiffness can be obtained as follow.

$$K_{tan} = \frac{dM}{dq} = \frac{1}{C_1 P + 3C_2 P(PM)^2 + 5C_3 P(PM)^4} \tag{2-9}$$

In applying the polynomial model in cyclic moment-rotation curves, the rotational tangent stiffness is determined using the predictor moment for the next time step and the incremental moment as follow.

$$\begin{aligned}
&\text{If} \quad M_{n+1} \geq 0 \quad \text{and} \quad \Delta M_{n+1} > 0 \\
&\quad K_{tan} = \frac{dM}{dq} = \frac{1}{C_1 P + 3C_2 P(PM)^2 + 5C_3 P(PM)^4} \\
&\text{else if} \quad M_{n+1} \geq 0 \quad \text{and} \quad \Delta M_{n+1} \leq 0 \\
&\quad K_{tan} = \frac{dM}{dq} = \frac{1}{C_1 P + 3C_2 P(P|M - M_i|/2)^2 + 5C_3 P(P|M - M_i|/2)^4} \\
&\text{else if} \quad M_{n+1} \leq 0 \quad \text{and} \quad \Delta M_{n+1} < 0 \\
&\quad K_{tan} = \frac{dM}{dq} = \frac{1}{C_1 P + 3C_2 P(PM)^2 + 5C_3 P(PM)^4} \\
&\text{else if} \quad M_{n+1} \leq 0 \quad \text{and} \quad \Delta M_{n+1} \geq 0 \\
&\quad K_{tan} = \frac{dM}{dq} = \frac{1}{C_1 P + 3C_2 P(P|M - M_i|/2)^2 + 5C_3 P(P|M - M_i|/2)^4} \\
&\text{end}
\end{aligned} \tag{2-10}$$

Where M_{n+1} is predictor moment for (n+1)-th step; ΔM_{n+1} is incremental moment at (n+1)-th step; M_i is the latest unloading or reloading moment along the cyclic curve.

The advantages of the two empirical models are that the models are standardized to fit into the experimental observation on all the connection types so they can be used to predict the rotational cyclic behavior once the geometrical and material properties of the

given connection type are known. However, as aforementioned, they can not consider the stiffness and strength degradation and the pinching phenomena frequently observed in the hysteretic behavior of beam-column connections.

Table 2.2 Standardized Connection Moment-Rotation Functions

Connection Type	Curve-fitting Parameters	Standardized Constant	Maximum Deviation of Standardized Curve from Experimental Curve	Number of Tests
Double-web-angle connection	$C_1=3.66\times10^{-4}$ $C_2=1.15\times10^{-6}$ $C_3=4.57\times10^{-8}$	$P=d^{-2.4}\cdot t^{-1.18}\cdot g^{0.15}$	6%	19
Single-web-angle connection	$C_1=4.28\times10^{-3}$ $C_2=1.45\times10^{-9}$ $C_3=1.51\times10^{-16}$	$P=d^{-2.4}\cdot t^{-1.18}\cdot g^{0.15}$	10%	8
Header-plate connection	$C_1=5.1\times10^{-5}$ $C_2=6.2\times10^{-10}$ $C_3=2.4\times10^{-13}$	$P=t^{-1.6}\cdot g^{1.6}\cdot d^{-2.3}\cdot w^{0.5}$	4%	16
Top-and-seat-angle connection	$C_1=8.46\times10^{-4}$ $C_2=1.01\times10^{-4}$ $C_3=1.24\times10^{-8}$	$P=t^{-0.5}\cdot d^{-1.5}\cdot f^{1.1}\cdot l^{-0.7}$	11%	55
End-plate connection without column stiffeners	$C_1=1.83\times10^{-3}$ $C_2=-1.04\times10^{-4}$ $C_3=4.57\times10^{-8}$	$P=d^{-2.4}\cdot t^{-0.4}\cdot f^{1.1}$	3%	12
End-plate connection with column stiffener	$C_1=1.79\times10^{-3}$ $C_2=1.76\times10^{-4}$ $C_3=2.04\times10^{-4}$	$P=d^{-2.4}\cdot t^{-0.6}$	6%	18
T-stud connection	$C_1=2.1\times10^{-4}$ $C_2=6.2\times10^{-6}$ $C_3=-7.6\times10^{-9}$	$P=d^{-1.5}\cdot t^{-0.5}\cdot f^{1.1}\cdot l^{-0.7}$	12%	17

2.3.2 Mechanical Models: Component-based Approach

The mechanical models are also aimed at predicting the rotational cyclic behavior of connections by assemblages of rigid and deformable elements (spring elements). They are frequently referred to as component-based models in the literature. The advantage of the component-based modeling is that the cyclic behavior of the whole connections can be represented by the uni-axial cyclic behavior of simple deformable elements.

In 1994, De Stefano et al. proposed a mechanical model to simulate the behavior of the double-angle connection subjected to large amplitude cyclic loading (De Stefano, et al. 1994). They pointed out that the angle behavior is primarily dependent on the flexural response of the angle leg adjacent to column flange. Beam element with distributed plasticity approach was used with a kinematic hardening model for the material model. The model is illustrated in Figure 2.5. However, the model is for predicting the cyclic behavior of the double-angle connection only.

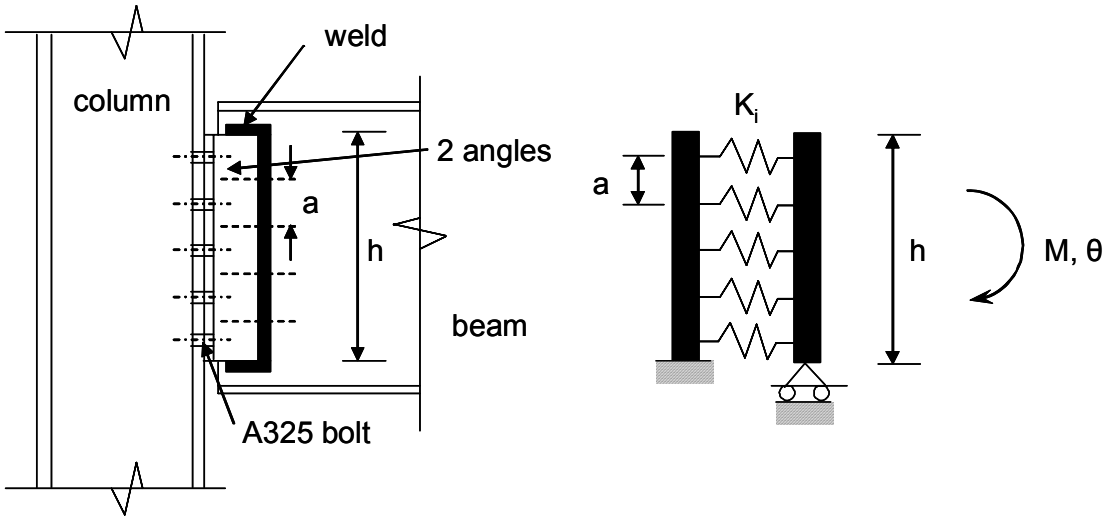

Figure 2.5 Mechanical Model for Double-angle Connection (De Stefano, et al. 1994)

In 1992, a component-based model was proposed by Madas, et al. (Madas and Elnashai 1992). The model consists of a rigid parallelogram surrounding the panel zone and spring elements representing fastening elements such as angles, end plate and bolts as shown in Figure 2.6. In the calculation of the stiffness of each component C and D, the connection elements such as bolts and column flange in bending are assumed to be connected in serial mode. The stiffness of the spring element for the panel zone is calculated according to the formulation proposed by Krawinkler et al. (Krawinkler, et al. 1971) and tri-linear cyclic model is applied as shown in Figure 2.6. The drawbacks of this model are that the stiffness and strength degradation and pinching phenomenon are not taken into account and the shear force is transferred to the panel zone only through flexural action of beams.

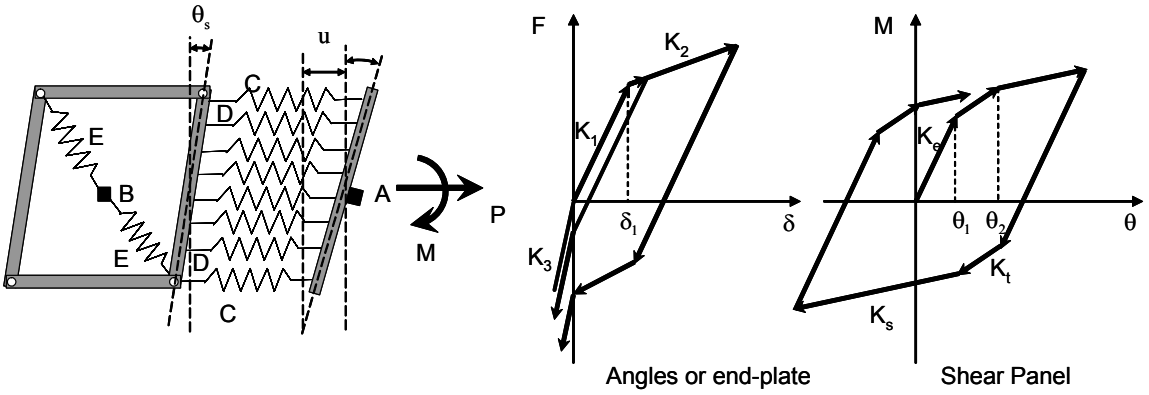

Figure 2.6 Mechanical Model and Cyclic Behavior of Components (Madas and Elnashai 1992)

In 2004, an advanced component-based model for cyclic behaviors of partially restrained composite joint was proposed by Rassati, et al. (Rassati, et al. 2004). While it

has been proven to reproduce complex 3D connection behaviors, it is not suitable in practical applications because of enormous input and computation overhead.

In 2006, the cyclic behavior of the components was modeled by NN based material modeling approach in order to resolve the drawback of the original model (Yun, et al. 2006a). For development of the NN based material model, a self-learning simulation methodology was applied and three past states of stress-strain pairs was used to train the NN model. Considering the potential of NN's learning capability, it is very promising approach for modeling the cyclic behavior of beam-column connections.

2.3.3 Three-Dimensional Finite Element Model

Three-dimensional finite element model is the most accurate approach to predict the cyclic response of beam-column connections. Recently, many general-purpose nonlinear finite element analysis packages and advanced finite element mesh generation tools are routinely available, such as ABAQUS, ANSYS, I-DEAS and HYPERWORKS, etc. For detailed modeling of components of the connection, modeling techniques such as metal frictional contact, assembly torque, geometric and material nonlinearity are easily employed in complex three-dimensional finite element models. With such a detailed finite element model, realistic responses under cyclic loadings can be simulated by classical metal plasticity model with mixed hardening definitions such as kinematic and non-linear isotropic hardening model. A number of studies on three-dimensional finite element analysis of beam-column connections have been reported (Citipitioglu, et al. 2002; Bursi and Jaspart 1998; Sherbourne and Bahaari 1996; Bahaari and Sherbourne 1996; Sherbourne and Bahaari 1994). However, there are several drawbacks in the three-

dimensional finite element models of connections subjected to cyclic loadings. While the approach can provide the most accurate prediction of the capacity of connections, the computational time and cost are enormous and there are still unresolved issues with respect to modeling of post-yield behavior such as local buckling, fracture and tearing of components.

Figure 2.7 illustrates results from a three-dimensional finite element analysis of a welded-flange-bolted-web connection (Yun, et al. 2006a). All the components including beam, column, shear tab, bolts and weld materials are modeled using three-dimensional solid elements to reproduce experimental results. According to the test results, top flange of the beam was torn out. The experimental observation could be inferred by the result from the three-dimensional finite element analysis as illustrated in Figure 2.7.

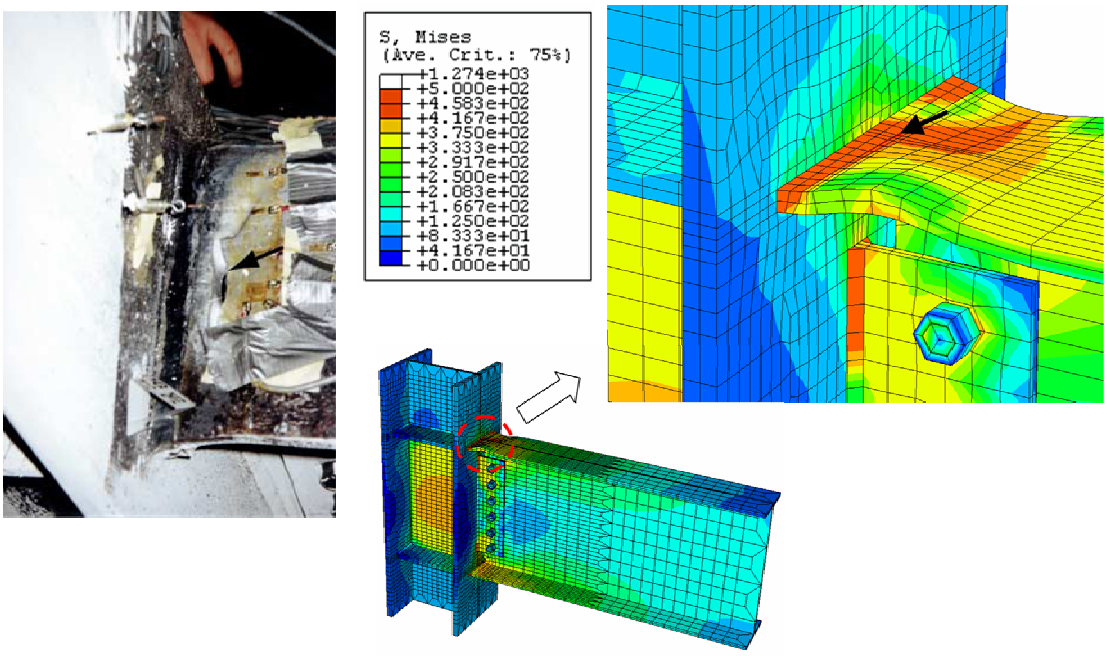

(a) Top Beam Flange Torn Out (Stojadinovic 1998) (b) Contour of Von Mises Stress

Figure 2.7 3D Finite Element Analysis of Welded-Flange-Bolted-Web Connection

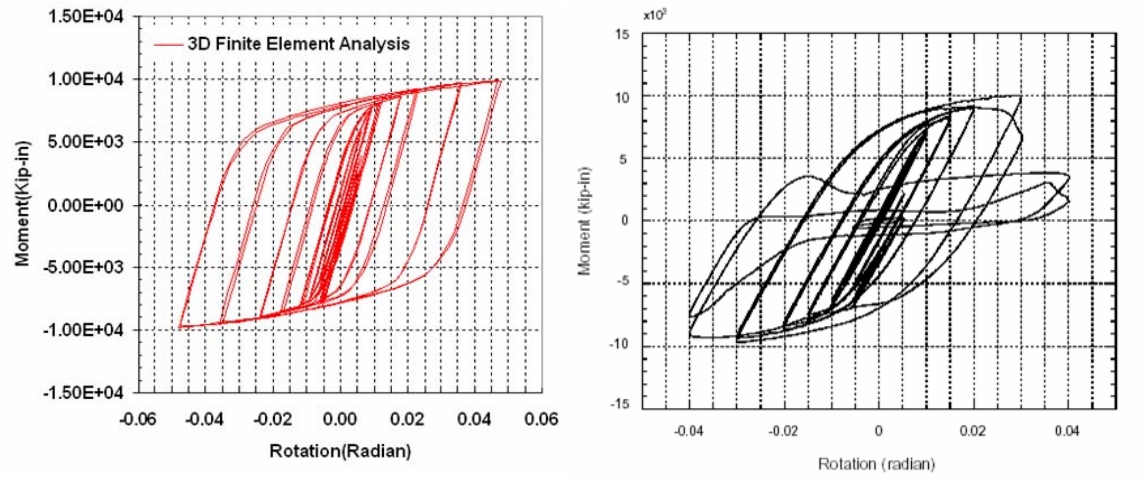

(a) 3D Finite Element Analysis Result (b) Experimental Result(Stojadinovic 1998)

Figure 2.8 Comparison of Cyclic Behavior between 3D FE Analysis and Experiment

A comparison of Figure 2.8 shows that the three-dimensional finite element analysis can reasonably predict the cyclic behavior of the test specimen until tearing of the beam flange occurs. However, as shown in Figure 2.8, the three-dimensional finite element analysis has difficulties in reproducing the post-limit behavior.

2.4 Neural Network Based Modeling Approach

Since neural network (NN) based material modeling methodology was first proposed by Ghaboussi et al. (Ghaboussi, et al. 1991), there have been other related studies on constitutive modeling of soil and concrete material through NN (Ghaboussi, et al. 1998a; Ghaboussi and Sidarta 1998b; Hashash, et al. 2003; Jung and Ghaboussi 2006). The main advantages of the NN based material models are that 1) the NN based material models can represent the material behavior properly if they are trained with comprehensive

training data and 2) they can represent any complex cyclic material behavior including the post-limit behavior such as local buckling, fracture and tearing of components. The training process of the NN material model is similar to validation with comprehensive experimental observations in conventional phenomenological material models.

However, there has been no research on the NN based cyclic material modeling for steel beam-column connections. Recently, a conventional NN based material constitutive model has been applied to model the cyclic behavior of steel beam-column connections with component-based approach (Yun, et al. 2006a). Since there is strong path-dependency in the cyclic behavior of beam-column connections, three-point scheme representation is used in which three recent states of stresses and strains are included in the input of the NN. Generally, there are two forms in NN representation for modeling the path-dependent material behavior; total form, Equation (2-11) and incremental form, Equation (2-12). Either of the two forms can learn the path-dependent material behavior. The two NN based constitutive models for connecting components are expressed as follows.

$$\boldsymbol{\sigma}_i^{NN} = \hat{\boldsymbol{\sigma}}_{NN}\left(\left\{\boldsymbol{\varepsilon}_i, \boldsymbol{\varepsilon}_{i-1}, \boldsymbol{\sigma}_{i-1}, \boldsymbol{\varepsilon}_{i-2}, \boldsymbol{\sigma}_{i-2}, \boldsymbol{\varepsilon}_{i-3}, \boldsymbol{\sigma}_{i-3}\right\} : \left\{\text{NN architecture}\right\}\right) \tag{2-11}$$

$$\Delta\boldsymbol{\sigma}_i^{NN} = \Delta\hat{\boldsymbol{\sigma}}_{NN}\left(\left\{\Delta\boldsymbol{\varepsilon}_i, \boldsymbol{\varepsilon}_{i-1}, \boldsymbol{\sigma}_{i-1}, \boldsymbol{\varepsilon}_{i-2}, \boldsymbol{\sigma}_{i-2}, \boldsymbol{\varepsilon}_{i-3}, \boldsymbol{\sigma}_{i-3}\right\} : \left\{\text{NN architecture}\right\}\right) \tag{2-12}$$

The advantage of the NN based constitutive model is its capability of learning the post-limit behavior such as local buckling and tearing of components, while classical metal plasticity model can not represent this post-limit behavior.

The component based model for beam-column connections is illustrated in Figure 2.9 with exaggerated schematic deformations. The parallelogram with dimension d_b (depth of beam) by d_c (depth of column) is modeled by four rigid elements. The corners

of the parallelogram are modeled as simple pin connections. The top/bottom flanges (or angles) and bolts connections are modeled as simple uni-axial spring elements. The spring elements at the center line of bolts are combined with rigid body elements in order to transfer flexural actions from beam to column. The beam and column joining to the connection are modeled with ordinary beam-column elements. A translational spring element is used to transfer the shear force from beam to column.

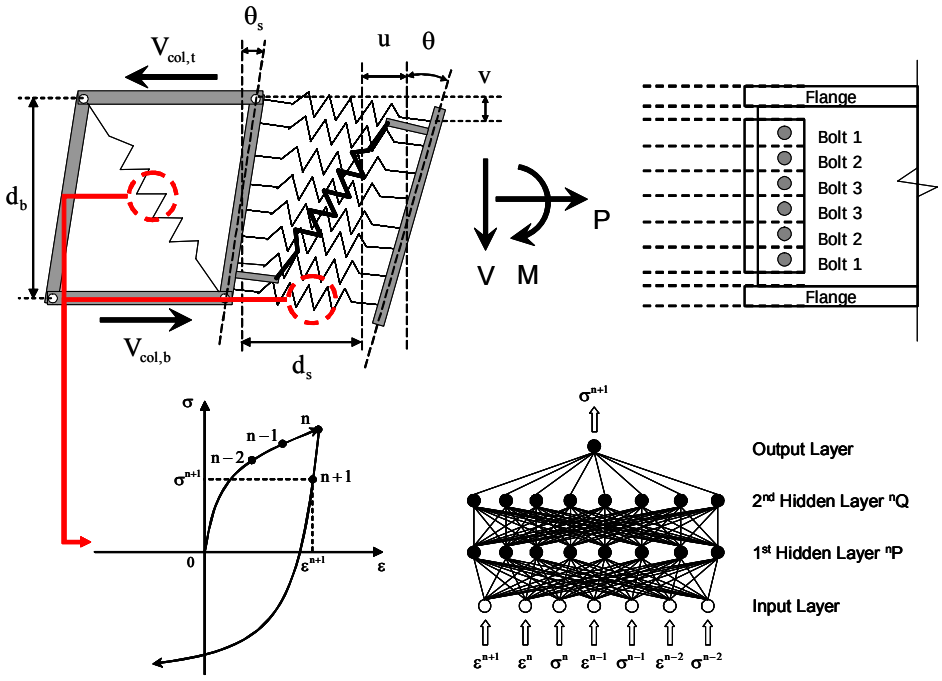

Figure 2.9 Mechanical Model with Neural Network based Constitutive Model (Yun, et al. 2006a)

Rotational stiffness of the shear panel spring is determined by the procedure proposed by Krawinkler (Krawinkler 1978). Using the principle of virtual work on the deformed configuration illustrated in Figure 2.10, the rotational stiffness of the shear

panel zone can be obtained. Translational spring stiffness as shown in Figure 2.10(b) can be derived from the rotational spring stiffness following the procedure below.

$$W_{int} = M_s\gamma = K_R\gamma^2$$
$$W_{ext} = \left(M_{b,r} + M_{b,l}\right)\gamma - \left(V_{col,t} + V_{col,b}\right)\gamma\frac{d_b}{2} \quad ; \quad W_{int} = W_{ext} \tag{2-13}$$

From equilibrium conditions in the deformed configuration in Figure 2.10(a), the shear demand can be obtained as follows.

$$V = \left(\frac{M_{b,l} + M_{b,r}}{d_b}\right) - \left(\frac{V_{col,t} + V_{col,b}}{2}\right) \tag{2-14}$$

From the third equation of (2-13) and (2-14), the rotational spring of shear panel can be expressed as follows.

$$K_R = d_b\left(\frac{V}{\gamma}\right) \tag{2-15}$$

In order for the work done by the given action to remain invariant, the following equality must be satisfied.

$$\frac{1}{2}K_R\gamma^2 = \frac{1}{2}K_T\left(L_{diag} - L'_{diag}\right)^2 = \frac{1}{2}K_T\Delta^2 \tag{2-16}$$

Where L_{diag} is the diagonal length of shear panel zone in original configuration and L'_{diag} is the diagonal length of the shear panel zone in a deformed configuration.

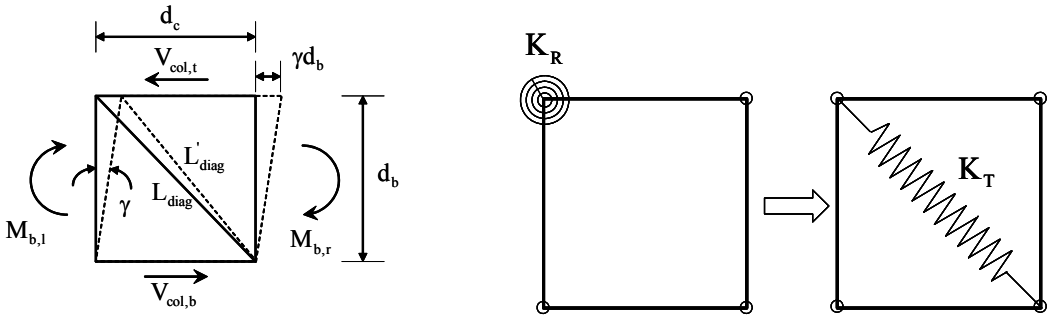

(a) Deformed configuration of shear panel zone (b) Modeling of shear panel zone

Figure 2.10 Deformed Configuration and Idealization of Shear Panel Zone Stiffness

By substituting Equation (2-15) into Equation (2-16) and using the relationship $V_y = 0.55F_y d_c t_c$ and $\gamma_y = F_y/\sqrt{3}G$, the initial stiffness of the translational spring can be obtained as follows. Then effective area of the translational spring for the shear panel zone is obtained using the equation (2-17).

$$K_T = \frac{0.55F_y^2 d_b d_c t_c}{\sqrt{3}G\Delta_y^2} \quad \text{where } \Delta_y = \sqrt{d_b^2 + d_c^2} - \sqrt{d_b^2 + \left(d_c - \gamma_y d_b\right)^2} \tag{2-17}$$

where F_y is yield stress of steel; d_b depth of beam; d_c depth of column; t_c thickness of shear panel; G shear modulus of steel; Δ_y deformation of the spring at yielding point. Finally, the deformation of each component is defined by three variables: rotation $\theta_e=\theta-\theta_s$, axial deformation, u and vertical deformation, v. Therefore, the total axial force P and the moment M transmitted by n components (except shear panel spring) and the moment M_{cf} at the column face are expressed in terms of the stresses determined by the NN based material constitutive model.

$$P(t) = \sum_{i=1}^{n} \sigma_i^{NN}(t) A_i^{eff}, \quad M(t) = \sum_{i=1}^{n} \sigma_i^{NN}(t) A_i^{eff} z_i - \frac{d_s}{2} V(t) \tag{2-18}$$

$$M_{cf}(t) = \frac{d_s}{2} V(t) - \sum_{i=1}^{n} \sigma_i^{NN}(t) A_i^{eff} z_i + (V_{col,t} + V_{col,b}) \frac{d_b}{2} \quad (2\text{-}19)$$

where n is the number of components; σ_i^{NN} stress of i-th component; t time step; A_i^{eff} effective area of i-th component; z_i distance from neutral axis to i-th component; d_s distance from column face to center line of bolts; V(t) shear force transferred to column; d_b depth of beam and $V_{col,t}$ and $V_{col,b}$ column shear forces in the column above and below the connection.

The flexibility and the learning capability of the NN based material models are the unique advantage of the proposed model in learning the complex force-displacement relationship of the components due to buckling, frictional slip, fracture, slacking of fastened bolts as well as yielding of materials. The nonlinear force-displacement relationship which might include fractures of the corresponding components can be obtained through the NN based hysteretic model in conjunction with the self-learning simulation.

2.5 Recommendations to Improve Accuracy and Practicality of Connection Model

Through the phenomenological and mechanical modeling approaches, some of the experimental observations on beam-column connections could have been well reproduced in numerical simulations. However, the key point is that there is no generally accepted rule or model for the cyclic behavior of beam-column connections because the cyclic behavior is highly dependent on loading scenario, connection types, construction or manufacturing quality as well as complex hierarchical yield mechanisms between components. Even though there are standardized empirical models starting from

geometrical and material properties, their uses are mostly limited to monotonic loading cases and they are constructed from limited number of experimental cases. Therefore, there has been strong need for a practical, accurate and viable dynamic hysteretic model for components that significantly affect the response of structural systems such as beam-column connections.

In this report, the NN based modeling approach has been adopted to improve the accuracy in prediction of the cyclic behavior of connections and the practicality of the model in design point of view. The NN has a remarkable capability to extract information from complicated or imprecise data such as cyclic behavior of structures from experiments. Although the earlier versions of the NN material models were effective in capturing the multi-axial material behavior, not only did they have limitations in learning cyclic behavior of materials but also they were only tested under cyclic uni-axial state of stress.

CHAPTER 3 NOVEL NEURAL NETWORK BASED INELASTIC HYSTERETIC MATERIAL MODEL

3.1 Introduction

Even with the great advances made in material modeling and computational simulation, inelastic analysis of materials and structural components remain challenging, especially under cyclic loading. In classical plasticity models, the cyclic behavior and Bauschinger effect has been modeled through a combination of isotropic and kinematic hardening. In most of the hardening models, the shape of the yield surface is assumed to remain unchanged in spite of the fact that the actual material behavior is known to lead changes in the shape of the yield surface (Green and Naghdi 1965; Shiratori and Ikegami 1968).

Over the past several decades, numerous cyclic plasticity and visco-plasticity models have been proposed in order to describe the material behavior under cyclic loading conditions (Chaboche 1989; Lemaitre and Chaboche 1990; Bodner and Partom 1975; Ristinmaa 1999). Numerous inelastic hysteretic models have also been developed for applications in earthquake engineering to represent the behavior of structural components, such as base isolators, reinforced concrete or steel members and their connections (Iwan 1966; Wen 1976). These models represent various phenomena, such as stiffness/strength degradation and pinching, under arbitrary cyclic loadings. Modeling and calibrating of the observed phenomenological behavior of structural components have been proven to be difficult.

Neural network (NN) based constitutive modeling methods, first proposed by Ghaboussi, et al. (Ghaboussi, et al. 1991; Ghaboussi and Sidarta 1997), offer an alternative method for modeling of the complex behavior of materials and structural

components. A unique advantage of NN based constitutive models is that they are trained to learn the material behavior directly from the stress-strain data that are generated from experiments. If the training data contain sufficient information, then the trained NN can learn the material behavior and function as a constitutive model in computational mechanics. Recognizing that generating sufficient training data from material experiments may not always be possible, Ghaboussi, et al. (Ghaboussi, et al. 1998a) proposed a new method for training the NN material model from the results of structural experiments. However, prediction of the complicated hysteretic behavior of materials with NN material models has remained a challenge. A new method is proposed in this chapter for modeling of the cyclic behavior of materials and structural components. The effectiveness of the proposed method has been demonstrated through a series of examples with actual and numerically simulated experiments.

3.2 Neural Networks in Material Modeling

Multi-layered NN consists of artificial neurons that are arranged within layers. The neurons in each layer are connected to all the neurons in the next layer with weighted connections. Input signals are propagated from the input layer, through the hidden layers to the output layer. Three simple operations are performed in each neuron: 1. weighted sum of the incoming signals are calculated; 2. output of the neuron is determined by passing the weighted sum through a nonlinear activation function (e.g. hyperbolic tangent function); and, 3. The output is sent to the neurons in the next layer. Multi-layered NNs are first trained with training data that consist of target input and output pairs. The connection weights are adjusted during the training phase. Training of the NN is an

adaptive process in which the connection weights are adjusted so that NN produces target output in response to the input pattern from the training data set (Hertz, et al. 1991). A number of methods for training the NNs are available. In this report, a local adaptive learning scheme called RPROP (Resilient Back-propagation) algorithm is used (Riedmiller and Braun 1993).

When the input and output of the NN consist of stresses and strains, it can be trained to learn the material behavior, as first demonstrated by Ghaboussi et al. (Ghaboussi, et al. 1991; Ghaboussi and Sidarta 1997). A numerical implementation of the trained NN material model was suggested by Hashaah et al. (Hashash, et al. 2004). The performance of the trained NN material model depends on the quality and quantity of the information on the material behavior in the training data. The most common form of the NN material model uses strains as inputs and stresses as outputs. However, the current state of strains is not sufficient to determine the state of stresses in most materials due the path dependence. In order to train the NN material models to learn the path dependence, several past states of stresses and strains are included as the inputs to the NN.

A new version of standard multi-layered feed forward NNs was proposed by Ghaboussi et al. (Ghaboussi, et al. 1997) and used in of modeling material behavior (Ghaboussi and Sidarta 1998b; Ghaboussi, et al. 1991; Zhang 1996; Lefik and Schrefler 2003). As shown in Figure 3.1, several independent NN modules are nested. The first module of the NN, called the base module, is created first. Other modules, called history modules in material modeling, are added in hierarchical sequences. Each NN module is fully connected within itself and it constitutes a complete regular NN. The “nested”

feature refers to the way that the modules are connected. Each new module has only one way connections to the existing modules.

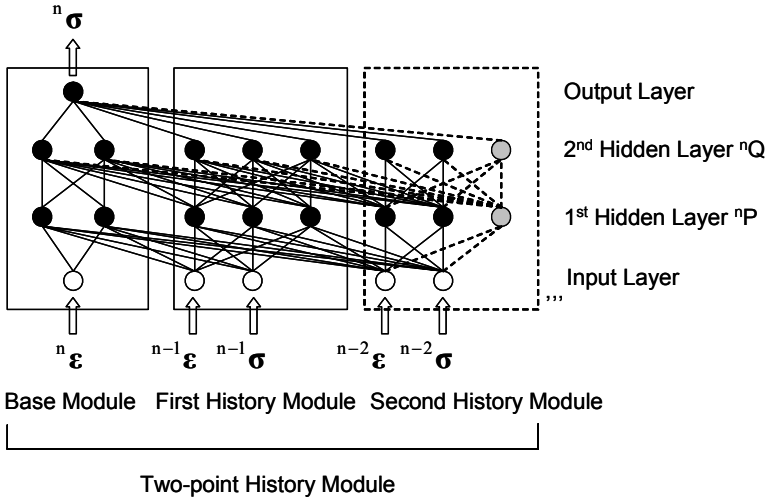

Figure 3.1 Example of Nested Adaptive Neural Network for Material Model

The adaptive method allows the neurons in hidden layers to be automatically added to hidden layers during the training of the NN. Initially, the training of the NN is started with a small number of hidden neurons. The learning rate is monitored during the training and if the capacity of the current network is reached, new neurons are added to hidden layers. Immediate training after the addition of new neurons is limited to new connections only while the old connections are kept frozen. In this way, the new connections are adapted to learn the portion of the knowledge that has not been learned by the previous network.

In order to model the inelastic hysteretic behavior of materials by NNs, there have been two approaches. In the case of the first approach, current state of the material depends on the current and past histories of observable variables only (total stress/strain,

incremental stress/strain, etc.) (Ghaboussi and Sidarta 1998b; Ghaboussi, et al. 1991; Zhang 1996; Lefik and Schrefler 2003). In the second approach, the current state of the material depends on the current and/or the past histories of observable variables and a set of internal state variables (back stress and drag stress, etc.) (Furukawa and Yagawa 1998; Furukawa and Hoffman 2004). In the early application of the NN to a material constitutive modeling (Ghaboussi, et al. 1991; Zhang 1996), the first approach were mainly used. Recently, Furukawa, et al. proposed an accurate cyclic plasticity model using a NN material model (Furukawa and Hoffman 2004). In 1998, Furukawa, et al. also suggested an implicit constitutive modeling for visco-plasticity using NNs following the second approach (Furukawa and Yagawa 1998). They demonstrated a good learning capability of the NN based model if a variety of training data with different conditions are used.

In this report, inspired by the inner product-based NN model of piezoceramic actuators (Xuanju and Yonghong 2005), a novel NN based cyclic material model with an implicit evolutional representation of new internal variables has been developed in order to represent the complex inelastic hysteretic models of materials and structural components. There have been systematic developments in the field of electromagnetic hysteresis (Xuanju and Yonghong 2005; Cincotti, et al. 1998; Mayergoyz 1991; Tong, et al. 2005). Among them, Xuanju and Yonghong (Xuanju and Yonghong 2005) proposed a new input value in order to transform a multi-valued mapping to a single-valued mapping in hysteresis for the application to piezoceramic actuators. However, the mathematical proof on the single-valuedness shows a discrepancy in modeling the material behavior. Moreover, stresses and strains (or forces and displacements) in mechanics are in the form

of tensor or vector rather than scalar values. Therefore, in this chapter, further investigations on its applicability to hysteretic behaviors of materials and structural components are conducted. It is noteworthy that the hysteretic behavior in electromagnetic devices is fundamentally different than the hysteretic behavior of materials that have to obey conservation laws of mechanics. The objective of this chapter is to propose a new NN based model for inelastic hysteretic behavior of materials with new internal variables and validate its performance through a series of examples.

3.3 Neural Network based Inelastic Hysteretic Material Model

There are four modes of hysteresis in one-dimensional stress and strain relationship, as shown in Figure 3.2. However, the mode II only is admissible in the behavior of materials. The other three hysteretic modes either violate the conservation laws of mechanics or stability conditions, or both.

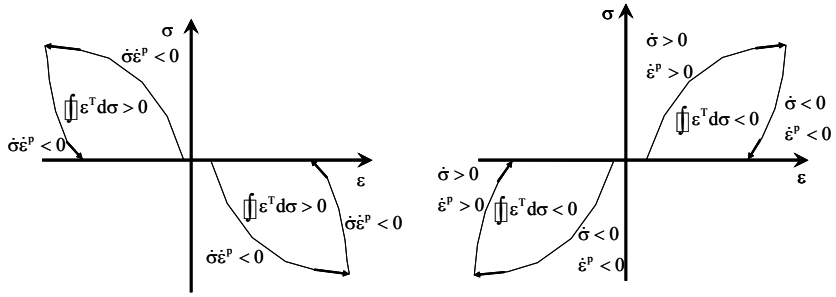

(a) Model I (b) Mode II

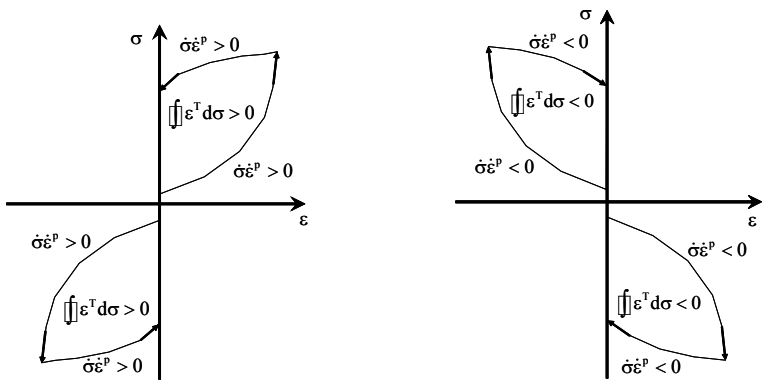

(c) Mode III (d) Mode IV

Figure 3.2 Modes of Hysteretic Behavior of Materials in Uni-axial Cases

It is worth noting that the plastic energy and the complementary strain energy inequalities in multi-dimensional problems are only applicable for the stress and strain tensors, while the individual engagement of components of stress and strain tensors may appear to violate these inequalities and appear to follow the modes I, II, or III. Mode II is the only hysteretic mode admissible for the material behavior in uni-axial or tensor-valued cases. The following is a definition of the admissible hysteresis in mechanics of materials.

Definition: Given $\hat{\sigma}: A \to B$ and $\sigma \in B$ over a closed stress cycle, the level set of $\hat{\sigma}$ with a value σ is written by $I_{\hat{\sigma}}(\sigma) = \{\varepsilon \in A : \hat{\sigma}(\varepsilon) = \sigma\}$. If the number of the level set is not less than 2, that is, $n[I_{\hat{\sigma}}(\sigma)] \geq 2$, the function $\hat{\sigma}$ is said to describe a hysteresis loop. The closed stress cycle satisfies the stability and energy constraints, $d\boldsymbol{\sigma}^T d\boldsymbol{\varepsilon}^e \geq 0$ and $\oint \boldsymbol{\varepsilon}^T d\boldsymbol{\sigma} \leq 0$. The opposite definition is also established by interchanging σ with ε.

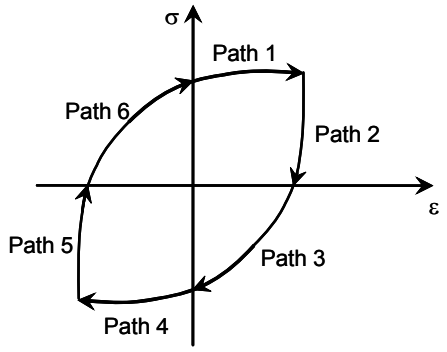

Figure 3.3 Admissible hysteretic curve in mechanics and classification of path

According to the definition of hysteresis, one strain value is corresponding to multiple stresses. The one-to-many mapping can be claimed to be a major cause that prevents NNs from learning hysteretic behaviors. Rigorously speaking, it is not a mathematical functional relationship. The essential idea for a new NN based cyclic material model is to transform the one-to-many mapping to single-valued mapping. In order to accomplish the single-valuedness between input and output of the NN based model for the hysteresis, two internal variables are introduced. The internal variable can be chosen as phenomenological variables as long as they are suitable for explaining the experimental observations. It can be taken as either scalar or tensor values. Since the NNs deal with discrete data in an incremental setting, the internal variables are necessarily in terms of discrete values of stresses and strains. The following internal variables are introduced.

$$\xi_n = \sigma_{n-1}\varepsilon_{n-1} \quad \Delta\eta_{\varepsilon,n} = \sigma_{n-1}\Delta\varepsilon_n \quad \Delta\eta_{\sigma,n} = \varepsilon_{n-1}\Delta\sigma_n \tag{3-1}$$

The subscript n indicates n-th incremental step. The second internal variable is for the strain control form and the third internal variable for the stress control form. These internal variables are illustrated in Figure 3.4.

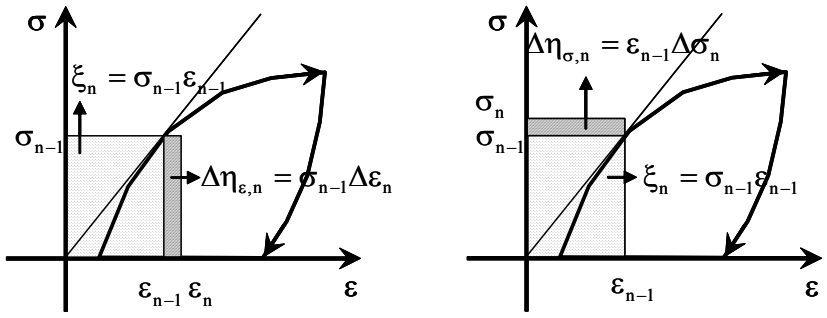

(a) Strain control form (b) Stress control form

Figure 3.4 Internal variables defined for NN based cyclic material model

The internal variable ξ_n implies its previous state along the equilibrium path by its energy quantity. On the other hand, the internal variable $\Delta\eta_{\varepsilon,n}$ or $\Delta\eta_{\sigma,n}$ implies the direction for next time or load step along the equilibrium path. A rigorous proof for the single-valuedness in the case of uni-axial material behavior of mechanical systems is given in the following lemma.

Lemma: For the given uni-axial closed hysteresis in mechanics as defined in Figure 3.3, the following relations are total and one-to-one or many-to-one relations, $f : R^3 \to R$, between domain and codomain.

$$\sigma_n = \left\{\sigma\left(\xi_n, \Delta\eta_{\varepsilon,n}, \varepsilon_n\right) : A_1B_1 \le \xi_n \le A_2B_2, A_1C_1 \le \Delta\eta_{\varepsilon,n} \le A_2C_2, B_1 \le \varepsilon_n \le B_2\right\}$$
$$\varepsilon_n = \left\{\varepsilon\left(\xi_n, \Delta\eta_{\sigma,n}, \sigma_n\right) : A_1B_1 \le \xi_n \le A_2B_2, B_1D_1 \le \Delta\eta_{\sigma,n} \le B_2D_2, A_1 \le \sigma_n \le A_2\right\} \quad \text{(3-2a, b)}$$

where ξ_n, $\Delta\eta_{\varepsilon,n}$ and $\Delta\eta_{\sigma,n}$ are defined in equation (3-1); $A_1 \le \sigma_n \le A_2$, $B_1 \le \varepsilon_n \le B_2$, $C_1 \le \Delta\varepsilon_n \le C_2$ and $D_1 \le \Delta\sigma_n \le D_2$; and n is n-th time step.

Proof:

In order to show that the relations in Equation (3-2a, b) are single-valued functional mappings from domain in R^3 to codomain in R, the closed hysteresis is subdivided into six paths as in Figure 3.3. The signs of the independent variable in the six paths shown in Figure 3.3 are given in tables 1 and 2 for the strain and stress controlled cases. The one-to-one or many-to-one relationship from domain space $(\xi, \Delta\eta_\varepsilon, \varepsilon)$ to codomain space (σ) can be easily inferred from these tables.

Table 3.1 Combinations of signs of input variables for strain control form

	ξ	$\Delta\eta_\varepsilon$	ε		σ
Path 1	+	+	+		+
Path 2	+	–	+		+
Path 3	–	+	+	→	–
Path 4	+	+	–		–
Path 5	+	–	–		–
Path 6	–	+	–		+

Table 3.2 Combinations of signs of input variables for stress control form

	ξ	$\Delta\eta_\sigma$	σ		ε
Path 1	+	+	+		+
Path 2	+	–	+		+
Path 3	–	–	–	→	+
Path 4	+	+	–		–
Path 5	+	–	–		–
Path 6	–	–	+		–

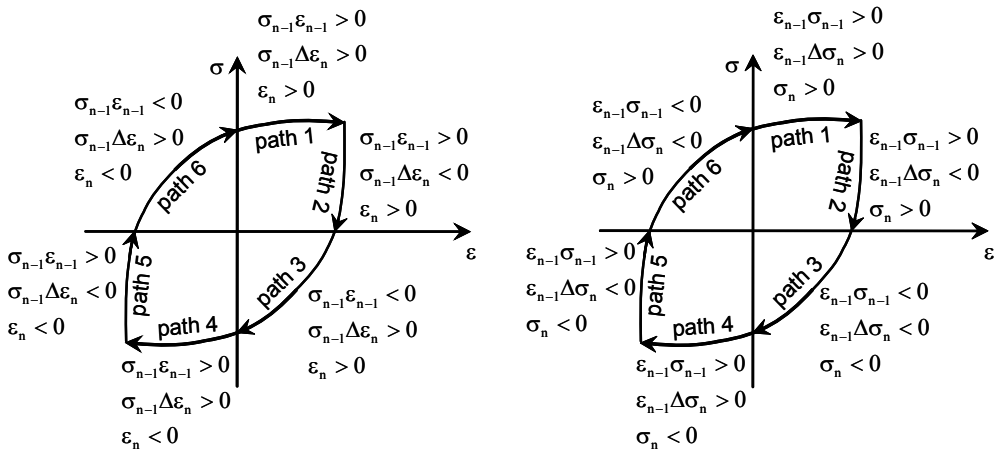

(a) Strain control form (b) Stress control form

Figure 3.5 Classification of domain in strain control form and stress control form

Remarks:

The proof given in this Chapter is acceptable only for uni-axial material behavior. Even though numerical experiments with the internal variables from tensors, that is, $\xi_n = \boldsymbol{\sigma}_{n-1}^{T}\boldsymbol{\varepsilon}_{n-1}$ $\Delta\eta_{\varepsilon,n} = \boldsymbol{\sigma}_{n-1}^{T}\Delta\boldsymbol{\varepsilon}_n$ are shown to be valid, the rigorous proof with tensors still remains unresolved. In this report, the internal variables constructed by tensors are not used.

Therefore, a new implicit stress-strain relation is created with the new internal variables for the uni-axial hysteretic behavior of materials. The single-valued attribute of this implicit relation makes it suitable for the NN constitutive models; expressed in the following equation and illustrated in Figure 3.7.

$$\begin{aligned}\sigma_n &= \hat{\sigma}_{NN}\left(\left\{\varepsilon_n, \varepsilon_{n-1}, \sigma_{n-1}, \xi_{\varepsilon,n}, \Delta\eta_{\varepsilon,n}\right\} : \left\{\text{NN architecture}\right\}\right) \text{ or} \\ \varepsilon_n &= \hat{\varepsilon}_{NN}\left(\left\{\sigma_n, \sigma_{n-1}, \varepsilon_{n-1}, \xi_{\sigma,n}, \Delta\eta_{\sigma,n}\right\} : \left\{\text{NN architecture}\right\}\right)\end{aligned} \qquad \text{(3-3a, b)}$$

In this equation σ = stress; ε = strain and $\hat{\sigma}_{NN}$ and $\hat{\varepsilon}_{NN} : R^5 \rightarrow R$ are functional mappings to be established through NNs. The first equation represents the strain controlled NN and the second equation the stress controlled NN. The two internal variables in each case can be combined in the representation; $\varsigma_{\varepsilon,n} = \xi_n + \Delta\eta_{\varepsilon,n} = \sigma_{n-1}\varepsilon_{n-1} + \sigma_{n-1}\Delta\varepsilon_n$ and $\varsigma_{\sigma,n} = \xi_n + \Delta\eta_{\sigma,n} = \varepsilon_{n-1}\sigma_{n-1} + \varepsilon_{n-1}\Delta\sigma_n$. The information contained in the single internal variable ($\varsigma_{\varepsilon,n}$ or $\varsigma_{\sigma,n}$) or two internal variables appears (ξ_n and $\Delta\eta_{\varepsilon,n}$ or $\Delta\eta_{\sigma,n}$) to be the same based on numerical experiments. According to numerical tests, using the combined single internal variable shows better training performance than using the two internal variables in the case of multi-dimensional problems whereby many inputs are presented to the NN.

When any softening behavior is included in hysteretic curves, the softening path both in the stress and strain control form can lead to one-to-many mapping depending on the hysteretic path. Figure 3.6(a) shows the same sign combination of input values in softening region of the stress control form as the one of path 2. Likewise, in the case of strain control form, the sign combination of path 1 is the same as the softening path. To overcome this possible problem, the stresses and strains from the previous step (σ_{n-1}, ε_{n-1}) are added as part of the input to the NN as shown in Equations (3-3a, b). According to numerical tests, it is also observed that the addition strengthens the representation of the path dependency.

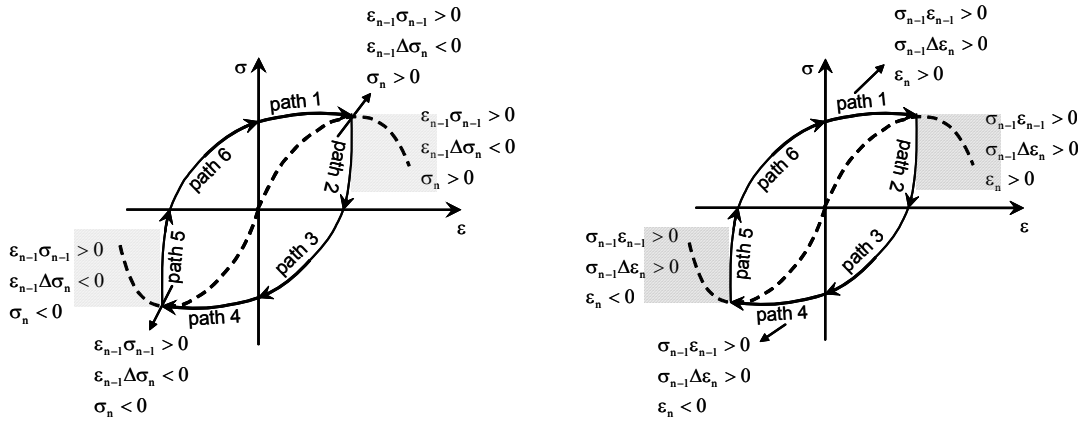

(a) Softening region in stress control form (b) Softening region in strain control form

Figure 3.6 Exception of the single-valued mapping in case of softening region under stress control form

The strain control form in Equation (3.3a) is chosen in this chapter. As was pointed out earlier, this form is more general and is it not limited to work-hardening materials; it can also represent the strain softening hysteretic behavior of materials. Moreover, this form is more suitable finite element applications.

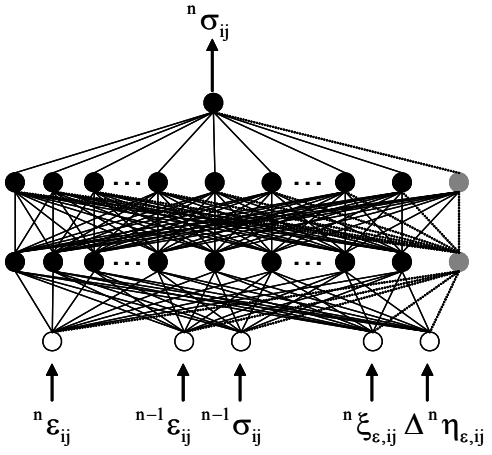

Figure 3.7 Novel NN based cyclic material model; gray-colored neurons and connections indicates adaptively added nodes of NANN

The proposed NN is not limited to representing the hysteretic behavior in terms of stresses and strains. It can also represent the cyclic behavior of samples in terms of force-displacement relations. Both types of data have been used in verifying the proposed model. Data from both physical experiments and simulated experiments are used.

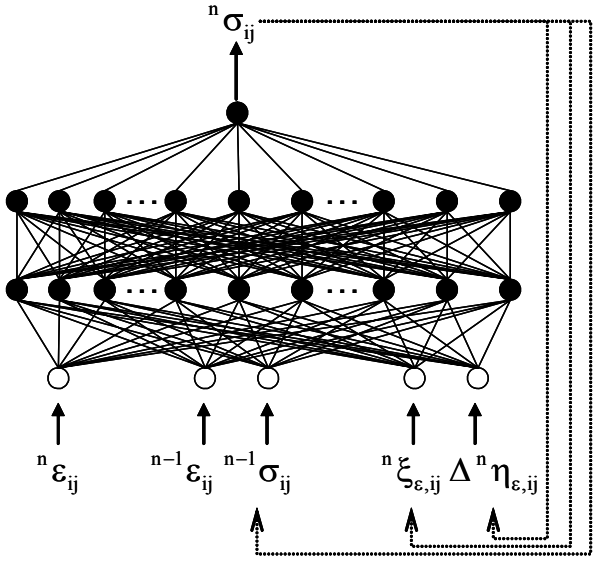

Figure 3.8 Testing of the trained NN material model in recurrent mode

The trained NN models are used in finite element analysis in recurrent mode, illustrated in Figure 3.8; the stresses predicted by the trained NN models are used as input values in the next step. It is important to test the NN in recurrent form since they will be used in that mode. This tests the robustness of the trained NNs in the presence of the inherent stepwise errors. NNs in the examples presented in Chapter have been used in recurrent form.

3.4 Implementation of NN Material Models in Non-linear FE Analysis

In a general nonlinear finite element formulation, the iterative solution schemes such as Newton-Raphson, modified Newton-Raphson, Quasi-Newton and Arc-length methods are frequently used to find convergent response points. In the iterative process, calculation of internal resisting forces in material or element level is the primary source of nonlinearities in the case of material nonlinear problems because the internal resisting forces are mostly dictated by the material constitutive law provided. Therefore, the unbalanced force comes from the difference between external loads and internal resisting forces as in equation (3-4).

$$\mathbf{K}_t \Delta \mathbf{U}_n^{(k)} = \mathbf{P}_n - \mathbf{I}_n^{(k-1)} = \mathbf{P}_n - \sum \int \mathbf{B}^T \boldsymbol{\sigma} dv \tag{3-4}$$

Where $\mathbf{K}_t$ indicates global tangent stiffness matrix; $\mathbf{P}_n$ total external loading vector at n-th load step; $\mathbf{I}_n^{(k-1)}$ internal resisting force vector at (k-1)-th iteration step in n-th load step and $\mathbf{B}$ strain-displacement matrix. The stress $\boldsymbol{\sigma}$ in equation (3-4) is updated at every iterative step. In conventional incremental material constitutive models, an infinitesimal strain increment $d\boldsymbol{\varepsilon}$ is related to infinitesimal stress increment $d\boldsymbol{\sigma}$ through constitutive differential equations. Therefore, in order to calculate material responses, a numerical integration is needed in the form of either explicit or implicit integration scheme. Since the NN based material model directly predicts material responses in terms of stresses as shown in equation (3-5), it is advantageous numerically in that it does not need any numerical integration. As such, after solving the incremental equilibrium equation (3-4), the internal resisting force vector is calculated by passing input strains and internal variables through the NN during the calculation of the material responses as follow:

$$\mathbf{I}_n^{(k-1)} = \sum \int \mathbf{B}^T \hat{\boldsymbol{\sigma}}_{NN}(\{\varepsilon_n^{(k)}, \varepsilon_{n-1}, \sigma_{n-1}, \xi_{\varepsilon,n}, \Delta\eta_{\varepsilon,n}^{(k)}\} : \{\text{NN architecture}\})dv \tag{3-5}$$

In nonlinear finite element analysis, the global tangent stiffness matrix is directly assembled from elemental stiffness matrices as shown in equation (3-6).

$$\mathbf{K}_t = \sum_{i=1}^{nelem} \int_{vi} \mathbf{B}^T \mathbf{D}_{NN}^{ep} \mathbf{B} dv_i \qquad \mathbf{D}_{NN}^{ep} = \begin{pmatrix} D_{NN,11}^{ep} & \cdots & D_{NN,1n}^{ep} \\ \vdots & \ddots & \vdots \\ D_{NN,n1}^{ep} & \cdots & D_{NN,nn}^{ep} \end{pmatrix} \tag{3-6}$$

Particularly, for an elasto-plastic material constitutive model, the elasto-plastic material stiffness matrix should be explicitly defined for use in FE codes. However, since the NN based material models directly predict material responses in terms of stresses or forces in material or element level without explicit material stiffness matrix, there have been difficulties in its numerical implementation into nonlinear finite element codes in which global tangent stiffness matrix needs to be explicitly computed. As alternative approaches, the conjugate gradient method was used with modified Newton-Raphson iterations in which global tangent stiffness matrix is formed by element-by-element computations of element tangent stiffness matrices via NN based material models (Zhang 1996). Otherwise, elements of material stiffness matrix were probed using small increments of stress and strain component (Wu 1991). The material tangent stiffness of a material model in general FE codes is a relationship between the rates of stress and strain as follow.

$$\mathbf{D}^{ep} = \frac{\partial(d\boldsymbol{\sigma})}{\partial(d\boldsymbol{\varepsilon})} \tag{3-7}$$

With a finite strain increment $\Delta\boldsymbol{\varepsilon}$ which is $\Delta\boldsymbol{\varepsilon} >> d\boldsymbol{\varepsilon}$, the material tangent stiffness is not uniquely defined since it can be calculated at any sub-increment of size $d\boldsymbol{\varepsilon}$. Therefore, an algorithmic material tangent stiffness is widely used in numerical implementation of a

wide variety of nonlinear constitutive models (Simo and Taylor 1985). This is a consistent linearization of nonlinear incremental constitutive relations.

$$\mathbf{D}^{ep} = \frac{\partial(^{n+1}\Delta\boldsymbol{\sigma})}{\partial(^{n+1}\Delta\boldsymbol{\varepsilon})}, \text{ where } {}^{n+1}\Delta\boldsymbol{\sigma} = {}^{n+1}\boldsymbol{\sigma} - {}^{n}\boldsymbol{\sigma} \text{ and } {}^{n+1}\Delta\boldsymbol{\varepsilon} = {}^{n+1}\boldsymbol{\varepsilon} - {}^{n}\boldsymbol{\varepsilon} \tag{3-8}$$

Recently, an explicit formulation method of the algorithmic material tangent stiffness for NN based material models was proposed (Hashash, et al. 2004). In this report, the numerical implementation method has been employed to derive the material tangent stiffness matrix for the proposed NN model. The NN based algorithmic (or consistent) tangent stiffness is expressed in terms of activation values from hidden layers, input/output values, connection weights as well as scale factors, as in equation (3-19). Since the new internal variables are expressed in terms of current stress and strain increment, the algorithmic material tangent stiffness for the proposed NN based material model can be derived without difficulties. The algorithmic tangent stiffness in conjunction with incremental nonlinear finite element analysis can be expressed as following.

$$\mathbf{D}^{ep} = \frac{\partial \Delta^{n+1}\sigma_i}{\partial \Delta^{n+1}\varepsilon_j} = \frac{\partial({}^{n+1}\sigma_i - {}^{n}\sigma_i)}{\partial \Delta^{n+1}\varepsilon_j} = \frac{\partial^{n+1}\sigma_i}{\partial \Delta^{n+1}\varepsilon_j} \tag{3-9}$$

Applying chain rules in equation (3-9) gives rise to the following relationship.

$$\frac{\partial^{n+1}\sigma_i}{\partial \Delta^{n+1}\varepsilon_j} = \frac{\partial^{n+1}\sigma_i}{\partial^{n+1}\sigma_i^{NN}} \frac{\partial^{n+1}\sigma_i^{NN}}{\partial \Delta^{n+1}\varepsilon_j} = \frac{\partial^{n+1}\sigma_i}{\partial^{n+1}\sigma_i^{NN}} \frac{\partial^{n+1}\sigma_i^{NN}}{\partial^{n+1}\varepsilon_j^{NN}} \frac{\partial^{n+1}\varepsilon_j^{NN}}{\partial \Delta^{n+1}\varepsilon_j} \tag{3-10}$$

Then each derivative of the right hand side of equation (3-10) can be expressed in terms of parameters of NNs.

$$\frac{\partial^{n+1}\sigma_i}{\partial^{n+1}\sigma_i^{NN}} = S_i^{\sigma} \tag{3-11}$$

$$\frac{\partial^{n+1}\varepsilon_j^{NN}}{\partial\Delta^{n+1}\varepsilon_j}=\frac{1}{S_j^{\varepsilon}}\frac{\partial^{n+1}\varepsilon_j}{\partial\Delta^{n+1}\varepsilon_j}=\frac{1}{S_j^{\varepsilon}}\frac{\partial({}^{n+1}\Delta\varepsilon_j+{}^{n}\varepsilon_j)}{\partial\Delta^{n+1}\varepsilon_j}=\frac{1}{S_j^{\varepsilon}} \tag{3-12}$$

$$\frac{\partial^{n+1}\sigma_i^{NN}}{\partial^{n+1}\varepsilon_j^{NN}}=\sum_{k=1}^{NC}\left\{\frac{\partial^{n+1}\sigma_i^{NN}}{\partial^{n+1}C_k}\left(\sum_{l=1}^{NB}\frac{\partial^{n+1}C_k}{\partial^{n+1}B_l}\frac{\partial^{n+1}B_l}{\partial^{n+1}\varepsilon_j^{NN}}\right)\right\} \tag{3-13}$$

The derivative of the activation function tanh(f(x)) with respect to x is as following.

$$\frac{\partial\tanh\left(f(x)\right)}{\partial x}=\left(1-\left(\tanh(x)\right)^2\right)\frac{\partial f(x)}{\partial x} \tag{3-14}$$

Then the last derivative on the right hand side of the equation (3-13) can be expressed as follows;

$$\frac{\partial^{n+1}B_l}{\partial^{n+1}\varepsilon_j^{NN}}=\left\{1-\left({}^{n+1}B_l\right)^2\right\}\frac{\partial\left\{\beta\left(\sum_{k=1}^{s-m}w_{lk}^{B\varepsilon}\,{}^{n+1}\varepsilon_k^{NN}+\sum_{k=1}^{m}w_{lk}^{BSV}\,{}^{n}SV_k\right)\right\}}{\partial^{n+1}\varepsilon_j^{NN}} \tag{3-15}$$

Since ${}^{n}\mathbf{SV}=\left\{{}^{n}\varepsilon^{NN};{}^{n}\sigma^{NN};{}^{n}\varsigma_{\varepsilon}^{NN}\right\}=\left\{{}^{n}\varepsilon^{NN};{}^{n}\sigma^{NN};{}^{n}\sigma^{NN}\cdot{}^{n+1}\varepsilon^{NN}\right\}$, the right hand side of equation (3-15) can be rewritten as following.

$$\frac{\partial^{n+1}B_l}{\partial^{n+1}\varepsilon_j^{NN}}=\left\{1-\left({}^{n+1}B_l\right)^2\right\}\beta\left(w_{lj}^{B\varepsilon}+w_{lj}^{BSV}\,{}^{n}\sigma_j^{NN}\right) \tag{3-16}$$

Similarly, the other two derivatives of equation (3-13) can be found as follows;

$$\frac{\partial^{n+1}C_k}{\partial^{n+1}B_l}=\left\{1-\left({}^{n+1}C_k\right)^2\right\}\beta w_{kl}^{CB} \tag{3-17}$$

$$\frac{\partial^{n+1}\sigma_i^{NN}}{\partial^{n+1}C_k}=\left\{1-\left({}^{n+1}\sigma_i^{NN}\right)^2\right\}\beta w_{ik}^{\sigma C} \tag{3-18}$$

Then the algorithm tangent stiffness can be found as following.

$$D_{NN,ij}^{ep} = \frac{\partial \Delta^{n+1}\sigma_i}{\partial \Delta^{n+1}\varepsilon_j} =$$

$$\frac{S_i^{\sigma}}{S_j^{\varepsilon}}\beta^3 \sum_{k=1}^{NC}\left[\left(\left\{1-\left({}^{n+1}\sigma_i^{NN}\right)^2\right\}\beta w_{ik}^{\sigma C}\right)\right. \tag{3-19}$$

$$\left.\times\left(\sum_{l=1}^{NB}\left[\left\{1-\left({}^{n+1}C_k\right)^2\right\}\beta w_{kl}^{CB}\right]\left[\left\{1-\left({}^{n+1}B_l\right)^2\right\}\beta\left(w_{lj}^{B\varepsilon}+w_{lj}^{BSV\ n}\sigma_j^{NN}\right)\right]\right)\right]$$

Where $D_{NN,ij}^{ep}$ indicates the algorithmic material tangent stiffness; β steepness parameter (1 or ½); S_i^{σ} and S_i^{ε} Scale factors input and output values, respectively; C_k activation values from the second hidden layer; B_l activation value from the first hidden layer; w_{ij} connection weight between neuron i and neuron j. Compared with the conventional nonlinear finite element analysis procedure with elasto-plastic material, the proposed NN based constitutive formulations do not need either yield surface or plastic potential that are required in numerical integrations within material packages. The NN based model has been implemented into a widely used general-purpose finite element code ABAQUS using its extended capability for user-defined materials.

3.5 Numerical examples

In order to investigate the performance of the proposed model, real physical experimental results as well as simulated cyclic testing results are used in either one-dimensional or multi-dimensional problems. Because of lack of experimental cases from which stress and strain tensor values at sufficient material points under plane stress condition can be obtained, training data are generated from a numerical simulation with a mathematical cyclic plasticity model in the numerical test with a multi-dimensional problem. Using the training data, the proposed model is trained and tested for its performance with FE

analysis. It is worth noting that reproductions of any existing material model through the proposed model are not final objective of this study. As aforementioned in the introduction, the proposed model can be developed from available structural testing results through auto-progressive training methodology (Ghaboussi, et al. 1998a).

3.5.1 Behavior of Plain Concrete under Uni-Axial Cyclic Loading

Experimental data from a cyclic testing on samples of plain concrete by AC2-9 Karsan and Jirsa (Karsan and Jirsa 1969) is employed to train the proposed NN based model. The NN used in training and testing has two hidden layers, each with 20 nodes. Training is performed up to 5000 epochs. Testing is performed in recurrent mode as explained earlier. The NN based model is as following.

$$\sigma_n = \hat{\sigma}_{NN}\left(\left\{\varepsilon_n, \varepsilon_{n-1}, \sigma_{n-1}, \xi_{\varepsilon,n}, \Delta\eta_{\varepsilon,n}\right\} : \left\{5-20-20-1\right\}\right) \tag{3-20}$$

The performance of the proposed model and its comparison with an analytical model is illustrated in Figure 3.9. The phenomenological material model by Palermo et al. (Palermo and Vecchio 2003) is also shown in the figure. The trained NN is able to reasonably represent the normalized stress-strain behavior. This trained NN is used to model a different experimental data by Sinha et al. (Sinha, et al. 1964) in order to explore its generalization capability.

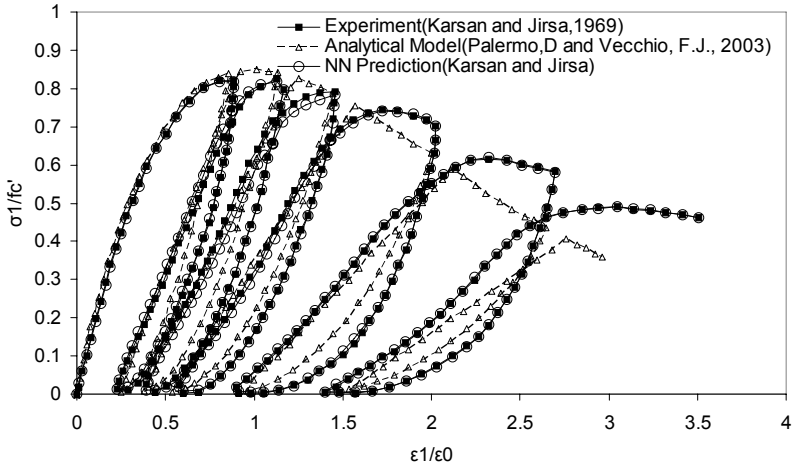

Figure 3.9 Results of training the proposed models and its comparison with an analytical model

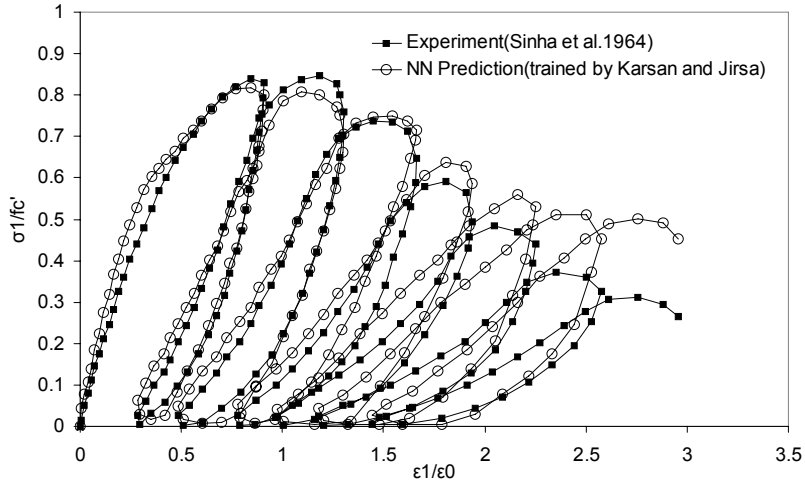

Figure 3.10 Trained NN tested on different test data

As shown in Figure 3.10, the trained NN material model can reasonably predict the cyclic behavior of a novel set of testing data. Particularly, it is worth noting that the generalization of the proposed model can be achieved using comprehensive training data and functional approximation capability of the NN.

3.5.2 Modeling of Cyclic Behavior of Beam-Column Connections

The purpose of this example is to verify the performance of the NN based cyclic material model in reproducing the cyclic behavior of beam-column connections from testing. As the experiment cases, three full-size beam-column connection tests conducted under the SAC testing program of Phase I are chosen (SAC 1995a; SAC 1995b; SAC 1999). The first connection was tested in 1995. It was a repaired one that consists of standard beam (W30x99), column (W13x176), beam haunch and stiffeners as shown in Figure 3.11. During the test, the connection experienced severe local buckling and yielding of beam flange outside haunch and replacement flange. The second connection was tested in 1995 and it experienced beam top and bottom flange buckling, panel zone yielding and column bending and twisting and terminated with severe lateral torsional buckling at the face of haunch. The test of the third connection (bolted flange plate connection) was carried out in 1999. The key observations of the test were local flange and web buckling, ductile flange tearing, significant local buckling in compression flange and brittle fracture of the flange.

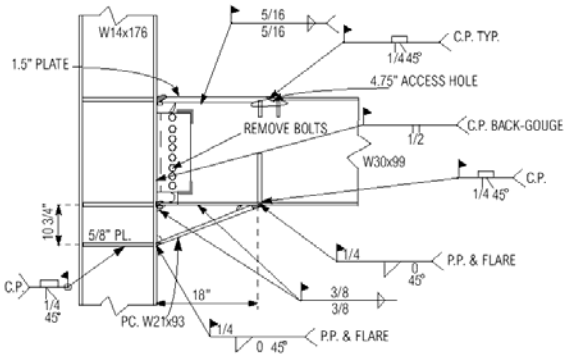

(a) Connection Details (UCSD-3R)

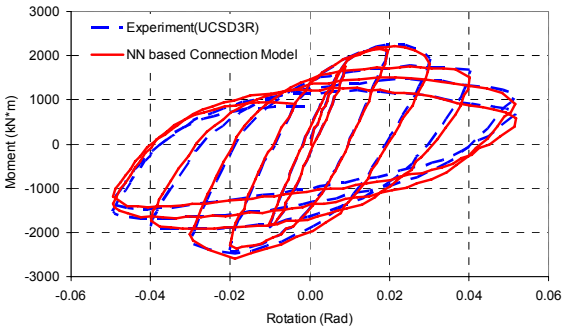

(b) Moment-Rotation Hysteretic Curve

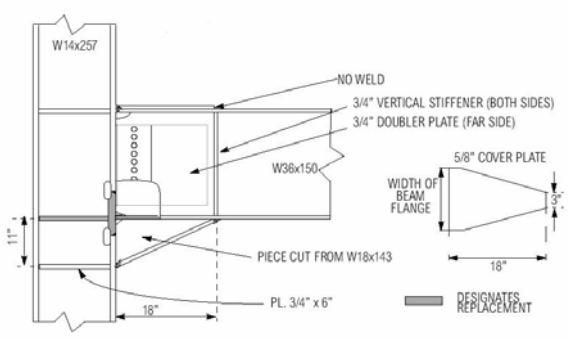

(c) Connection Details (UTA-1RB)

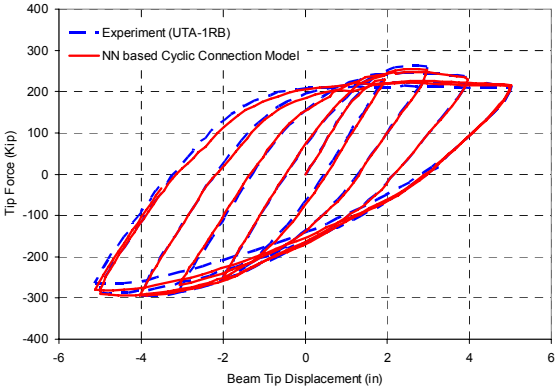

(d) Force-Displacement Hysteretic Curve

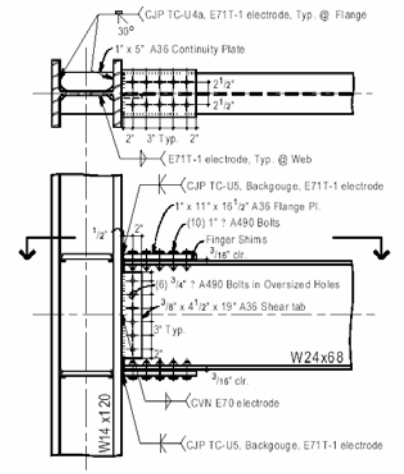

(e) Connection Details (SAC UIUC BFP 02)

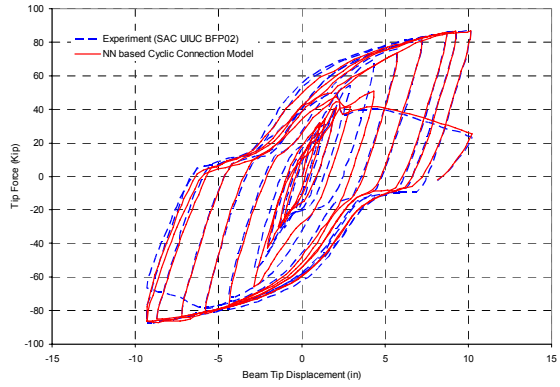

(f) Force-Displacement Hysteretic Curve

Figure 3.11 Comparisons with Experimental Data on Various Beam-Column Connections

The trained NN based cyclic connection model for the first connection is expressed as follow;

$$M_n = \mathbf{M}_{NN}\left(\left\{\theta_n, \theta_{n-1}, M_{n-1}, \xi_{\theta,n}, \Delta\eta_{\theta,n}\right\} : \left\{5-29-29-1\right\}\right) \tag{3-21}$$

The other trained NN based models for the second and third connections can also be expressed as equation (3-21) but with tip force and displacement instead of moment and rotation. The NN architectures used are {5-35-35-1} and {5-45-45-1} for the second and the third, respectively. The number of epochs in training the model was 20,000 for UTA 1RB and SAC UIUC BFP 02.

The series of comparisons in Figure 3.11 demonstrate the performance of the NN based cyclic connection model in reproducing the complex cyclic behavior of connections from experiments. In case of SAC UIUC BFP 02, the model is reproducing the unstable post-limit behavior as well as the pinched hysteresis which are encountered in bolted connection types. In case of UTA-1RB, the hysteretic curve is non-symmetric but the NN based model is shown to be reproducing the behavior well. The slight error is mainly caused by the accumulated error in testing since the testing is carried out in recurrent mode considering its later use in nonlinear finite element code. However, the error is practically negligible. The distinct capability of the NN based cyclic connection model is that it can reproduce experimental observations including destabilizing effects such as buckling and tearing. Furthermore, it can be easily implemented in nonlinear finite element codes.

3.5.3 Cyclic Behavior in Non-Uniform Stress States

Primary objective of this example is to validate the proposed model under a non-uniform stress state. To obtain the non-uniform stress state, a simulated cyclic testing is conducted with an exterior joint of a steel moment-frame building. The steel frame building is a three-story building which was designed as a part of SAC steel project as shown in Figure 3.12 (Gupta and Krawinkler 1999). The dimension of the building, sizes of the members and the material properties are shown in Figure 3.12. For the sake of simplicity, the beam-column connection is assumed to be fully rigid in the whole frame analysis.

The three-story building is modeled with 162 two-dimensional Bernoulli-Euler beam elements. One exterior joint is modeled by 176 two-dimensional plane stress elements. The models are illustrated in Figure 3.13. A commercial finite element code, ABAQUS was used for the numerical simulation. For the material nonlinearity, cyclic plasticity model with Von Mises yield surface and mixed hardening effects are used. The cyclic loading illustrated in Figure 3.14 is applied to the two exterior columns. The displacement histories along the three edges of the two-dimensional continuum model are calculated from the whole frame analysis. In order to apply the displacement boundary conditions to the continuum model, two-dimensional distributing coupling elements are used.

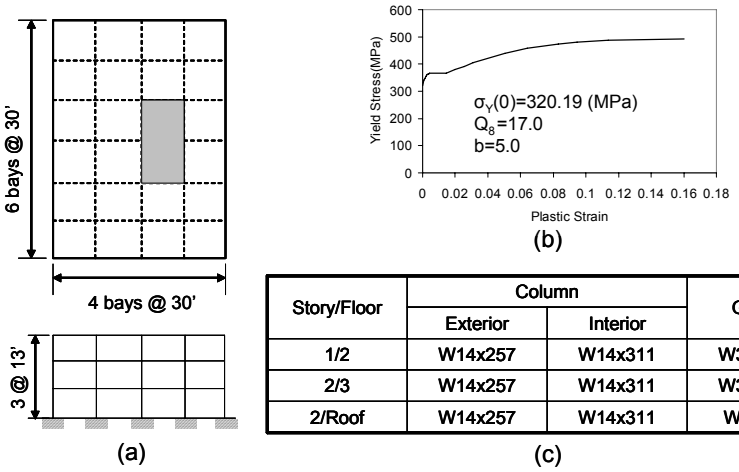

Story/Floor	Column		Girder
	Exterior	Interior	
1/2	W14x257	W14x311	W33x118
2/3	W14x257	W14x311	W30x116
2/Roof	W14x257	W14x311	W24x68

(c)

Figure 3.12 3-story building from SAC steel project; Global model for obtaining boundary displacements of beam-column finite element model

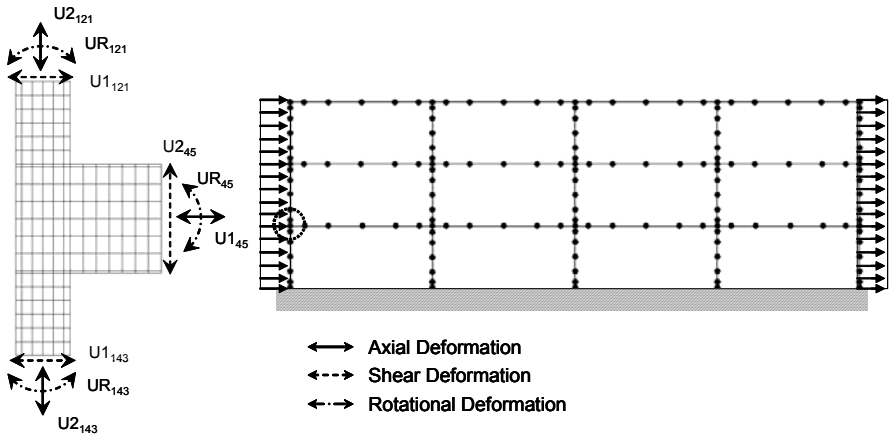

Figure 3.13 Frame Model for Global Analysis and 2D Continuum Model for Exterior Joint

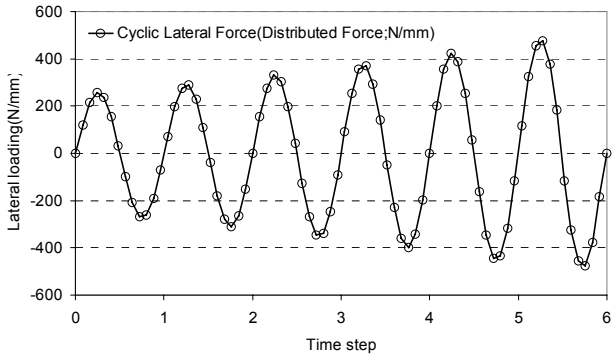

Figure 3.14 Lateral Cyclic Loading

3.5.3.1 Local Validation of the Proposed Model

The training data are extracted from the simulated cyclic testing on two-dimensional solid model. The stress and strain tensors of $\{\sigma_{11}, \sigma_{22}, \sigma_{12}\}$ and $\{\varepsilon_{11}, \varepsilon_{22}, \varepsilon_{12}\}$ at every gauss point of the solid model are extracted to construct input and target patterns for training the proposed model. The NN based model is expressed as follow.

$$\left\{ {}^{n+1}\sigma_{11}; {}^{n+1}\sigma_{22}; {}^{n+1}\sigma_{12} \right\} = \hat{\sigma}_{NN}\left(\left\{ {}^{n+1}\varepsilon_{11}; {}^{n+1}\varepsilon_{22}; {}^{n+1}\varepsilon_{12}; {}^{n}\varepsilon_{11}; {}^{n}\varepsilon_{22}; {}^{n}\varepsilon_{12}; {}^{n}\sigma_{11}; {}^{n}\sigma_{22}; {}^{n}\sigma_{12}; {}^{n+1}\varsigma_{\varepsilon,11}; {}^{n+1}\varsigma_{\varepsilon,22}; {}^{n+1}\varsigma_{\varepsilon,12} \right\} : \{12\text{-}27\text{-}27\text{-}3\} \right) \quad (3\text{-}22)$$

Total number of input pattern is 73,528 and the number of sampling time points are the same as the number of load increments of simulated cyclic testing which is 107 increments. The number of total epochs is 20,000 for training the NN model. The training process is minimization of the average error function expressed as following;

$$E[\mathbf{w}] = \frac{1}{2N_{\mu}} \sum_{\mu=1}^{N_{\mu}} \sum_{i=1}^{N_i} \left(\varsigma_i^{\mu} - O_i^{\mu} \right)^2 \quad (3\text{-}23a, b)$$

where N_μ indicates the total number of input patterns; N_i the number of output nodes; ς the target values; O the neural network prediction and **w** is the connection weight vector.

The average error indicated by a solid line in Figure 3.15 was calculated during the training course. It gradually decreases during the training. It means that the proposed model in equation (3-22) is reliably learning cyclic behaviors of the material under the highly non-uniform stress state. The average errors from testing at the three elements shown in Figure 3.15 are also gradually decreasing.

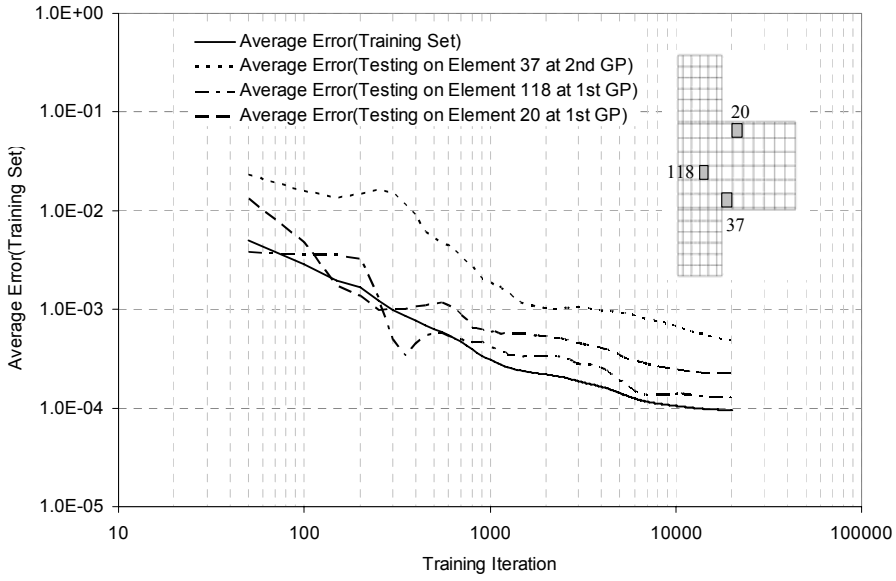

Figure 3.15 Performance evaluation of the training process

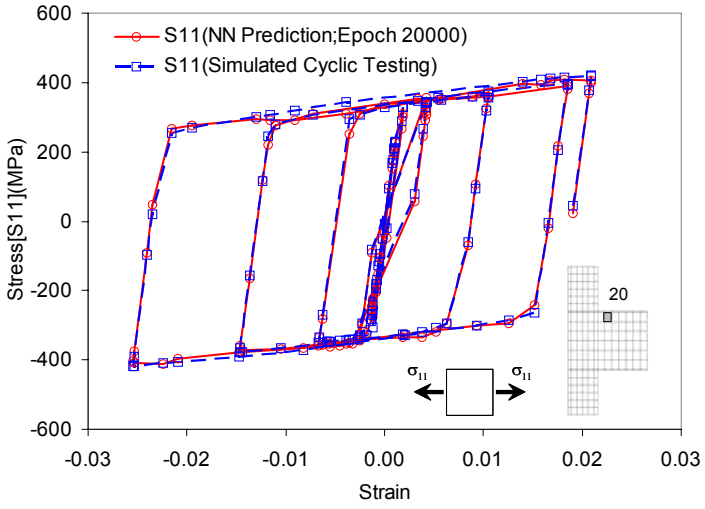

(a) S11 at element 20; integration point 1

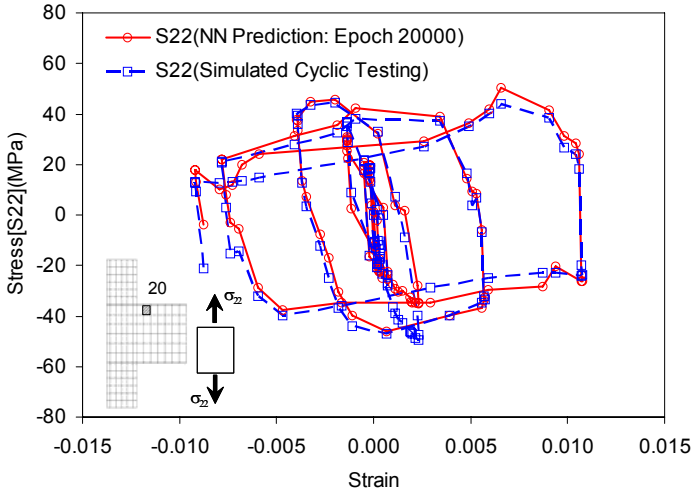

(b) S22 at element 20; integration point 1

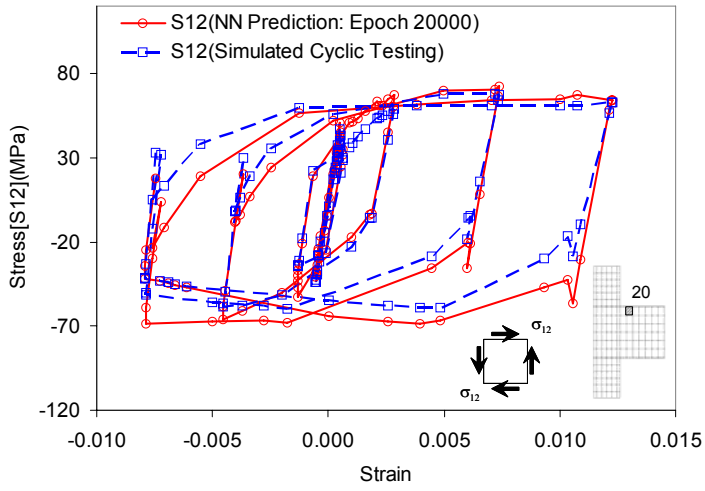

(c) S12 at element 20; integration point 1

Figure 3.16 Local stress hysteretic curves and comparison of the proposed model with the training data

As shown Figure 3.16, comparisons of three stress components for the simulated cyclic testing and the proposed NN model shows that the proposed model can reasonably reproduce cyclic material responses under the non-uniform stress state. Apparently, the proposed model has a learning capability of the local hysteretic behavior of materials by the training. Because the model experiences a large bending action from the beam section, the stress component σ_{11} (S_{11}); the horizontal component in the global coordinate system, is more uniform over the model than the other stress components. The range of the component σ_{11} is -489 (MPa) ~ +497.2 (MPa). On the contrary, the stress component σ_{22} (S22) shows a peculiarity in stress levels at the geometrical discontinuity as shown in Figure 3.21 (a). The range of the stress component σ_{22} (S22) is -398.5 (MPa) ~ +389.2 (MPa) and the range of the shear stress σ_{12} (S12) is -198.6 (MPa) ~ +193.9 (MPa). According to comparisons between the NN predictions and responses from the reference

model at other material points, the stress component σ_{11} (S_{11}) was always most accurate among all the components.

3.5.3.2 Global Validation of the Proposed Model

In this example, the trained NN based cyclic material model is tested as a substitute for a mathematical plasticity model with implementation of user-defined material routine in a commercial finite element code, ABAQUS. The finite element analysis with the trained NN based cyclic material model is called as 'forward analyses. The results from the forward analysis with the proposed model are compared with a mathematical metal cyclic plasticity model by Lemaitre and Chaboche (Lemaitre and Chaboche 1990). Finally, time series of sectional forces on the beam section are compared with the results from the mathematical model to validate the overall performance of the proposed cyclic material model. According to the simulated cyclic testing, large amounts of energy are dissipated under the action of axial forces at the beam section. As shown in Figure 3.17, Figure 3.18 and Figure 3.19, the proposed model is reasonably predicting the global response of the numerical model.

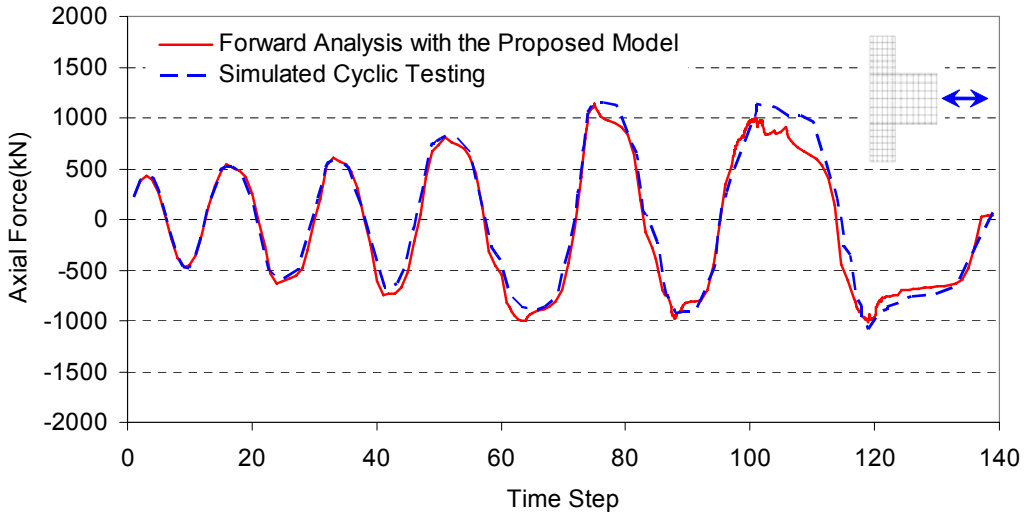

Figure 3.17 Time history of axial force at beam section

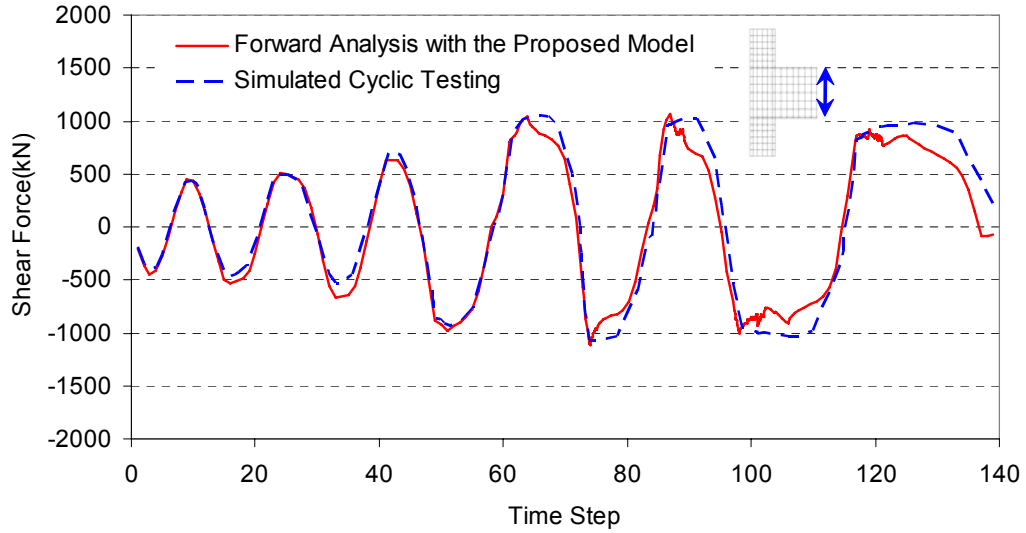

Figure 3.18 Time history of shear force at beam section

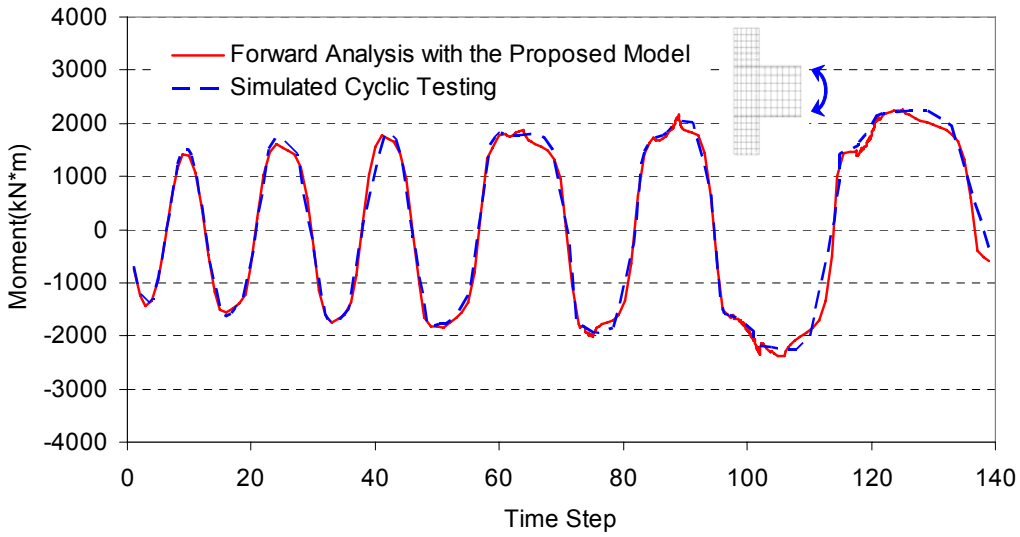

Figure 3.19 Time history of moment at beam section

The discrepancy in the last cycle can be caused by various reasons such as prediction errors of the proposed model in interpolative or extrapolative operations due to use of different incremental size, their accumulation through the loading scenario, approximately converged solution in nonlinear finite element analysis and secondary effects of the errors on coupling between each stress component due to geometric nonlinearity. These comparisons are proving that the proposed model trained in a material level is reproducing the equilibrium path in a structural level of the numerical model under a cyclic loading with acceptable accuracy. It is worth noting the fact that the proposed model can guarantee the reasonable learning capability even in multi-dimensional cases such as a continuum model. As such, the limitations of existing mathematical material models under cyclic loadings in terms of deterministic hardening model and assumption on invariant yield surface shape can be overcome by use of the proposed model.

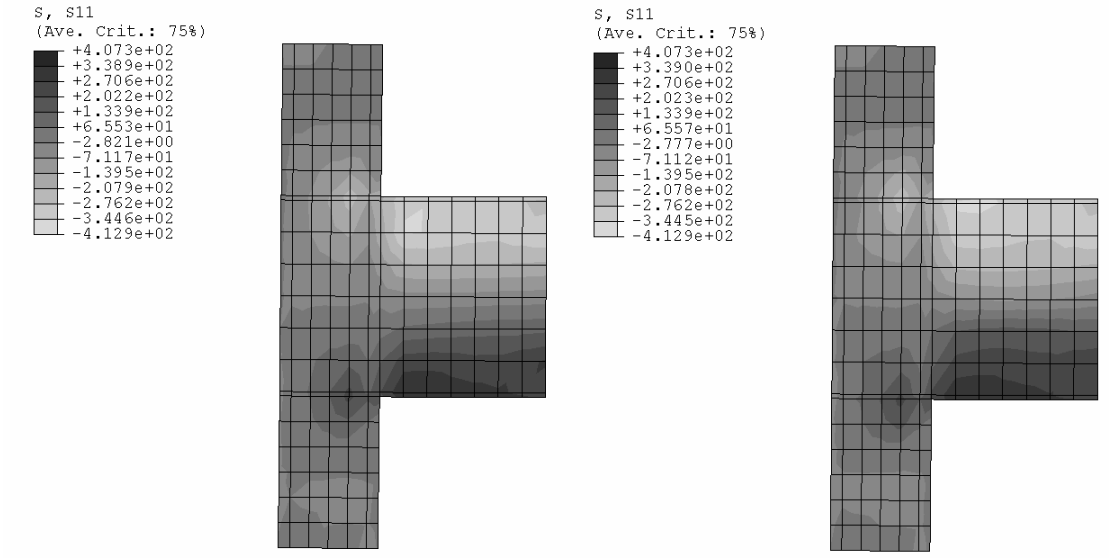

(a) Mathematical cyclic plasticity model (b) NN based cyclic material model

Figure 3.20 Comparison of stress component σ_{11} between cyclic plasticity model and the proposed model at time step 33

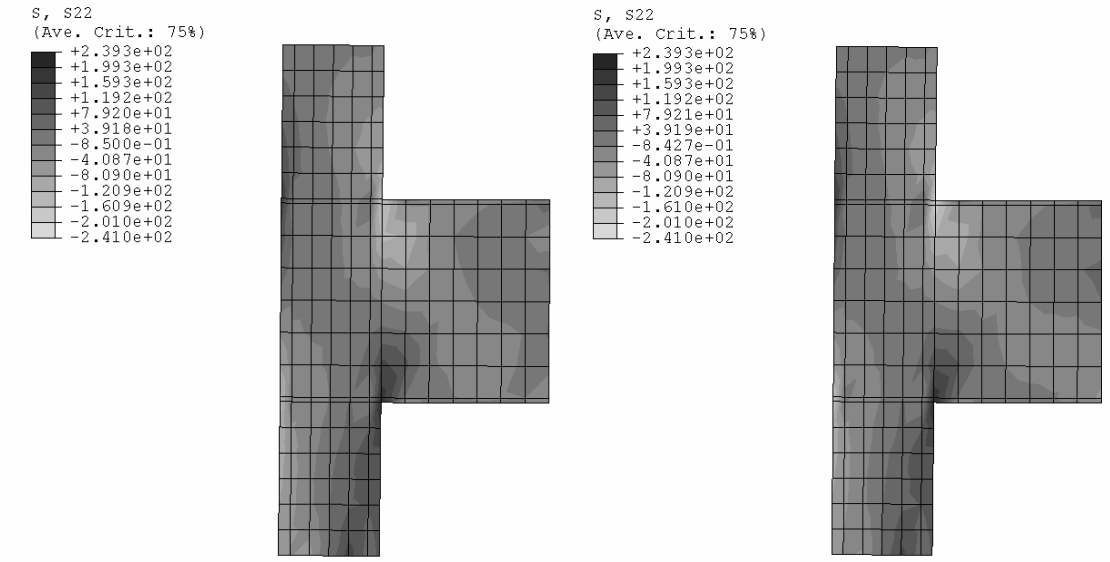

(a) Mathematical cyclic plasticity model (b) NN based cyclic material model

Figure 3.21 Comparison of stress component σ_{22} between cyclic plasticity model and the proposed model at time step 33

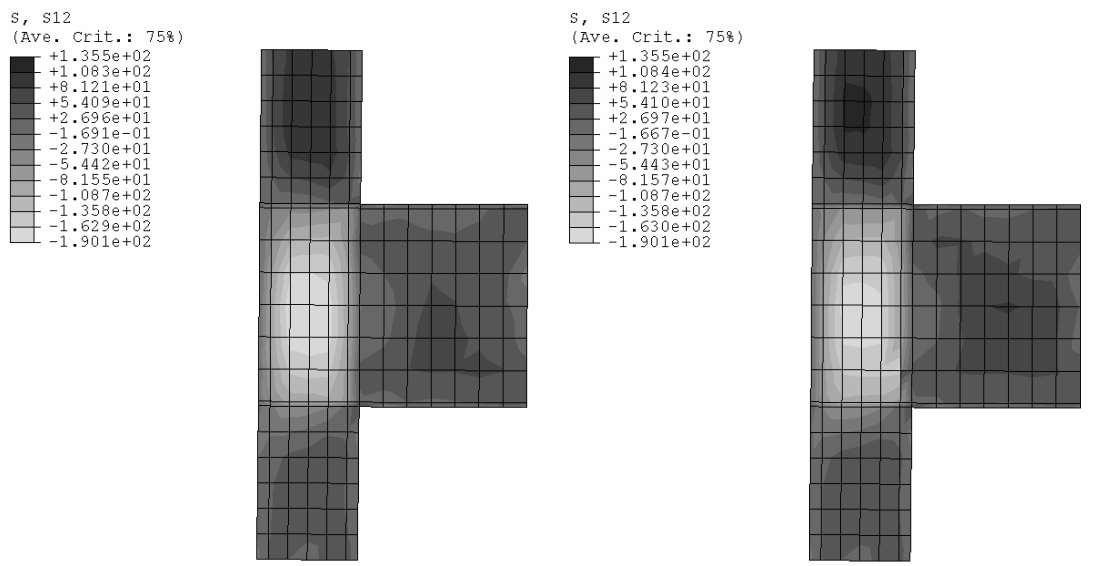

(a) Mathematical cyclic plasticity model (b) NN based cyclic material model

Figure 3.22 Comparison of stress component σ_{12} between cyclic plasticity model and the proposed model at time step 33

From Figure 3.20 through Figure 3.22, a series of contours of stress components; σ_{11} σ_{22} and σ_{12} obtained from the proposed model are illustrated with those from the mathematical model (Lemaitre and Chaboche 1990) at time step 33. The contours show distinctive evidence on the overall performance of the proposed model under cyclic loading.

3.6 Conclusions

In this report, a novel NN based cyclic material model is proposed by introducing new internal variables to learn any hysteretic behavior of materials or structural components under cyclic loadings. The key role of the new internal variables is to provide a necessary

condition for establishing a reasonable functional relationship between input and output values, which is one-to-one or many-to-one mapping.

First, admissible hysteretic curves in mechanics are discussed based on stability and energy constraints. Second, considering the admissible hysteretic curve, a mathematical proof on the establishment of the functional relationship is provided for both stress and strain control form. Third, following the new internal variables for the cyclic material model, a novel NN representation is proposed. The proposed model is the first ever cyclic material model which is based on energy description different from conventional phenomenological hardening-based plasticity model. In order to test the proposed model, the nested adaptive NN is used for the adaptive node creation functionality. For numerical examples, the algorithmic material tangent stiffness matrix is derived for the proposed model and implemented into a user-defined material module in a widely used commercial finite element code, ABAQUS. According to a series of numerical testing, the proposed model shows phenomenal performance in learning any cyclic behavior of uni-axial plain concrete and metal in one dimensional form. Moreover, the extension of the proposed model into multi-dimensional problems is shown to be reasonable through a 2-D beam-column connection problem.

As aforementioned, the conventional mathematical cyclic plasticity models, to a certain extent, include limitations in their deterministic descriptions based on hardening behavior and pitfalls in crude assumption of invariant yield surface shape. Through combining the proposed model with high fidelity of learning capability of NNs, the proposed model is expected to overcome the current limitation of mathematical plasticity

models and open significant applications in many engineering fields such as earthquake engineering.

CHAPTER 4 NONLINEAR FRAME ANALYSIS WITH NEURAL NETWORK BASED INELASTIC HYSTERETIC CONNECTION MODEL

4.1 Introduction

In capacity design concept, beam-hinging mechanism plays a critical role in the seismic performance of steel moment-frame buildings. Therefore, current building codes such as AISC-LRFD code, British Standards and Eurocode 3 require that nonlinear behavior of beam-column connections be characterized in the design process. Since the 1994 Northridge earthquake, many alternatives for seismically resistant connection designs had been researched tremendously. Thus, it resulted in more challenges in modeling the nonlinear behavior of the connections. According to the past experimental observations, there are wide variations in load-carrying capacity with different types of connections.

There are several approaches in incorporating nonlinear behavior of connections with finite element models. One common approach is to use fixity factors or rigidity index in order to modify the conventional stiffness matrices of beam-column element with full fixity at both ends (Ang and Morris 1984; Dhillon and Abdelmajid 1990). In addition to the linear analysis approach, large displacement analysis approach to investigate behaviors of frames with semi-rigid connections was also researched both under static and dynamic loading conditions (Goto and Chen 1987; Chan and Ho 1994). Although only moment-rotation relation is of practical interest, in general, connections are subjected to combined axial forces and moments. Therefore, formal stress-resultant plasticity formulation for beams and columns has been researched in various applications in steel, reinforced concrete and concrete-filled steel tubes since 1970's (Orbison, et al.

1982; Powell and Chen 1986; Takizawa and Aoyama 1976; Hajjar and Gourley 1997; Hajjar, et al. 1997; El-Tawil and Deierlein 1998). Although the stress-resultant plasticity formulation is accurate and computationally efficient, it is not applicable when localized destabilizing effects such as local buckling and tearing of components can be not neglected. Those complex responses are frequently observed in steel beam-column connections. As opposed to the stress-resultant plasticity formulation, there is also stress-space formulation whereby inelastic effects are explicitly modeled by uni-axial stress-strain constitutive relationship and the behavior is monitored at discrete points in cross section (Izzuddin and Elnashai 1989). However, the fiber-based modeling approach has a restriction that plane-sections should remain plane after deformations and combined effect with inelastic shear deformation can not be considered since inelastic effects are represented by only uni-axial deformations of the fiber elements.

In order to overcome the limitations on the stress-resultant plasticity model and the fiber-based analysis, this chapter introduces a fundamentally different model to represent nonlinear connection behavior whereby connection behavior is characterized by neural network (NN) based cyclic material model. This model is developed for earthquake analysis of steel moment-frame buildings with semi-rigid connections. The unique advantage of this model is that not only can it model inelastic cross-section deformations under combined axial forces and moments without following classical plasticity rules but also it can model any post-limit behavior of connections. In this chapter, geometric nonlinear three-dimensional beam-column element with NN based inelastic hysteretic connection models is formulated and its numerical implementation for nonlinear static and dynamic simulation is explained. Following co-rotational Updated Lagrangian

formulation, the reference configuration is updated in every iterative step and the tangent stiffness matrix is formulated as such. To obtain the converged responses along the equilibrium path, the incremental-iterative Newton-Raphson method is used. Instead of using the modified stiffness matrices to consider flexibility of the connections, a generalized constraint equation is applied both to static equilibrium equations and pseudo-static equilibrium equations for dynamic analysis. The generalized constraint equation can deal with both constraint conditions between degrees of freedom of the nodes with the same spatial coordinates and displacement boundary conditions.

In this chapter, following the co-rotational Updated Lagrangian formulation, the element tangent stiffness of the three-dimensional beam-column element is explicitly derived using the principle of virtual work and the stationary potential energy principle. It is followed by NN based inelastic hysteretic connection element proposed in this report. The numerical implementations for nonlinear static and dynamic analysis with the proposed connection element are also introduced. As numerical examples, nonlinear static and dynamic analysis of steel moment-frame buildings with the proposed elements are carried out and the proposed modeling method is verified with experimental data and three-dimensional finite element analysis results.

4.2 Formulation of Geometrically Nonlinear 3D Beam-Column Element

In order to derive a tangent stiffness matrix of the three-dimensional beam-column element, the following assumptions are made. 1) Material shows linear elastic behavior and element has prismatic section along its length. 2) There is no change in the shape of sections. 3) Displacements and rotations are assumed to be large and finite but the strain

is small. 4) Bi-moments of each element are not transformed to other components of moments even if it's transformed from local coordinate system to global coordinate system. 5) Shear deformation is neglected following Euler-Bernoulli beam theory. 6) In-between iterative steps, the relationship between incremental strains and stresses is assumed to be linear.

In the three-dimensional beam-column element, a displacement vector consists of 6 components $\{u_1,u_2,u_3,\omega_1,\omega_2,\omega_3\}$ with a right-handed coordinate system as shown in Figure 4.1. u_1, u_2 and u_3 are translational displacements in x, y and z direction, respectively and ω_1, ω_2 and ω_3 are rotations in x, y and z direction, respectively.

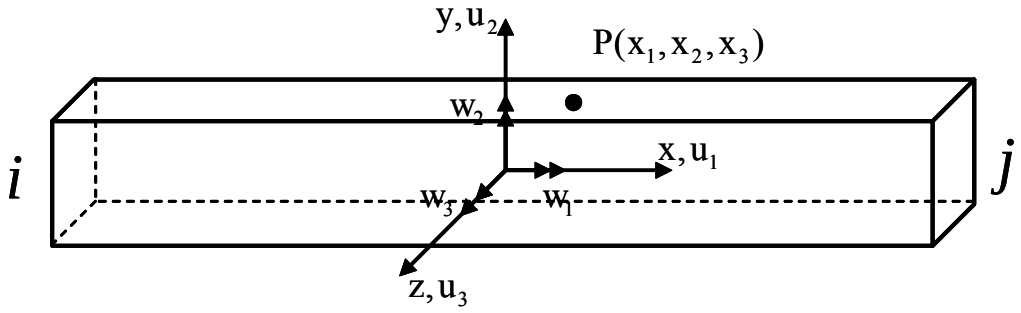

Figure 4.1 Three-Dimensional Beam-Column Element

If any arbitrary point P within a beam is assumed to move by (U_1,U_2,U_3), then the translational movements of the point P can be represented in terms of the six components as follows.

$$\begin{aligned} U_1 &= u_1 + \omega_2 x_3 - \omega_3 x_2 \\ U_2 &= u_2 - \omega_1 x_3 \\ U_3 &= u_3 + \omega_1 x_2 \end{aligned} \tag{4-1}$$

Then Green strain vector is expressed in a tensorial form as follow.

$$\varepsilon_{ij} = \frac{1}{2}\left(U_{i,j} + U_{j,i} + U_{k,i}U_{k,j}\right) \tag{4-2}$$

According to the second assumption, three in-plane strain components ε_{22}, ε_{33} and ε_{23} are assumed to be zero. Then the axial and shear strains are expressed as follows. $(\cdot)_{,1}$ means a derivative with respect to x_1.

$$\begin{aligned}
\varepsilon_{11} &= U_{1,1} + \frac{1}{2}\left[\cancel{\left(U_{1,1}\right)^2} + \left(U_{2,1}\right)^2 + \left(U_{3,1}\right)^2\right] \\
\varepsilon_{12} &= \frac{1}{2}\left(U_{1,2} + U_{2,1}\right) + \frac{1}{2}\left(\cancel{U_{1,1}U_{1,2}} + U_{2,1}U_{2,2} + U_{3,1}U_{3,2}\right) \\
\varepsilon_{13} &= \frac{1}{2}\left(U_{1,3} + U_{3,1}\right) + \frac{1}{2}\left(\cancel{U_{1,1}U_{1,3}} + U_{2,1}U_{2,3} + U_{3,1}U_{3,3}\right)
\end{aligned} \tag{4-3}$$

In equation (4-3), the lined terms are neglected. However, other nonlinear strains are all included in the following formulation. Substituting equation (4-1) into equation (4-3) gives rise to strain components in terms of six displacement components as follows.

$$\begin{aligned}
\varepsilon_{11} &= \left(u_{1,1} + \omega_{2,1}x_3 - \omega_{3,1}x_2\right) + \frac{1}{2}\left[\left(u_{2,1} - \omega_{1,1}x_3\right)^2 + \left(u_{3,1} + \omega_{1,1}x_2\right)^2\right] \\
\varepsilon_{12} &= \frac{1}{2}\left(u_{2,1} - \omega_3 - \omega_{1,1}x_3\right) + \frac{1}{2}\left[\left(u_{3,1} + \omega_{1,1}x_2\right)\omega_1\right] \\
\varepsilon_{13} &= \frac{1}{2}\left(u_{3,1} + \omega_2 + \omega_{1,1}x_2\right) - \frac{1}{2}\left[\left(u_{2,1} - \omega_{1,1}x_3\right)\omega_1\right] \\
\varepsilon_{22} &= \varepsilon_{33} = \varepsilon_{23} = 0
\end{aligned} \tag{4-4}$$

For development of the beam-column element, twelve degrees of freedom are defined as shown in Figure 4.2 and the nodal displacement vector is defined as follow.

$$\mathbf{u} = < u_1^i, u_2^i, u_3^i, \omega_1^i, \omega_2^i, \omega_3^i, u_1^j, u_2^j, u_3^j, \omega_1^j, \omega_2^j, \omega_3^j >^T \tag{4-5}$$

Then the displacement field can be expressed in terms of the nodal displacements and shape functions as follows. The axial displacement and other displacement components are separately interpolated. Therefore, the axial displacement is assumed to vary linearly

along the length and other displacement components are interpolated using the third-order shape functions.

$$
\begin{aligned}
u_1 &= N_5 u_1^i + N_6 u_1^j \\
u_2 &= N_1 u_2^i + N_2 \omega_3^i + N_3 u_2^j + N_4 \omega_3^j \\
u_3 &= N_1 u_3^i - N_2 \omega_2^i + N_3 u_3^j - N_4 \omega_2^j \\
\omega_1 &= N_1 \omega_1^i + N_3 \omega_1^j
\end{aligned}
\tag{4-6}
$$

Following assumptions in the Euler-Bernoulli beam theory, the shear deformation is neglected. Then the relationship, $\omega_3 = u_{2,1}$ and $\omega_2 = - u_{3,1}$, are established. The shape functions used to define the displacement field are expressed as follows. The shape functions are expressed in the natural coordinate system.

$$
\begin{aligned}
&N_1 = \left[1 - 3\beta^2 + 2\beta^3\right] \quad N_2 = L\left[\beta - 2\beta^2 + \beta^3\right] \\
&N_3 = \left[3\beta^2 - 2\beta^3\right] \quad N_4 = L\left[-\beta^2 + \beta^3\right] \\
&N_5 = \frac{1-\xi}{2} \quad N_6 = \frac{1+\xi}{2} \quad \text{where} \quad \beta = \frac{1+\xi}{2}
\end{aligned}
\tag{4-7}
$$

where L indicates the length of the element considered.

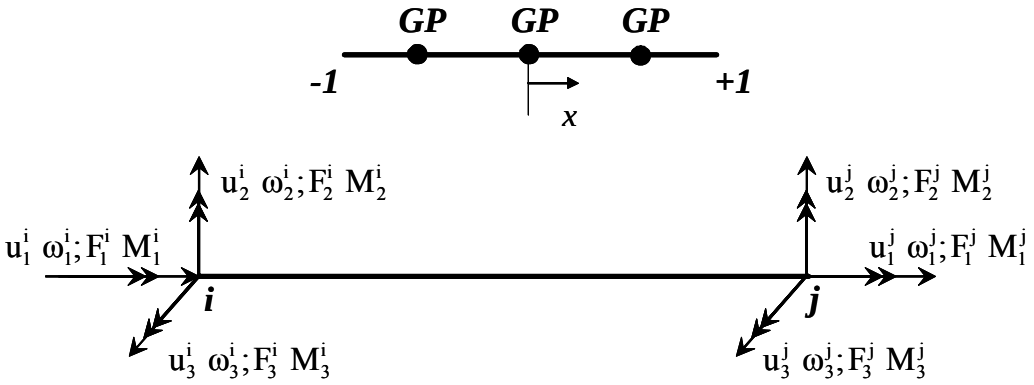

Figure 4.2 Degrees of freedom of Three Dimensional Beam-Column Element

In order to find the strain-displacement matrices, displacement fields in equation (4-6) are substituted into equations (4-4). Then the strain components in equation (4-4) are expressed as follows. The strains are expressed in engineering Green strains instead of tensorial Green strains.

$$\begin{aligned}
\varepsilon_{11} &= \left(\mathbf{B}_{\mathrm{a}}^{l} - \mathrm{x}_2 \mathbf{B}_{\mathrm{b2}}^{l} - \mathrm{x}_3 \mathbf{B}_{\mathrm{b3}}^{l} + \frac{1}{2} \mathbf{B}_{\mathrm{a}}^{nl} \right) \mathbf{u} \\
2\varepsilon_{12} &= \left(-\mathrm{x}_3 \mathbf{B}_{\mathrm{s}}^{l} + \frac{1}{2} \mathbf{B}_{\mathrm{s12}}^{nl} \right) \mathbf{u} \\
2\varepsilon_{13} &= \left(\mathrm{x}_2 \mathbf{B}_{\mathrm{s}}^{l} + \frac{1}{2} \mathbf{B}_{\mathrm{s13}}^{nl} \right) \mathbf{u}
\end{aligned} \tag{4-8}$$

The *l* and *nl* mean linear and nonlinear components, respectively. In equation (4-8), $\mathbf{B}_{\mathrm{a}}^{nl}$ relates the nonlinear portion of the axial strain to the nodal displacement vector. $\mathbf{B}_{\mathrm{s12}}^{nl}$ and $\mathbf{B}_{\mathrm{s13}}^{nl}$ relate the nonlinear portion of the shear strain to the nodal displacement vector. Then the nonlinear strains can be expressed in terms of the strain-displacement matrices in vector form as follows.

$$\boldsymbol{\varepsilon}^{nl} = \begin{Bmatrix} \varepsilon_{11}^{nl} \\ 2\varepsilon_{12}^{nl} \\ 2\varepsilon_{13}^{nl} \end{Bmatrix} = \frac{1}{2} \mathbf{A}\boldsymbol{\Theta} = \frac{1}{2} \mathbf{A}\mathbf{G}\mathbf{u}; \quad \mathbf{A} = \begin{bmatrix} \vartheta_1^{\mathrm{T}} & 0 & 0 \\ \vartheta_2^{\mathrm{T}} & \vartheta_1^{\mathrm{T}} & 0 \\ \vartheta_3^{\mathrm{T}} & 0 & \vartheta_1^{\mathrm{T}} \end{bmatrix} \text{ and } \boldsymbol{\Theta} = \begin{Bmatrix} \vartheta_1 \\ \vartheta_2 \\ \vartheta_3 \end{Bmatrix} = \mathbf{G}\mathbf{u} \tag{4-9}$$

In equation (4-9), $\vartheta_1 = \begin{langle} 0 & \mathrm{U}_{2,1} & \mathrm{U}_{3,1} \end{rangle}^{\mathrm{T}}$, $\vartheta_2 = \begin{langle} 0 & 0 & \mathrm{U}_{3,2} \end{rangle}^{\mathrm{T}}$ and $\vartheta_3 = \begin{langle} 0 & \mathrm{U}_{2,3} & 0 \end{rangle}^{\mathrm{T}}$ are the displacement gradients. **G** matrix consists of the first derivative of shape functions. The G matrix can be explicitly expressed in local coordinate system before transforming to natural coordinate system as follow.

$$\mathbf{G} = \begin{bmatrix} \mathbf{G}_1 \\ \mathbf{G}_2 \\ \mathbf{G}_3 \end{bmatrix}_{9\mathrm{x}12} \tag{4-10}$$

$$\mathbf{G}_1 = \begin{bmatrix} 0 & 0 & 0 & 0 & 0 & 0 \\ 0 & N_1' & 0 & -x_3 N_1' & 0 & N_2' \\ 0 & 0 & N_1' & x_2 N_1' & -N_2' & 0 \\ & & 0 & 0 & 0 & 0 & 0 & 0 \\ & & 0 & N_3' & 0 & -x_3 N_3' & 0 & N_4' \\ & & 0 & 0 & N_3' & x_2 N_3' & -N_4' & 0 \end{bmatrix} \tag{4-11}$$

$$\mathbf{G}_2 = \begin{bmatrix} 0 & 0 & 0 & 0 & 0 & 0 & 0 & 0 & 0 & 0 & 0 & 0 \\ 0 & 0 & 0 & 0 & 0 & 0 & 0 & 0 & 0 & 0 & 0 & 0 \\ 0 & 0 & 0 & N_1 & 0 & 0 & 0 & 0 & 0 & N_3 & 0 & 0 \end{bmatrix} \tag{4-12}$$

$$\mathbf{G}_3 = \begin{bmatrix} 0 & 0 & 0 & 0 & 0 & 0 & 0 & 0 & 0 & 0 & 0 & 0 \\ 0 & 0 & 0 & -N_1 & 0 & 0 & 0 & 0 & 0 & -N_3 & 0 & 0 \\ 0 & 0 & 0 & 0 & 0 & 0 & 0 & 0 & 0 & 0 & 0 & 0 \end{bmatrix} \tag{4-13}$$

In order to get nonlinear parts of strain-displacement matrices, each component of nonlinear Green strain vector in equation (4-9) can be described as follows. Note that a relationship of $\vartheta_i^T \vartheta_j = \vartheta_j^T \vartheta_i$ (i,j=1,2,3) is satisfied.

$$\begin{aligned} \varepsilon_{11}^{nl} &= \frac{1}{2} \vartheta_1^T \vartheta_1 \\ \dot{\varepsilon}_{11}^{nl} &= \frac{1}{2}\left(\dot{\vartheta}_1^T \vartheta_1 + \vartheta_1^T \dot{\vartheta}_1 \right) = \vartheta_1^T \dot{\vartheta}_1 = \vartheta_1^T \mathbf{G}_1 \dot{\mathbf{u}} = \mathbf{B}_a^{nl} \dot{\mathbf{u}} \end{aligned} \tag{4-14}$$

$$\begin{aligned} \varepsilon_{12}^{nl} &= \frac{1}{2}\left(\vartheta_2^T \vartheta_1 + \vartheta_1^T \vartheta_2 \right) = \frac{1}{2}\left(2\vartheta_2^T \vartheta_1 \right) = \vartheta_1^T \vartheta_2 \\ \dot{\varepsilon}_{12}^{nl} &= \left(\dot{\vartheta}_1^T \vartheta_2 + \vartheta_1^T \dot{\vartheta}_2 \right) = \left(\vartheta_2^T \mathbf{G}_1 + \vartheta_1^T \mathbf{G}_2 \right) \dot{\mathbf{u}} = \mathbf{B}_{s12}^{nl} \dot{\mathbf{u}} \end{aligned} \tag{4-15}$$

$$\begin{aligned} \varepsilon_{13}^{nl} &= \frac{1}{2}\left(\vartheta_3^T \vartheta_1 + \vartheta_1^T \vartheta_3 \right) = \frac{1}{2}\left(2\vartheta_3^T \vartheta_1 \right) = \vartheta_1^T \vartheta_3 \\ \dot{\varepsilon}_{13}^{nl} &= \left(\dot{\vartheta}_1^T \vartheta_3 + \vartheta_1^T \dot{\vartheta}_3 \right) = \left(\vartheta_3^T \mathbf{G}_1 + \vartheta_1^T \mathbf{G}_3 \right) \dot{\mathbf{u}} = \mathbf{B}_{s13}^{nl} \dot{\mathbf{u}} \end{aligned} \tag{4-16}$$

Therefore, the nonlinear strain-displacement vector can be expressed as follow.

$$\mathbf{B}_{\mathrm{a}}^{nl} = \begin{Bmatrix} \mathbf{B}_{\mathrm{a}}^{nl} \\ \mathbf{B}_{\mathrm{s12}}^{nl} \\ \mathbf{B}_{\mathrm{s13}}^{nl} \end{Bmatrix} = \begin{Bmatrix} \vartheta_1^{\mathrm{T}}\mathbf{G}_1 \\ \vartheta_2^{\mathrm{T}}\mathbf{G}_1 + \vartheta_1^{\mathrm{T}}\mathbf{G}_2 \\ \vartheta_3^{\mathrm{T}}\mathbf{G}_1 + \vartheta_1^{\mathrm{T}}\mathbf{G}_3 \end{Bmatrix} \tag{4-17}$$

where $\mathbf{B}_{\mathrm{a}}^{nl}$ is 3x12 matrix. Note that a relationship $\dot{\vartheta}_{\mathrm{i}}^{\mathrm{T}}\vartheta_{\mathrm{j}} = \vartheta_{\mathrm{j}}^{\mathrm{T}}\dot{\vartheta}_{\mathrm{i}}$ is also satisfied. Because **G** is a constant matrix, its material rate is zero. It is worth noting that the nonlinear strain-displacement matrices are functions of the displacement gradient which should be functions of time while the linear strain-displacement matrices are constant which can be calculated once in the initial configuration. Then the relation between the material rate of the Green strain and the material rate of the nodal displacement is used to derive the tangent stiffness matrix in the following section. Taking material derivatives of the strains in equation (4-8), the rate form can be expressed as follows.

$$\begin{aligned} \dot{\varepsilon}_{11} &= \left(\mathbf{B}_{\mathrm{a}}^{l} - \mathrm{x}_2\mathbf{B}_{\mathrm{b2}}^{l} - \mathrm{x}_3\mathbf{B}_{\mathrm{b3}}^{l} + \mathbf{B}_{\mathrm{a}}^{nl}\right)\dot{\mathbf{u}} \\ 2\dot{\varepsilon}_{12} &= \left(-\mathrm{x}_3\mathbf{B}_{\mathrm{s}}^{l} + \mathbf{B}_{\mathrm{s12}}^{nl}\right)\dot{\mathbf{u}} \\ 2\dot{\varepsilon}_{13} &= \left(\mathrm{x}_2\mathbf{B}_{\mathrm{s}}^{l} + \mathbf{B}_{\mathrm{s13}}^{nl}\right)\dot{\mathbf{u}} \end{aligned} \tag{4-18}$$

Then the incremental form of Green strain-displacement relation can be determined by multiplying both side of equation (4-18) by a small time increment Δt. By taking a variation of Green strain and displacement vector, the variational form can also be obtained as follow.

$$\Delta\boldsymbol{\varepsilon} = \left(\mathbf{B}^{l} + \mathbf{B}^{nl}\right)\Delta\mathbf{u} \quad \text{and} \quad \delta\boldsymbol{\varepsilon} = \left(\mathbf{B}^{l} + \mathbf{B}^{nl}\right)\delta\mathbf{u} \tag{4-19}$$

Then $\mathbf{B}^{l}$ can be expressed in local coordinate system as follow. In Lagrangian formulation, it is not affected by the deformation or motion of the element.

$$\mathbf{B}^{l}=\left[\begin{array}{cccccc|c} N_5^{'} & -x_2N_1^{''} & -x_3N_1^{''} & 0 & x_3N_2^{''} & -x_2N_2^{''} & \\ 0 & 0 & 0 & -x_3N_1^{'} & 0 & 0 & \\ 0 & 0 & 0 & x_2N_1^{'} & 0 & 0 & \end{array}\right.$$
$$\left.\begin{array}{cccccc} N_6^{'} & -x_2N_3^{''} & -x_3N_3^{''} & 0 & x_3N_4^{''} & -x_2N_4^{''} \\ 0 & 0 & 0 & -x_3N_3^{'} & 0 & 0 \\ 0 & 0 & 0 & x_2N_3^{'} & 0 & 0 \end{array}\right] \tag{4-20}$$

Where (·)' and (·)" indicate a first and second derivative with respect to x_1. Unlikely, $\mathbf{B}^{nl}$ is a linear function of the element nodal displacement.

4.2.1 Co-rotational Updated Lagrangian Finite Element Formulation

In the Updated Lagrangian formulation, three configuration systems are defined as illustrated in Figure 4.3; 1) the initial configuration is C_0, 2) the reference configuration C_1 and 3) the current configuration C_2. In the incremental Updated Lagrangian formulation, the reference configuration C_1 is continuously updated during iteration. As illustrated in Figure 4.3, a position vector ${}^{2}\overline{\mathbf{x}}$ in the current configuration C_2 can be updated by ${}^{2}\overline{\mathbf{x}} = {}^{1}\overline{\mathbf{x}} + {}^{12}\mathbf{u}$ and the total displacement ${}^{2}\mathbf{u}$ referred to the initial configuration C_0 is updated by ${}^{2}\mathbf{u} = {}^{1}\mathbf{u} + {}^{12}\mathbf{u}$. The two superscripts on the left-side of a vector indicate the configuration at the beginning and the end of the incremental step. The subscript on the left-side of a vector indicates the configuration to which the vector refers. Particularly, in the co-rotational Updated Lagrangian formulation, any rigid body motion from C_1 to C_2 is excluded in order to obtain true values of incremental member forces. Then, the finite element equations are determined from a virtual work expression written at C_2 referring to C_1.

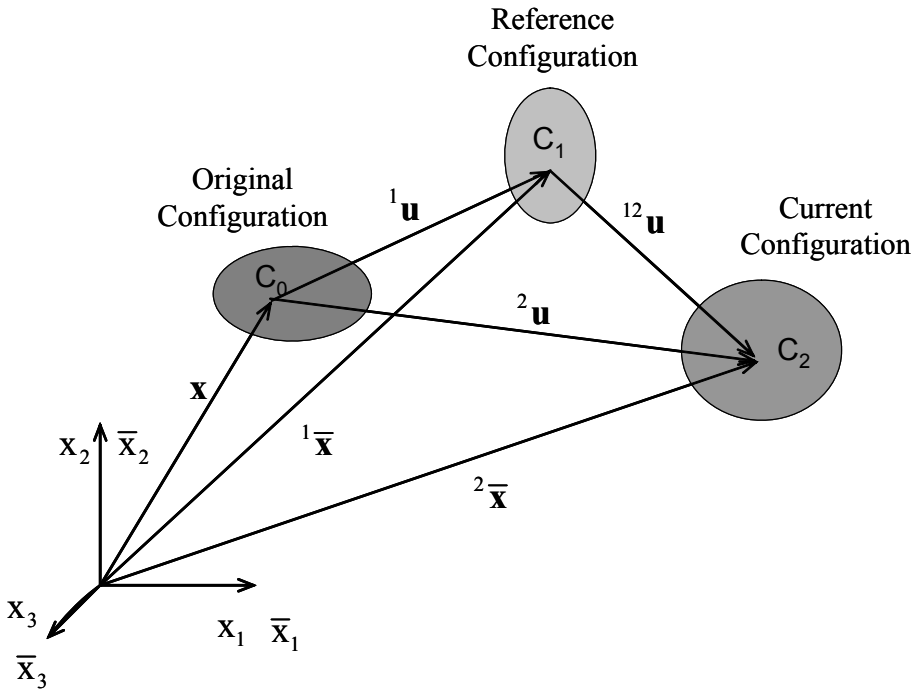

Figure 4.3 Definition of Original, Reference and Current Configuration for Updated Lagrangian Formulation

4.2.2 Tangent Stiffness Matrix Formulation

In order to obtain the geometric tangent stiffness of three dimensional beam-column element, an incremental equilibrium equation should be derived from a virtual work expression. First, a potential energy of a structural system is represented as follow.

$$\Pi_P = \frac{1}{2}\int_V \varepsilon_{ij}\sigma_{ij}dV - \int_V u_i b_i dV - \int_S u_i T_i dS \tag{4-21}$$

where b_i is component of a body force vector; T_i is a component of a traction vector. By taking a variation of the potential energy and applying the stationary potential energy principle, variation of the potential energy should be zero as follow.

$$\delta\Pi_P = \int_V \delta\varepsilon_{ij}\sigma_{ij}dV - \int_V \delta u_i b_i dV - \int_S \delta u_i \left[\overline{T}_i \frac{d\overline{S}}{dS}\right] dS = 0 \tag{4-22}$$

These integrals are all carried out in an initial configuration or in a reference configuration.

$$\begin{aligned}\delta\Pi_p &= \delta\mathbf{u}^T\int_V \mathbf{B}^T\boldsymbol{\sigma}dV - \delta\mathbf{u}^T\int_V \mathbf{N}^T\mathbf{b}dV - \delta\mathbf{u}^T\int_S \mathbf{N}^T\left[\overline{\mathbf{T}}\frac{d\overline{S}}{dS}\right]dS \\ &= \delta\mathbf{u}^T\left(\int_V \mathbf{B}^T\boldsymbol{\sigma}dV - \int_V \mathbf{N}^T\mathbf{b}dV - \int_S \mathbf{N}^T\left[\overline{\mathbf{T}}\frac{d\overline{S}}{dS}\right]dS\right) = 0\end{aligned} \tag{4-23}$$

where $\overline{\mathbf{T}}$ is a surface traction vector in a deformed configuration.; dV and dS are infinitesimal volume and surface in the initial configuration C_0; $\delta\mathbf{u}^T$ a variation of nodal displacement vector; $\mathbf{N}^T$ shape function matrix and $\mathbf{B}^T$ a strain-displacement matrix. For any $\delta\mathbf{u}^T$, the equation (4-23) should be satisfied. Then the equilibrium equation can be written at current configuration C_2 as follow, noting that ${}^2\overline{\mathbf{T}} = {}^2\mathbf{p}\,{}^2\overline{\mathbf{n}}$ (by Cauchy stress principle).

$$\int_V \mathbf{B}^T\,{}^2_0\boldsymbol{\sigma}dV - \int_{\overline{V}} \mathbf{N}^T\,{}^2\mathbf{b}\,d^2\overline{V} - \int_S \mathbf{N}^T\,{}^2\mathbf{p}\,{}^2\overline{\mathbf{n}}\,d^2\overline{S} = 0 \tag{4-24}$$

In the Updated Lagrangian formulation, the finite element formulation is determined from the virtual work expression written at C_2 referring to C_1. Using the relationships $d^2\overline{V} = \left|{}^2_1\mathbf{F}\right| d^1\overline{V}$ and ${}^2\mathbf{p}\,{}^2\underset{\sim}{\overline{\mathbf{n}}}\,d^2\overline{S} = {}^2\mathbf{p}\left|{}^2_1\mathbf{F}\right|{}^2_1\overline{\mathbf{F}}^{T\,1}\underset{\sim}{\overline{\mathbf{n}}}\,d^1\overline{S}$ (the Nansen's formula), the equilibrium equation can be written in the reference configuration C_1 as follow.

$$\int_{{}^1\overline{V}} \mathbf{B}^T\,{}^2_1\boldsymbol{\sigma}\,d^1\overline{V} - \int_{{}^1\overline{V}} \mathbf{N}^T\,{}^2\mathbf{b}\left|{}^2_1\mathbf{F}\right| d^1\overline{V} - \int_{{}^1\overline{S}} \mathbf{N}^T\,{}^2\mathbf{p}\left|{}^2_1\mathbf{F}\right|{}^2_1\overline{\mathbf{F}}^{T\,1}\underset{\sim}{\overline{\mathbf{n}}}\,d^1\overline{S} = 0 \tag{4-25}$$

where ${}^2_1\mathbf{F}$ and ${}^2_1\overline{\mathbf{F}}$ are the Lagrangian and Eulerian deformation gradients, respectively. To obtain the finite element equation, the rate form of equation (4-25) is required. In order to find the tangent stiffness, the first term in equation (4-25) only is considered. Then the first term in equation (4-25) can be expressed as a sum of each component.

$$\int_{{}^1\bar{V}} \mathbf{B}^{T}\,{}^2_1\boldsymbol{\sigma}\, d\,{}^1\bar{V} = \int_{{}^1\bar{V}} \mathbf{B}_a^{T}\,{}^2_1\sigma_{11}\, d\,{}^1\bar{V} + \int_{{}^1\bar{V}} \mathbf{B}_{s12}^{T}\,{}^2_1\tau_{12}\, d\,{}^1\bar{V} + \int_{{}^1\bar{V}} \mathbf{B}_{a13}^{T}\,{}^2_1\tau_{13}\, d\,{}^1\bar{V} \tag{4-26}$$

The strain-displacement matrices can be expressed in terms of matrices in equation (4-18).

$$\begin{aligned}
\mathbf{B}_a &= \mathbf{B}_a^l - x_2\mathbf{B}_{b2}^l - x_3\mathbf{B}_{b3}^l + \mathbf{B}_a^{nl} = \mathbf{B}_{ab}^l + \mathbf{B}_a^{nl} \\
\mathbf{B}_{s12} &= -x_3\mathbf{B}_s^l + \mathbf{B}_{s12}^{nl} = \mathbf{B}_{s12}^l + \mathbf{B}_{s12}^{nl} \\
\mathbf{B}_{s13} &= x_2\mathbf{B}_s^l + \mathbf{B}_{s13}^{nl} = \mathbf{B}_{s13}^l + \mathbf{B}_{s13}^{nl}
\end{aligned} \tag{4-27}$$

Taking the derivative of equation (4-26) with respect to time, the first term in the equation is expressed as follow. In the derivation, the relationship $\left(\dot{\mathbf{B}}_a^{nl}\right)^T = \left(\dot{\vartheta}_1^T\mathbf{G}_1\right)^T = \mathbf{G}_1^T\dot{\vartheta}_1$ should be used.

$$\begin{aligned}
&\int_{{}^1\bar{V}} \mathbf{B}_a^{T}\,{}^2_1\dot{\sigma}_{11}\, d\,{}^1\bar{V} + \int_{{}^1\bar{V}} \dot{\mathbf{B}}_a^{T}\,{}^2_1\sigma_{11}\, d\,{}^1\bar{V} = \\
&\left[\int_{{}^1\bar{I}} (\mathbf{B}_{ab}^l + \mathbf{B}_a^{nl})^T EA(\mathbf{B}_{ab}^l + \mathbf{B}_a^{nl})\, d\,{}^1\bar{x}\right]{}^2\dot{\mathbf{u}} + \int_{{}^1\bar{I}}\int_{{}^1\bar{A}} \mathbf{G}_1^T\dot{\vartheta}_1\,{}^2_1\sigma_{11}\mathbf{I}_3\, d\,{}^1\bar{A}\, d\,{}^1\bar{x} \\
&= \left[\int_{{}^1\bar{I}} (\mathbf{B}_{ab}^l + \mathbf{B}_a^{nl})^T EA(\mathbf{B}_{ab}^l + \mathbf{B}_a^{nl})\, d\,{}^1\bar{x} + \int_{{}^1\bar{I}}\int_{{}^1\bar{A}} \mathbf{G}_1^T\,{}^2_1\sigma_{11}\mathbf{I}_3\mathbf{G}_1\, d\,{}^1\bar{A}\, d\,{}^1\bar{x}\right]{}^2\dot{\mathbf{u}}
\end{aligned} \tag{4-28}$$

where E indicates Young's modulus and A indicates sectional area. $\mathbf{G_1}$ is in equation (4-11). $\mathbf{I}_3$ indicates a 3x3 identity matrix. Similarly, the derivative of the second and the third terms in equation (4-26) can be expressed as follows. In the derivation, the relationship $\left(\dot{\mathbf{B}}_{s12}^{nl}\right)^T = \left(\dot{\vartheta}_2^T\mathbf{G}_1 + \dot{\vartheta}_1^T\mathbf{G}_2\right)^T = \left(\mathbf{G}_1^T\dot{\vartheta}_2 + \mathbf{G}_2^T\dot{\vartheta}_1\right)$ is used for a shear strain energy term with $2\varepsilon_{12}$.

$$
\begin{aligned}
&\int_{{}^1\bar{V}} \mathbf{B}_{a12}^{T}\, {}_1^2\dot{\tau}_{12}\, d{}^1\bar{V} + \int_{{}^1\bar{V}} \dot{\mathbf{B}}_{a12}^{T}\, {}_1^2\tau_{12}\, d{}^1\bar{V} = \\
&\left[\int_{{}^1\bar{I}} (\mathbf{B}_{s12}^{l} + \mathbf{B}_{s12}^{nl})^{T} GA (\mathbf{B}_{s12}^{l} + \mathbf{B}_{s12}^{nl}) d{}^1\bar{x}\right] {}^2\dot{\mathbf{u}} + \int_{{}^1\bar{I}}\int_{{}^1\bar{A}} \left(\mathbf{G}_1^{T}\dot{\vartheta}_2 + \mathbf{G}_2^{T}\dot{\vartheta}_1\right) {}_1^2\tau_{12}\mathbf{I}_3 d{}^1\bar{A} d{}^1\bar{x} = \\
&\left[\int_{{}^1\bar{I}} (\mathbf{B}_{s12}^{l} + \mathbf{B}_{s12}^{nl})^{T} GA (\mathbf{B}_{s12}^{l} + \mathbf{B}_{s12}^{nl}) d{}^1\bar{x} + \int_{{}^1\bar{I}}\int_{{}^1\bar{A}} \mathbf{G}_1^{T}\, {}_1^2\tau_{12}\mathbf{I}_3\mathbf{G}_2 d{}^1\bar{A} d{}^1\bar{x}\right. \\
&\left. + \int_{{}^1\bar{I}}\int_{{}^1\bar{A}} \mathbf{G}_2^{T}\, {}_1^2\tau_{12}\mathbf{I}_3\mathbf{G}_1 d{}^1\bar{A} d{}^1\bar{x}\right] {}^2\dot{\mathbf{u}}
\end{aligned}
\tag{4-29}
$$

Likewise, $\left(\dot{\mathbf{B}}_{s13}^{nl}\right)^{T} = \left(\dot{\vartheta}_3^{T}\mathbf{G}_1 + \dot{\vartheta}_1^{T}\mathbf{G}_3\right)^{T} = \left(\mathbf{G}_1^{T}\dot{\vartheta}_3 + \mathbf{G}_3^{T}\dot{\vartheta}_1\right)$ is used with $2\varepsilon_{13}$.

$$
\begin{aligned}
&\int_{{}^1\bar{V}} \mathbf{B}_{a13}^{T}\, {}_1^2\dot{\tau}_{13}\, d{}^1\bar{V} + \int_{{}^1\bar{V}} \dot{\mathbf{B}}_{a13}^{T}\, {}_1^2\tau_{13}\, d{}^1\bar{V} = \\
&\left[\int_{{}^1\bar{I}} (\mathbf{B}_{s13}^{l} + \mathbf{B}_{s13}^{nl})^{T} GA (\mathbf{B}_{s13}^{l} + \mathbf{B}_{s13}^{nl}) d{}^1\bar{x}\right] {}^2\dot{\mathbf{u}} + \int_{{}^1\bar{I}}\int_{{}^1\bar{A}} \left(\mathbf{G}_1^{T}\dot{\vartheta}_3 + \mathbf{G}_3^{T}\dot{\vartheta}_1\right) {}_1^2\tau_{13}\mathbf{I}_3 d{}^1\bar{A} d{}^1\bar{x} = \\
&\left[\int_{{}^1\bar{I}} (\mathbf{B}_{s13}^{l} + \mathbf{B}_{s13}^{nl})^{T} GA (\mathbf{B}_{s13}^{l} + \mathbf{B}_{s13}^{nl}) d{}^1\bar{x} + \int_{{}^1\bar{I}}\int_{{}^1\bar{A}} \mathbf{G}_1^{T}\, {}_1^2\tau_{13}\mathbf{I}_3\mathbf{G}_3 d{}^1\bar{A} d{}^1\bar{x}\right. \\
&\left. + \int_{{}^1\bar{I}}\int_{{}^1\bar{A}} \mathbf{G}_3^{T}\, {}_1^2\tau_{13}\mathbf{I}_3\mathbf{G}_1 d{}^1\bar{A} d{}^1\bar{x}\right] {}^2\dot{\mathbf{u}}
\end{aligned}
\tag{4-30}
$$

where G indicates shear modulus. Then the tangent stiffness matrix can be assorted as follow.

$$
\begin{aligned}
&\left[\mathbf{K}_t^0 + \mathbf{K}_t^1 + (\mathbf{K}_t^1)^{T} + \mathbf{K}_t^2 + \mathbf{K}_g\right] {}^2\dot{\mathbf{u}} = {}^2\dot{\mathbf{P}} \\
&{}^2\dot{\mathbf{P}} = < {}^2\dot{F}_1^i, {}^2\dot{F}_2^i, {}^2\dot{F}_3^i, {}^2\dot{M}_1^i, {}^2\dot{M}_2^i, {}^2\dot{M}_3^i, {}^2\dot{F}_1^j, {}^2\dot{F}_2^j, {}^2\dot{F}_3^j, {}^2\dot{M}_1^j, {}^2\dot{M}_2^j, {}^2\dot{M}_3^j >^{T}
\end{aligned}
\tag{4-31}
$$

Where ${}^2\dot{\mathbf{P}}$ and ${}^2\dot{\mathbf{u}}$ indicate the rate of the nodal force and displacement vector in the current configuration C_2, respectively. The each component of the tangent stiffness can be found as follow.

$$
\begin{aligned}
\mathbf{K}_t^0 &= \int_{{}^1\bar{l}}\int_{{}^1\bar{A}} \mathbf{B}_{ab}^{l\,\mathrm{T}}\mathrm{E}\mathbf{B}_{ab}^{l}\,\mathrm{d}^1\bar{A}\mathrm{d}^1\bar{x} + \int_{{}^1\bar{l}}\int_{{}^1\bar{A}} \mathbf{B}_{s12}^{l\,\mathrm{T}}\mathrm{G}\mathbf{B}_{s12}^{l}\,\mathrm{d}^1\bar{A}\mathrm{d}^1\bar{x} + \int_{{}^1\bar{l}}\int_{{}^1\bar{A}} \mathbf{B}_{s13}^{l\,\mathrm{T}}\mathrm{G}\mathbf{B}_{s13}^{l}\,\mathrm{d}^1\bar{A}\mathrm{d}^1\bar{x} \\
\mathbf{K}_t^1 &= \int_{{}^1\bar{l}}\int_{{}^1\bar{A}} \mathbf{B}_{ab}^{l\,\mathrm{T}}\mathrm{E}\mathbf{B}_{ab}^{nl}\,\mathrm{d}^1\bar{A}\mathrm{d}^1\bar{x} + \int_{{}^1\bar{l}}\int_{{}^1\bar{A}} \mathbf{B}_{s12}^{l\,\mathrm{T}}\mathrm{G}\mathbf{B}_{s12}^{nl}\,\mathrm{d}^1\bar{A}\mathrm{d}^1\bar{x} + \int_{{}^1\bar{l}}\int_{{}^1\bar{A}} \mathbf{B}_{s13}^{l\,\mathrm{T}}\mathrm{G}\mathbf{B}_{s13}^{nl}\,\mathrm{d}^1\bar{A}\mathrm{d}^1\bar{x} \\
\mathbf{K}_t^2 &= \int_{{}^1\bar{l}}\int_{{}^1\bar{A}} \mathbf{B}_{ab}^{nl\,\mathrm{T}}\mathrm{E}\mathbf{B}_{ab}^{l}\,\mathrm{d}^1\bar{A}\mathrm{d}^1\bar{x} + \int_{{}^1\bar{l}}\int_{{}^1\bar{A}} \mathbf{B}_{s12}^{nl\,\mathrm{T}}\mathrm{G}\mathbf{B}_{s12}^{l}\,\mathrm{d}^1\bar{A}\mathrm{d}^1\bar{x} + \int_{{}^1\bar{l}}\int_{{}^1\bar{A}} \mathbf{B}_{s13}^{nl\,\mathrm{T}}\mathrm{G}\mathbf{B}_{s13}^{l}\,\mathrm{d}^1\bar{A}\mathrm{d}^1\bar{x} \\
\mathbf{K}_g &= \int_{{}^1\bar{l}}\int_{{}^1\bar{A}} \mathbf{G}_1^{\mathrm{T}}\,{}^2_1\sigma_{11}\mathbf{I}_3\mathbf{G}_1\,\mathrm{d}^1\bar{A}\mathrm{d}^1\bar{x} + \int_{{}^1\bar{l}}\int_{{}^1\bar{A}} \mathbf{G}_1^{\mathrm{T}}\,{}^2_1\tau_{12}\mathbf{I}_3\mathbf{G}_2\,\mathrm{d}^1\bar{A}\mathrm{d}^1\bar{x} + \\
&\int_{{}^1\bar{l}}\int_{{}^1\bar{A}} \mathbf{G}_2^{\mathrm{T}}\,{}^2_1\tau_{12}\mathbf{I}_3\mathbf{G}_1\,\mathrm{d}^1\bar{A}\mathrm{d}^1\bar{x} + \int_{{}^1\bar{l}}\int_{{}^1\bar{A}} \mathbf{G}_1^{\mathrm{T}}\,{}^2_1\tau_{13}\mathbf{I}_3\mathbf{G}_3\,\mathrm{d}^1\bar{A}\mathrm{d}^1\bar{x} + \int_{{}^1\bar{l}}\int_{{}^1\bar{A}} \mathbf{G}_3^{\mathrm{T}}\,{}^2_1\tau_{13}\mathbf{I}_3\mathbf{G}_1\,\mathrm{d}^1\bar{A}\mathrm{d}^1\bar{x}
\end{aligned}
\tag{4-32}
$$

In Newton-Raphson iteration, the reference configuration is updated at every step. In such a case, the displacement increment ${}^{12}\mathbf{u}$ becomes zero. Therefore, the $\mathbf{K}_t^1$ and $\mathbf{K}_t^2$ are vanished because they depend on $\mathbf{B}^{nl}$ which is determined from $\partial\,{}^{12}\mathrm{u}_i/\partial\,{}^1\mathrm{x}_j$. Therefore, the incremental equilibrium equation can be expressed as follow.

$$
\left[\mathbf{K}_t^0 + \mathbf{K}_g\right]{}^2\dot{\mathbf{u}} = {}^2\dot{\mathbf{P}} \tag{4-33}
$$

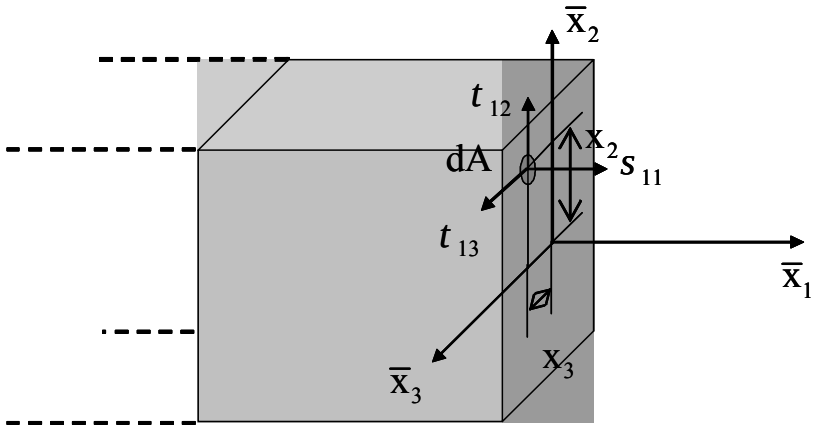

Figure 4.4 Stress Components on a Cross Section of 3D Beam-Column Element

Neglecting in-plane deformations ($\varepsilon_{22} = \varepsilon_{33} = \varepsilon_{23} = 0$), the stress resultants are calculated using stress components shown in Figure 4.4.

$$F_1 = \int_A \sigma_{11} dA \quad F_2 = \int_A \tau_{12} dA \quad F_3 = \int_A \tau_{13} dA$$
$$M_1 = \int_A (x_3 \tau_{12} - x_2 \tau_{13}) dA \quad M_2 = \int_A x_3 \sigma_{11} dA \quad M_3 = -\int_A x_2 \sigma_{11} dA \tag{4-34}$$

In equation (4-34), F_1 indicates axial force and F_2 and F_3 are shear forces in x_2 and x_3 direction, respectively. M_2 and M_3 are bending moments around x_2 and x_3 axis, respectively.

4.2.3 Incremental Internal Resisting Force Vector

In the Updated Lagrangian formulation, the geometry at reference configuration C_1 should be updated at each iteration step. Based on the updated geometry, the increment of the displacement vector from C_1 to C_2 with respect to global coordinate system (x_1, x_2, x_3) should be transformed to the increment with respect to local coordinate (x'_1,x'_2,x'_3) system referring to the reference configuration C_1.

$$\Delta^{12}\mathbf{u}'(x_1', x_2', x_3') = \mathbf{T}\Delta^{12}\mathbf{u}(x_1, x_2, x_3)$$
$$\Delta^{12}\mathbf{u}' = < \Delta^{12}u_{1i}, \Delta^{12}u_{2i}, \Delta^{12}u_{3i}, \Delta^{12}\omega_{1i}, \Delta^{12}\omega_{2i}, \Delta^{12}\omega_{3i}; \tag{4-35}$$
$$\Delta^{12}u_{1j}, \Delta^{12}u_{2j}, \Delta^{12}u_{3j}, \Delta^{12}\omega_{1j}, \Delta^{12}\omega_{2j}, \Delta^{12}\omega_{3j} >^T$$

where **T** indicates a transformation matrix. The three configurations and displacement increments are illustrated in Figure 4.5. In order to calculate the incremental resisting force vector due to the increment of deformations, rigid body motions should be excluded from the increment of the displacement vector. The deformed shapes projected on two planes are illustrated with rigid body rotations in Figure 4.6. Then the pure rotations caused by bending moments can be expressed as follows.

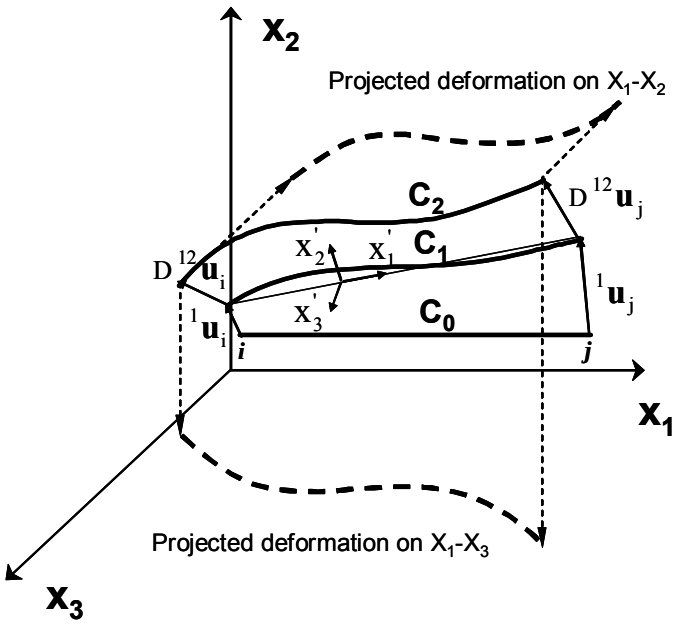

Figure 4.5 Deformation States of 3D Beam-Column Element at Three Different Configurations

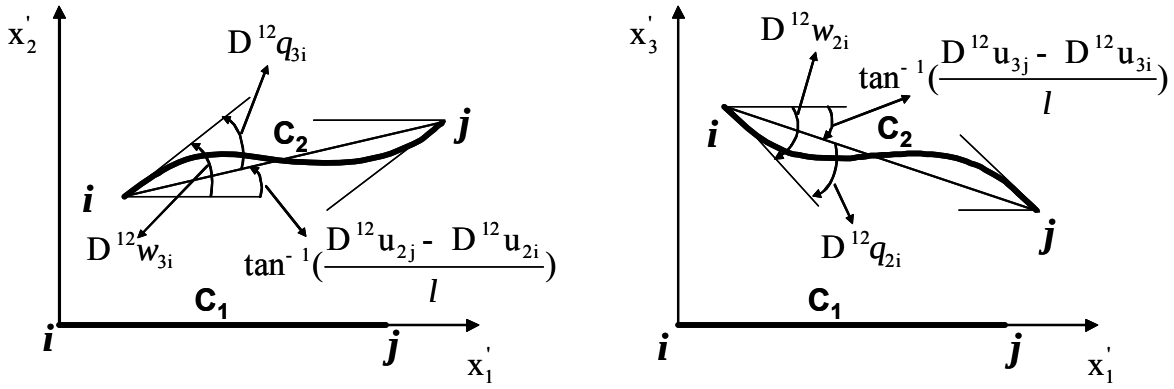

(a) Projected Deformation on x_1-x_2 plane (b) Projected Deformation on x_1-x_3 plane

Figure 4.6 Decomposition of Rigid Body Motion from Incremental Displacement Vector

$$
\begin{aligned}
{}^{12}\Delta q_{3i} &= {}^{12}\Delta w_{3i} - \tan^{-1}\left(\frac{{}^{12}\Delta u_{2j} - {}^{12}\Delta u_{2i}}{l}\right) \\
{}^{12}\Delta q_{3j} &= {}^{12}\Delta w_{3j} - \tan^{-1}\left(\frac{{}^{12}\Delta u_{2j} - {}^{12}\Delta u_{2i}}{l}\right) \\
{}^{12}\Delta q_{2i} &= {}^{12}\Delta w_{2i} + \tan^{-1}\left(\frac{{}^{12}\Delta u_{3j} - {}^{12}\Delta u_{3i}}{l}\right) \\
{}^{12}\Delta q_{2j} &= {}^{12}\Delta w_{2j} + \tan^{-1}\left(\frac{{}^{12}\Delta u_{3j} - {}^{12}\Delta u_{3i}}{l}\right) \\
{}^{12}\Delta f &= {}^{12}\Delta q_{1j} - {}^{12}\Delta q_{1i}
\end{aligned}
\tag{4-36}
$$

These rotations are referred to the reference configuration C_1 as shown in Figure 4.6. Due to the large displacement, there is a coupling effect between axial, bending and torsional deformation called Bowing effect. Specifically, the change in axial length caused by bending and torsional deformations should be considered when the incremental internal resisting force vector is calculated. Therefore, the total axial deformation during an incremental step can be calculated as follow.

$$
\begin{aligned}
\Delta L = &\sqrt{({}^{2}x_{1j} - {}^{2}x_{1i})^2 + ({}^{2}x_{2j} - {}^{2}x_{2i})^2 + ({}^{2}x_{3j} - {}^{2}x_{3i})^2} - \\
&\sqrt{({}^{1}x_{1j} - {}^{1}x_{1i})^2 + ({}^{1}x_{2j} - {}^{1}x_{2i})^2 + ({}^{1}x_{3j} - {}^{1}x_{3i})^2} + d_b
\end{aligned}
\tag{4-37}
$$

Where ${}^{2}x_{ki}(k = 1,2,3)$ indicates coordinate values at i-node of the element in the current configuration C_2; ${}^{1}x_{ki}(k = 1,2,3)$ indicates coordinate values at j-node of the element in the reference configuration C_1. The δ_b indicates the Bowing shortening in axial length which can be calculated from nonlinear terms of Green strain ε_{11} defined in equation (4-3). The section is assumed to be doubly symmetry with respect to two local two directions. The shortening can be expressed in terms of the increments of two bending rotations and torsional displacement as follow.

$$
\begin{aligned}
d_b &= \int_0^l \varepsilon_{11}^{nl} dx = \frac{1}{2}\int_0^l [(u_{2,1})^2 + (u_{3,1})^2] dx_1 + \frac{1}{2A}\int_0^l \int_A [2u_{3,1}\omega_{1,1}x_2 - 2u_{2,1}\omega_{1,1}x_3 \\
&\qquad + (\omega_{1,1})^2(x_2^2 + x_3^2)] dA dx_1 \\
&= \frac{l}{30}(2D^{12}q_{2i}^2 - D^{12}q_{2i}^2 \times D^{12}q_{2j}^2 + 2D^{12}q_{2j}^2) \\
&+ \frac{l}{30}(2D^{12}q_{3i}^2 - D^{12}q_{3i}^2 \times D^{12}q_{3j}^2 + 2D^{12}q_{3j}^2) \\
&+ \frac{(I_{22} + I_{33})}{2A}(D^{12}q_{1j} - D^{12}q_{1i})^2
\end{aligned}
\tag{4-38}
$$

I_{22} and I_{33} are moment of inertia in two local directions of the element. And A indicates sectional area. Multiplying the incremental axial deformation and rotations in equation (4-36) and (4-38) by element tangent stiffness, the incremental internal resisting force can be calculated at the current configuration C_2. The incremental internal resisting force vector is accumulated for the calculation of the residual loading.

4.2.4 Equivalent Load Vector

When any distributed loading is imposed on the three-dimensional beam-column element, the equivalent load vector is calculated from the virtual work expression for the external energy in equation (4-22).

$$
\begin{aligned}
\mathbf{P}_b &= \int_{-l/2}^{+l/2} \mathbf{N}^T \boldsymbol{\rho} A dx_1 = \int_{-1}^{+1} \mathbf{N}^T \boldsymbol{\rho} A |\mathbf{J}| dx = \sum_{k=1}^{3} \mathbf{N}(x_k)^T \boldsymbol{\rho} A |\mathbf{J}| W_k \\
\mathbf{P}_t &= \int_S \mathbf{N}^T \boldsymbol{\Phi} dS = \int_{-l/2}^{+l/2} \mathbf{N}^T \boldsymbol{\Phi} dx_1 = \int_{-1}^{+1} \mathbf{N}^T \boldsymbol{\Phi} |\mathbf{J}| dx = \sum_{k=1}^{3} \mathbf{N}(x_k)^T \boldsymbol{\Phi}(x_k) |\mathbf{J}| W_k
\end{aligned}
\tag{4-39}
$$

$\mathbf{P}_b$ indicates an equivalent load vector from body force and $\mathbf{P}_t$ indicates an equivalent load vector from any surface traction. $\boldsymbol{\rho}$ vector is $<0,-1,0>^T$ when gravity is defined in negative x_2 direction. $\boldsymbol{\Phi}$ is a traction vector $< F_1, F_2, F_3 >^T$ and $|\mathbf{J}|$ is determinant of

Jacobian matrix which is constant $|\mathbf{J}| = dx_1 / dx = l/2$ in this case and W_k is the weight factor for numerical integration. The **N** matrix can be extended as follow.

$$\mathbf{N} = \begin{bmatrix} N_1 & 0 & 0 & 0 & 0 & 0 & N_2 & 0 & 0 & 0 & 0 & 0 \\ 0 & N_1 & 0 & 0 & 0 & N_2 & 0 & N_3 & 0 & 0 & 0 & N_4 \\ 0 & 0 & N_1 & 0 & -N_2 & 0 & 0 & 0 & N_3 & 0 & -N_4 & 0 \end{bmatrix} \tag{4-40}$$

Each interpolation function in equation (4-40) is defined in equation (4-7).

4.3 Formulation of Neural Network based Hysteretic Connection Element

There are two-fold reasons for inclusion of the flexibility of connections into seismic response analysis of building structures. First, the nonlinear behavior of connections has been known to affect significantly the overall response of low to medium-rise moment-resisting frames under dynamic loading. Even though the flexibility of connections can lead to larger lateral drift than rigid connection cases, the hysteretic damping at connections provides superior energy-absorption capacity to rigid connections under earthquake loading and reduces inertia forces owing to its ductile behavior. Second, test results on steel connection in the SAC program indicate a large variability in load-carrying capacity of steel beam-column connections. The observed variability is caused by many effects (Nakashima, et al. 1998), including:

Complex 3D loading scenarios (biaxial and shear, axial loads, torsional effects)

Variations in weld details and quality (number of weld passes, thickness, weld material)

Variations in geometric properties (angle thickness, number of bolts, bolt pretension, etc)

Geometric imperfections, residual stresses due to welding and strain hardening of panel zone, etc

The combined effect of the above features can have significant influence on inelastic rotational capacity, crack initiation and propagation in beam-column connections as well as other semi-rigid connection types of moment resisting frames. In order to better understand the seismic response of moment resisting frame building structures, incorporation of actual response of connection in assessment and design is required. Noting that modeling of the complex behavior of connections such as buckling and tearing, etc is still challenging, an alternative method to model the complex nonlinear behavior of connections is in needs.

There have been two different modeling types in inelastic analysis of steel/RC frame structures: lumped inelasticity and distributed inelasticity approach. The lumped inelasticity model is frequently called as plastic hinge approach. The lumped inelasticity model is efficient computationally because the plastic hinges are usually assumed to be located at the end of beam element and the plastification of cross sections can be readily represented in terms of stress resultants of spring elements. In practical point of view, any moment and force interaction equation can also be directly incorporated into computational simulations. On the other hand, the distributed inelasticity approach is more accurate than the lumped inelasticity model but computational expense is enormous because the inelasticity of the whole volume of structures is checked through modeling in both of longitudinal and transversal directions (called fiber model). Moreover, the distributed inelasticity model is not appropriate for modeling the complex nonlinear behavior of connections since connection details are very much different from any standard section. Therefore, to propose the implicit generalized inelastic hysteretic connection model, the lumped inelasticity approach is adopted in this report. The

generalized inelastic hysteretic connection model is illustrated in Figure 4.8. The model has zero length and can be placed at any position between three-dimensional beam-column elements. The stiffness of connection sub-assemblage can be easily combined with the tangent stiffness of the normal three-dimensional beam-column element. One example of modeling of connections is illustrated in Figure 4.7.

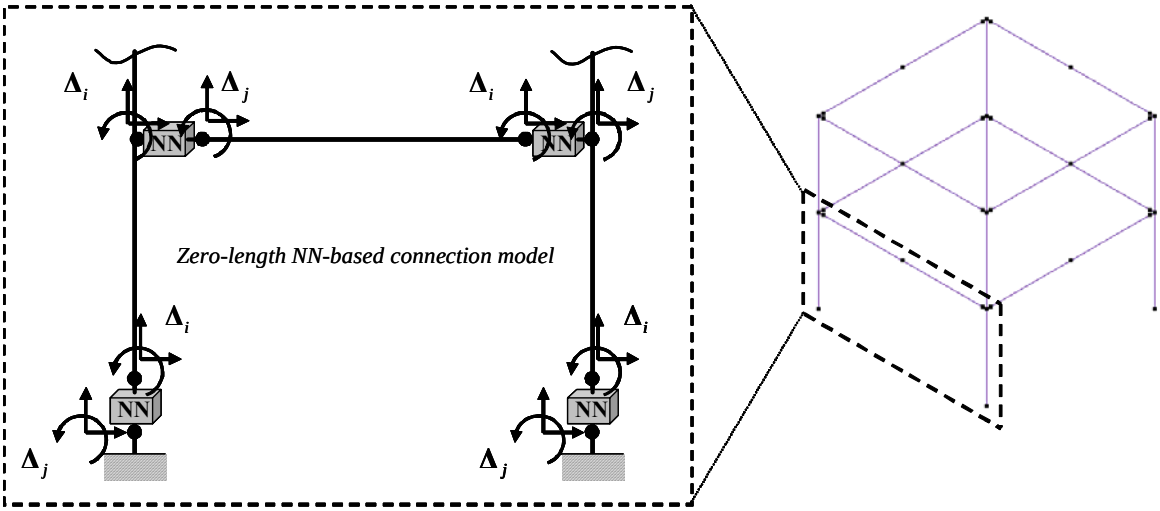

Figure 4.7 Modeling of Connections in Frame Structures

For the sake of simplicity, only the interactions between axial force and biaxial moments are considered in the formulation. However, it is noteworthy that the formulation can be extended to full interactions between all the six stress resultants if the failure mode is associated with all the six stress resultants. In order to make it easy to implement it to any incremental nonlinear finite element codes, an incremental equilibrium equation of the connection is expressed as follow. A tangent stiffness matrix relates the increments of the actions to those of the deformations.

$$\begin{Bmatrix} dF_1 \\ dM_2 \\ dM_3 \end{Bmatrix} = \begin{bmatrix} \frac{\partial F}{\partial \delta} & \frac{\partial F}{\partial \alpha_2} & \frac{\partial F}{\partial \alpha_3} \\ \frac{\partial M_2}{\partial \delta} & \frac{\partial M_2}{\partial \alpha_2} & \frac{\partial M_2}{\partial \alpha_3} \\ \frac{\partial M_3}{\partial \delta} & \frac{\partial M_3}{\partial \alpha_2} & \frac{\partial M_3}{\partial \alpha_3} \end{bmatrix} \begin{Bmatrix} d\delta \\ d\alpha_2 \\ d\alpha_3 \end{Bmatrix} = [\mathbf{D}_{mat}^{NN}] \begin{Bmatrix} d\delta \\ d\alpha_2 \\ d\alpha_3 \end{Bmatrix} \tag{4-41}$$

where $\begin{Bmatrix} d\delta \\ d\alpha_2 \\ d\alpha_3 \end{Bmatrix} = \begin{Bmatrix} du_1^j - du_1^i \\ d\theta_2^j - d\theta_2^i \\ d\theta_3^j - d\theta_3^i \end{Bmatrix}$

The $d\delta$, $d\alpha_2$ and $d\alpha_3$ are increments of axial deformation and rotational displacement around two local axes. $\mathbf{D}_{mat}^{NN}$ indicates an explicit form of the tangent stiffness of connections. This tangent stiffness of connections is expressed in terms of neural network parameters as follows.

$$D_{mat,ij}^{NN} = \frac{\partial \Delta^{n+1} F_i}{\partial \Delta^{n+1} U_j} =$$
$$\frac{S_i^F}{S_j^U} \beta^3 \sum_{k=1}^{NC} \left[\left(\left\{ 1 - \left({}^{n+1}F_i^{NN} \right)^2 \right\} w_{ik}^{FC} \right) \right. \tag{4-42}$$
$$\left. \times \left(\sum_{l=1}^{NB} \left[\left\{ 1 - \left({}^{n+1}C_k \right)^2 \right\} w_{kl}^{CB} \right] \left[\left\{ 1 - \left({}^{n+1}B_l \right)^2 \right\} \left(w_{lj}^{BU} + w_{lj}^{BSV\ n} F_j^{NN} \right) \right] \right) \right]$$

Where β steepness parameter (1 or ½); S_i^{σ} and S_i^{ε} Scale factors input and output values, respectively; C_k activation values from the second hidden layer; B_l activation value from the first hidden layer; w_{ij} connection weight between neuron i and neuron j. The tangent stiffness of connection elements is expanded to the size of the global tangent stiffness using the transformation matrix shown as follow.

$$\begin{Bmatrix} d\delta \\ d\alpha_2 \\ d\alpha_3 \end{Bmatrix} = \begin{bmatrix} 1 & 0 & 0 & 0 & 0 & 0 & -1 & 0 & 0 & 0 & 0 & 0 \\ 0 & 0 & 0 & 1 & 0 & 0 & 0 & 0 & 0 & -1 & 0 & 0 \\ 0 & 0 & 0 & 0 & 1 & 0 & 0 & 0 & 0 & 0 & -1 & 0 \end{bmatrix} \{d\mathbf{u}\} = \mathbf{T}\{d\mathbf{u}\} \tag{4-43}$$

where $\{d\mathbf{u}\} = < du_1^i \; du_2^i \; du_3^i \; d\omega_1^i \; d\omega_2^i \; d\omega_3^i \; du_1^j \; du_2^j \; du_3^j \; d\omega_1^j \; d\omega_2^j \; d\omega_3^j >^T$

where **T** is a transformation matrix. Then the tangent stiffness of connections can be expanded as follow.

$$\mathbf{K}_{ep} = \mathbf{T}^T \mathbf{D}_{mat}^{NN} \mathbf{T} \tag{4-44}$$

Then the connection stiffness is assembled with the global tangent stiffness. Comparing with the existing elasto-plastic analysis method of frame structures, the unique advantage of this formulation is that there is no need to have any yield surface for calculating the plastic reduction matrix. Noting that interaction equations for the complex connection regions are rare, the present formulation approach has an obvious advantage for modeling connection behavior. If comprehensive training data are used in training the proposed model, the model can simulate any complex non-linear behavior of connections within general nonlinear frame analysis program. Moreover, self-learning simulation methodology makes it possible to develop the proposed model for connections from structural testing measurements. The self-learning simulation methodology will be explained in the following Chapter 5.

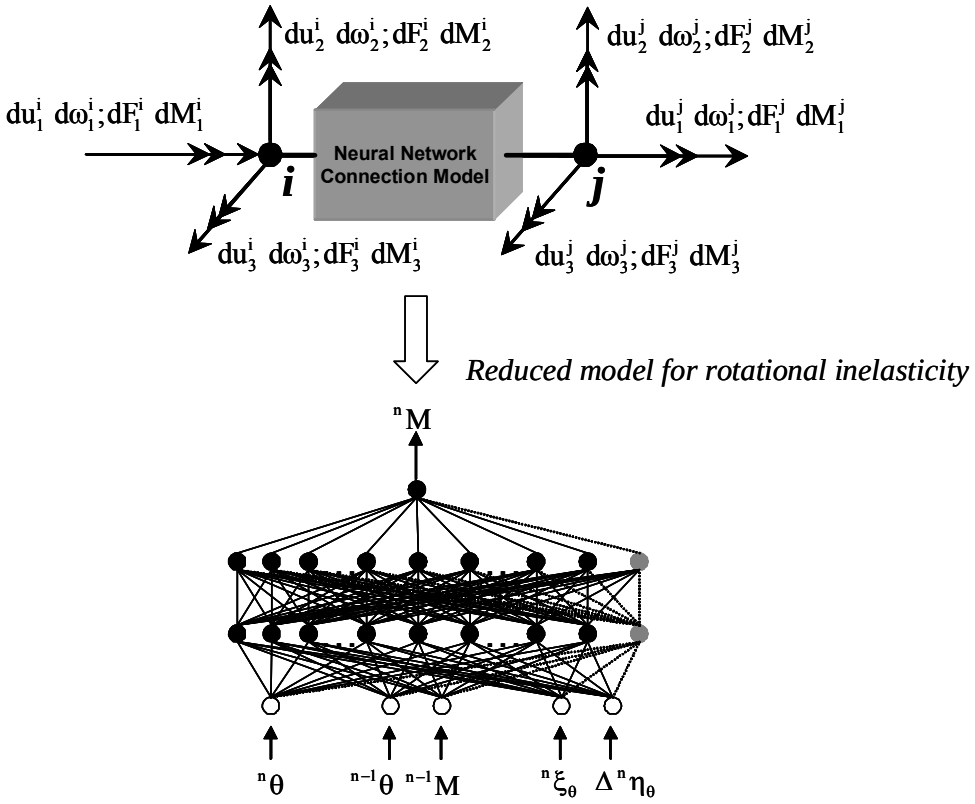

Figure 4.8 Neural Network based Connection Model for Inelastic Analysis of Frame Structures

4.4 Numerical Procedures for Nonlinear Analysis

In this section, detailed numerical procedures for the nonlinear static and dynamic simulations with the proposed formulation in the previous sections are presented. For a stable numerical procedure under random cyclic loadings, incremental-iterative Newton-Raphson method is used for finding convergent response points along the equilibrium path.

4.4.1 Generalized Constraint Equation for Displacement Boundary Conditions

The generalized inelastic hysteretic connection model is placed at any expected plastic hinge location to connect three-dimensional beam-column elements. If a failure mode is governed by the interaction between axial force and bending moment, then degrees of freedom corresponding to shear deformation can be modeled by a linear elastic spring with infinite stiffness or condensed out. Particularly, in a process of the self-learning simulation, displacement measurements should be applied to structures. In this report, a generalized constraint equation is applied to the global stiffness equation before solving the incremental equilibrium equation at each iteration step. If part of degrees of freedom is constrained with others by linear multi-point constraint equations, it can be expressed as follow.

$$G_{i1}\Delta_1 + G_{i2}\Delta_2 + ... + G_{ij}\Delta_j + ... + G_{i1}\Delta_{neq} = H_i \tag{4-45}$$

G_{ij} is the coefficient associated with j-th degrees of freedom in i-th constraint equation. H_i is a constant that characterizes the relationship between the degrees of freedom. The equation (4-45) can be expressed in matrix form as follow.

$$\left[\mathbf{G}_e \mid \mathbf{G}_c\right]\begin{Bmatrix}\boldsymbol{\Delta}_e \\ \boldsymbol{\Delta}_c\end{Bmatrix} = \{\mathbf{H}\} \tag{4-46}$$

$\boldsymbol{\Delta}_e$ and $\boldsymbol{\Delta}_c$ are degrees of freedom to be eliminated and to remain, respectively. The equation (4-45) is used to condense out the incremental equilibrium equation. Then the degrees of freedom to be eliminated can be expressed in terms of degrees of freedom to remain as follow.

$$\mathbf{G}_e\boldsymbol{\Delta}_e + \mathbf{G}_c\boldsymbol{\Delta}_c = \mathbf{H}$$
$$\boldsymbol{\Delta}_e = \mathbf{G}_e^{-1}\left(\mathbf{H} - \mathbf{G}_c\boldsymbol{\Delta}_c\right) = \bar{\boldsymbol{\Gamma}}_e + \boldsymbol{\Gamma}_{ec}\boldsymbol{\Delta}_c \tag{4-47}$$

After rearranging the incremental equilibrium equation, it can be expressed as follow.

$$\begin{Bmatrix} d\mathbf{F}_e \\ d\mathbf{F}_c \end{Bmatrix} = \begin{bmatrix} \mathbf{K}_{ee}^t & \mathbf{K}_{ec}^t \\ \mathbf{K}_{ce}^t & \mathbf{K}_{cc}^t \end{bmatrix} \begin{Bmatrix} d\boldsymbol{\Delta}_e \\ d\boldsymbol{\Delta}_c \end{Bmatrix} \tag{4-48}$$

As shown in equation (4-48), the tangent stiffness matrix is divided into sub-matrices that represent stiffness and coupling between eliminated degrees of freedom and active degrees of freedom. Substituting the incremental form of equation (4-47) into equation (4-48), the equation (4-48) can be rewritten as follows.

$$d\mathbf{F}_e = \mathbf{K}_{ee}^t d\boldsymbol{\Delta}_e + \mathbf{K}_{ec}^t d\boldsymbol{\Delta}_c = \mathbf{K}_{ee}^t d\bar{\boldsymbol{\Gamma}}_e + \mathbf{K}_{ee}^t \boldsymbol{\Gamma}_{ec} d\boldsymbol{\Delta}_c + \mathbf{K}_{ec}^t d\boldsymbol{\Delta}_c$$
$$d\mathbf{F}_c = \mathbf{K}_{ce}^t d\boldsymbol{\Delta}_e + \mathbf{K}_{cc}^t d\boldsymbol{\Delta}_c = \mathbf{K}_{ce}^t d\bar{\boldsymbol{\Gamma}}_e + \mathbf{K}_{ce}^t \boldsymbol{\Gamma}_{ec} d\boldsymbol{\Delta}_c + \mathbf{K}_{cc}^t d\boldsymbol{\Delta}_c \tag{4-49}$$

where $d\bar{\boldsymbol{\Gamma}}_e = \mathbf{G}_e^{-1} d\mathbf{H}$. Then the effective incremental equation can be derived as follow.

$$(d\mathbf{F}_c - \mathbf{K}_{ce}^t d\bar{\boldsymbol{\Gamma}}_e) = (\mathbf{K}_{ce}^t \boldsymbol{\Gamma}_{ec} + \mathbf{K}_{cc}^t) d\boldsymbol{\Delta}_c \tag{4-50}$$

However, the effective stiffness is unsymmetrical. To make it symmetry, the effective force is modified using contragradience rule between force and displacement vector.

$$d\mathbf{F}_{c,\text{eff}} = d\mathbf{F}_c - \mathbf{K}_{ce}^t d\bar{\boldsymbol{\Gamma}}_e + \boldsymbol{\Gamma}_{ec}^T (d\mathbf{F}_e - \mathbf{K}_{ee}^t d\bar{\boldsymbol{\Gamma}}_e) \tag{4-51}$$

Then the effective tangent stiffness matrix becomes symmetric as follow.

$$d\mathbf{F}_{c,\text{eff}} = \mathbf{K}_{\text{eff}}^t d\boldsymbol{\Delta}_c$$
$$\mathbf{K}_{\text{eff}}^t = \mathbf{K}_{cc}^t + \mathbf{K}_{ce}^t \boldsymbol{\Gamma}_{ec} + \boldsymbol{\Gamma}_{ec}^T \mathbf{K}_{ec}^t + \boldsymbol{\Gamma}_{ec}^T \mathbf{K}_{ee}^t \boldsymbol{\Gamma}_{ec} \tag{4-52}$$

After solving the equation (4-52) for increment of the displacement at the active degrees of freedom $d\boldsymbol{\Delta}_c$, the solution corresponding to the eliminated degrees of freedom can be calculated using the equation (4-47). This condensation process can be easily applied to the problems where any prescribed displacement boundary condition is imposed by

taking non-homogeneous form of equation (4-45). Similarly, the same process can also be applied to an effective equilibrium equation from the dynamic equation of motion.

4.4.2 Numerical Procedures for Nonlinear Static Analysis

In this section, the detailed numerical procedures used for nonlinear static analysis of frame structures with the proposed generalized inelastic hysteretic connection model are exhaustively explained. The geometrical nonlinearity is considered using the geometric stiffness derived in Section 4.2.2 based on the incremental Updated Lagrangian formulation method and the material nonlinearity is assumed to be concentrated at the locations where the inelastic model is defined. For solving the incremental equilibrium equation, incremental-iterative Newton-Raphson solution algorithm is used in which the tangent stiffness is reformed referring to the last equilibrated state at every iteration step. The detailed flow chart for geometric and material nonlinear analysis procedures are as follows.

Step 1) Read the basic finite element data given at the initial configuration C_0: nodal coordinates, element connectivity data with sectional, material properties and local directional data and loading data.

Step 2) Calculate the equivalent load vector and fixed end force vector from various loading information. 'nelem' is total number of elements.

$$^{0}\mathbf{F} = \sum_{i=1}^{\text{nelem}} {}^{0}\mathbf{f}_{i} \tag{4-53}$$

Assume that the current incremental step is n and Start the current incremental step n.

Step 3) Calculate the unbalanced force vector including unbalanced force left-over from the previous incremental step.

$$\Delta^{0}\mathbf{R}_{n} = {}^{0}\mathbf{F}/\text{nincr} + \mathbf{R}_{n-1} \tag{4-54}$$

where 'nincr' is the total number of incremental steps and $\mathbf{R}_{n-1}$ the unbalanced force left-over from the previous incremental step.

Assume that the current iteration step is k and Start the current iteration step k.

Step 4) Initialize the global tangent stiffness matrix and increment of the internal resisting force vector.

$$\mathbf{K}_{t,n}^{(k)} = \mathbf{0} \quad \text{and} \quad \Delta\mathbf{I}_{n}^{(k)} = \mathbf{0} \tag{4-55}$$

Step 5) Assemble the current tangent stiffness matrix from elemental matrices of 3D beam-column element and generalized inelastic connection element.

$$\mathbf{K}_{t,n}^{(k)} = \sum_{i=1}^{nelem} \mathbf{T}^{T}(\mathbf{k}_{i,e}^{(k)} + \mathbf{k}_{i,g}^{(k)})\mathbf{T} + \sum_{i=1}^{nNNelem} \mathbf{T}^{T}(k_{i,e}^{NN})\mathbf{T} \tag{4-56}$$

where $\mathbf{T}$ is a transformation matrix defined in Appendix. 'nNNelem' is total number of the proposed connection elements.

Step 6) Apply the constraint equation if necessary and Calculate the effective tangent stiffness and load vector with equations (4-51) and (4-52).

Step 7) Solve the incremental equilibrium equation for the incremental displacement vector.

$$\begin{aligned} D\mathbf{U}_{n}^{(k)} &= [\mathbf{K}_{t,n}^{(k)}]^{-1} D\mathbf{R}_{n}^{(k)} \\ D\mathbf{R}_{n}^{(k)} &= D\mathbf{R}_{n}^{(k-1)} - D\mathbf{I}_{n}^{(k-1)} \end{aligned} \tag{4-57}$$

Step 8) Calculate the incremental internal resisting force vector of the three-dimensional beam-column elements and connection elements. For the beam-column elements, the increment of internal resisting forces is calculated as follows.

$$\Delta \mathbf{I}_n^{(k)} = \sum_{i=1}^{nelem} [\mathbf{k}_{i,e}^{(k)} + \mathbf{k}_{i,g}^{(k)}] \Delta \mathbf{u}_{i,n}^{(k)} \tag{4-58}$$

Detailed equations used for the calculation can be found in section 4.2.3. For the NN based inelastic connection element, the increment of the internal resisting force vector and the algorithmic tangent stiffness are calculated differently. For the one-dimensional case in terms of moment-rotation pairs, the procedure for calculating them is illustrated in Figure 4.9.

Step 9) Update the configuration to the latest configuration.

$$\Delta \mathbf{X}_n^{(k)} = \Delta \mathbf{X}_n^{(k-1)} + \Delta \mathbf{U}_n^{(k)} \tag{4-59}$$

Step 10) Calculate the unbalanced force vector.

$$\Delta \mathbf{R}_n^{(k+1)} = \Delta \mathbf{R}_n^{(k)} - \Delta \mathbf{I}_n^{(k)} \tag{4-60}$$

Step 11) Check the convergence. If satisfied, go to Step 3 and apply next load increment. Otherwise, repeat the iteration step from Step 4.

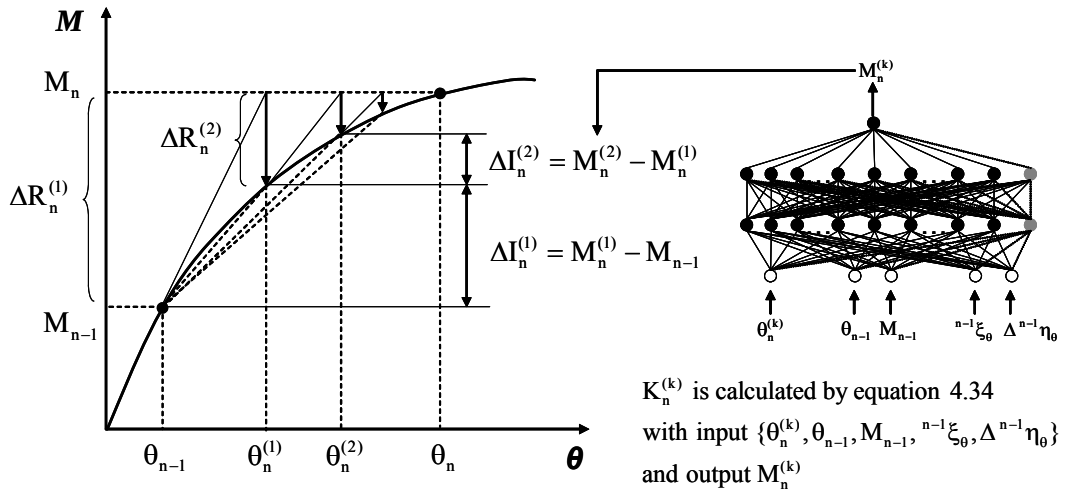

Figure 4.9 Use of Neural Network for Calculations of Increment of Internal Resisting Force and Tangent Stiffness

As shown in Figure 4.9, the latest converged load step is referred when forward passing of the neural network is performed for calculation of the internal resisting force vector and tangent stiffness. For the purpose of stable predictions by the NN based model, secant stiffness within a load incremental step is assumed to be tangent stiffness. According to numerical tests, the rough assumption gives reasonable predictions even though bookkeeping of the latest converged solution and the latest iterative solution is needed.

4.4.3 Numerical Procedures for Nonlinear Dynamic Analysis

In this section, detailed numerical procedures used for the nonlinear dynamic analysis of frame structures with the proposed inelastic hysteretic connection model are explained. The dynamic equation of motion is integrated with Newmark average acceleration scheme which has integration parameters, β=1/4 and γ=1/2. For finding the convergent

response points between each time step, Newton-Raphson iterative solution scheme is used in which the tangent stiffness is updated at each iteration step. In dynamic simulations, the geometric nonlinearity is considered because its effect can be significant on the examples with large deformation under large axial forces. Using the numerical damping parameter α (Hilber, et al. 1977), the dynamic equation of motion can be written as follow.

$$\begin{aligned}
&\mathbf{M}\ddot{\mathbf{U}}_{n+1} + (1+\alpha)\mathbf{C}\dot{\mathbf{U}}_{n+1} - \alpha\mathbf{C}\dot{\mathbf{U}}_{n} + (1+\alpha)\mathbf{K}\mathbf{U}_{n+1} - \alpha\mathbf{K}\mathbf{U}_{n} = (1+\alpha)\mathbf{F}_{n+1} - \alpha\mathbf{F}_{n} \\
&\mathbf{U}_{n+1} = \mathbf{U}_{n} + \Delta t\dot{\mathbf{U}}_{n} + \Delta t^{2}\left[\left(\frac{1}{2} - \beta\right)\ddot{\mathbf{U}}_{n} + \beta\ddot{\mathbf{U}}_{n+1}\right] \\
&\dot{\mathbf{U}}_{n+1} = \dot{\mathbf{U}}_{n} + \Delta t\left[(1-\gamma)\ddot{\mathbf{U}}_{n} + \gamma\ddot{\mathbf{U}}_{n+1}\right]
\end{aligned} \tag{4-61}$$

where **M**, **C** and **K** are mass matrix, damping matrix and tangent stiffness matrix, respectively; n indicates n-th time step. The consistent mass matrix can be formulated using interpolation functions.

$$\mathbf{M} = \int_{V} \rho\,\mathbf{N}^{T}\mathbf{N}\,dV \tag{4-62}$$

The damping matrix is calculated by Rayleigh damping approach as follow.

$$\mathbf{C} = a_0\mathbf{M} + a_1\mathbf{K} \tag{4-63}$$

The mass and stiffness proportional damping parameter can be determined as follow.

$$a_0 = \zeta\frac{2\omega_i\omega_j}{\omega_i + \omega_j} \qquad a_1 = \zeta\frac{2}{\omega_i + \omega_j} \tag{4-64}$$

where ς is a modal damping ratio which is assumed to be the same for the two different modes i and j. ω_i and ω_j are natural angular frequency at i-th and j-th mode. In order to use the incremental-iterative solution scheme for nonlinear problems, the equation of motion in (4-61) is reformulated in the difference form. When there is any constraint

equation, the effective equation of motion can be reformulated through the condensation process as explained in section 4.4.1.

$$\mathbf{K}_{\text{eff}}\Delta\mathbf{U}_n = \Delta\mathbf{F}_{\text{eff},n} \tag{4-65}$$

The effective tangent stiffness and loading vector in equation (4-65) can be expressed as follow. The derivation can be found in a reference (Chopra 2000).

$$\begin{aligned}
&\mathbf{K}_{\text{eff}}\Delta\mathbf{U}_n = \Delta\mathbf{F}_{\text{eff},n} \\
&\text{where}\quad \mathbf{K}_{\text{eff}} = \mathbf{K} + \frac{g}{b\Delta t}\mathbf{C} + \frac{1}{b(\Delta t)^2}\mathbf{M} \\
&\qquad \Delta\mathbf{F}_{\text{eff},n} = \Delta\mathbf{F}_{\text{eff},n-1} + \mathbf{a}\dot{\mathbf{U}}_{n-1} + \mathbf{b}\ddot{\mathbf{U}}_{n-1}
\end{aligned} \tag{4-66}$$

After applying the generalized constraint equation, the effective equation of motion can be expressed in terms of active degrees of freedom.

$$\begin{aligned}
\bar{\mathbf{K}} &= \left(\mathbf{K}_{\text{eff},cc} + \mathbf{K}_{\text{eff},ce}\boldsymbol{\Gamma}_{ec} + \boldsymbol{\Gamma}_{ec}^{\mathrm{T}}\mathbf{K}_{\text{eff},ec} + \boldsymbol{\Gamma}_{ec}^{\mathrm{T}}\mathbf{K}_{\text{eff},ee}\boldsymbol{\Gamma}_{ec}\right) \\
\Delta\bar{\mathbf{F}}_n &= \Delta\mathbf{F}_{\text{eff},n,c} - \mathbf{K}_{\text{eff},ce}\bar{\boldsymbol{\Gamma}}_e + \boldsymbol{\Gamma}_{ec}^{\mathrm{T}}(\Delta\mathbf{F}_{\text{eff},n,e} - \mathbf{K}_{\text{eff},ee}\bar{\boldsymbol{\Gamma}}_e) \\
\Delta\bar{\mathbf{F}}_n &= \bar{\mathbf{K}}\Delta\mathbf{U}_{n,c}
\end{aligned} \tag{4-67}$$

For the sake of simplicity, the numerical damping parameter is omitted in the following flow chart.

$$\mathbf{M}\Delta\ddot{\mathbf{U}}_{n+1} + \mathbf{C}\Delta\dot{\mathbf{U}}_{n+1} + \mathbf{K}\Delta\mathbf{U}_{n+1} = \Delta\mathbf{F}_{n+1} \tag{4-68}$$

Step 1) Calculate the initial acceleration from initial conditions and time step Δt.

$$\Delta\ddot{\mathbf{U}}_0 = \mathbf{M}^{-1}(\mathbf{F}_0 - \mathbf{C}\Delta\dot{\mathbf{U}}_0 - \mathbf{K}\Delta\mathbf{U}_0) \tag{4-69}$$

Step 2) Calculate parameters for effective force vector

$$\mathbf{a} = \frac{1}{b\Delta t}\mathbf{M} + \frac{g}{b}\mathbf{C} \quad \text{and} \quad \mathbf{b} = \frac{1}{2b}\mathbf{M} + \Delta t\left(\frac{g}{2b} - 1\right)\mathbf{C} \tag{4-70}$$

Assume that current time step is n and start time integration at the current step.

Step 3) Calculate the effective loading vector

$$\Delta \mathbf{F}_n = \Delta \mathbf{F}_{n-1} + a\mathbf{M}\dot{\mathbf{U}}_{n-1} + b\mathbf{C}\ddot{\mathbf{U}}_{n-1} \tag{4-71}$$

Assume that the current iteration step is k and Start the current iteration step k (Newton-Raphson iteration)

Step 4) Assemble the current tangent stiffness matrix from elemental matrices of the three-dimensional beam-column elements and the connection element and calculate the effective stiffness matrix.

$$\mathbf{K}_{\text{eff}} = \mathbf{K}_{t,n}^{(k)} + \frac{g}{b\Delta t}\mathbf{C} + \frac{1}{b(\Delta t)^2}\mathbf{M} \tag{4-72}$$

where $\mathbf{K}_{t,n}^{(k)}$ from equation (4.56)

Step 5) Apply the constraint equation to calculate effective incremental equilibrium equation in terms of active degrees of freedom. The equation (4-67) is used.

Step 6) Solve the incremental equilibrium equation for the incremental displacement vector.

$$\Delta \mathbf{U}_n^{(k)} = [\hat{\mathbf{K}}_n^{(k)}]^{-1} \Delta \hat{\mathbf{F}}_n^{(k)} \tag{4-73}$$

Step 7) Calculate the incremental internal resisting force vector $\Delta \mathbf{I}_n^{(k)}$ of the three-dimensional beam-column elements and connection elements. The computation is the same as the one for nonlinear static analysis but the compensation of the dynamic effect.

$$\Delta \hat{\mathbf{F}}_n^{(k+1)} = \Delta \hat{\mathbf{F}}_n^{(k)} - (\Delta \mathbf{I}_n^{(k)} + (\hat{\mathbf{K}}_n^{(k)} - \mathbf{K}_n^{(k)})\Delta \mathbf{U}_n^{(k)}) \tag{4-74}$$

Step 8) Update the configuration to the latest configuration.

$$\Delta \mathbf{X}_n^{(k)} = \Delta \mathbf{X}_n^{(k-1)} + \Delta \mathbf{U}_n^{(k)} \tag{4-75}$$

Step 9) Check the convergence. If satisfied, go on to Step 10 and repeat from Step 3 for next time step. Otherwise, repeat the iteration step from Step 4.

Step 10) Calculate velocity and acceleration values at the converged response point

$$\Delta\dot{\mathbf{U}}_n = \frac{g}{b\Delta t}\Delta\mathbf{U}_n - \frac{g}{b}\Delta\dot{\mathbf{U}}_{n-1} + \Delta t\left(1 - \frac{g}{2b}\right)\Delta\ddot{\mathbf{U}}_{n-1} \quad ; \quad \dot{\mathbf{U}}_n = \dot{\mathbf{U}}_{n-1} + \Delta\dot{\mathbf{U}}_n$$
$$\ddot{\mathbf{U}}_n = \mathbf{M}^{-1}\left(\mathbf{F}_n^{ext} - \mathbf{C}\dot{\mathbf{U}}_n - \int_V \mathbf{B}^T\boldsymbol{\sigma}\,dV\right) \tag{4-76}$$

Numerical examples for verifying the proposed connection model as well as the numerical procedure and implementation follow in next section.

4.5 Numerical Examples

The objectives of the numerical examples are to verify the proposed hysteretic connection models and the proposed formulations and algorithms in the nonlinear analysis. The numerical examples in this section consist of four parts.

1) Geometrical nonlinear static analysis of a simple strut with imperfection of 0.1 % under axial loading.

2) Nonlinear static and dynamic analysis of one-bay two-story frame

3) Nonlinear dynamic analysis with the proposed hysteretic connection model.

4) Nonlinear static analysis of NN based plastic hinge element under a non-proportional cyclic loading.

4.5.1 A Simple Strut subjected to Elastic Buckling Load

A simple strut is modeled with four beam-column elements and it has imperfection of 0.1% of the length 10 m. The beam has a tube section which has outside diameter of 193.7 mm and thickness of 6.3 mm. Its elastic Euler buckling load is calculated as $P_{cr}=\pi EI/L^2=323.7$ kN. The Young's modulus used is $2.05\text{x}10^8$ kN/m^2 and the poisson

ratio is 0.3. The axial force is incrementally imposed up to 80% of the buckling load before the solution response diverges because of well-known limitation of the load controlled Newton-Raphson algorithm. The geometrical nonlinearity is considered as formulated in the previous section. This example is analyzed by Chan and Chi (Chan and Chui 2000) and the present result is compared with the result from general nonlinear finite element software, ABAQUS (ABAQUS/Standard 2004) as illustrated in Figure 4.10.

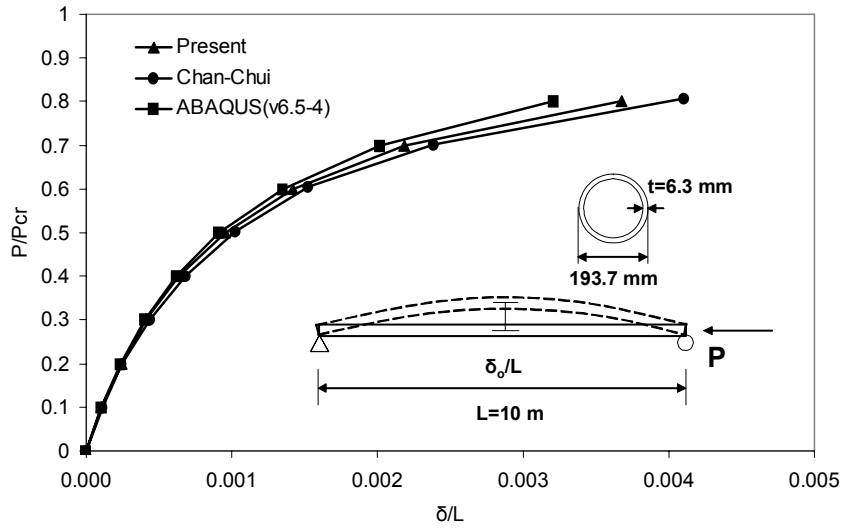

Figure 4.10 Simple Strut subjected to Elastic Buckling Load

4.5.2 Nonlinear Static and Dynamic Analysis

In this example, a one-bay two-story frame with nonlinear connection behavior is analyzed to investigate the effect of nonlinear characteristics at connections on the global response. The overall structural dimensions and numerical model used is illustrated in Figure 4.11. The beams are modeled by two elements and the column is modeled by one

element. For the consideration of P-Δ effect, gravity loading is represented by concentrated loading at each node on the beam. The nonlinear behavior of the connections is modeled by Ramberg-Osgood Model calibrated with a test result (Ostrander 1970) on a flush and plate connection illustrated in Figure 4.13. For comparisons between various connection types, the connections are also modeled by rigid and linear connections. The moment-rotation relationship is illustrated in Figure 4.12. In order to check the capacity of the frame with the flexible connection, push-over analysis is performed with gradually increasing horizontal forces. The horizontal displacement at the second floor versus load factor λ is plotted in Figure 4.14. For verification of the proposed formulation and algorithm with flexible connection models, the results are compared with ABAQUS results. According to the result, the proposed formulation proves to reasonably estimate the maximum load-carrying capacity of frame structures with flexible connections. Particularly, because of the P-Δ effect, the second-order analysis results are showing larger displacements than the first-order analysis results with the same load factor.

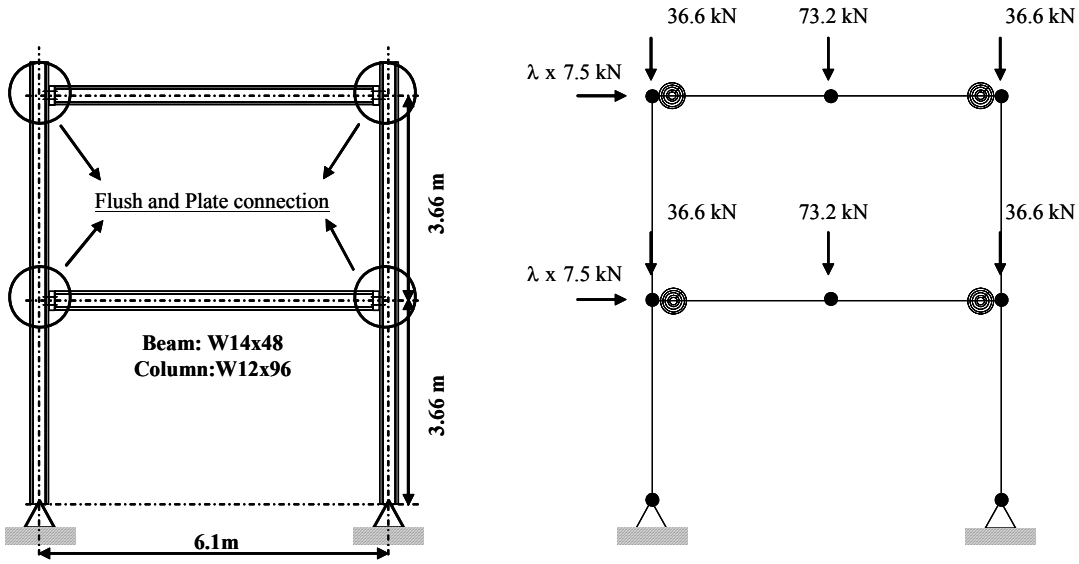

(a) Geometrical dimension (b) Numerical Model

Figure 4.11 One-bay two-story frame with flush and plate connections

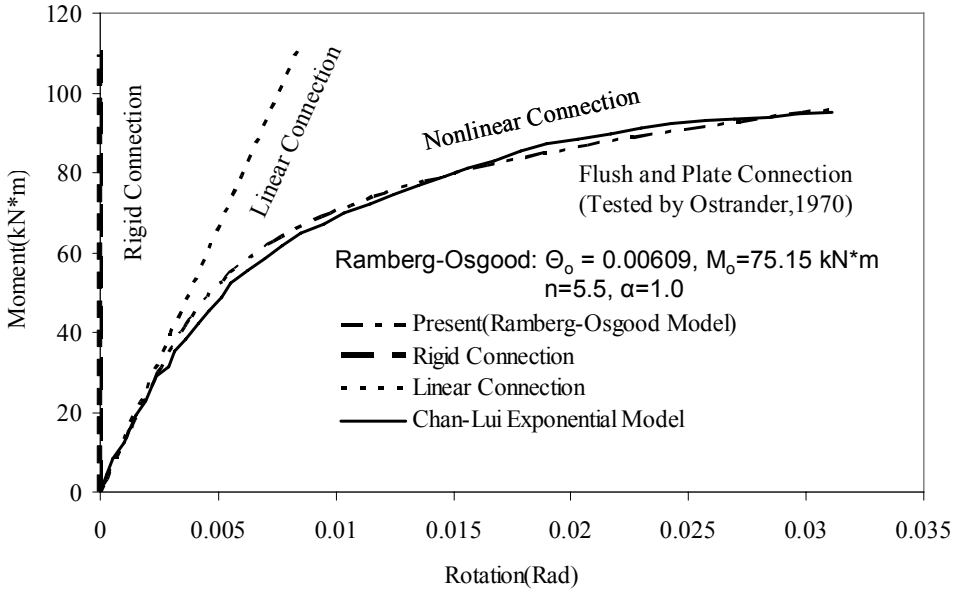

Figure 4.12 Moment-Rotation Relationship of Various Connection Modeling

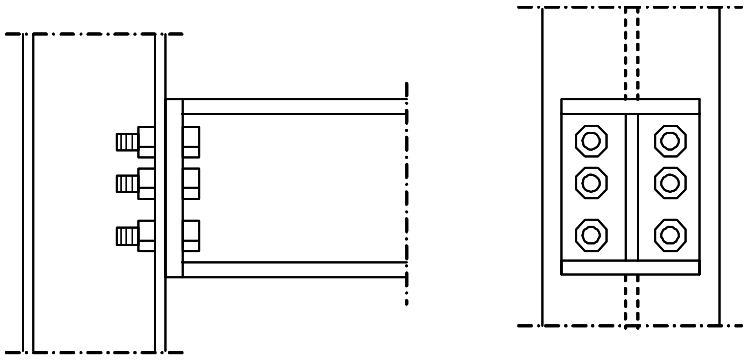

Flush and Plate Connection (Tested by Ostrander,1970)

Figure 4.13 Flush and Plate Connection

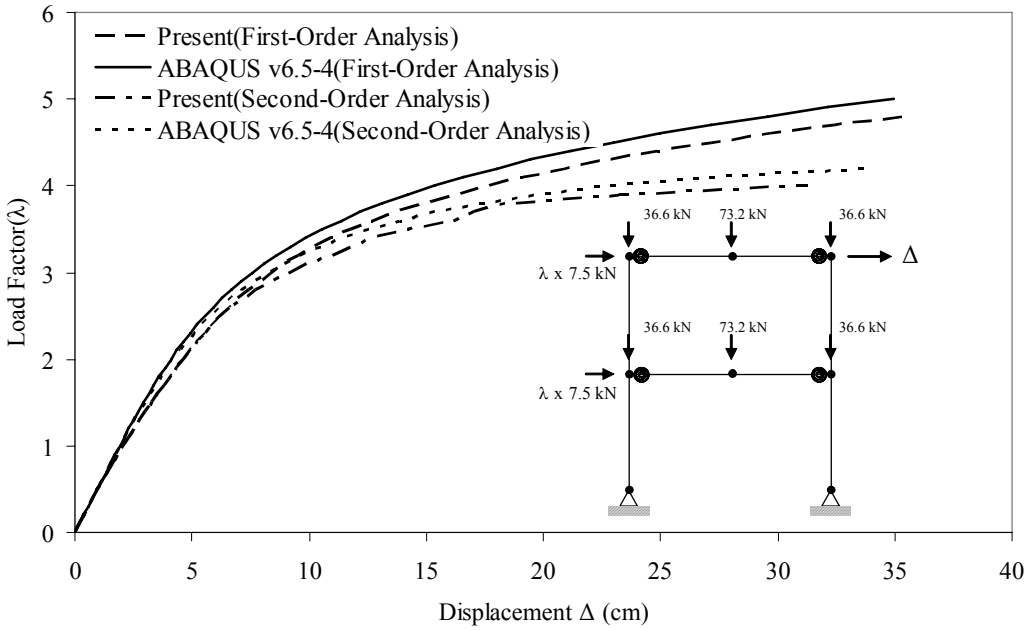

Figure 4.14 Push-over Analysis Results and Comparison with ABAQUS (v6.5-4)

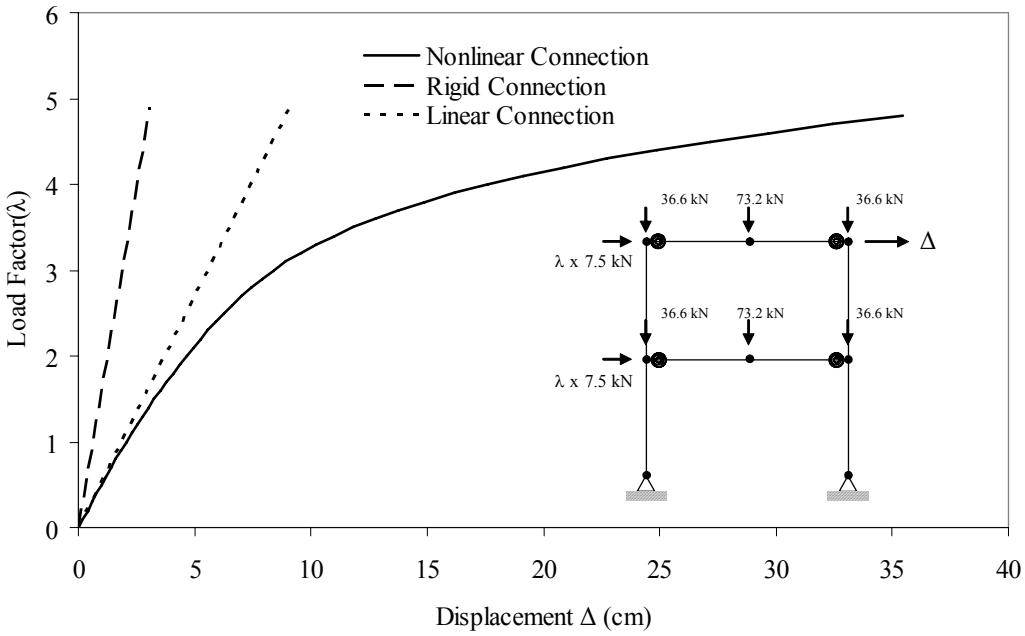

Figure 4.15 Push-over Analysis Results with Various Connection Modeling

Evidently, the flexible connection behavior has significant influence on the load carrying capacity of the two-story frame as shown in Figure 4.15. Therefore, the accurate modeling of the connection behavior is very important in the assessment of resistance of frame structures to static loading. In the following example, the dynamic response characteristic of the same frame is investigated.

To investigate the effect of the connection modeling type on the dynamic responses of frame structures, the same one-bay two-story building is simulated under an impact loading. The numerical model and loading condition without gravity loading effect and with gravity loading effect are illustrated in Figure 4.16 and Figure 4.17, respectively. The gravity loading is represented by lumped masses 7.46 ton in the middle of beams and 3.73 ton at each connection. When the gravity loading effect is considered, multi-step simulation is performed: 1) First, nonlinear static simulation is performed and 2) it is

followed by nonlinear dynamic simulation which starts from the converged state and configuration. For the verification purpose, the responses with gravity effect and without gravity effect are compared with ABAQUS results. In this case, the rotational behavior of connection is modeled by spring elements which have linear stiffness as shown in Figure 4.12. The displacement history at the second floor is illustrated in Figure 4.18 and Figure 4.19. According to the results, reasonable dynamic response can be obtained by the proposed formulation and algorithm for both of linear and nonlinear response.

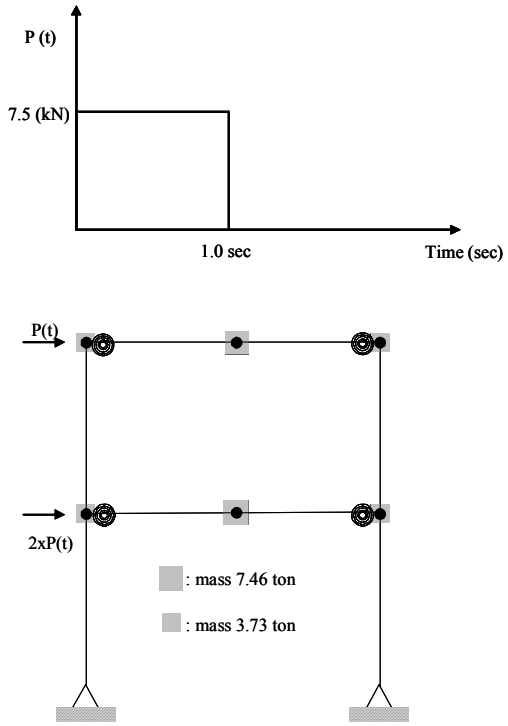

Figure 4.16 Impact Loading and Numerical Model without Gravity Loading Effect

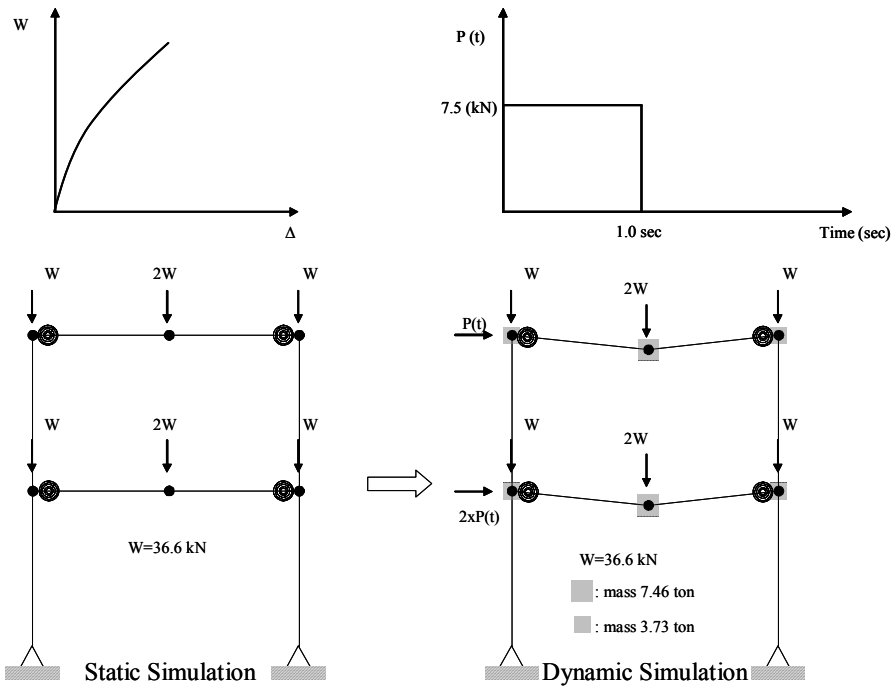

Figure 4.17 Loading and Numerical Model with Gravity Loading Effect (Multi-Step Simulation)

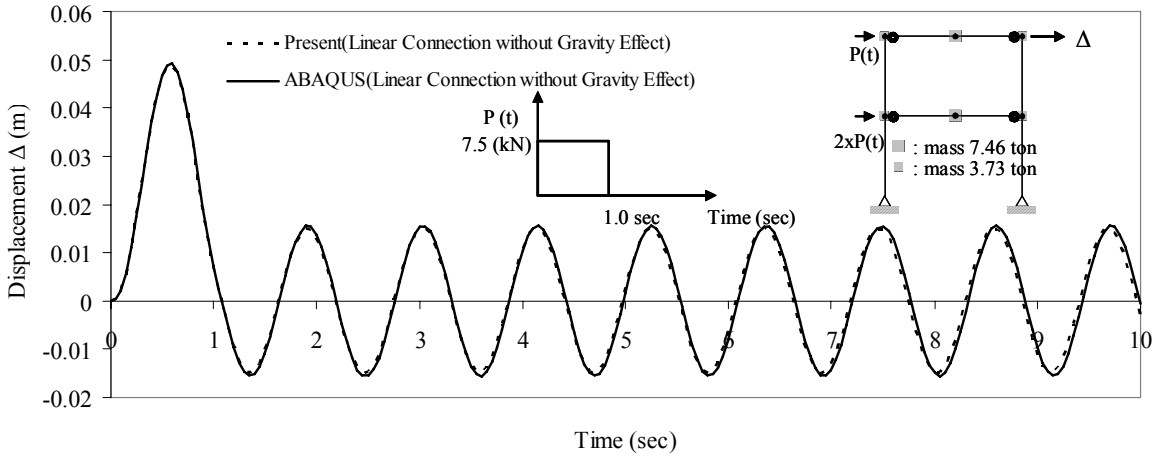

Figure 4.18 Dynamic Response of Two-story Frame with Linear Connection Model without Gravity Loading Effect

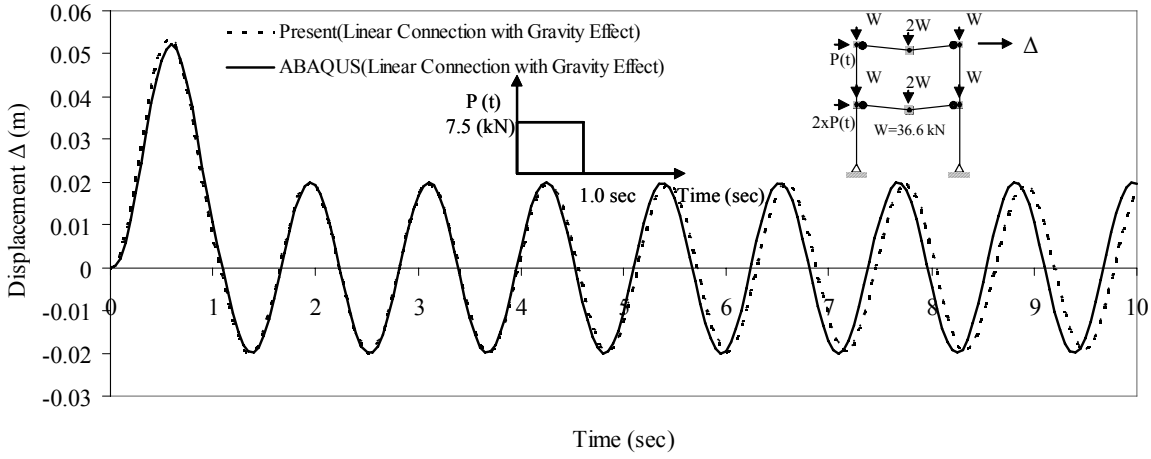

Figure 4.19 Dynamic Response of Two-story Frame with Linear Connection Model with Gravity Loading Effect

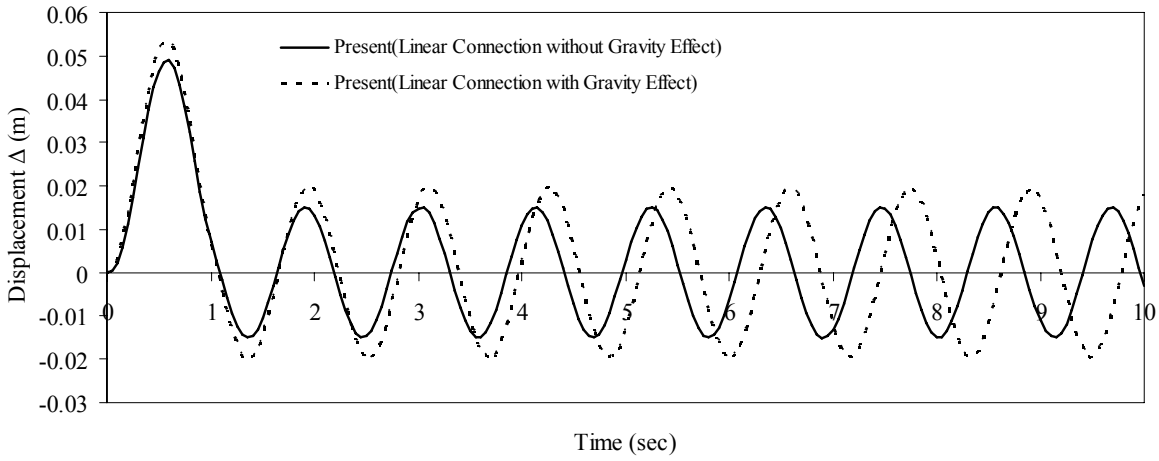

Figure 4.20 Comparison of Top Displacement between the results with Gravity Effect and without Gravity Effect

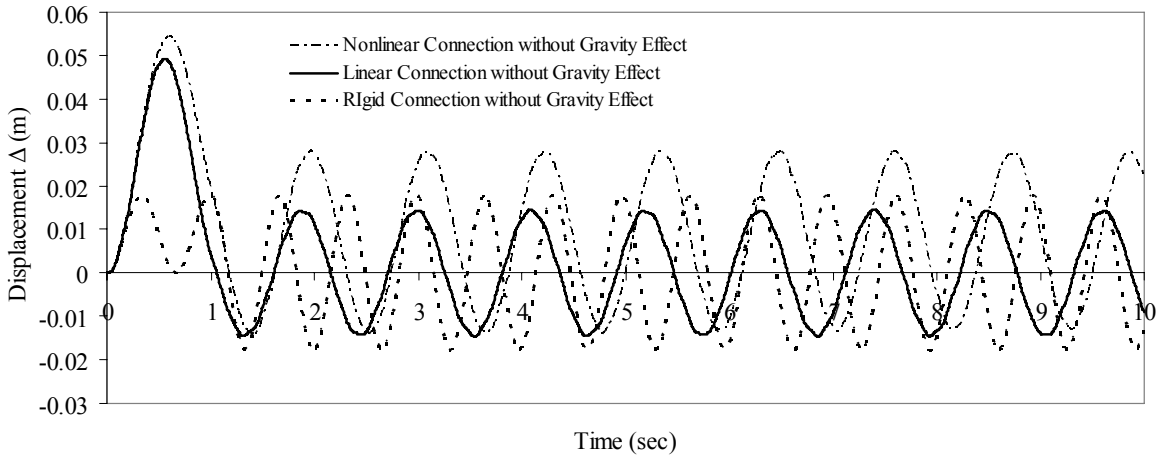

Figure 4.21 Dynamic Response with Various Connection Types (Rigid, Linear and Nonlinear Connection)

According to the comparison between the results with gravity effect and without gravity effect in Figure 4.20, the amplitude during free vibration phase has become increased by 25% because of the consideration of geometric nonlinearity. Moreover, the vibration period has also become increased significantly because of the P-Δ effect. The effect of flexibility at connection regions on the dynamic response is salient as shown in Figure 4.21. Owing to the flexibility, the amplitude has increased and also gradually decreased after 1 second because of hysteretic damping at connections.

4.5.3 Dynamic Analysis of a Frame with NN based Connection Model

A primary objective of this example is to verify the proposed NN based model in nonlinear dynamic simulation. In the lumped inelasticity approach, phenomenological models representing the cyclic behavior of flexible connections are usually utilized to investigate dynamic responses of frame structures within dynamic simulation computer

codes for a given cyclic loading. Since the phenomenological models are usually obtained from exhaustive regression of experimental data and curve-fitting process, they are dependent on experimental data. If either given cyclic loading or structural detail changes, the model should also change. However, once the proposed NN based connection model is trained by enriched experimental data, it can represent such a complex hysteretic behavior.

The test model is a half model of a two-story frame with semi-rigid connections. The frame was tested using an explicit pseudo-dynamic testing method by Elnashai et al. (Elnashai, et al. 1998). The instrumentation and dimension are shown in Figure 4.22 and geometrical dimension of the test specimen is summarized in Table 4.1.

Table 4.1 Geometrical Properties of Test Specimen (Elnashai, et al. 1998)

Components	Dimension
Beam	Welded Section: H 250 x 130 x 9 x 9
Column	Rolled Section: H 150 x 150 x 7 x10
Top/Bottom Angle	L 75x 75 x 9: Length 150
Web Angle	L 75 x75 x 8: Length 190
Bolt	Diameter 16 mm

Two concentrated masses, 8000 kg at each story, are assumed in the numerical model. For an input ground motion, the 1940 Imperial Valley (El centro) N-S component acceleration record of 15-sec duration was used. The peak ground acceleration is scaled up to 0.45g. The time step 0.01 sec was used in the pseudo-dynamic testing. Mass proportional damping only is assumed with 5% and 0.5% damping ratio for the first and second mode, respectively. The numerical model is described in Figure 4.23.

For the purpose of verification, two-stage verification method is employed. First, the semi-rigid connections are modeled using a phenomenological model (Ramberg-Osgood model) and the phenomenological model is shown to be able to reasonably predict dynamic responses through comparisons with experimental results in terms of horizontal displacement history at each story. Second, the proposed NN based connection model is trained with the verified simulated testing results (called reference data or model) and used in the incremental nonlinear finite element code developed in this report. Then, the performance of the proposed model is verified in predicting the response of the two-story steel frame structure with semi-rigid connections under earthquake loading. It is noteworthy that not only can the proposed model be developed directly from any available accurate local connection behavior but also it can be developed from self-learning simulation described in the following chapter.

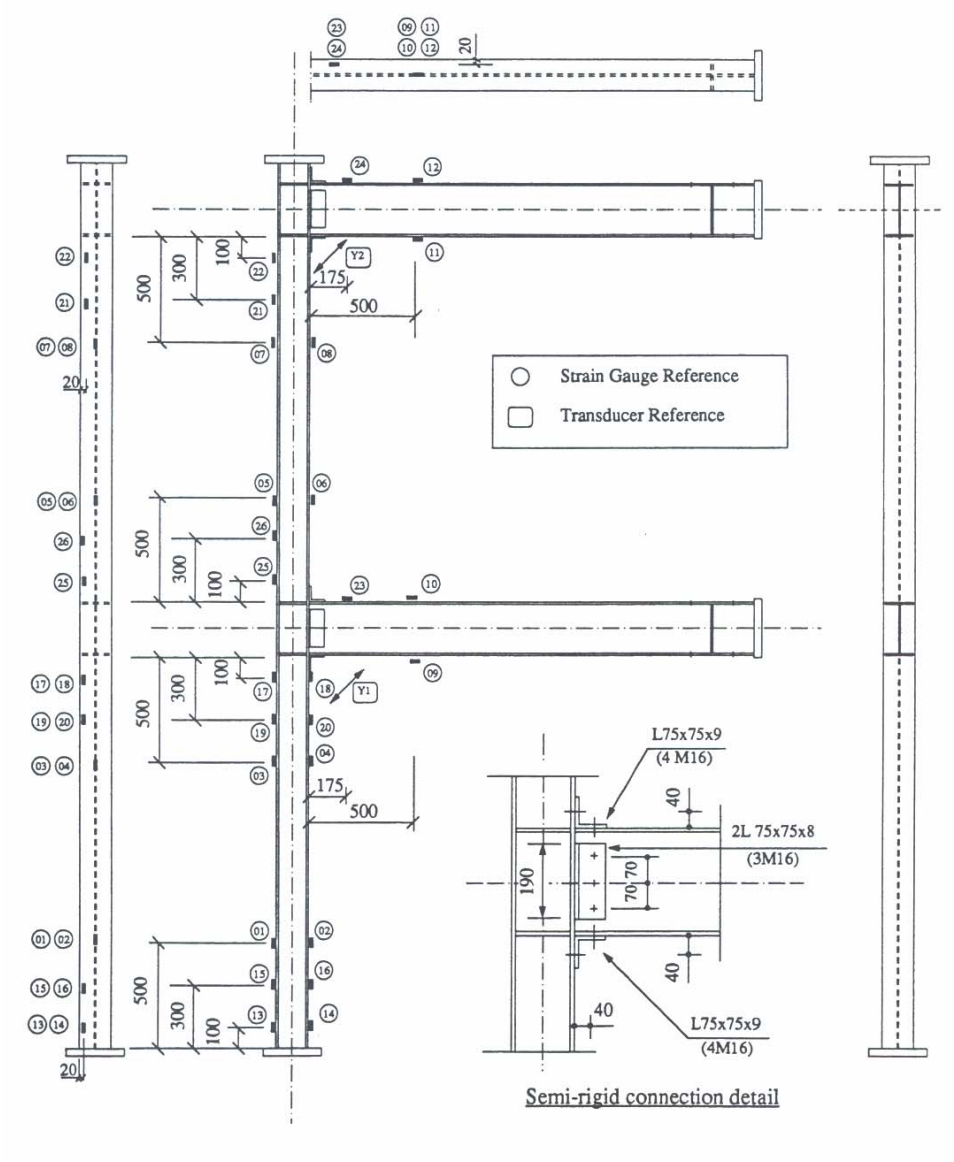

Figure 4.22 Instrumentation and Dimension of Test Model (Elnashai, et al. 1998)

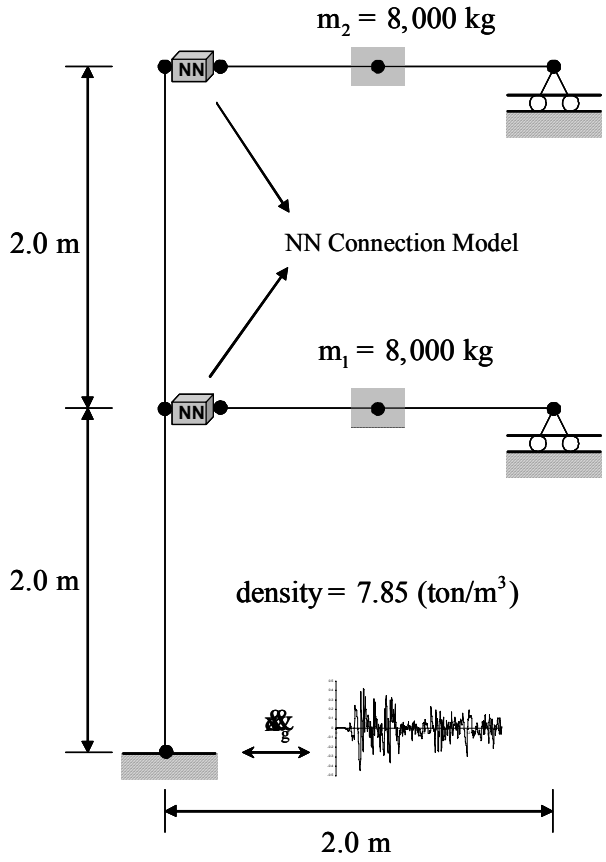

Figure 4.23 Numerical Model and its Dimension for Simulation

The capacity of the semi-rigid connection is calculated utilizing JMRC (Joint Moment Rotation Curve) software (Faella, et al. 2000). The JMRC can reasonably predict the initial rotational stiffness and the flexural resistance for any type of steel beam-column connections. The computed capacity of the connection is summarized in Table 4.2. In the Ramberg-Osgood model, the reference moment (M_0) giving rise to a permanent rotation (θ_0) corresponds to the plastic flexural resistance (M_{Rd}) of connections in JMRC.

Table 4.2 Capacity of Semi-Rigid Connection from JMRC

	Initial Rotational Stiffness (kN/Rad)	Flexural Resistance (kN*m)
Semi-Rigid Connection (Bolted with Angles)	13916.85	36.044

Two elements are used for columns and three elements are used for modeling beams. The Young's modulus is assumed to be 2.05 x 10^8 (kN/m^2) and poisson ratio is assumed to be 0.3. All the elements have density 7.85 (ton/m^3). Figure 4.24 shows comparisons of the displacement history between the experiment and the numerical simulation with semi-rigid connections. As shown in Figure 4.24, the numerical simulation (reference simulation) is reasonably predicting the maximum displacement amplitude. Toward the end of the verification, the proposed NN based model is trained with moment-ration data from the reference simulation. The connections at each story are modeled by two different NN based connection models so they are separately trained.

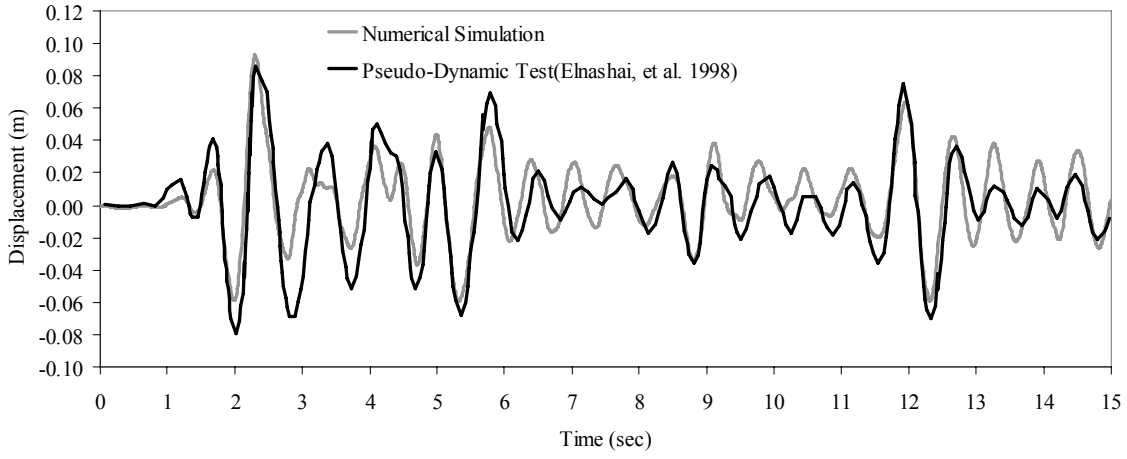

(a) Displacement at the Second Story

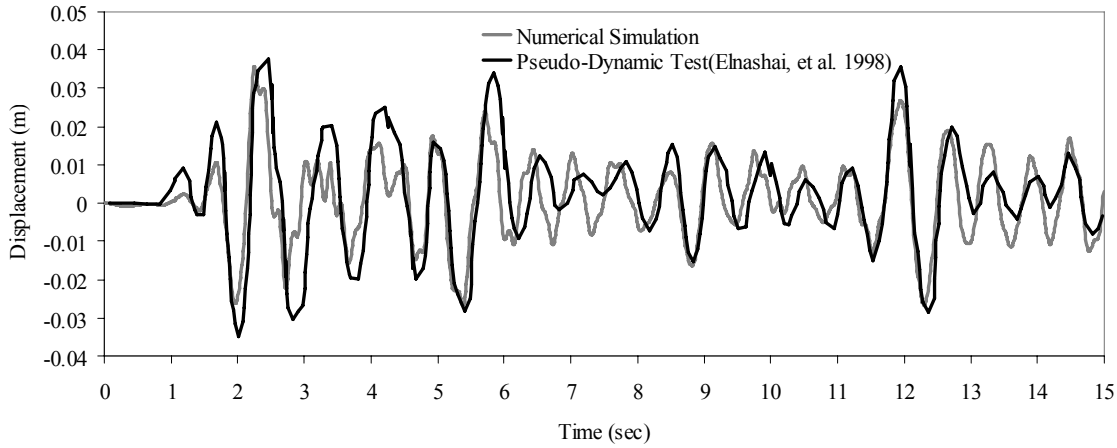

(b) Displacement at the First Story

Figure 4.24 Comparisons between Numerical Simulation and Experiment

The information about training of the proposed model is described in Table 4.3. The number of layers in the neural network is three excluding the input layer and 50 neurons are used per each hidden layer. The NN based connection model is represented as follows.

$$M_{n+1} = \hat{M}_{NN}\left(\{q_{n+1}, q_n, M_n, z_{q,n}\}: \{4-\ 50-\ 50-\ 1\}\right) \tag{4-77}$$

The standard Newton-Raphson iteration method is used for solving nonlinear equilibrium equation of motion.

Table 4.3 Training Information of the NN based Connection Model

	Number of Epochs used in Training	NN Architecture	Average Error in Training
NN based Model for 1st Floor	20,000	{4-50-50-1}	3.253×10^{-6}
NN based Model for 2nd Floor	20,000	{4-50-50-1}	5.699×10^{-6}

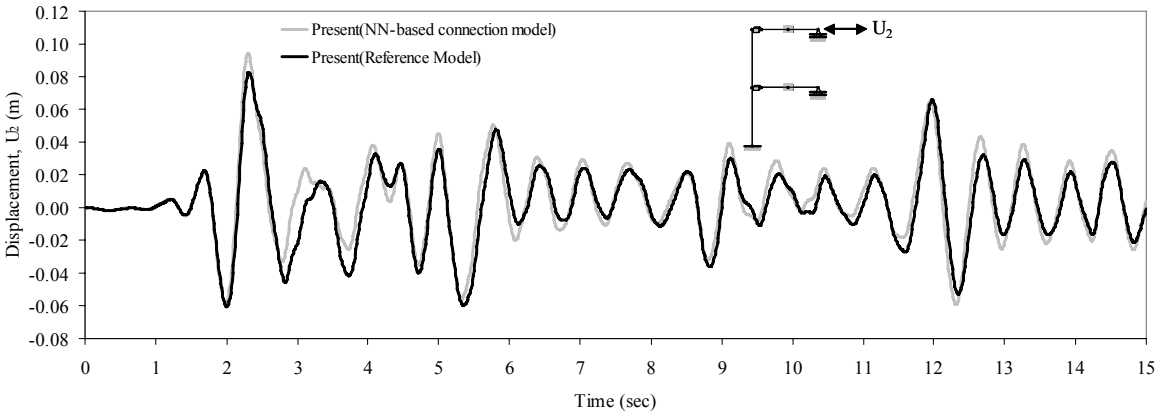

(a) Displacement at the Second Floor

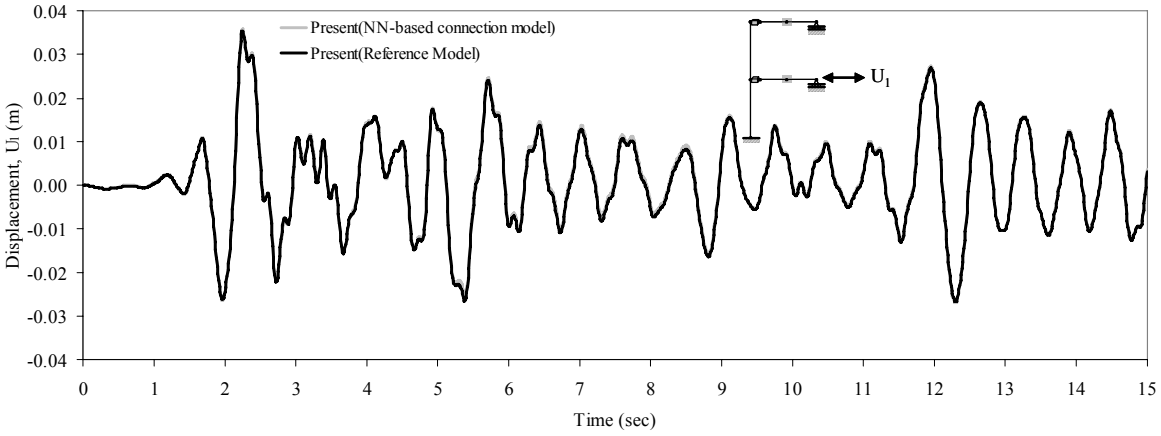

(b) Displacement at the First Floor

Figure 4.25 Comparison between NN based Connection Model and Reference Model

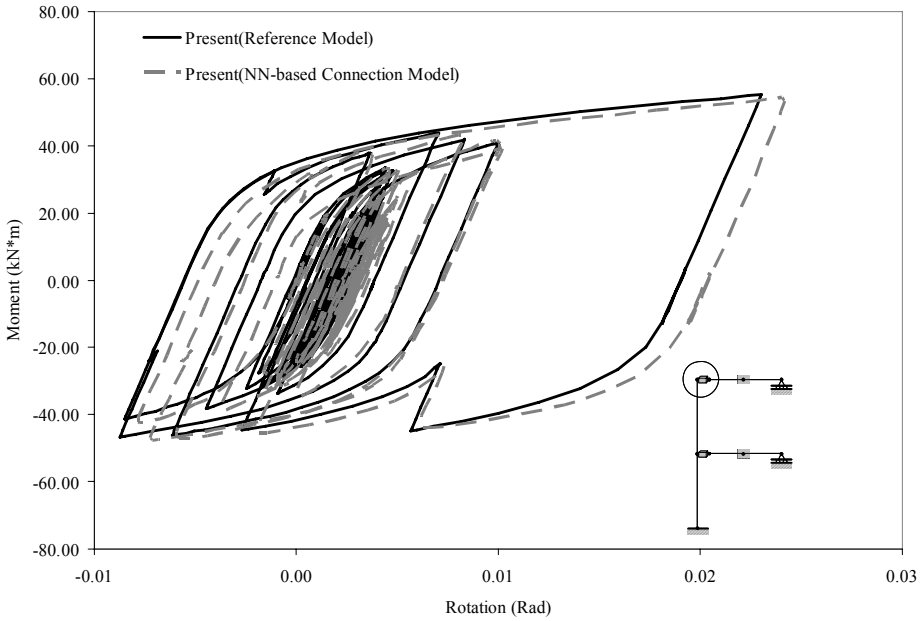

(a) Moment-Rotation at the Second Floor

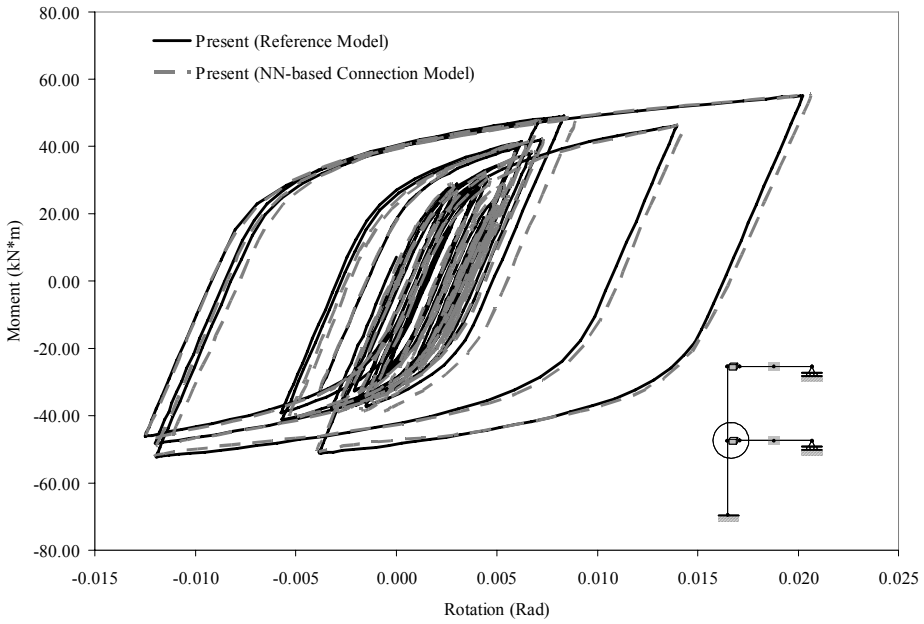

(b) Moment-Rotation at the First Floor

Figure 4.26 Comparison between Reference Model and NN based Model

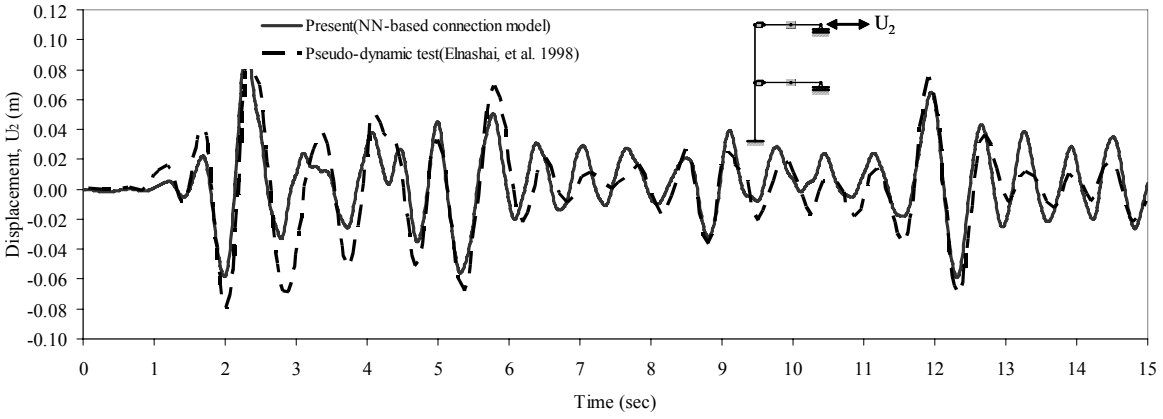

(a) Displacement at the Second Floor

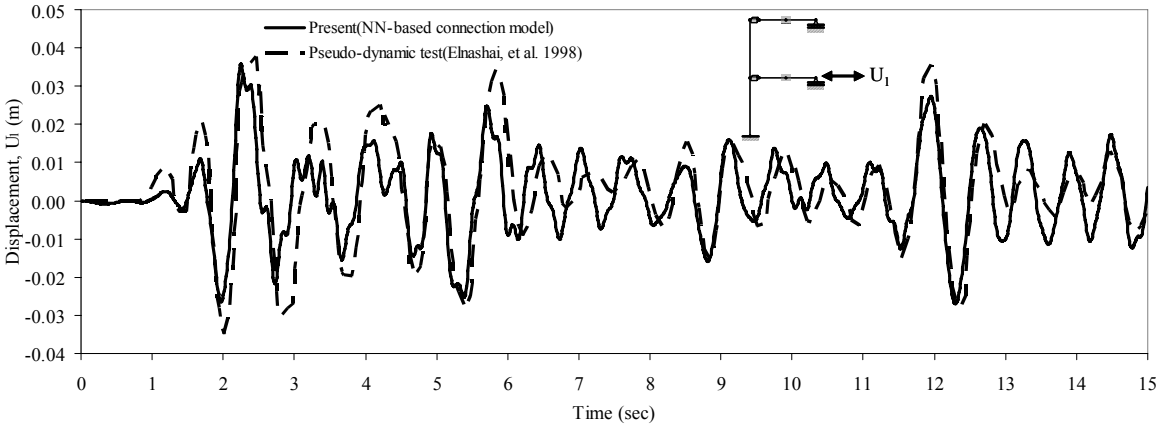

(b) Displacement at the First Floor

Figure 4.27 Comparison between Experimental Results and NN based Connection Model

The predicted global responses by the proposed NN based model are matching well with the reference simulation results and the experimental results according to the comparison illustrated in Figure 4.25 and Figure 4.26. The comparisons with experimental result are illustrated in Figure 4.27. Even under earthquake type loading, every spike in the response could be accurately predicted by the proposed NN based

connection. It is one of the main advantages of using the proposed NN based connection model for representing very complex nonlinear hysteretic behavior of connections and predicting the global response of structures by standard nonlinear dynamic analysis codes.

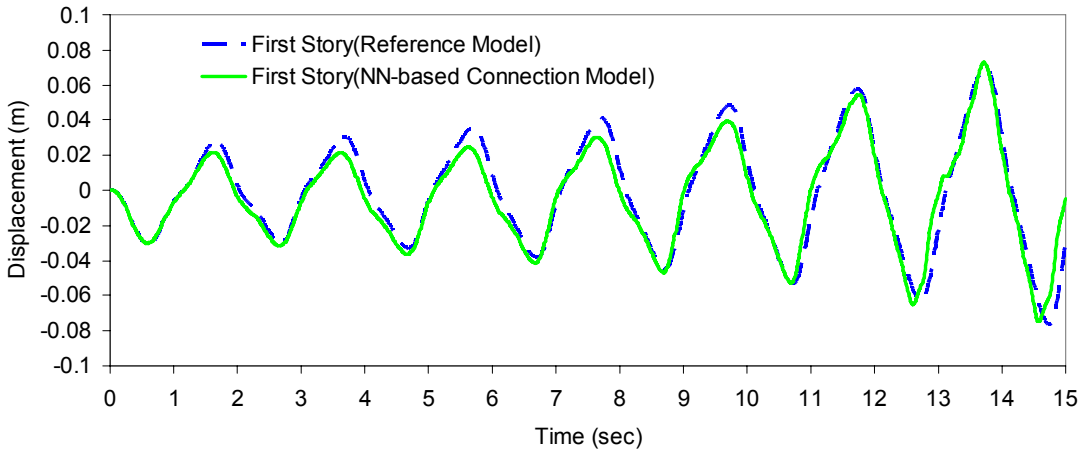

(a) Time History of Horizontal Displacement at the First Floor

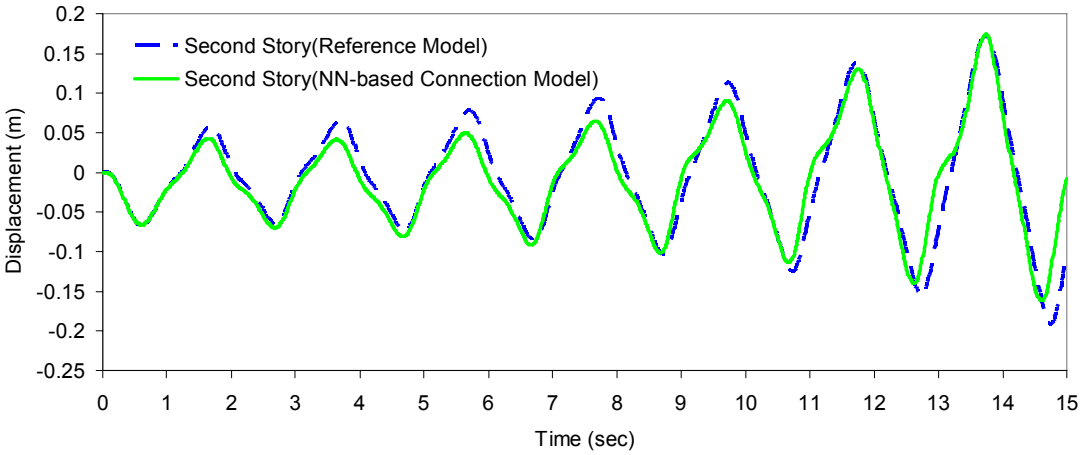

(b) Time History of Horizontal Displacement at the Second Floor

Figure 4.28 Prediction of Response to New Loading Condition

In order to check the generalization of the trained NN based model, totally new input motion (negatively damped harmonic motion) is applied instead of earthquake type loading. Figure 4.28 shows the comparison of the predicted displacement by the NN based connection model with the reference model. This implies that the proposed NN based connection model can be responsive to change of loading history. In the following section, the NN based connection model is applied to plastic hinge.

4.5.4 NN based Plastic Hinge Elements

In this example, the proposed NN based connection model is used by plastic hinge elements of a tubular cantilever. The plastic hinge element is named as NN based plastic hinge element. The primary purpose of this example is to introduce the NN based plastic hinge as a new inelastic analysis method of frame structures in which plastic hinges are formed at the end of the member. The secondary objective of this example is to confirm performance of the proposed NN based plastic hinge element in multi-dimensional problem whereby bi-moments are acting. There are three advantages in the proposed simulation method; 1) the NN based plastic hinge model can represent any complex hysteretic behavior from 3D finite element analysis. 2) The computation of tangent stiffness matrix and internal resisting forces is relatively easier than any existing method. 3) The trained NN based plastic hinge element can be reused and updated with new training data.

4.5.4.1 NN based Plastic Hinge under Monotonic Loading

In order to get training data for the NN based plastic element, three-dimensional finite element analysis is performed using solid element (C3D8) in ABAQUS. The tubular section has diameter, 609.6 mm and thickness, 38.9 mm. The bilinear material model is defined in which Young's modulus is E = 200,000 (MPa); poisson ratio is ν = 0.3; yield stress is σ_y = 248.2 (MPa) and hardening stiffness is 0.02E. The monotonic loading is applied at the tip of tubular column in X direction with the displacement boundary condition.

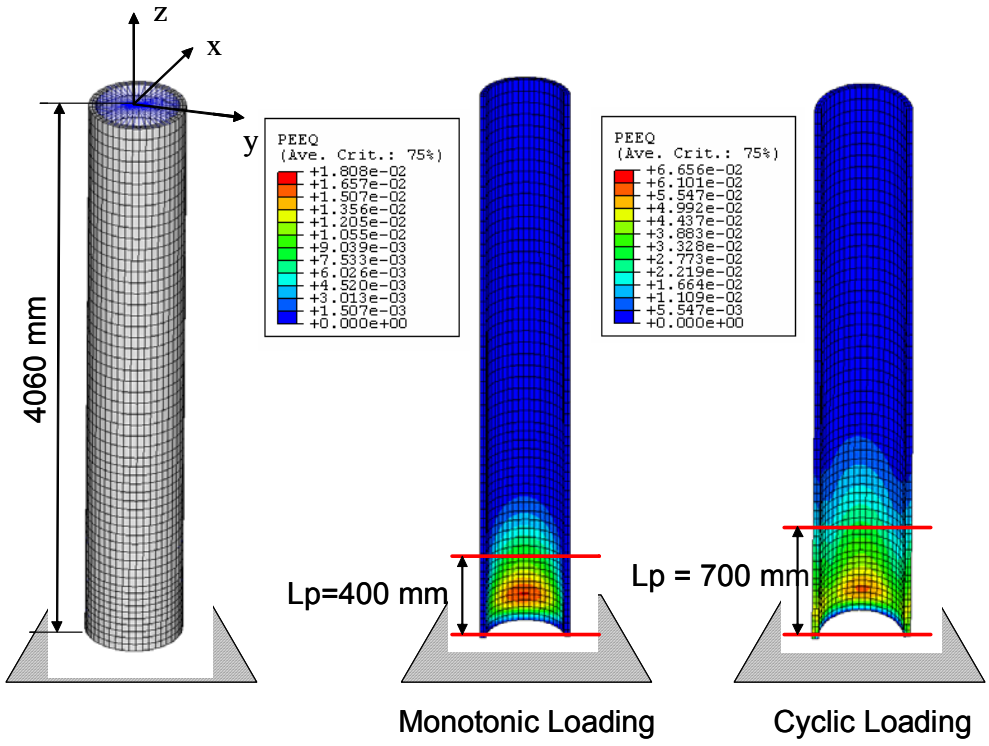

Figure 4.29 Three-Dimensional Finite Element Model and Assumed Plastic Hinge Length for Monotonic and Cyclic Loading (Contour Equivalent Plastic Strain)

To get rotational deformation through the assumed plastic hinge length, three-dimensional decoupling elements are used at then end of plastic hinge. The determined length of plastic hinge is illustrated in Figure 4.29. The moment at the plastic hinge is calculated by multiplying the force by distance from the tip of column to the center of plastic hinge. The moment-rotation data are used to train the NN based plastic hinge element. The training information is summarized in Table 4.4. The NN based plastic hinge is assumed to be initially rigid.

Table 4.4 Training Information of the NN based Plastic Hinge Element

Number of Epochs used in Training	NN Architecture	Average Error in Training
50,000	{4-20-20-1}	3.747×10^{-5}

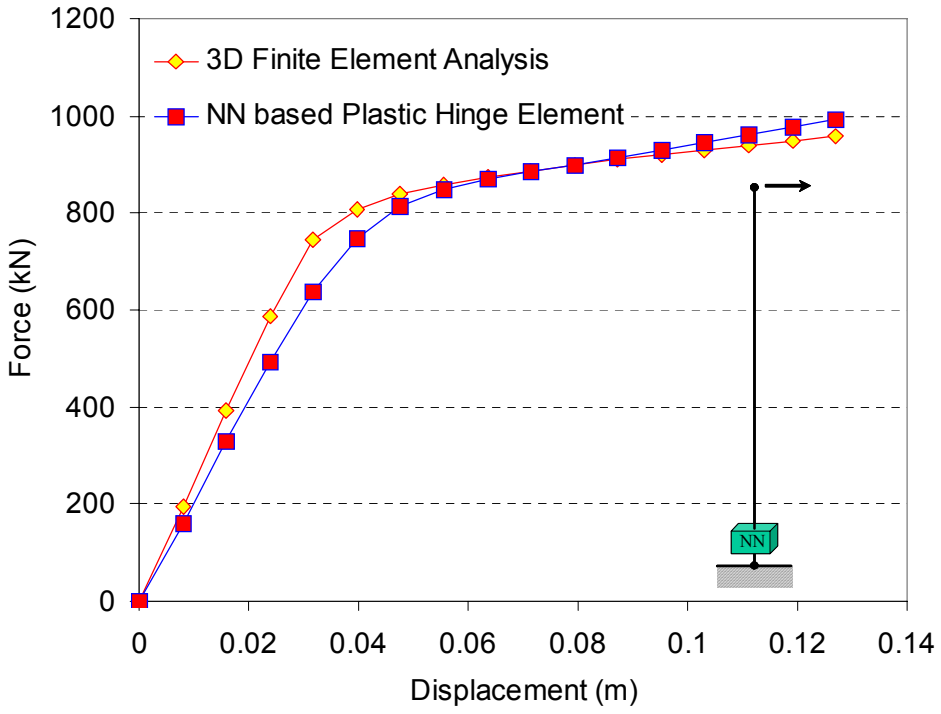

Figure 4.30 Force-Deflection Relationship for X Load Only

After training, the NN based plastic hinge is plugged into beam-column element model for finite element analysis. Figure 4.30 shows good agreement between 3D finite element analysis and NN based plastic hinge element. The training NN based plastic hinge element can be updated with additional information and be reused. It is noteworthy that the application of the NN based plastic hinge element is not limited to steel material only but also extended to concrete and composite material as long as the inelastic deformation is concentrated in the assumed region.

4.5.4.2 NN based Plastic Hinge under Non-Proportional Cyclic Loading

In this example, the same tubular cantilever as the previous example is subject to bi-axial moment actions.

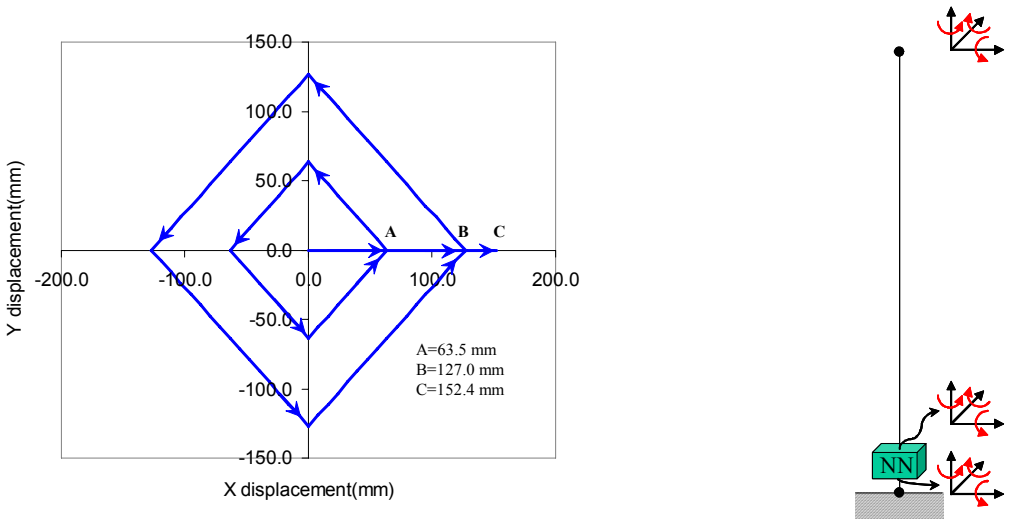

(a) Displacement Path Imposed (b) 3D Numerical Model

Figure 4.31 Loading Path and Numerical Model with NN based Plastic Hinge

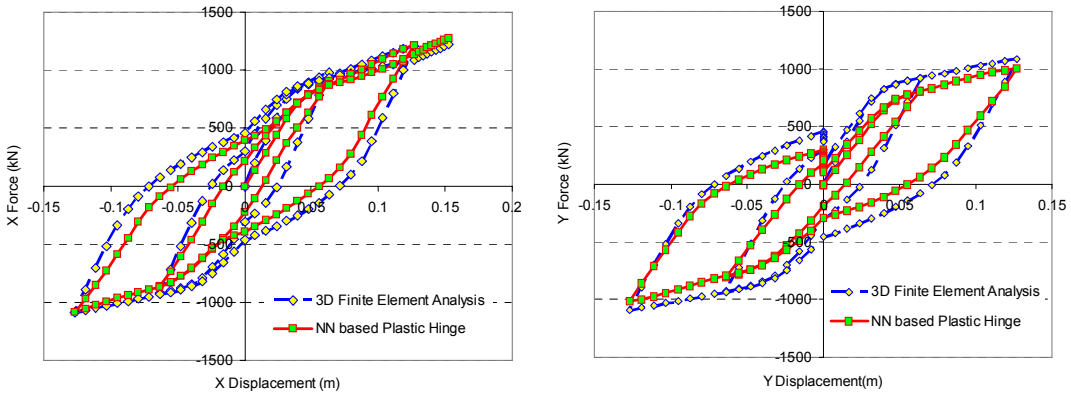

(a) Force-Displacement in X Direction (b) Force-Displacement in Y Direction

Figure 4.32 Comparison of Force-Displacement between 3D FE analysis and NN based Plastic Hinge Model

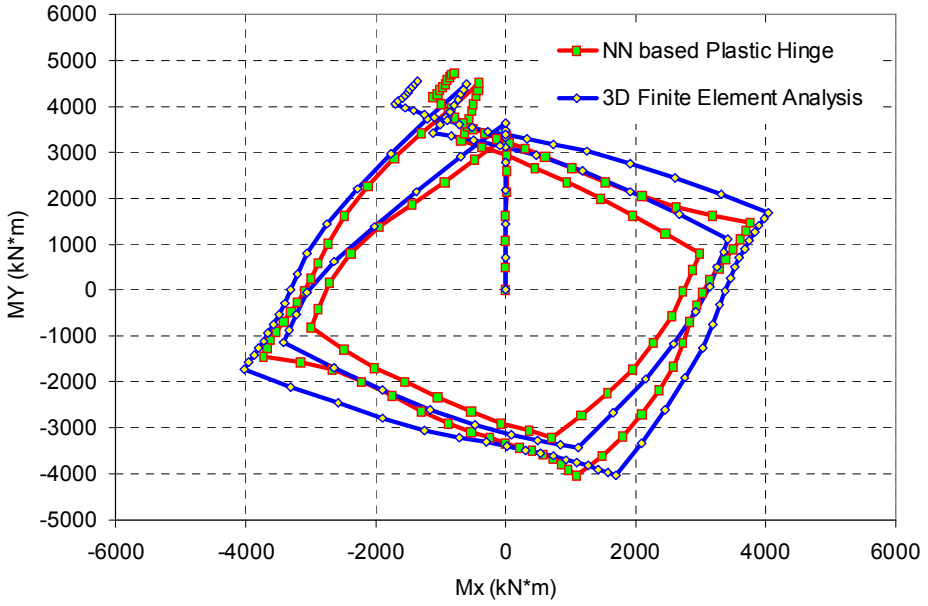

Figure 4.33 Variation of Actions within Yield Surface and Its Comparison with NN based Plastic Hinge Element

From three-dimensional finite element analysis, training data are also generated and the length of plastic hinge is assumed to be 700 mm distance from the support as illustrated

in Figure 4.29. The loading path is described in Figure 4.31 (a). The numerical model employing the NN based plastic hinge element has 18 degrees of freedom as shown in Figure 4.31 (b). The other degrees of freedoms (D_x, R_x, R_y and R_z) at the ends of NN based plastic hinge element except D_x and D_y are constrained. The column is modeled by 3D beam-column element and the same material specification as the previous model is used except the hardening stiffness. In this example, the hardening stiffness is set to 0.1E. The representation of the NN based plastic hinge element can be expressed as follow.

$$\begin{Bmatrix} M_{xn} \\ M_{yn} \end{Bmatrix} = \hat{\mathbf{M}}_{NN}\left(\left\{\theta_{x,n}, \theta_{y,n}, \theta_{x,n-1}, \theta_{y,n-1}, M_{x,n-1}, M_{y,n-1}, \varsigma_{\theta x,n}, \varsigma_{\theta y,n}\right\} : \{8-28-28-2\}\right) \quad (4\text{-}78)$$

Where M_x and M_y indicate moment in x and y direction; θ_x and θ_y rotation in x and y direction, n indicates n-th load step and ζ indicates internal variable for hysteretic behavior. As done in the previous example, the NN based plastic hinge element is assumed to be initially rigid. The training information is summarized as in Table 4.5.

Table 4.5 Training Information of the NN based Plastic Hinge Element

Number of Epochs used in Training	NN Architecture	Average Error in Training
50,000	{4-28-28-1}	9.227×10^{-6}

Figure 4.32 shows reasonable agreements between NN based plastic hinge model and 3D finite element model in both directions. Figure 4.33 shows that the NN based plastic hinge model can reproduce the process of action increments during yield surface updating.

4.6 Conclusions

In this chapter, NN based connection element has been developed for representing complex inelastic hysteretic behavior at connection regions and three-dimensional beam-column element has been formulated with consideration of geometric nonlinearity for second-order analysis. Combining three-dimensional beam-column element with the NN based connection element, nonlinear static and dynamic analysis procedures have been presented. Through a series of numerical examples with semi-rigid beam-column connections, the performance of the developed computer program has been verified and the importance of modeling of nonlinear behavior of connections has been revisited numerically.

Semi-rigid connections in a frame structure are modeled by the NN based connection model which is trained by synthetic data from a simulated testing and the trained NN based connection elements are plugged into finite element model under earthquake loading. According to the test result, not only could the NN based connection model provide accurate response prediction as it's trained but also it could predict dynamic response of the structure under a totally new loading condition. In the last two examples, the NN based connection model is applied in plastic hinge element and a new simulation method has been proposed in which the NN based plastic hinge model is combined with three-dimensional finite element analysis. According to the two tests, the proposed model has been proved to represent cyclic behavior under both uni- and multi-directional actions.

In summary, the unique advantages of the proposed model are that 1) It can represent complex inelastic hysteretic behavior 2) It can be used to solve new problems when it is

trained with comprehensive data and 3) Its numerical implementation is very efficient compared to any conventional connection model.

CHAPTER 5 SELF-LEARNING SIMULATION FRAMEWORK FOR DEVELOPMENT OF INELASTIC HYSTERETIC CONNECTION MODELS

5.1 Introduction

Behavior of connections significantly affects global responses of assembled structures subjected to cyclic or dynamic loadings. The connections are often the primary source of energy dissipation due to hysteretic damping and lead to significant changes in local stiffness and strength. In order to develop models for the connections, structural tests on the connections or systems have to be conducted. Although the local nonlinear behavior can be directly measured during structural tests and used to model the connections, the measurement results can become unreliable after exceeding the stability limit. For example, measuring apparatus such as strain gauges may not work properly any more under severely damaged conditions. Moreover, since responses of the assembled structures are of our primary interest, a methodology to characterize the local nonlinear behavior of connections from structural tests would be the most desired option. The modeling task of the connection behaviors from structural tests can be described in the context of complex inverse problems.

The neural network (NN) based model offers the potential for developing accurate and reliable models of the inelastic hysteretic behavior of material and structural components. The concept of NN constitutive models was first introduced by Ghaboussi, et al. (Ghaboussi, et al. 1991). In this chapter, the new NN based cyclic material model proposed by Yun, et al. (Yun, et al. 2006b) is used. However, the usual modeling of the material behavior with NNs requires the results of comprehensive material tests that may

not always be available, and in some case not possible. To facilitate the use of the NN based material model, auto-progressive training algorithm was proposed by Ghaboussi, et al. (Ghaboussi, et al. 1998a). It can perform on-line training of the NN based material model through the incorporation of experimental measurements with usual incremental nonlinear finite element analysis. This simulation methodology has been recently studied on the development of the constitutive model for soil (Sidarta and Ghaboussi 1998; Shin and Pande 2000; Hashash, et al. 2003).

This chapter presents a novel self-learning simulation framework to characterize the cyclic behavior of connections from structural tests; from its numerical implementations to applications to real experimental data. The proposed self-learning simulation framework is a new extension of the original auto-progressive training algorithm proposed by Ghaboussi, et al. (Ghaboussi, et al. 1998a). Owing to flexible learning capabilities of NNs, the proposed connection models can reproduce the actual cyclic response of the connection that may experience buckling, nonlinear frictional slip, fracture, slacking of fastened bolts as well as yielding of materials. Following the development of the new NN based cyclic connection model, the model is first ever applied in self-learning simulation mechanics in this chapter. In the following section, an overview on the self-learning simulation will be introduced and it is followed by detailed numerical implementations regarding the self-learning simulation and use of the NN based material model in standard finite element codes.

5.2 Self-Learning Simulation Framework

5.2.1 Numerical Procedures for Self-Learning Simulation

Self-learning simulation algorithm enables extracting the connection behavior directly from the global response of structures, (Ghaboussi, et al. 1998a; Sidarta and Ghaboussi 1998). Based on the parallel analysis scheme suggested by Hashash, et al. (Hashash, et al. 2003), the self-learning simulation framework has been developed in this report. Since its application is for developing the NN based inelastic hysteretic connection model, the simulation framework is constructed on nonlinear frame analysis program developed in this report. The overall flowchart for numerical procedures of the self-learning simulation is illustrated in Figure 5.1. There are three notable features in the numerical procedures; 1) Two parallel iterative procedures are performed, that is, Step I and Step II. 2) There is additional iterative loop called auto-progressive cycles between the loop for load increments and the loop for equilibrium iterations. 3) The outermost loop is for NN Pass which is one complete pass of all the load increments. It is intended to find better training data base for the NN based model by restarting the whole analysis with the latest NN based model and training data base.

Evolution of the NN based model is mainly attributed to the auto-progressive cycles. It is true that the auto-progressive cycle plays an essential role in evolving the NN based connection model during self-learning simulation because it directly makes the NN based model able to learn realistic behavior of connections through updating training data base followed by training. One specific auto-progressive cycle is illustrated in Figure 5.2. In order to develop a NN based connection model from structural testing, a set of

experimental measurements at control points in a tested specimen are required, for example, force and displacement history. The NN based connection model is trained during the computational simulation of the structural experiment. One auto-progressive cycle is completed by 1) conducting Newton-Raphson iterations of two FE models in Step I and Step II, 2) appending a new input pattern to training data base, 3) training the NN based model with the updated training data base and 4) checking criteria to stop the auto-progressive cycles. To avoid confusion in the following description, iteration means Newton-Raphson iteration and cycle means auto-progressive cycle.

At each load step (or time step) two FE analyses are performed: in the first FE analysis (called as Step I or FEM-A later) the measured forces are applied; and, in the second FE analysis (called as Step II or FEM-B later) the measured displacements are enforced. It is stipulated that the stress resultant vector in Step I represent acceptable approximation of the actual stress resultant vector, while the displacement vector in Step II is considered to be a good approximation of the actual displacement vector. At the end of iteration of the current cycle of the current load increment, the stress resultant vector from Step I and the displacement vector from Step II are appended into a training data base and the NN based connection model is retrained with the updated training data base. In the next auto-progressive cycle of the current load increment, the NN connection weights are kept but the last input pattern will be replaced by a new input pattern obtained in the next auto-progressive cycle. If the given criteria are satisfied, the auto-progressive cycle is stopped and the auto-progressive cycle continues for the next load increment. If they are not satisfied, the cycle continues. One complete pass for all the

load increments is called a Pass, and several passes may be required to completely train the NN based connection model.

In the following section, important issues relating to the self-learning simulation are described; Pre-training of the NN based model, Specific criteria for auto-progressive cycle, and Static and dynamic forward analysis.

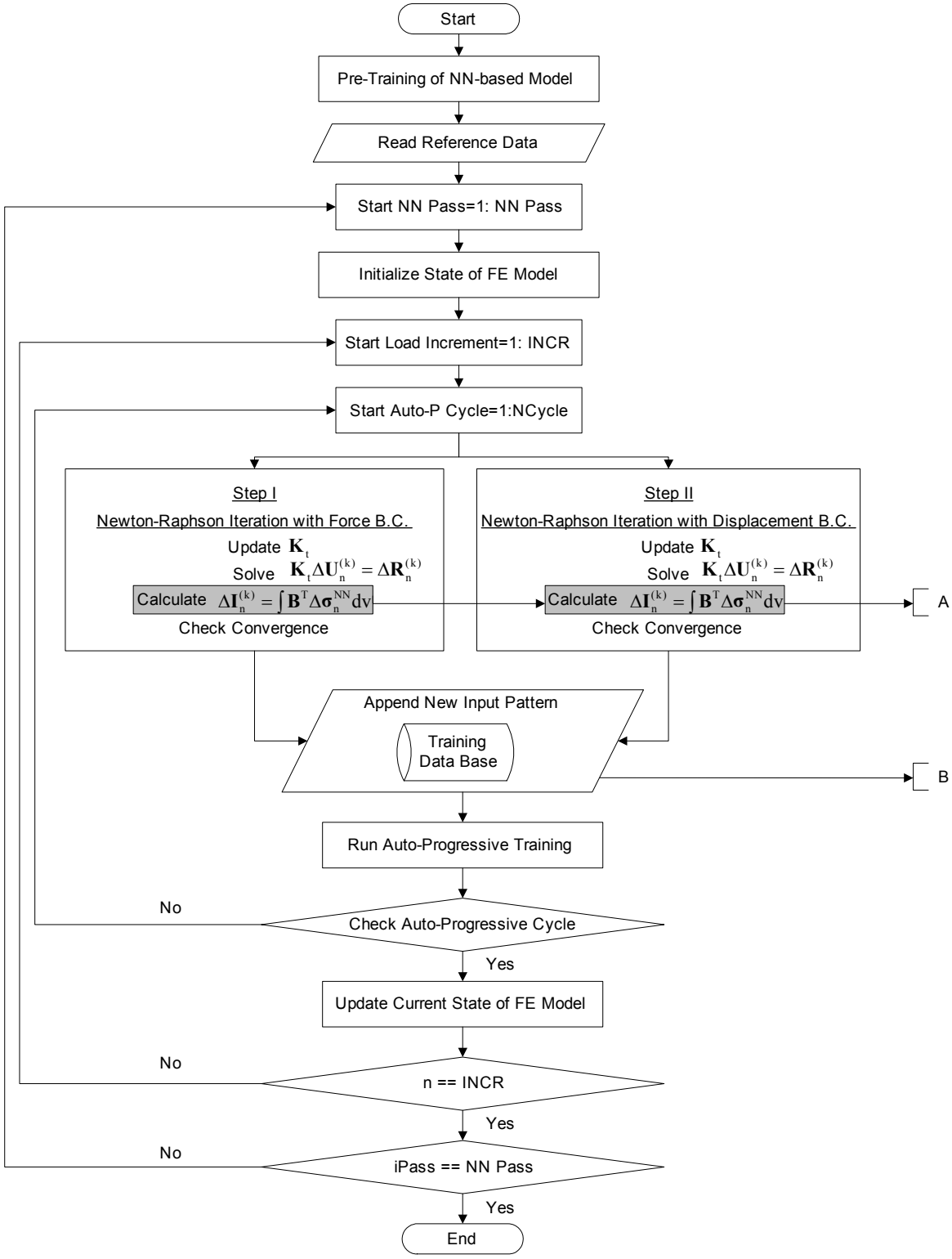

Figure 5.1 Flow Chart of Self-learning Simulation

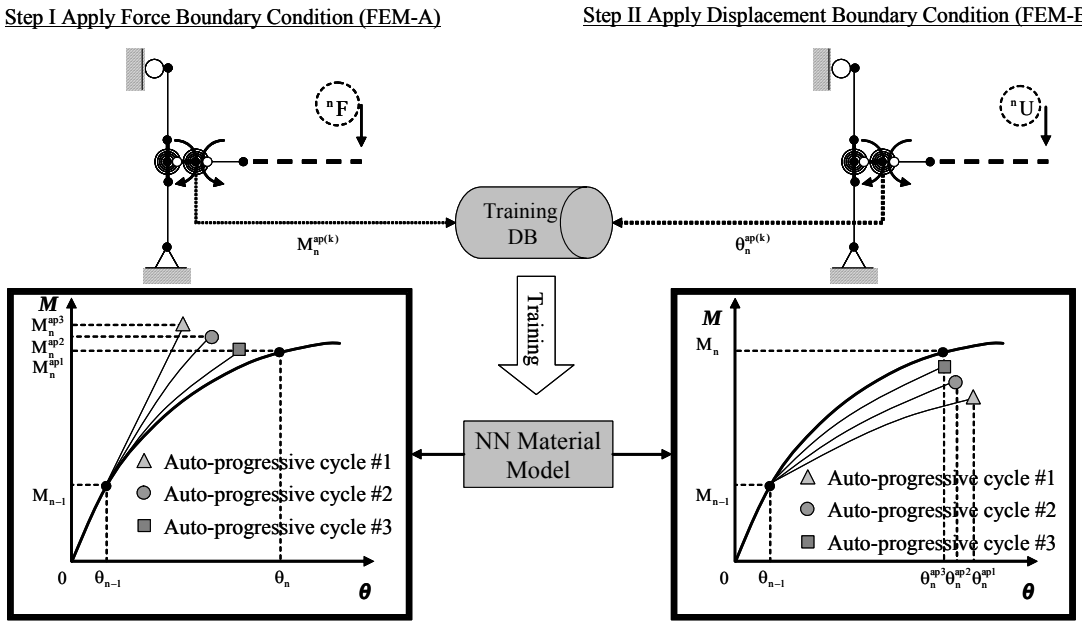

Figure 5.2 Auto-progressive Cycle

5.2.2 Pre-Training of Neural Network based Connection Model

Initial behavior of complex steel beam-column connections can not be easily defined while the linear elastic material assumption with Young's modulus and poisson ratio has been frequently used for pre-training the NN based material model. Fortunately, there are data bank and software available for calculating initial rotational stiffness and plastic flexural resistance of any type of beam-column connections (Weinand 1992; Kishi and Chen 1986). However, other pre-training data could be used for the NN based connection model as long as they give better approximation to initial stiffness than any other approximation. In this report, JMRC software is used to evaluate initial rotational stiffness of connections. For the proposed NN based model, very small range of stress resultants and displacements are selected and input patterns are automatically generated

in the research code. The pre-training data are enriched with additional data generated by varying the load step of the first load increment both in loading and unloading direction.

5.2.3 Criteria for Auto-progressive Cycle

The auto-progressive cycles are usually performed three to five cycles per each load increments. The auto-progressive cycles continues until a displacement error is satisfied with a user-defined tolerance. The displacement error is defined as the displacement difference between Step I and Step II. The displacement error is calculated as following.

$$\frac{\left\|\mathbf{U}_{\text{Step I}} - \mathbf{U}_{\text{Step II}}\right\|_{\max}}{\left\|\mathbf{U}_{\text{Step II}}\right\|_{\max}} < tol\_max \quad \text{or} \quad \frac{\sum_{i=1}^{\text{NRef}} \left\|\mathbf{U}_{\text{Step I}} - \mathbf{U}_{\text{Step II}}\right\|_i \Big/ \text{NRef}}{\left\|\mathbf{U}_{\text{Step II}}\right\|_{\max}} < tol\_avg \qquad (5\text{-}1)$$

where $\| \ \|$ represents Euclidean norm; $\mathbf{U}_{\text{step I}}$ and $\mathbf{U}_{\text{step II}}$ are displacement vectors from Step I and Step II, respectively; tol_max and tol_avg are user-defined tolerance for maximum error and average error, respectively and NRef indicates the total number of control points in tested specimen. The criteria are evaluated at all of the control points for calculating the max and average norm of the displacement vector.

5.2.4 Static and Dynamic Forward Analysis

After training the NN based connection model through the self-learning simulation, the NN based model can be used within nonlinear static and dynamic simulation codes as substitutes for any phenomenological model. This subsequent analysis following the self-learning simulation is called forward analysis. In this report, the NN based connection model can be trained in nonlinear static analysis mode. If any accurate experimental

result is available and the NN based connection model is trained directly from the experimental result, the NN based model also can be used in nonlinear dynamic analysis. In this report, nonlinear static analysis with the NN based model is named as static forward analysis and nonlinear dynamic analysis with the NN based model is named as dynamic forward analysis.

5.3 Algorithmic Formulation of NN based Model in Self-learning Simulation

During auto-progressive training of the self-learning simulation, the NN based connection model is used instead of any existing phenomenological connection model. A material package for the NN based connection model does two important roles like the existing model; 1) Calculation of the increment of the internal resisting force vector corresponding to the increment of displacement vector at the current iteration step and 2) Calculation of tangent stiffness matrices at the current iteration step. However, the NN based connection model does not need any design interaction equation or yield surface in stress resultant space while existing phenomenological model requires them for calculating predictor stress resultant and tangent stiffness matrix subsequently. Therefore, it is relatively easier to implement the NN based connection model in finite element codes than any other phenomenological based hysteretic models.

For the calculation of the above two quantities, forward propagations of input patterns through the trained NN are required within the material package. It is noteworthy that there are two algorithmic formulations for the forward propagations within the self-

learning simulation. Efficiencies of the variations are evaluated. The different algorithmic formulations are summarized in Table 5.1 and Table 5.2.

Table 5.1 Two Different Algorithmic Formulations for NN Forward Propagation in Step-I (FEM-a) of Self-learning Simulation

	Calculation of Tangent Stiffness	Calculation of Internal Resisting Force
Case I	$F_{NN}^{(i)} = \hat{F}_{NN}\left(U_n^{b(i)}, U_{n-1}^{b}, F_{n-1}^{a}, \xi_{U,n}^{ab}, \Delta\eta_{U,n}^{ab}; \{NN\}\right)$	$F_{NN}^{a(i)} = \hat{F}_{NN}\left(U_n^{a(i)}, U_{n-1}^{a}, F_{n-1}^{a}, \xi_{U,n}^{a}, \Delta\eta_{U,n}^{a} : \{NN\}\right)$
Case II	$F_{NN}^{(i)} = \hat{F}_{NN}\left(U_n^{a(i)}, U_{n-1}^{a}, F_{n-1}^{a}, \xi_{U,n}^{a}, \Delta\eta_{U,n}^{a} : \{NN\}\right)$	$F_{NN}^{a(i)} = \hat{F}_{NN}\left(U_n^{a(i)}, U_{n-1}^{a}, F_{n-1}^{a}, \xi_{U,n}^{a}, \Delta\eta_{U,n}^{a} : \{NN\}\right)$

Table 5.2 Two Different Algorithmic Formulations for NN Forward Propagation in Step-II (FEM-b) of Self-learning Simulation

	Calculation of Tangent Stiffness	Calculation of Internal Resisting Force
Case I	$F_{NN}^{(i)} = \hat{F}_{NN}\left(U_n^{b(i)}, U_{n-1}^{b}, F_{n-1}^{a}, \xi_{U,n}^{ab}, \Delta\eta_{U,n}^{ab}; \{NN\}\right)$	$F_{NN}^{b(i)} = \hat{F}_{NN}\left(U_n^{b(i)}, U_{n-1}^{b}, F_{n-1}^{b}, \xi_{U,n}^{b}, \Delta\eta_{U,n}^{b} : \{NN\}\right)$
Case II	$F_{NN}^{(i)} = \hat{F}_{NN}\left(U_n^{b(i)}, U_{n-1}^{b}, F_{n-1}^{b}, \xi_{U,n}^{b}, \Delta\eta_{U,n}^{b} : \{NN\}\right)$	$F_{NN}^{b(i)} = \hat{F}_{NN}\left(U_n^{b(i)}, U_{n-1}^{b}, F_{n-1}^{b}, \xi_{U,n}^{b}, \Delta\eta_{U,n}^{b} : \{NN\}\right)$

The key role of the auto-progressive training cycle is to narrow the displacement error between force controlled analysis (Step I or FEM-a) and displacement controlled analysis (Step II or FEM-b). Although the self-learning simulation usually starts with pre-training data generated within a small linear elastic range, the error comes from undefined behavior of the NN based connection model beyond the range. Testing of the two different cases in self-learning simulation is demonstrated in the following section.

5.3.1 Comparison of Two Algorithmic Formulations in Self-learning Simulation

In order to investigate the efficiency of the two different algorithmic formulations, self-learning simulations are carried out. A one-bay and two-story steel moment-resisting

frame is selected for a testing model (Stelmack, et al. 1986). The frame has semi-rigid connections with bolted angles as shown in Figure 5.3. In order to eliminate any modeling error related to connections and support conditions between the tested structure and its numerical model, synthetic data from simulated testing results are used as reference data. The semi-rigid connections are modeled by Ramberg-Osgood Model with the initial rotational stiffness of 4,520 (kN-m) and yielding moment of 14.69 (kN-m) as the reference (Stelmack, et al. 1986). The Ramberg-Osgood parameter (n) relating to the shape is set to 5.0. For numerical modeling of the tested structure, one beam-column element per each beam and column is used and the NN based connection model is used to represent the moment-rotation behavior and placed at the column face. The geometrical nonlinearity is not considered since P-Δ effect is not significant.

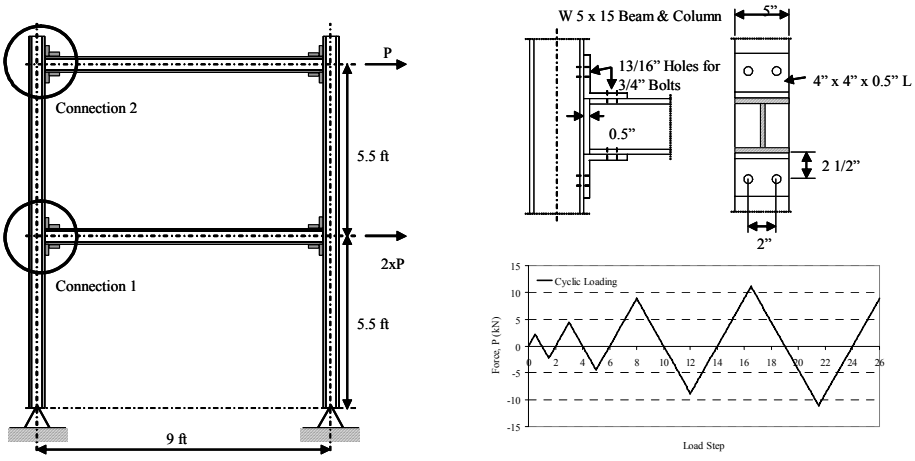

Figure 5.3 Two-story Frame Structure with Semi-Rigid Connections (Stelmack, et al. 1986)

For a loading condition, a cyclic loading with continuously increasing amplitudes as shown in Figure 5.3 is applied with total 260 load steps. Single NN group is used to

represent the four NN based connection models because the nonlinear moment-rotational behaviors of connections at the first and second story are similar except the range of moments and rotations. The parameters used in self-learning simulations are also summarized in Table 5.3. For the two cases, the same parameters were used for exact comparisons.

Table 5.3 Parameters used in Self-learning Simulation

	Parameters used in Self-learning Simulation	
Number of NN Pass tried	6	
Number of auto-progressive cycles in each load step	3	
Criteria for the auto-progressive cycle	Tol_avg	0.005
	Tol_max	0.005
NN architecture	{4-15-15-1}	
Scale factors used	$abs(\theta^n, \theta^{n-1}, M^{n-1}, \varsigma^n, M^n)$ $< (0.15, 0.15, 150.0, 22.5, 150.0)$	

According to self-learning simulation results, if input patterns for calculation of internal resisting force vector consist of force from Step-I and displacement from Step-II, the auto-progressive training was failed during the first NN Pass because of inconsistency in calculating internal resisting force vectors. Evidently, such input patterns for internal resisting force vector can not keep consistency in self-learning simulation. Therefore, the results from the input pattern could not be obtained. This means that consistency in calculation of the internal resisting force vector is very important during self-learning simulation.

The self-learning simulation was successfully completed up to the sixth NN Pass in both Case I and Case II. The static forward analysis results from Case I and Case II are displayed from Figure 5.4 to Figure 5.7. The moment-rotation hysteretic curves at both connection 1 and connection 2 are compared.

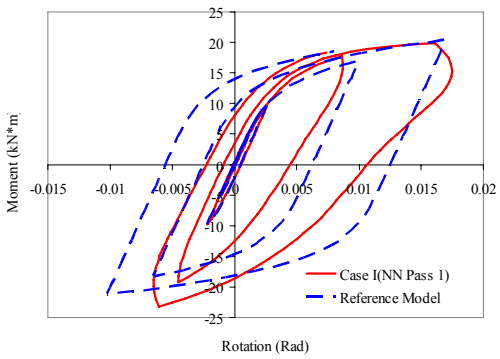

(a) NN Pass 1

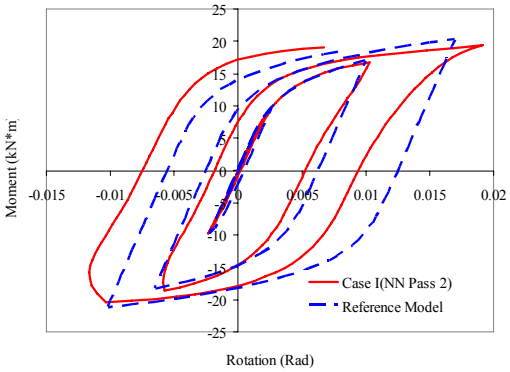

(b) NN Pass 2

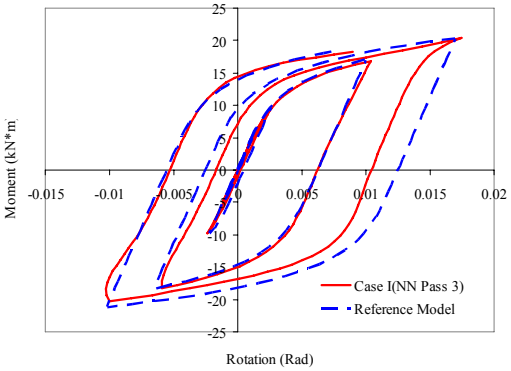

(c) NN Pass 3

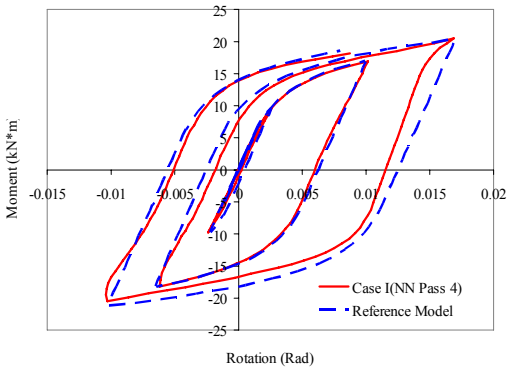

(d) NN Pass 4

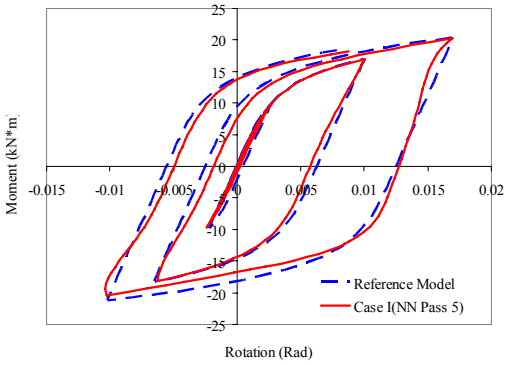

(d) NN Pass 5

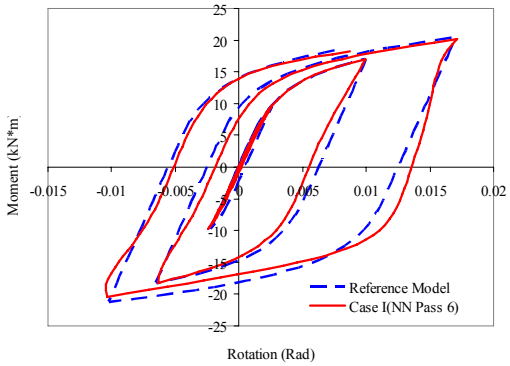

(e) NN Pass 6

Figure 5.4 Moment-Rotation of Connection 1 from Static Forward Analysis: Case I

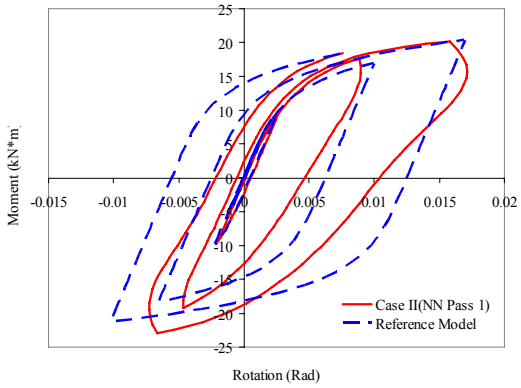

(a) NN Pass 1

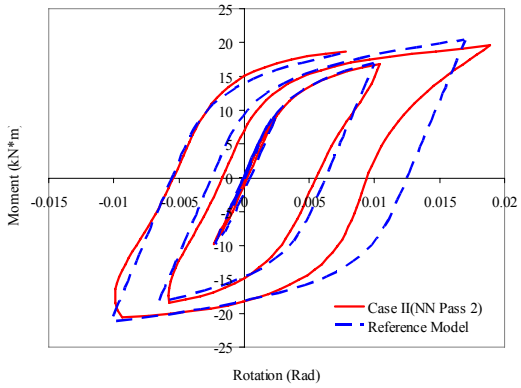

(b) NN Pass 2

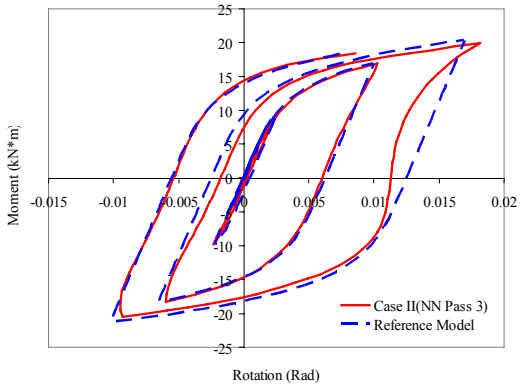

(c) NN Pass 3

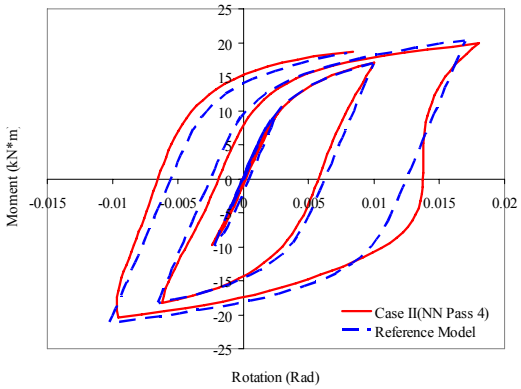

(d) NN Pass 4

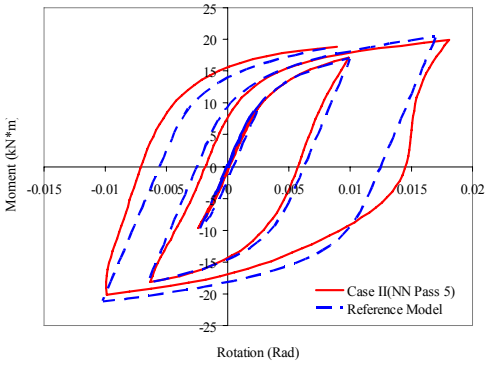

(d) NN Pass 5

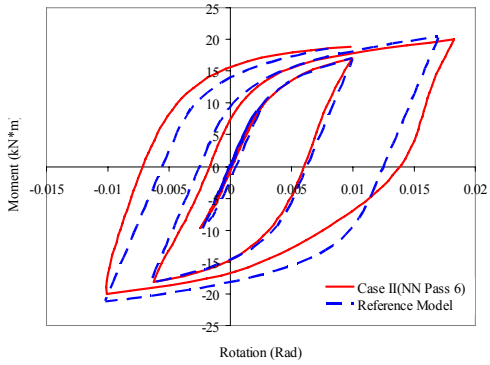

(e) NN Pass 6

Figure 5.5 Moment-Rotation of Connection 1 from Static Forward Analysis: Case II

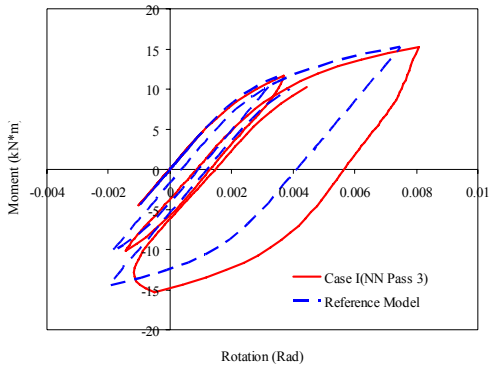

(a) NN Pass 3

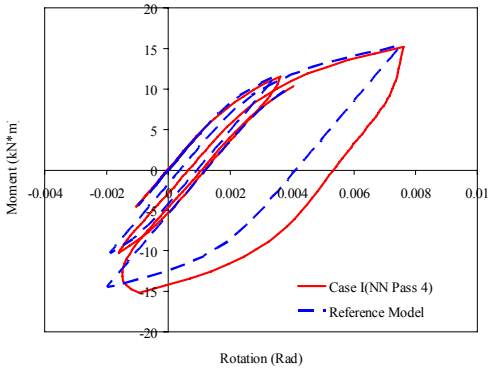

(b) NN Pass 4

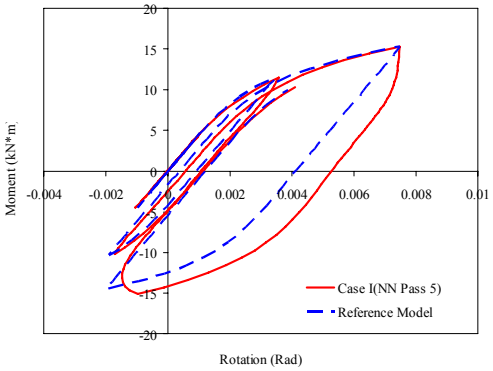

(c) NN Pass 5

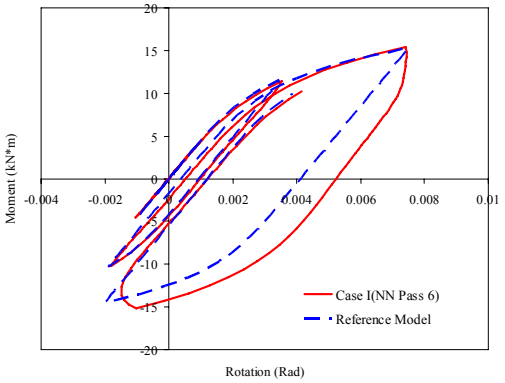

(d) NN Pass 6

Figure 5.6 Moment-Rotation of Connection 2 from Static Forward Analysis: Case I

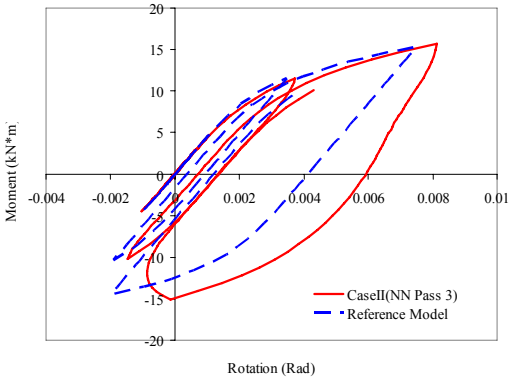

(a) NN Pass 3

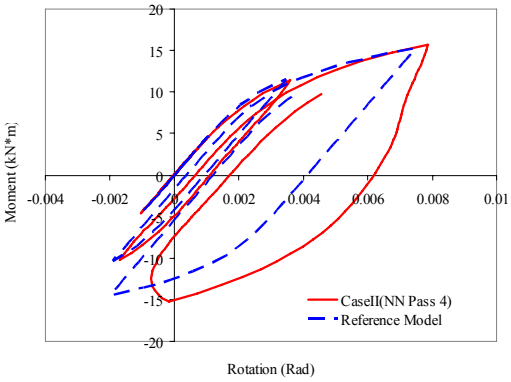

(b) NN Pass 4

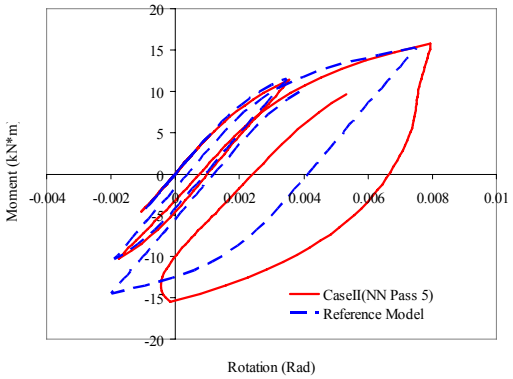

(c) NN Pass 5

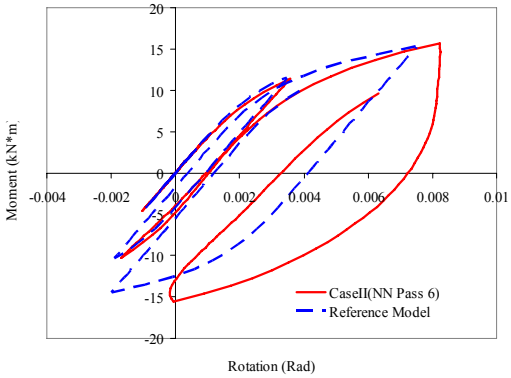

(d) NN Pass 6

Figure 5.7 Moment-Rotation at Connection 2 from Static Forward Analysis: Case II

As the number of NN Passes increases, the NN based connection model gradually learns the nonlinear cyclic behavior of the reference model in the two cases. It implies that the consistent tangent stiffness calculated by the trained NN based model becomes more close to exact tangent stiffness as the auto-progressive training is carried out. It was observed that Case I shows gradual improvements in Connection 2 as opposed to exacerbations in Case II.

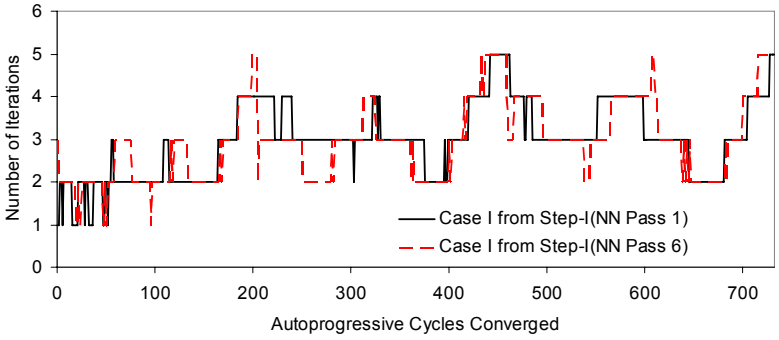

(a) Step I in Case I

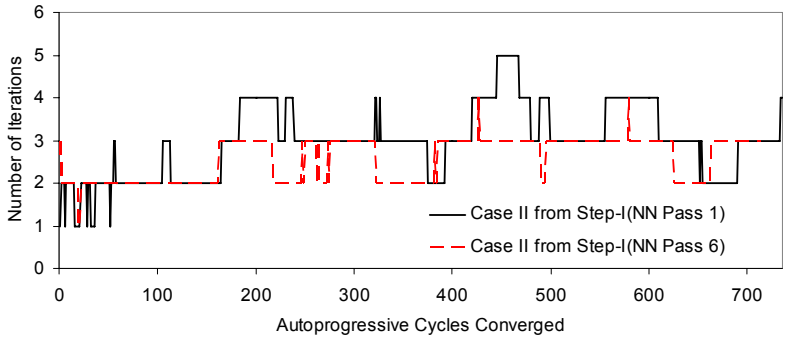

(b) Step I in Case II

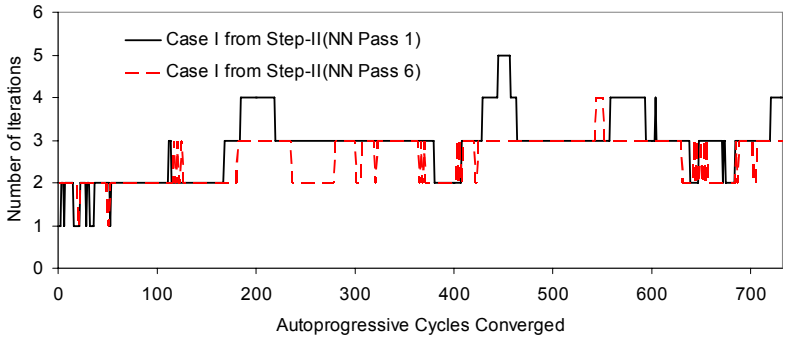

(c) Step II in Case I

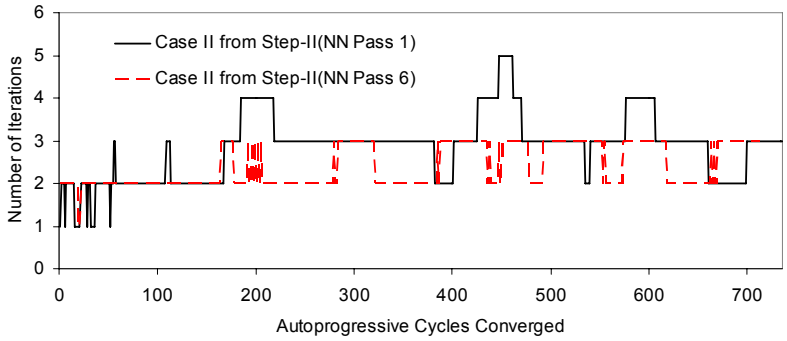

(b) Step II in Case II

Figure 5.8 Number of Iterations for Converged Solutions versus Auto-progressive Cycles Converged (Total Number of Load Step = 260)

However, it can not be fully ensured that the differences are purely caused by the differences in input patterns. During self-learning simulations, the number of iterations for each auto-progressive cycle is plotted in Figure 5.8. The number of iterations is plotted for only converged auto-progressive cycles. As shown in Figure 5.8, most of the cycles are converged within less than 5 iterations. When comparing between NN Pass 1 and NN Pass 6, the number of iterations are obviously reduced in NN Pass 6. When comparing between Case I and Case II, Case II showed less number of iterations than that of Case I at the sixth NN Pass. It is noteworthy that the convergence rate increases as the number of NN Pass increases.

5.3.2 Sensitivity to Load Step Size of the NN based Model

In this example, sensitivity of Case I and Case II to load step sizes is investigated with the same example as that of the previous section. Less sensitive feature of the NN based model to load step size is very important because uses of the NN based model in nonlinear finite element code require interpolative or extrapolative capabilities during simulations due to the recurrent uses of the NN based model. For this investigation, the loading step size has become two (total 130 load steps) and three (total 65 load steps) times larger than the original one and a series of the self-learning simulations are carried out. The obtained NN based models from the self-learning simulation are reused in static forward analysis and their performance are compared as follows.

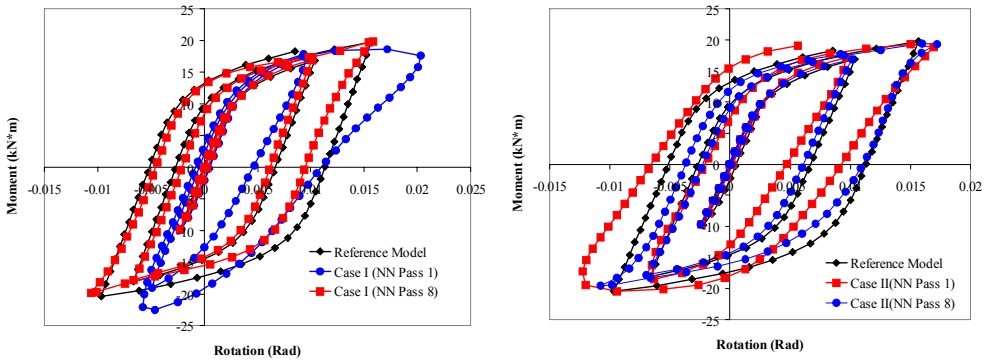

(a) Case I (b) Case II

Figure 5.9 Moment-Rotation from Static Forward Analysis in case of 130 Load Steps

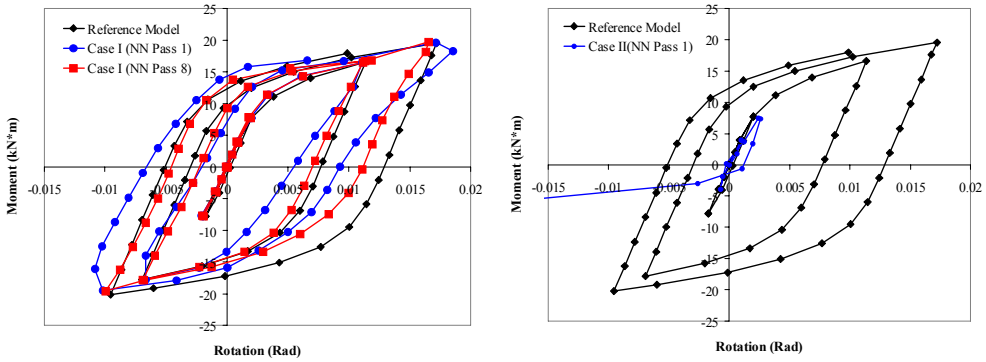

(a) Case I (b) Case II

Figure 5.10 Moment-Rotation from Static Forward Analysis in case of 65 Load Steps

As illustrated in Figure 5.9 and Figure 5.10, Case I was successfully completed in the self-learning simulation up to the eighth NN Pass with the two different load step sizes while Case II failed in the last load step size as shown in Figure 5.10(b). In case of 65 load steps, the number of iterations versus auto-progressive cycle converged are shown in Figure 5.11.

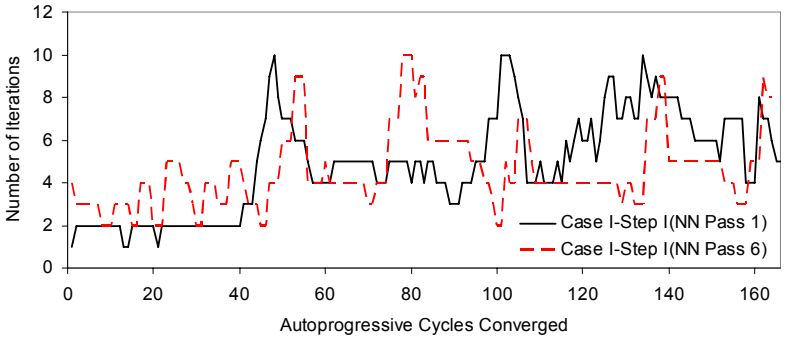

(a) Step I in Case I

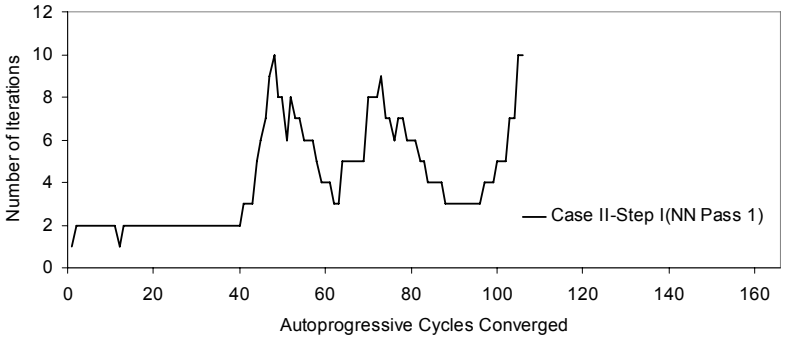

(b) Step I in Case II

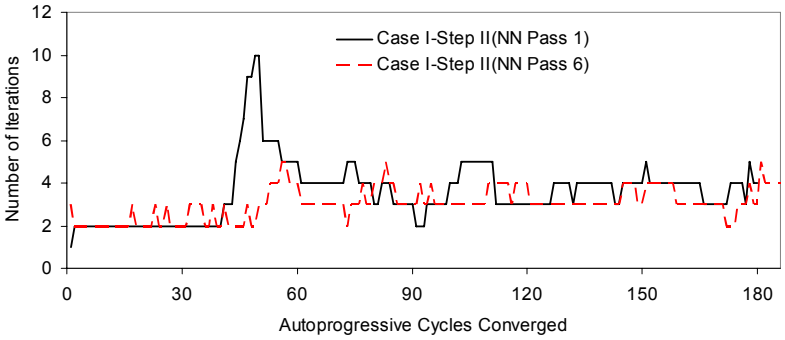

(c) Step II in Case I

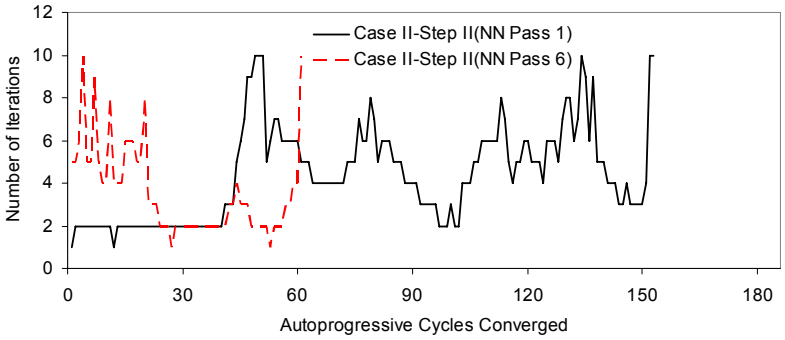

(b) Step II in Case II

Figure 5.11 Number of Iterations versus Auto-progressive Cycles Converged (Total Number of Load Step = 65)

As shown in Figure 5.11(a) and (c), the number of iterations for converged solutions per each cycle in Case I was reduced as the number of NN Pass increased from NN Pass 1 to NN Pass 6. As opposed to Case I, many cycles could not reach converged solutions in Case II. Particularly, even one of the cycles at sixth NN Pass of Step-I with Case II input patterns was not converged as shown in Figure 5.11(b).

5.3.3 Observations and Discussions

There are two important observations in the self-learning simulation using synthetic experimental data with different input patterns and load step sizes. Input pattern of Case I gave better trained NN based connection model than that of Case II as opposed to the fact that Case II resulted in faster convergence than that of Case I. However, when larger load step sizes (total number of load steps = 65) were used, the Newton-Raphson iterations in Step-I and Step-II module failed to converge with input patterns of Case II. As opposed

to failure of Case II in the self-learning simulation, trained NN based connection model could be obtained with input patterns of Case I.

Based on the observations, the mechanism in the auto-progressive training can be attributed to two important concepts which are ‘directionality’ and ‘consistency’ of the NN based connection model. The directionality is associated with building the trained NN data base by stress resultant data from Step I and displacement data from Step II as in Figure 5.13. As such, the NN based connection model can be gradually trained to follow the realistic behavior of connections. On the other hand, the consistency is associated with calculating the current internal resisting forces using the independent input pattern as in 2) of Figure 5.12. It consists of the stress resultants and displacements calculated in the current iteration module, that is, either Step-I or Step-II only. The detailed numerical procedures within NN based connection model package is illustrated in Figure 5.12.

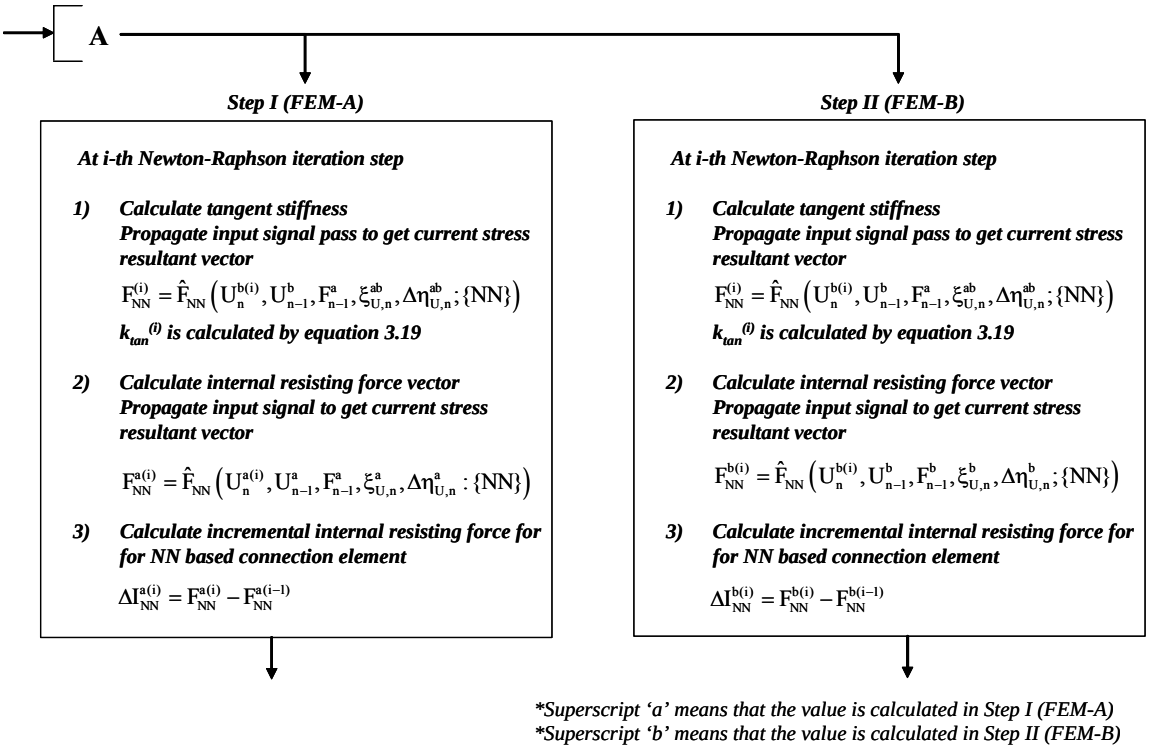

Figure 5.12 Numerical Procedure for NN based Connection Model in Self-learning Simulation

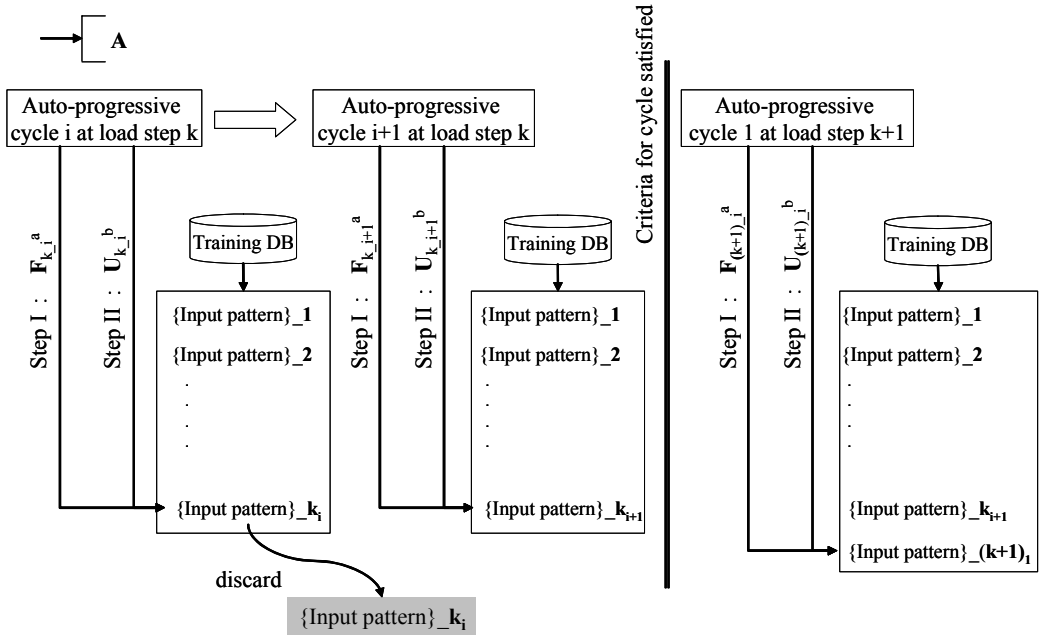

Figure 5.13 Building of Training Data Base during Self-learning Simulation

The observation implies that Case I establishes better algorithmic formulation to the NN based connection model than Case II with large load step size. Therefore, Case I with standard Newton-Raphson iterative scheme is used throughout this dissertation. Even though other parameters relating to NNs can affect the performance of the NN based model, the effect of the other parameters are minor and they are inherent parameters when NN is used in material constitutive modeling. Such parameters include scale factors, number of neurons in hidden layers, number of epochs for training.

5.4 Self-Learning Simulation with Experimental Data

In this example, self-learning simulations are carried out with real experimental data on half of a two-story steel frame with semi-rigid connections.

5.4.1 Testing of Semi-Rigid Frame and Its Observations

The tested structure introduced in section 4.5.3 is used in the self-learning simulation (Elnashai, et al. 1998; Takanashi, et al. 1992). The frame with top-and-seat-angle-with-double-web-angle (TSADW) connections was tested under a cyclic loading with a static testing procedure. The test (SRB02) was carried out using a hybrid load-displacement control procedure to simulate the first mode response. The second floor actuator was used to impose a horizontal displacement history and the actuator restoring force was measured. It was used to drive the first floor actuator so that the ratio of actuator forces at the second and the first floor was maintained at 2:1. This could ensure the first-mode-

dominated response during the testing. The testing was paused several times at the zero force position for allowing visual inspection of the connection components. Interrupt of testing could be one of the sources of uncertainties and variations in the observed responses.

According to the test results on SRB02, pinching of the force-displacement hysteresis loop was observed at the displacements larger than 8 cm because of yielding and separation of connection angles. However, the test results showed very stable hysteretic behavior up to the end of the testing.

5.4.2 Self-learning Simulation with NN based Connection Model

Based on the observations from the test, two finite element (FE) models with NN models are tested. The first FE model consists of three NN based connection models placed at the locations of the connections and column base as shown in Figure 5.14. The three NN models are independently trained during self-learning simulations, that is, they do not share training data base with one another. The second FE model consists of six NN based connection models and they are classified into three NN groups according to sign of bending moments and their magnitudes as shown in Figure 5.15. Two control points at the ends of beams are used to impose the displacement and force boundary conditions. Total 38 three-dimensional beam-column elements are used in the model. For the simulations, the geometrical nonlinearity is considered. In the case of the first FE model, total number of degrees of freedom is 97 and 88 before and after constraining degrees of freedom at the nodes of connections, respectively. The material is defined by Young's modulus of 2.08×10^8 (kN/m^2) and poisson ratio of 0.3.

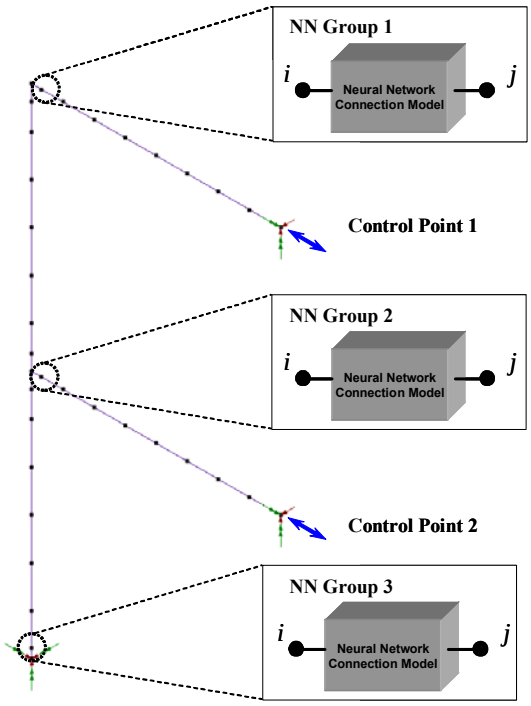

Figure 5.14 Nonlinear Finite Element Model I for Self-Learning Simulation

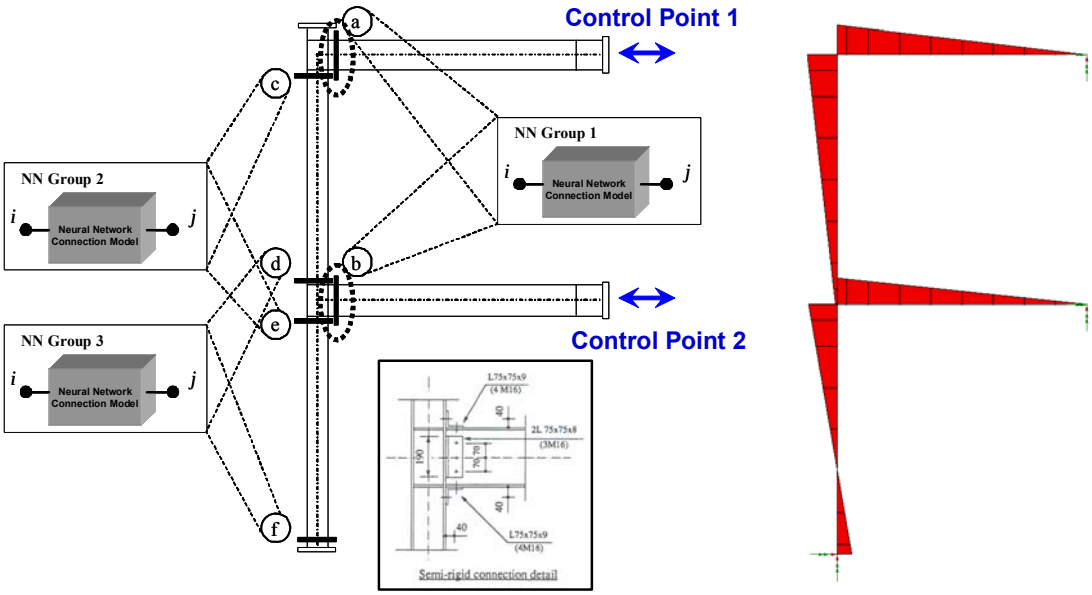

Figure 5.15 Nonlinear Finite Element Model II for Self-Learning Simulation

The force and displacement measurements from the experiment are used in Step-I and Step-II, respectively. The parameters used in the auto-progressive training of the self-learning simulation are listed in Table 5.4.

Table 5.4 Parameters used in Self-learning Simulation

	Parameters used in Self-learning Simulation	
Number of NN Pass tried	2	
Number of auto-progressive cycles in each load step	3	
Criteria for the auto-progressive cycle	Tol_avg	0.05
	Tol_max	0.05
NN architecture	NN Group 1: {4-15-15-1} NN Group 2: {4-15-15-1} NN Group 3: {4-15-15-1}	
Scale factors used	abs(θ^n, θ^{n-1}, M^{n-1},ς^n,M^n) < [1.5, 1.5, 800.0, 230.0, 800.0]	

Total number of load steps was 455. Before starting the self-learning simulation, a set of pre-training data are generated assuming the linear elastic rotational behavior of connections. For the FE model I, the range of moments in the pre-training data set is between -5.0 (kN-m) and +5.0 (kN-m) and that of rotations is between -0.000359 (Rad) and 0.000359 (Rad). For the FE model II, the ranges are -15.0 (kN-m) ~ +15.0 (kN-m) and -0.0014695 (Rad) ~ +0.0014695 (Rad), respectively. Total two NN Passes are carried out. The trained NN based connection models obtained from the self-learning simulations are used in the following static forward analysis.

The FE model I with rigid and bilinear connection behavior is used for comparisons. A comparison of Figure 5.16 and Figure 5.17 proves the importance of accurate modeling of nonlinear behavior of connections. For the bilinear model, an initial stiffness of 7200.0 (kN-m/rad), a hardening stiffness of 1235.38 (kN-m/rad) and a rotation at yield point of

0.004 (Rad) are assumed. On the other hand, a self-learning simulation is carried out with the FE model I to obtain NN based connection models. Results from static forward analysis with the NN models, as opposed to that from analytical models, are showing better agreement with experimental results than other analytical models for connections. Figure 5.18 and Figure 5.19 are showing force-displacement hysteretic curves from the static forward analysis with the model obtained from self-learning simulations up to NN Pass 1 and NN Pass 2, respectively.

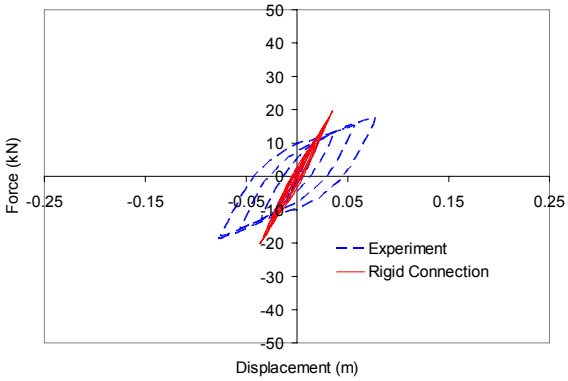

(a) Force-Displacement at the First Floor

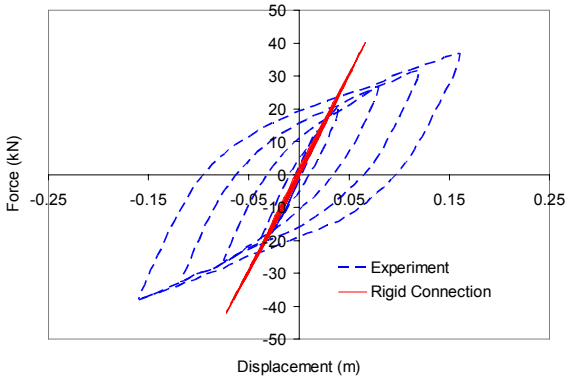

(b) Force-Displacement at the Second Floor

Figure 5.16 Force-Displacement Hysteresis with Rigid Connection (FE Model I)

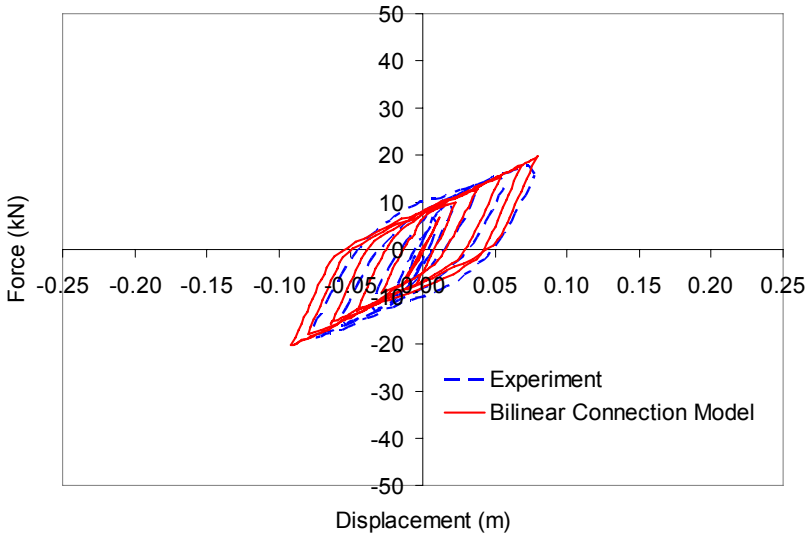

(a) Force-Displacement at the First Floor

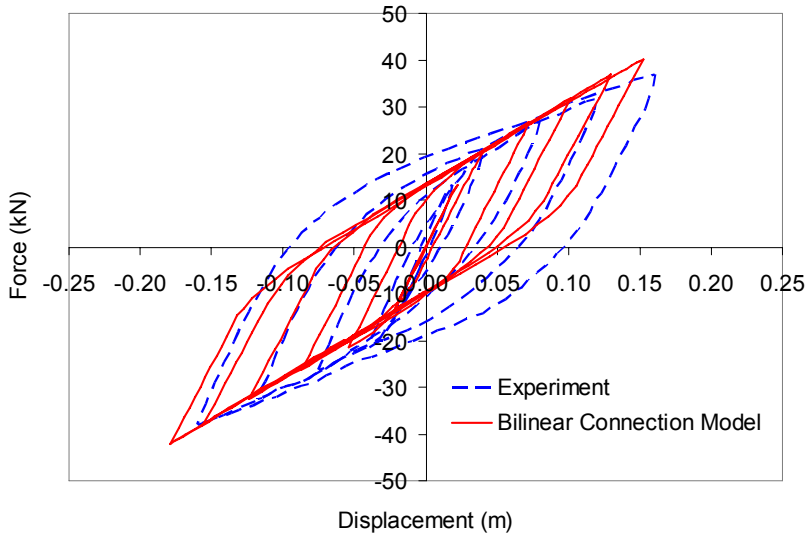

(b) Force-Displacement at the Second Floor

Figure 5.17 Force-Displacement Hysteresis with Bilinear Model for Connections (FE Model I)

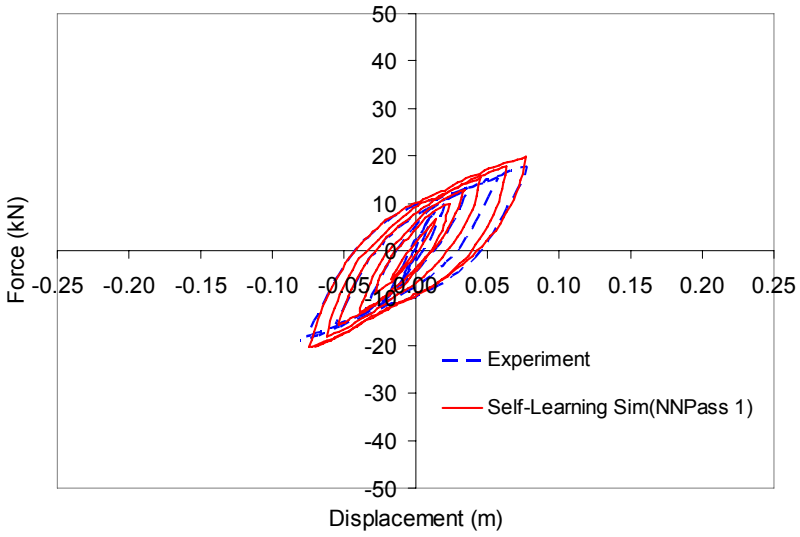

(a) Force-Displacement at the First Floor

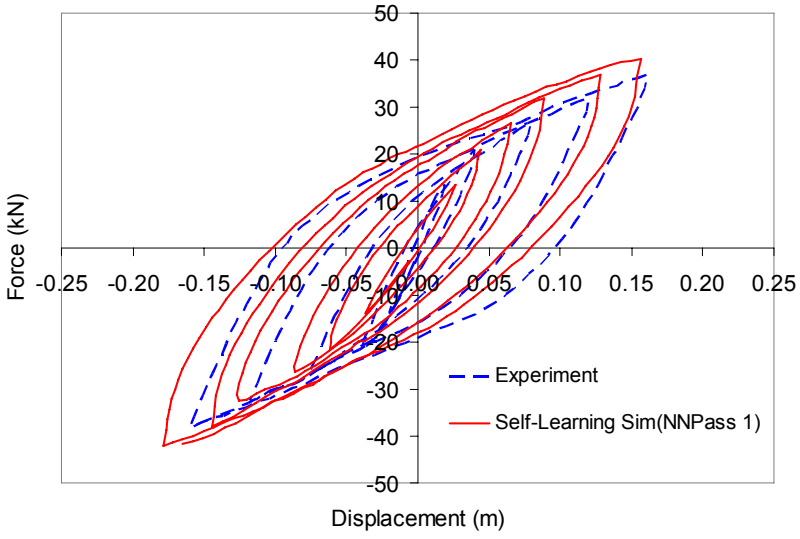

(b) Force-Displacement at the Second Floor

Figure 5.18 Force-Displacement Hysteresis from Static Forward Analysis with NN Models Trained up to NN Pass 1 (FE Model I)

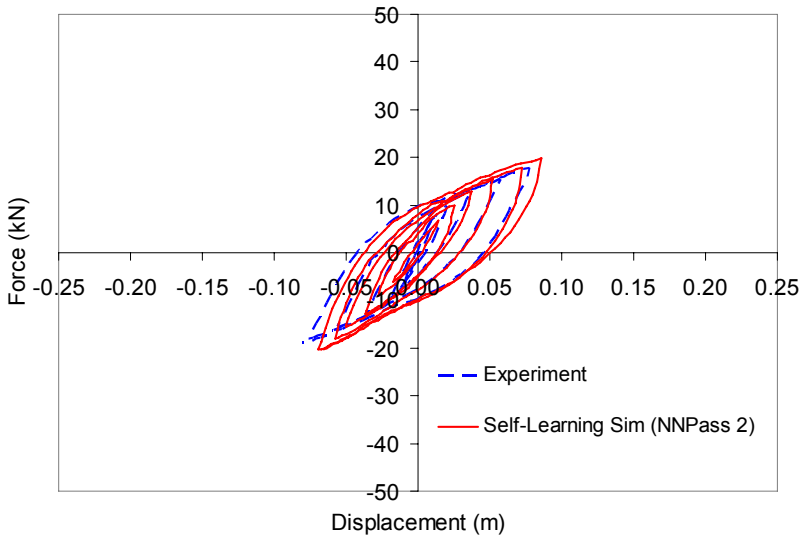

(a) Force-Displacement at the First Floor

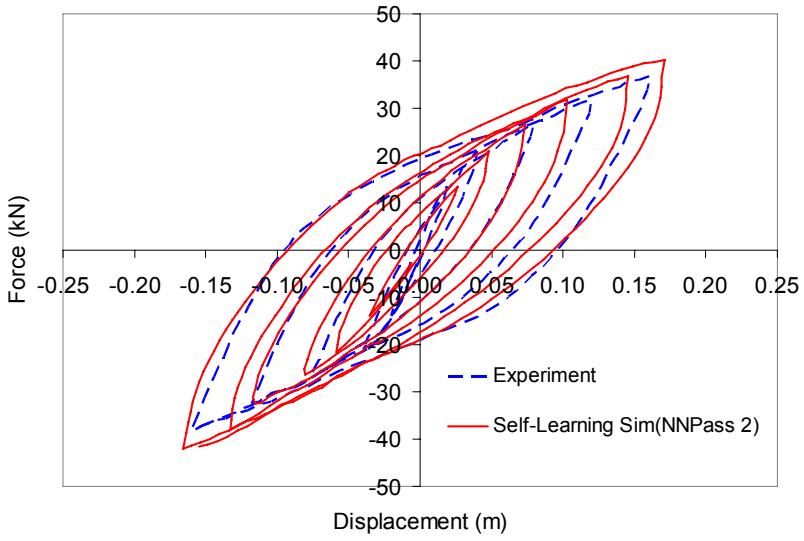

(b) Force-Displacement at the Second Floor

Figure 5.19 Force-Displacement Hysteresis from Static Forward Analysis with NN Models Trained up to NN Pass 2 (FE Model I)

Apparently, the NN based connection models are representing even pinching effect in the hysteretic curves which could not be properly represented by the bilinear model. Comparing the results from NN Pass 1 and NN Pass 2, there is obvious improvement in

the hysteretic curves. In particular, it is worthwhile to mention that sufficiently reasonable accuracy can also be obtained even with NN based models which are auto-progressively trained up to the first NN Pass. The deformed shape and bending moment diagram at load step 379 from the static forward analysis are illustrated in Figure 5.20.

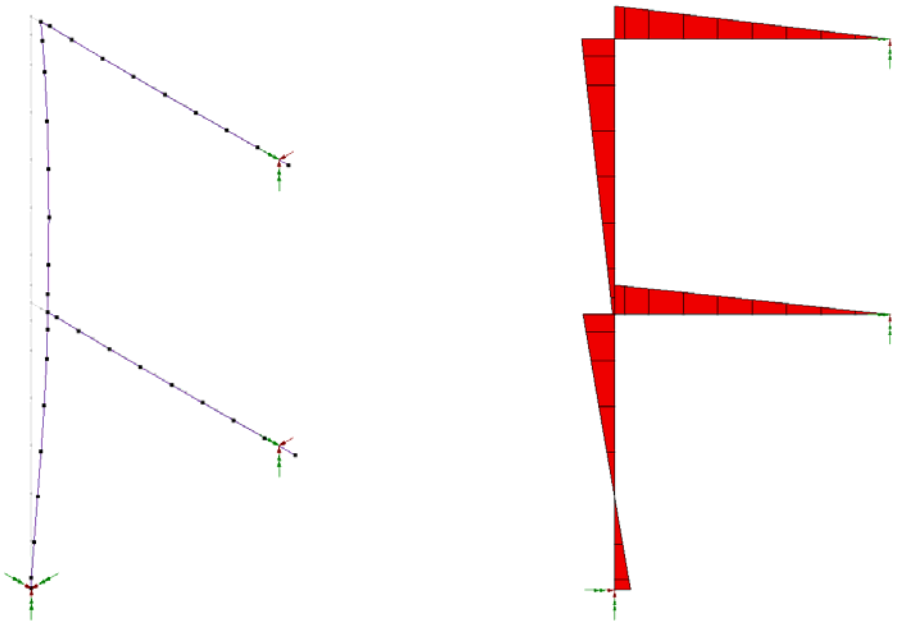

(a) Deformed Shape (b) Bending Moment Diagram

Figure 5.20 Deformed Shape and Bending Moment Diagram from Static Forward Analysis with NN based Connection Models

A self-learning simulation with the FE model II was also carried out to obtain the NN based connection models. Using the obtained models, a static forward analysis was conducted under force boundary conditions. As shown in Figure 5.21, a comparison of the moment-horizontal displacements for experimental data and the static forward analysis verifies that the self-learning simulations can capture the local nonlinear connection behavior from test measurements.

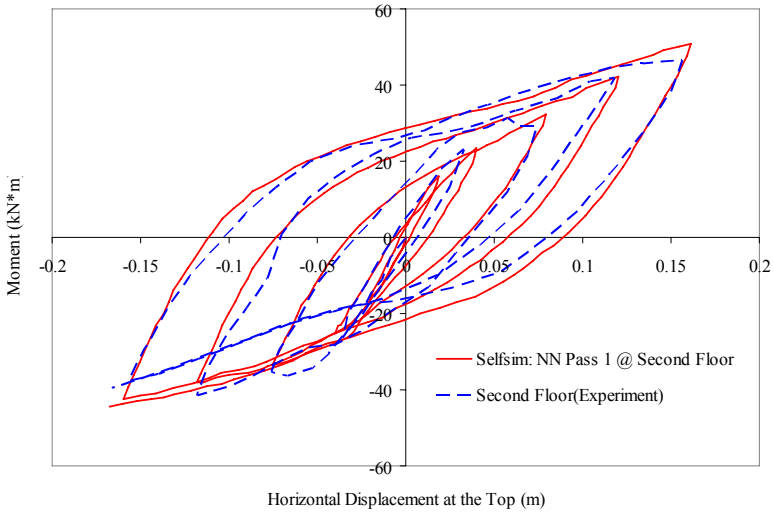

(a) Moment-Horizontal Displacement of Semi-rigid Connection at the Second Floor

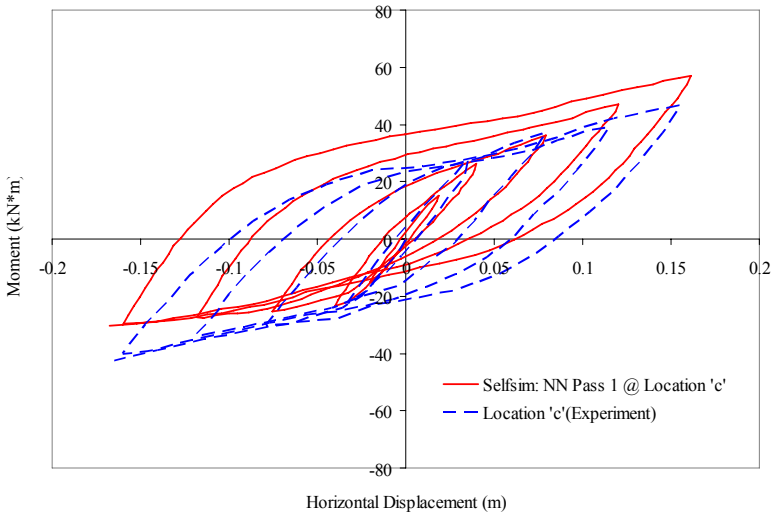

(b) Moment-Horizontal Displacement Hysteretic Curve at Location ‘c’

Figure 5.21 Comparisons between Experimental Data and NN based Connection Model from Self-learning Simulation (FE Model II)

One of the unique advantages of NN based connection models from self-learning simulation is that it can learn realistic experimental observations which may include pinching in hysteresis, yielding, buckling of connecting elements and any other destabilizing effects. The local behavior at connections we are interested in can be

masked at the beginning of simulations and only global responses of tested structures at control points are required to auto-progressively train the NN based connection model. Moreover, the obtained training data base from the self-learning simulation can be continuously updated with new experimental data available.

5.5 Further Research and Applications of Self-Learning Simulation

In the current application with lumped spring element approach, further research is required to have the NN based model evolve to the actual local behaviors because there could be multiple combinations of the trained NN based models that produce a single global response given. For resolving this non-uniqueness problem in the solution, more refined model such as a component-based model is suitable whereby the NN based model represents uni-axial inelastic hysteretic behavior of connecting components. There are unresolved uncertainties in component level because contributions of the failure modes in component level to the connection behavior are dependent on various loading scenario and construction quality of connections. It is also noteworthy that understanding of the connection and global behavior is more important than the component behavior in practical applications.

The self-learning simulation with the NN based inelastic hysteretic model opens up vast applications in earthquake engineering. Beyond its application in beam-column connections, any structural and geotechnical component can be modeled by the NN based inelastic hysteretic model and the self-learning simulation can be carried out to extract training data for the models as long as experimental data are provided. The trained NN based model can be updated with new set of experimental data and the NN based model

is suitable for cases with noisy structural test data because of its fault tolerance. For example, the proposed modeling approach to inelastic hysteretic behavior of structures can be incorporated with on-line hybrid simulation and testing because measured force and displacement data from quasi-static testing under earthquake loading can be directly used in self-learning simulation. The predictive and generalized capability of the NN based model can also be used for further development of testing algorithm in the context of expanding capability of on-line hybrid simulation and testing.

5.6 Conclusions

In this Chapter, self-learning simulation methodology, as a novel modeling approach to inelastic hysteretic behavior of beam-column connections, has been proposed. Performances of the self-learning simulation have been verified with synthetic experimental data. The example with synthetic experimental data has two-fold objectives. The first objective is to investigate the effect of the algorithmic formulation using the NN based model on the performance of self-learning simulation. For the purpose, two algorithmic formulation methods in calculating tangent stiffness matrix have been tested in self-learning simulation. The second objective is to investigate the sensitivity to load step sizes of the two methods. For this purpose, larger load step sizes are applied to the two algorithmic formulation methods and it was found out that the calculation of the tangent stiffness using measured forces from Step-I and measured displacement from Step-II gave stable convergence in auto-progressive training although it needs more iterations than the opposed method. Even though calculation of tangent stiffness using force and displacement from either Step-I only or Step-II only gave less number of

iterations, not only was it observed that it can mislead the NN based model during training but also self-learning simulation failed with larger load step size due to failure in convergence. Therefore, further research is needed to investigate the theoretical stability in convergence with the algorithmic formulation using the NN based connection model in self-learning simulation. From the testing in this report, it is recommended to use the formulation method of Case I for successful self-learning simulation in terms of stable convergence and accuracy.

After the investigation, actual experimental data have been used in self-learning simulation. From the simulation, unique advantages of the self-learning simulation have been shown through comparisons with analytical connection models such as rigid and bilinear connection model.

CHAPTER 6 GENERALIZED HYBRID NEURAL NETWORK BASED INELASTIC HYSTERETIC MODEL

6.1 Introduction

Capacity of beam-column connections plays an important role in determining the global response of structural systems. In current design codes, connections that can transfer 20 % to 90 % of moment capacity of joining members are classified into partially restrained connections. Except two extreme cases, that is, fully rigid connections and pinned connections, most of the connections used in practice are classified into partially restrained connections. Because of the complexity in geometrical properties and configurations of connections, moment-rotation relationships of the partially restrained connections are highly nonlinear and they are very much dependent on design parameters such as beam depth, thickness of components and bolt diameter, etc. In order to design connections, the non-linear moment-rotation curve from experiments or verified analytical models is required in current design codes. In highly seismic zones, a cyclic behavior of the connections is also very important for a seismic performance evaluation of structures. Although the correlation between design parameters and capacity of connections subjected to the cyclic loading has been sufficiently interpreted through experiments, further research on generally accepted inelastic hysteretic model for beam-column connections are still required.

Neural network (NN) is a massively parallel processor that can store experiential knowledge and make itself available for later use. It features adaptive learning, self-organizing capability during training and fault imprecision during applications. The biggest advantage of using NNs is that it can solve problems that are too complex for

conventional methods; problems that do not have an algorithmic solution or for which an algorithmic solution is too complex to be found. As aforementioned, it has been proved that there is obvious correlations between design parameters and capacities of beam-column connections under monotonic and cyclic loading (FEMA-355D 2000). While it is almost impossible to quantify the correlation between the design parameters and dynamic behavior of beam-column connections with any conventional methodology, the NN with its remarkable capability to extract essential information from complicated and/or imprecise data can be applied to the quantification.

The application of the NN in prediction of the cyclic connection behavior has been very rarely researched. In 1995, the NN was used to predict the moment-rotation curve of single web beam-column connections (Abdalla and Stavroulakis 1995). In 1997, Anderson et al. also used the NN to predict a bilinear approximation of the moment-rotation curve of minor axis end-plate beam-column connections (Anderson, et al. 1997). In 1997, Stavroulakis et al. proposed a two-stage NN approach for the elasto-plastic analysis of steel structures with semi-rigid connections. In the approach, the NN is trained to predict moment-rotation curves of connections subjected to monotonic loading only and the structural analysis problem is reformulated as a quadratic programming problem with which ordinary structural design engineers are unfamiliar. In 2004, Sakla used the NN to predict the load-carrying capacity of eccentrically loaded single-angle struts (Sakla 2004). Nonetheless, the research on the application of the NN in the modeling of complex cyclic behavior of connections is still in its infant stage.

In this chapter, a generalized hybrid neural network (GHNN) based inelastic hysteretic connection model is proposed. The GHNN based connection model is an

extension of the NN based cyclic material model proposed in this report toward its full practical applications in earthquake engineering. The identified design variables that significantly affect failure mechanisms of connections are included as inputs to a physical principle based module whereby important mechanical variables defining capacity of connections are calculated as outputs from the design variables using principle of mechanics or empirical equations. The physical principle based module is combined with the NN based cyclic material model so that the complex dynamic behavior of connections can be predicted from design variables and different loading histories. In order to validate the proposed GHNN based connection model, extended-end-plate connection without column stiffeners is chosen and its design variables are generated using Latin Hypercube Sampling technique to ensure its uniform distribution of variables in multivariate design space. Since there is few comprehensive experimental data on dynamic behavior of the given connection, an empirical model, Frye and Morris' polynomial model (Frye and Morris 1975), is employed to generate abundant moment versus rotation curves with different design variables. According to a series of systematic testing, the proposed model is shown to have remarkably generalized performance, which means that it can reasonably response to totally new set of situations with different design variables and even different loading history. Considering use of the model in general finite element codes, the testing is conducted in recurrent mode in which the earlier prediction of moment is fed back to input for prediction of moment at next time step.

6.2 Basic Concept of the Proposed Model

The basic concept about the GHNN based inelastic hysteretic connection model can be described with respect to information flow from design variables through mechanical parameters and displacement vector to the end of stress resultants vector as shown in Figure 6.1. The stress resultants of the connection element can be expressed as a function of design variables (e.g. size of the joining members, thickness of components and bolt diameter, etc.) and deformation vector of the element. The mathematical function for the stress resultant vector can be expressed as follow.

$$\mathbf{F}(t) = F\left(\mathbf{U}(t), \mathbf{DV}\right) \tag{6-1}$$

where **DV** indicates a vector of design variables; **U** a displacement vector and **F** a stress resultant vector. Many experimental observations manifest the functional mapping in equation (6-1). For instance, plastic rotation of beam-column connections is significantly affected by beam depth (FEMA-355D 2000) and the stress resultant actions certainly depend on deformations of the connection according to principle of mechanics. Therefore, the design parameters are considered as variables that affect the cyclic behavior of connections. However, the design variables that is mostly expressed in terms of geometrical dimensions are not adequate for directly quantifying the stress resultant-displacement states of the connections because their effects on the capacity of connections is not obvious, for example, the increase of end plate thickness can weaken or strengthen the capacity and ductility of connections. Therefore, mechanical parameters are introduced to consider the effect of design variables on the capacity of connections. Then the equation (6-1) can be rewritten as follow.

$$\mathbf{F}(t) = F\left(\mathbf{U}(t), \mathbf{MP}\right) = F\left(\mathbf{U}(t), G(\mathbf{DV})\right)$$
$$\mathbf{MP} = G(\mathbf{DV}) \tag{6-2}$$

where **MP** indicates a mechanical parameter vector that is a function of design variables. Since the mechanical parameters feature the capacity of connections, using them as inputs to NN along with other state variables or internal variables can be considered as natural. In summary, two functional mappings can be employed in the information flow from design variables to the stress resultant force vector; the first is a mapping G from design variable to mechanical parameters and the second is a mapping F from mechanical parameters to the stress resultant vector.

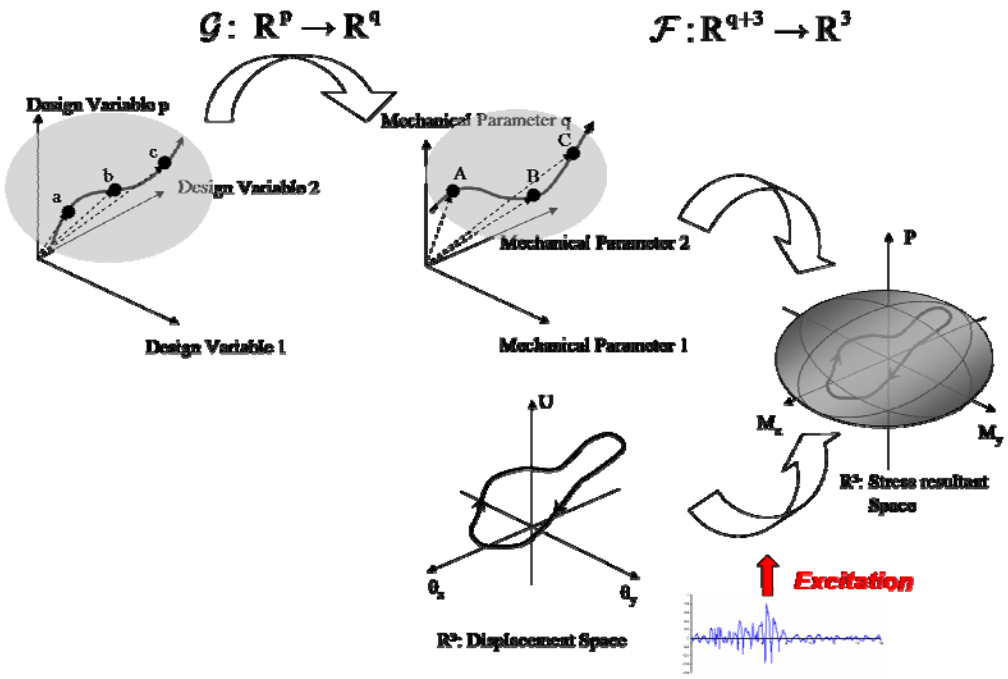

Figure 6.1 Information Flow from Design Variables through Stress Resultants in GHNN based Inelastic Hysteretic Connection Model

According to the summary and Figure 6.1, the first mapping G can be easily obtained by using basic principle of mechanics. Therefore, so called physical principle based module is constructed first to relate design variables to mechanical parameters. The most challenging mapping is the second one F because it should have responsive capability to represent any hysteretic behavior of connections. In this report, the NN is used for the mapping F because not only should the mapping be physically responsive to change in mechanical parameters and state variables (displacements and stress resultant forces) but also it should be responsive to loading scenarios. According to literature survey, any conventional technique including mathematical approaches can not realize such a dynamic hysteretic model for connections with full performance.

6.3 The Proposed Inelastic Hysteretic Model for Connections

Following the basic concept on the information flow described in the previous section, a generalized hybrid NN (GHNN) based inelastic hysteretic model is proposed whereby two hierarchical modules are integrated; one is physical principle based module and the other is NN based module. The GHNN based inelastic hysteretic model is as shown in Figure 6.2. Since the design variables and mechanical parameters can be customized to any specific connection type and the model can predict dynamic responses of connections, the model is called as generalized. Since the model also consists of two modules as aforementioned, it is called as hybrid.

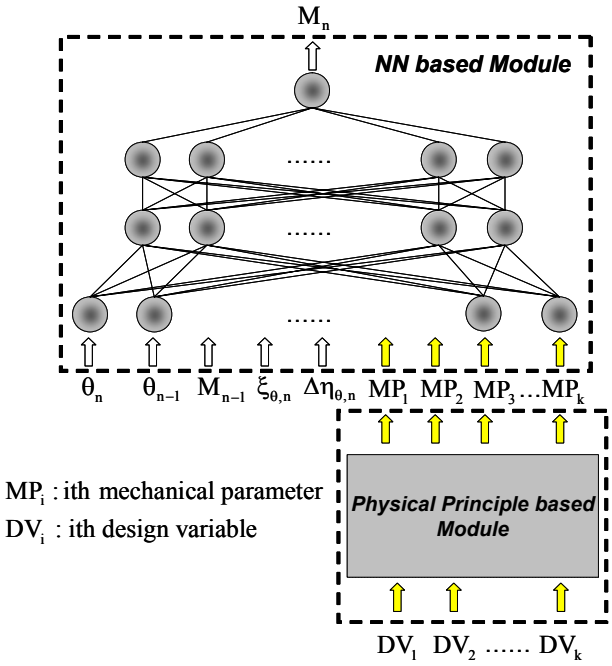

Figure 6.2 Generalized Hybrid NN based Inelastic Hysteretic Model

Since the behavior of beam-column connections is usually expressed in terms of moment and rotation, not only do the input and output variables in the model consist of moment, rotational displacement and internal variables related to moment-rotational evolutions but also the design variables and mechanical parameters are related to moment-rotational capacity of the connections. The equation (6-3) describes the trained GHNN based connection model in the common notation for NN applications.

$$M_n = \hat{\mathbf{M}}_{NN}\left(\left\{\theta_n, \theta_{n-1}, M_{n-1}, \xi_{\theta,n}, \Delta\eta_{\theta,n}, G(DV_1, .., DV_k)\right\} : \left\{\text{NN architecture}\right\}\right) \quad (6\text{-}3)$$

The unique advantage of the GHNN based model is that not only it can reproduce complex inelastic hysteretic behavior from experiments but also it can predict hysteretic responses of the given connections subjected to totally new design and loading scenario. If users have abundant and comprehensive information to train the proposed model, the model can be fairly generalized. The generalized feature of the model has two-fold

meaning; one is that it responses to new design and loading properly and the other is that a suite of libraries of the model for various connection type cans be constructed.

6.3.1 Physical Principle based Module

The physical principle based module connects a set of design variables to mechanical parameters since obvious correlation between design variables and mechanical parameters in connection behaviors have been experimentally observed (FEMA-355D 2000; Kishi and Chen 1990). Owing to its generalized feature, the physical principle based module can be customized to each specific connection type. Specifically, the design variables are chosen for each type of connections according to the experimental results. In this report, two connection types - extended-end-plate connection and top-and-seat-angle-with-double-web-angle connection (TSADW) - are chosen to demonstrate the performance of the proposed model. In the following section, the design variables chosen for the two connection types and mechanical parameters are explained.

6.3.1.1 Mechanical Parameters for Connections

For the seismic performance of beam-column connections, stiffness, strength and ductility are very important factors that should be ensured in the seismic design. They have strong correlation with one another. In this report, four mechanical parameters that manifest the capacity of connections are determined; 1) initial stiffness, 2) yielding moment, 3) failure moment and 4) rotational ductility. They are all essential indexes that can represent the capacity of connections. The four mechanical parameters are illustrated in Figure 6.3.

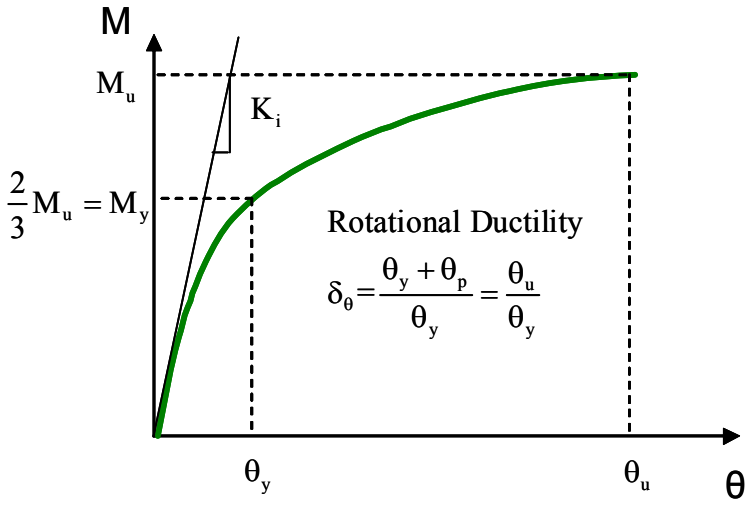

Figure 6.3 Mechanical Parameters of Physical Principle based Module

In structural analysis of a building structure with partially restrained connections, the rotational stiffness of the connections must be considered with a special model in addition to the member stiffness of the beam and column since the connection stiffness has considerable impact upon the structural behavior. Therefore, the rotational initial stiffness is chosen as one of the mechanical parameters used in the proposed model. Moreover, the ductile performance connections are required in highly seismic zones. The ductile deformation capacity of connections is a function of yield mechanisms and critical failure modes. To ensure the ductile performance of connections before failure, the prediction of the yield mechanisms and failure modes and reliable estimate of resistance associated with the estimated yield mechanisms and failure modes are required. As aforementioned in Chapter 2, there could be many different yield mechanisms and failure modes for each connection type. Particularly, the yield moment is associated with the geometry of components and the material properties as well. There exist many equations

that define yield and failure moment in terms of geometrical and material properties of connections (FEMA-355D 2000; Kishi and Chen 1990), Therefore, the yielding and failure moment are chosen as the mechanical parameters. In case of TSADW connections, the ultimate moment at the column face can be calculated assuming the collapse mechanisms in top and seat angles and web angles as shown in Figure 6.4.

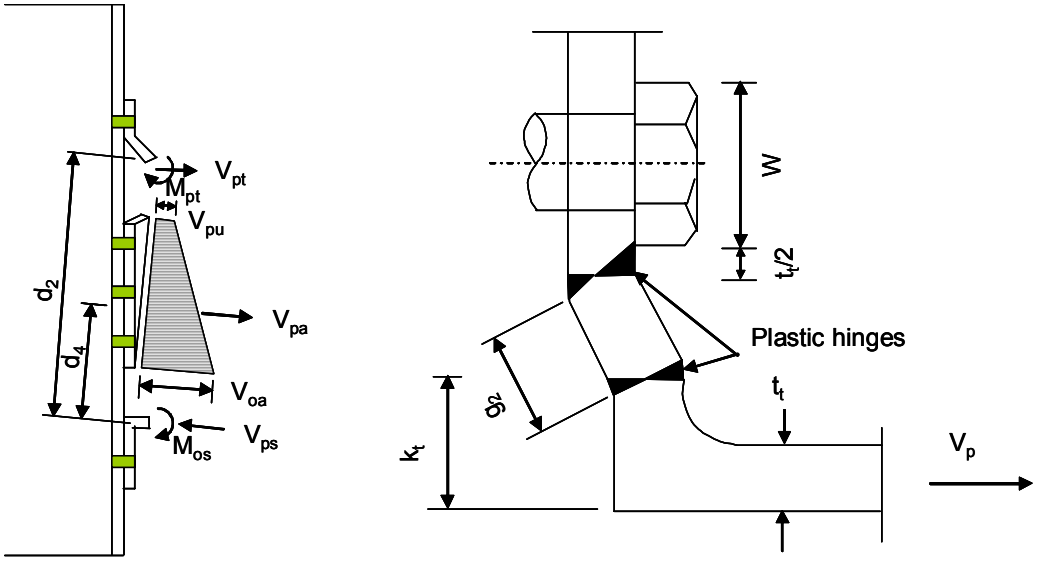

Figure 6.4 Collapse Mechanism of TSADW connection (Kishi and Chen 1990)

Then the ultimate moment resistance can be calculated as follow.

$$M_u = \frac{s_y l_s t_s^2}{4} + M_{pt} + V_{pt} d_2 + 2\left(\frac{V_{pu} + V_{oa}}{2}\right) l_p d_4$$

in which (6-4)

$$d_4 = \frac{(2V_{pu} + V_{oa})}{3(V_{pu} + V_{oa})} l_p + l_l + \frac{t_s}{2}$$

Where l_s indicates width of the seat angle; l_p width of the web angle, l_l distance from bottom flange of beam to lower edge of web angle; t_s thickness of seat angle and other

variables are indicated in Figure 6.4. M_{pt} and V_{pt} in (6-4) are bending moment and shearing force acting on the plastic hinges shown in Figure 6.4. Drucker's yielding criterion can be expressed by the fourth-order equation as follow.

$$\left(\frac{V_{pt}}{V_{ot}}\right)^4 + \frac{g_2}{t_t}\left(\frac{V_{pt}}{V_{ot}}\right) = 1 \qquad (6\text{-}5)$$

where V_{ot} indicates plastic shear capacity of the top-angle leg without coupling. From equation (6-5), V_{pt} can be calculated and M_{pt} is calculated by $M_{pt}=V_{pt}g_2/2$. The ductility of connections is commonly expressed in terms of the rotational ductility. The rotational ductility is defined as follow.

$$d_q = \frac{q_y + q_p}{q_y} = \frac{q_u}{q_y} \qquad (6\text{-}6)$$

where θ_p and θ_y indicate plastic and yield rotation, respectively. All of the mechanical parameters chosen for the proposed model can characterize the capacity of connections from yielding through failure. In the following section, design variables used in the proposed model for two specific connection types are explained.

6.3.1.2 Design Variables for Connections

In case of the extended-end-plate connections, flexural resistance of end plate and axial resistance of bolts are engaged in the energy dissipation during cyclic behavior. According to experimental observation on this type of connections, the more in plastic engagement the bolts are, the more hysteretic pinching are amplified. As illustrated in Figure 2.2(a), the ductility is very low when bolts are failed. If the end plate is stiffened, yield of the beam and good energy dissipation can be ensured as shown in Figure 2.2(c).

Therefore, the thickness of end plate and column flange and the diameter of bolts are very important design parameters for the extended-end-plate connections. In addition, as shown in Figure 6.5, there is strong correlation between capacity and beam depth. Therefore, the beam depth is also chosen as one of the design variables for the extended-end-plate connections.

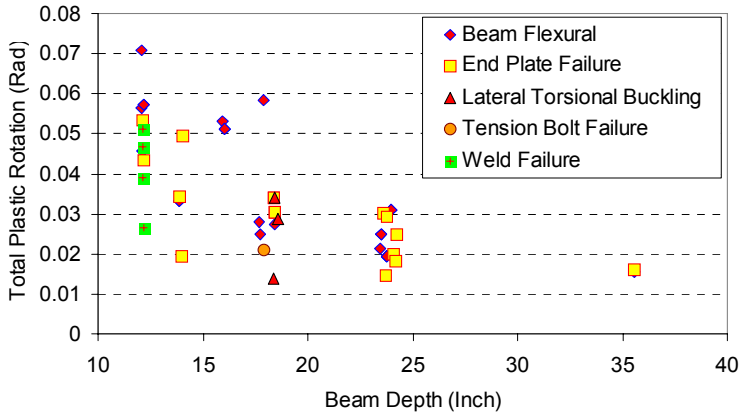

Figure 6.5 Effect of Beam Depth on End-Plate Connection Capacity (Redrawn from (FEMA-355D 2000))

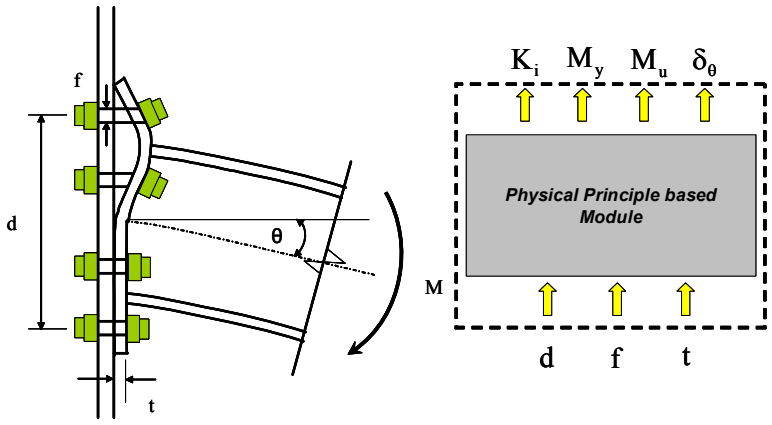

Figure 6.6 Design Variables of Extended-End-Plate Connections

The design parameters for the extended-end-plate connection are illustrated in Figure 6.6.

In case of TSADW connections, the yield mechanisms are limited to flexural yielding of the upstanding leg of the top angle and yielding of the shear panel zone. The latter is possible but less unlikely than the former. Since this is a flexible partially restrained connection, it provides large amount of plastic rotational capacity compared to other stiff partially restrained connection types. Because of its flexibilities, it has not been used in highly seismic zone. When other yield mechanisms such as looseness of the bolt holes and elongation of the bolts are engaged, it provides less plastic rotation capacity. According to the past experimental observations on this type of connections, five design variables are selected as illustrated in Figure 6.7. They are thickness of top and seat angles, thickness of web angles, width of top and seat angle, distance between flange and center of bolts and depth of the joining beam.

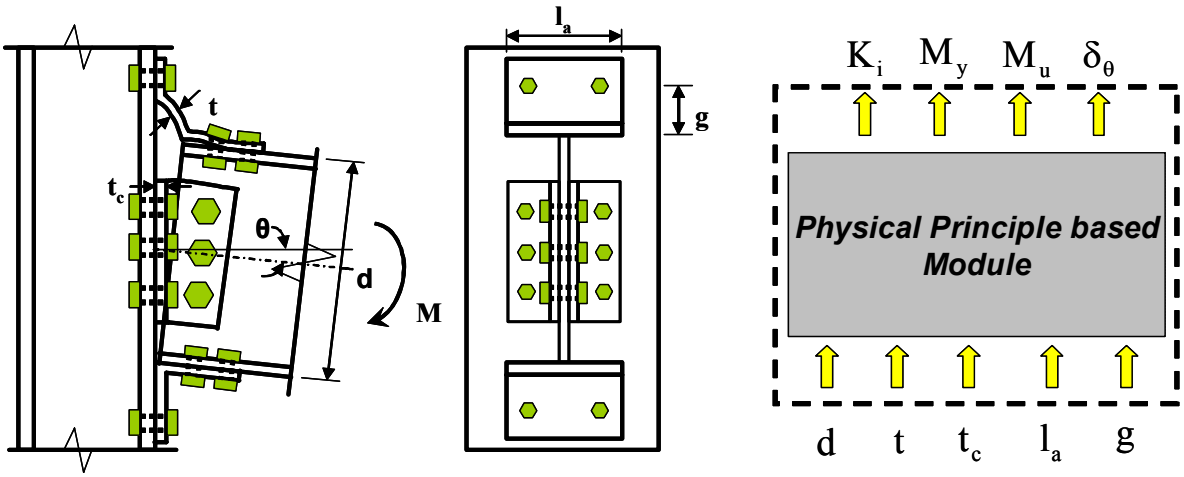

Figure 6.7 Design Variables of Top-and-Seat Angle Connections

6.3.2 Neural Network based Module for Modeling Hysteretic Behavior

The NN based cyclic material model proposed in this report is employed for establishing the functional mapping F from state and mechanical variables to stress resultants. The two internal variables also play an important role in learning the hysteretic behavior as demonstrated in Chapter 3. The only difference is that the mechanical variables from the physical principle based module are presented as inputs to the NN based module. Since the state variables and the mechanical parameters can be directly interpreted in the stress resultant space and the evolutions in inelasticity region, the proposed GHNN based model can be responsive to the change in mechanical parameters which have strong interrelation with design variables of each connection type. The proposed GHNN based inelastic hysteretic model for connection is illustrated as in Figure 6.8.

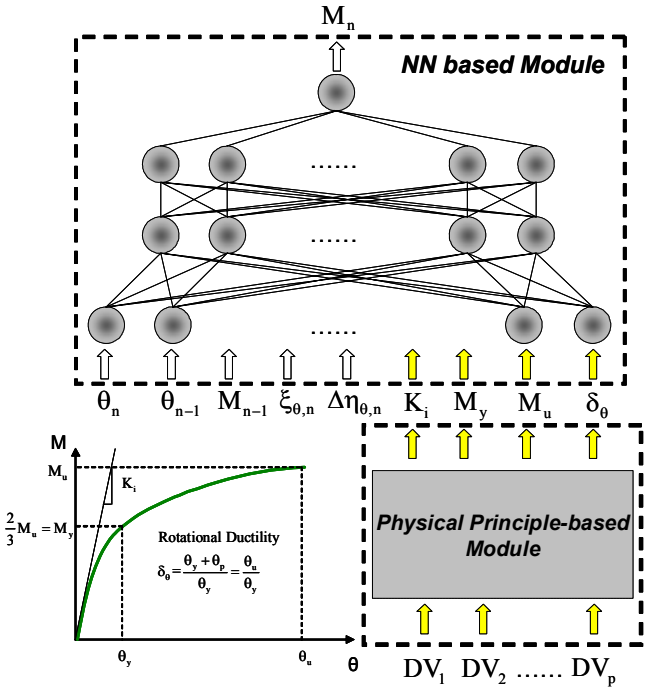

Figure 6.8 Generalized Hybrid NN based Inelastic Hysteretic Model for Connections

6.4 Validation of the Proposed Model with Experimental Data

The primary objective of the tests in this section is to verify the performance of the proposed model with real and synthetic experimental data of the two most common connection types. Since the key advantage of using the proposed model is its capability of reproducing complex inelastic hysteretic response of the experimental data, the proposed model is tested with earthquake records. The generalized feature of the proposed model is also verified with testing of the proposed model under totally new earthquake motions, design variables and combinations of them as well.

6.4.1 Extended-End-Plate Connection

In the test of the proposed model with this connection type, synthetic experimental data are used which are artificially generated design variables and generated from polynomial model. There are three reasons why the synthetic experimental data are used for testing of the proposed model on the extended-end-plate connections. The first reason is because most of the past experiments on this type of connections were conducted under monotonic loading only. The second reason is because while there are several studies on the seismic behavior of the connection type, not only is it unknown whether the rotational deformation history includes contribution from the column and the shear panel zone or not in some cases but also there are variations in the locations where the rotational deformation is measured. The third reason is because standardized beam sections, high strength bolts and thickness of plates can hinder the testing of the proposed model under

large variations in design variables and mechanical parameters. Therefore, if we use the limited real experimental case, the proposed model can be tested into the given narrow domain only.

6.4.1.1 Generation of Synthetic Experimental Data

In order to obtain the design variables which ensure full coverage of the given range, Latin Hypercube Sampling (LHS) technique is used (Iman and Conover 1982). LHS technique is an efficient sampling method for uncertainty analysis such as variation in design spaces. Since the scheme is beyond the topics of this report, it will not be explained any more in this section. The basic assumption in LHS is that there is no correlation between design variables. Figure 6.9 shows the sampled points in the space of the design variables which are generated in the LHS technique. D represents the distance between the outermost bolts and t stands for thickness of the end plate and f stands for the diameter of the bolts.

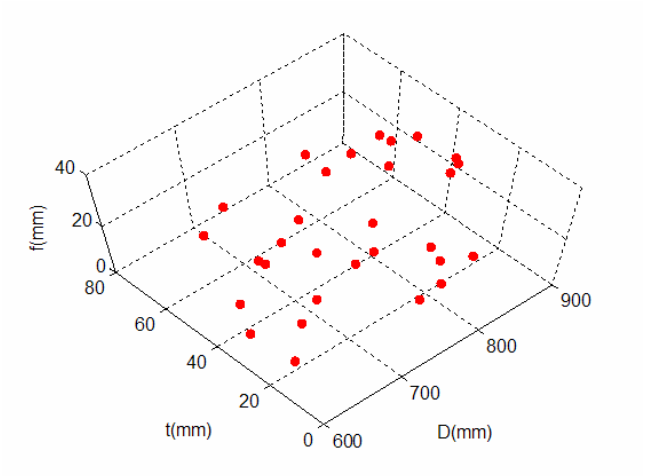

Figure 6.9 Sampled Points in Design Space by LHS technique (D-t-f)

Table 6.1 Sampled Designs of Extended End Plate Connection

Label of Samples	D (mm)	t (mm)	f (mm)	Label of Samples	D (mm)	t (mm)	f (mm)
1	908.75	12.93	37.85	18	825.54	28.08	36.94
2	812.34	62.98	26.21	19	877.24	61.25	30.80
3	840.60	51.49	26.51	20	610.39	18.28	33.25
4	745.77	30.60	17.23	21	760.79	45.13	16.77
5	834.84	39.64	33.88	22	792.82	22.83	23.79
6	669.70	9.59	22.39	23	710.42	21.59	21.53
7	622.06	53.82	27.60	24	730.56	28.76	18.94
8	638.93	58.30	23.54	25	781.94	56.75	20.12
9	674.35	5.25	31.64	26	862.55	41.16	20.70
10	797.28	47.88	12.93	27	660.76	35.32	34.77
11	742.27	26.18	28.47	28	899.27	33.45	18.34
12	721.53	42.40	15.23	29	770.93	48.09	29.93
13	702.82	8.06	29.28	30	880.34	20.59	36.08
14	857.52	52.01	32.38	$600.0 \text{ mm} \le D \le 910.0 \text{ mm}$ $5.0 \text{ mm} \le t \le 63.5 \text{ mm}$ $12.7 \text{ mm} \le f \le 38.1 \text{ mm}$			
15	686.38	15.27	13.72				
16	608.36	11.46	24.62				
17	642.95	37.48	15.37				

Table 6.1 shows numerical values of each design variable generated through LHC sampling technique.

The moment-rotation curves for the extended-end-plate connection are obtained from an empirical equation proposed by Frye and Morris (Frye and Morris 1975). The rotation of the connection is expressed as an odd-powered polynomial function.

$$q = C_1(PM) + C_2(PM)^3 + C_3(PM)^5 \quad (6\text{-}7)$$

Where M and θ are moment and rotation, respectively; C_1, C_2 and C_3 are curve-fitting parameters; P is a standardized parameter which is a function of the significant geometrical parameters such as connecting member size, plate thickness, etc. The parameters corresponding to the extended-end-plate connection are summarized in Table 6.2.

Table 6.2 Parameters for Extended-End-Plate Connection

C_1	C_2	C_3	P	# of Test	Maximum Deviation of Standardized Curve from Experimental Curve
1.83×10^{-3}	-1.04×10^{-4}	6.38×10^{-6}	$P=D^{-2.4}t^{-0.4}f^{1.1}$	12	3%
D : depth of beam (in) t : thickness of end plate (in) f : diameter of bolt (in)					

For each sampled set of design variables, mechanical parameters are determined as follow. According to regression analysis of test results (FEMA-355D 2000), the achievable plastic rotation by the extended-end-plate connection type can be expressed as follow.

$$q_{pmean} = 0.0607 - 0.0013 \times d_b \tag{6-8}$$

where d_b indicates depth of beams. The unit for d_b is inch and θ_{pmean} radian. The plastic rotational capacity is the rotation up to the point when significant losses in strength and stiffness start. From the mean value of the plastic rotation, the ultimate moment can be calculated using Equation (6-7). The initial stiffness can be obtained from Equation (6-7) as follow.

$$K_i = \frac{dM}{dq} = \frac{1}{C_1 P} \tag{6-9}$$

Then the yield moment is assumed to be 2/3 of ultimate flexural strength following the specification in Eurocode 3 in its Annex J. The rotational ductility is calculated by Equation (6-6). The total 30 sampled moment-rotation curves are illustrated in Figure 6.10.

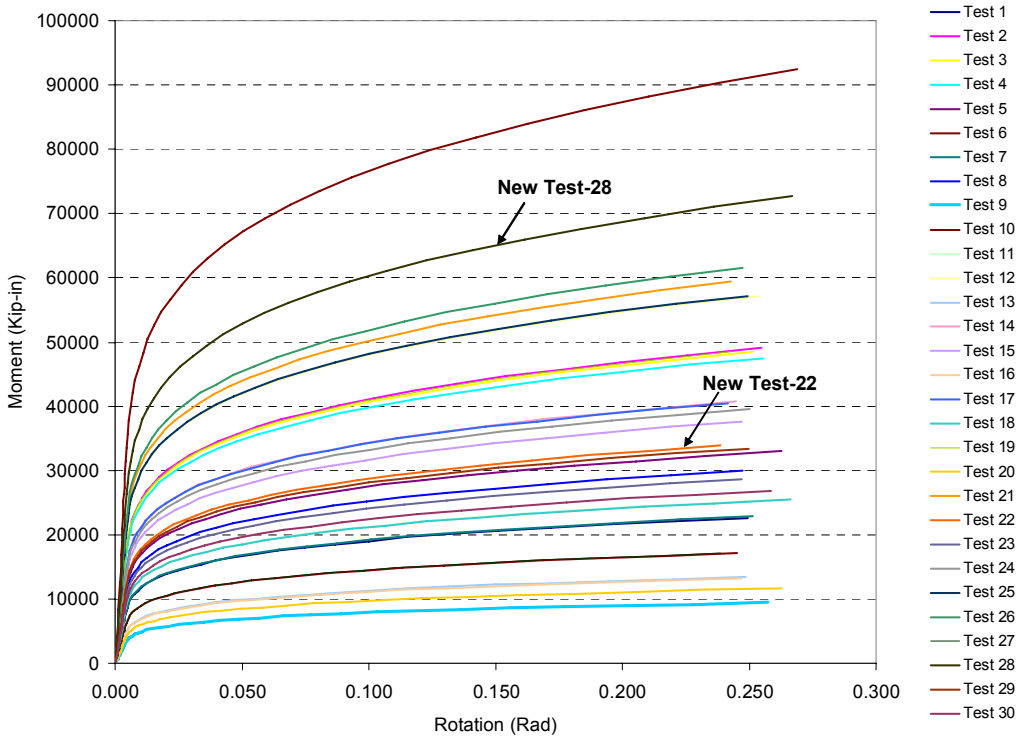

Figure 6.10 Moment-Rotation Curves with Sampled Design Variables

6.4.1.2 The Performance under Cyclic Loading

In this test, the performance of the proposed model is evaluated under cyclic loading. To generate the cyclic moment-rotation curve, the polynomial model is implemented into the finite element code developed for this report. Young's modulus used for steel is assumed to be 29,753.3 (ksi) and poisson ratio is assumed to be 0.3. The finite element model and the cyclic loading used are illustrated in Figure 6.11. The GHNN based model is trained with total 28 moment-rotation curves and it is tested with new Test-22 and Test-28 under the same cyclic loading.

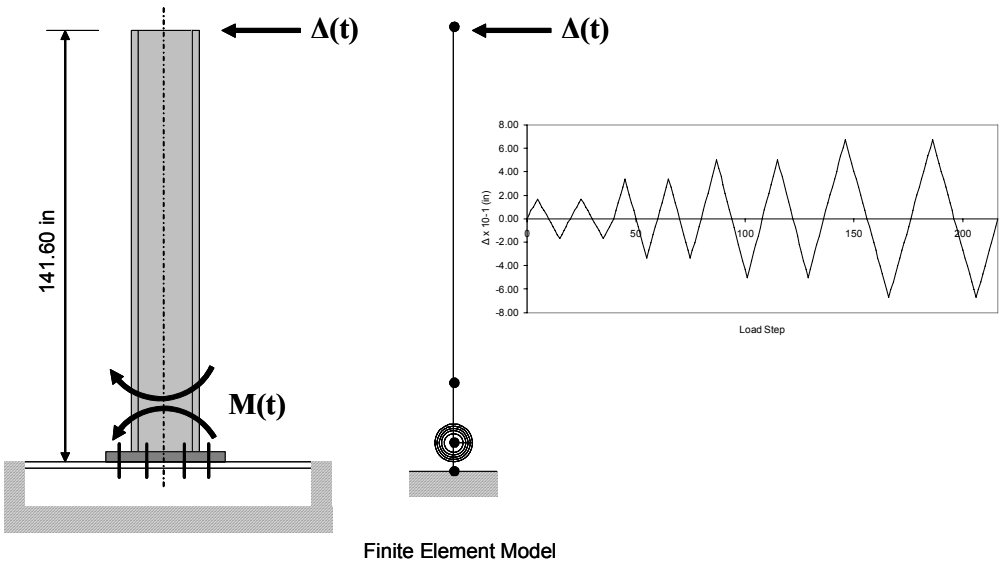

Figure 6.11 Finite Element Model of Column with End-Plate Connection

Table 6.3 shows the training information of the proposed model. During the training, one neuron per each hidden layer is added and the total number of epochs in training is 20,000. The testing of the proposed model is conducted in recurrent mode considering use in general finite element codes. The equation (6-10) describes the trained GHNN based model.

$$M_n = \hat{\mathbf{M}}_{NN}\left(\left\{\theta_n, \theta_{n-1}, M_{n-1}, \xi_{\theta,n}, \Delta\eta_{\theta,n}, G(D,t,f)\right\} : \left\{9-25-25-1\right\}\right) \qquad (6\text{-}10)$$

Table 6.3 Training Information for Cyclic Loading

	Number of Epochs used in Training	NN Architecture	Average Error in Training
NN based Model	20,000	{9-25-25-1}	5.24×10^{-7}

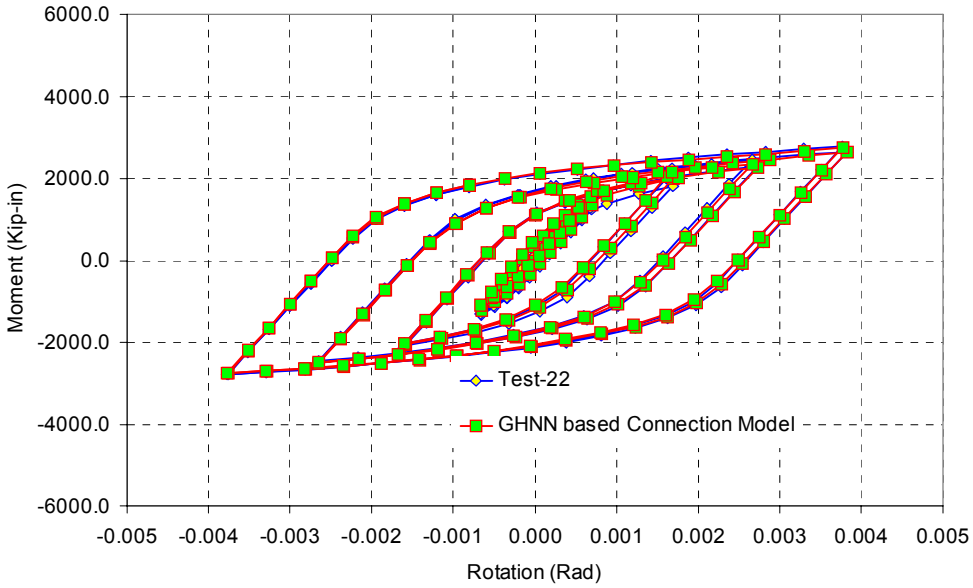

Figure 6.12 Predicted Cyclic Moment-Rotation Curve of Design 22

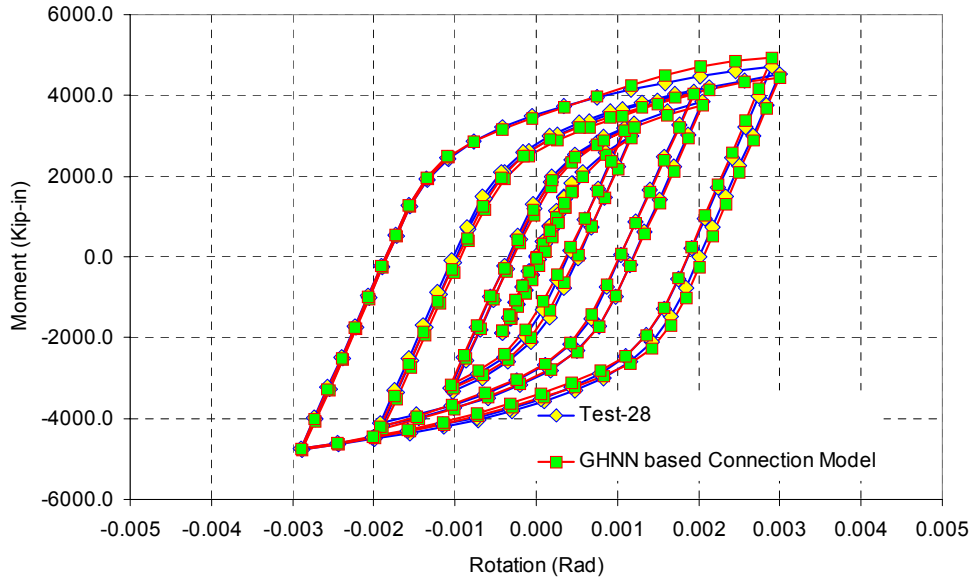

Figure 6.13 Predicted Cyclic Moment-Rotation Curve of Design 28

Figure 6.10 and Figure 6.13 show the predicted cyclic moment-rotation curves of new test-22 and test-28, respectively. According to the test results, it is evidenced that the proposed model can accurately predict the flexural response of completely different designs from the trained designs.

6.4.1.3 The Performance under Earthquake Loading

In this test, the performance of the GHNN based inelastic hysteretic model is demonstrated under earthquake ground records. The dynamic hysteretic moment-rotation curves of the sampled designs are calculated by nonlinear dynamic analysis of a cantilever column as shown in Figure 6.14. The model has total 9 degrees of freedom (three degrees of freedom per each node). The tangent stiffness of the rotational spring element for the column base is derived from the polynomial model in Chapter 2 and non-pinching cyclic behavior is assumed.

In order to verify fully generalized feature of the proposed model, new ground motion is also employed when the trained GHNN based model is tested. The ground motions to be used in training the proposed model are selected from an ensemble of 20 historical strong ground motions (Christopoulos, et al. 2002; PEER). To select ground motions that form envelopes of the group of the response spectrum, the elastic response spectra are drawn in Figure 6.15. Eventually, four records (Record 1, Record 2, Record 4 and Record 11) out of the 20 ground motions are selected and one new record (Record 5) is selected as shown in Figure 6.16 and Figure 6.17, respectively.

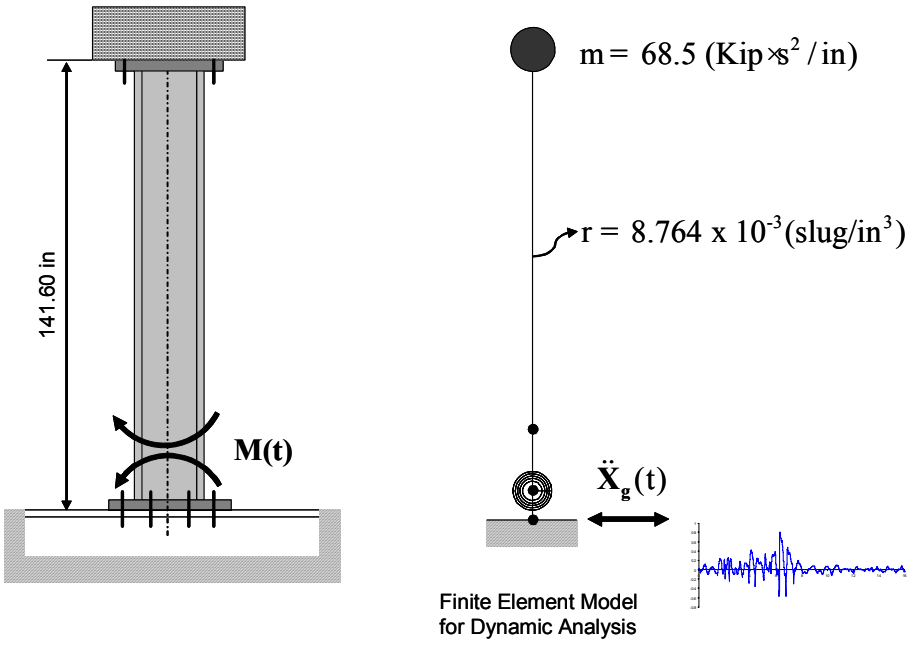

Figure 6.14 Dynamic Model of Column with End-Plate Connection

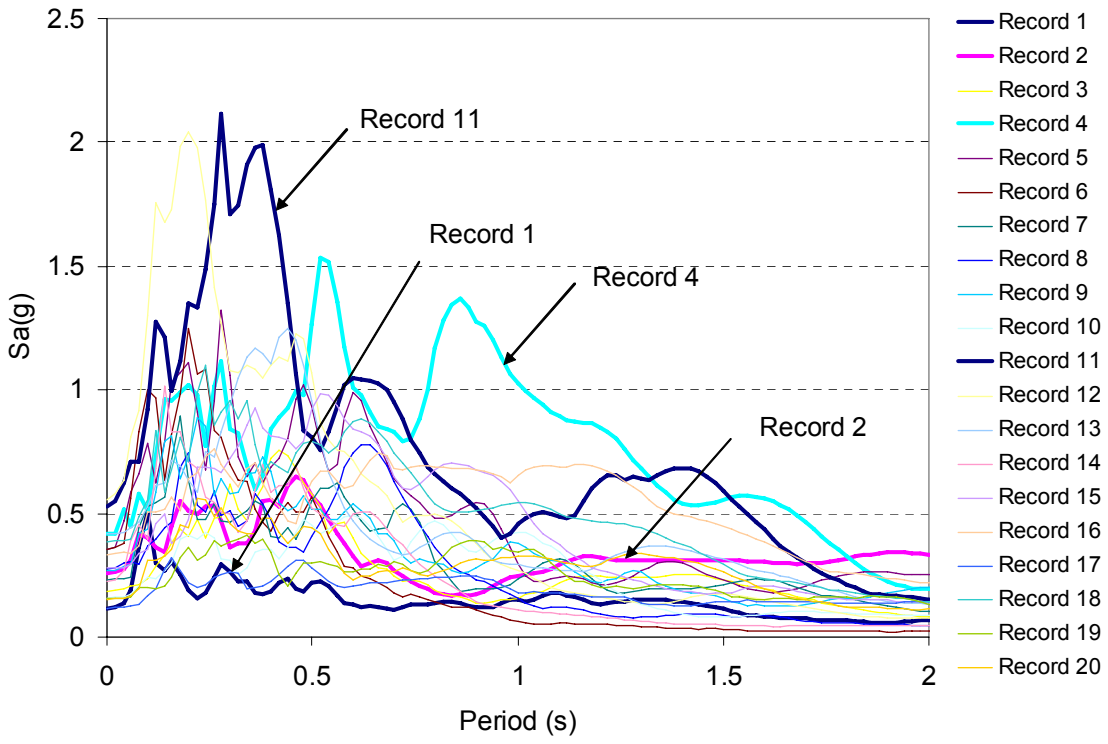

Figure 6.15 Elastic Response Spectra of Ground Motions Considered (5% damping)

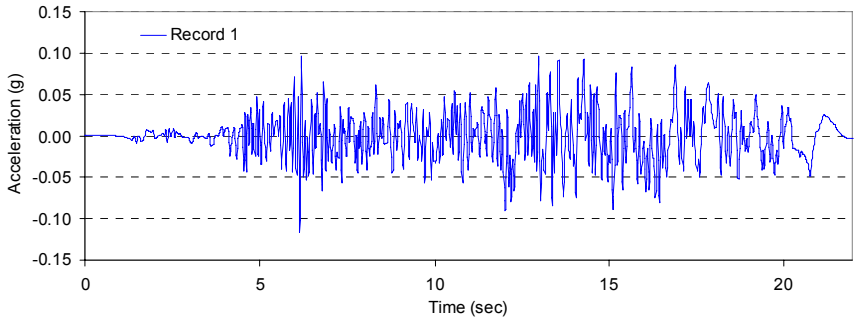

(a) Superstition Hills (Brawley), 1987

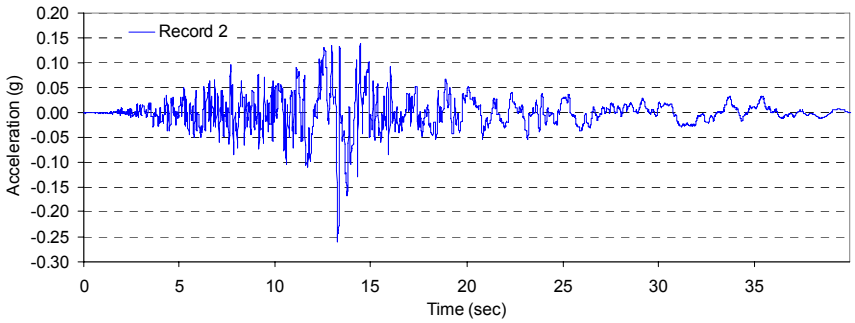

(b) Superstition Hills (El Centro Imp. Co. Cent), 1987

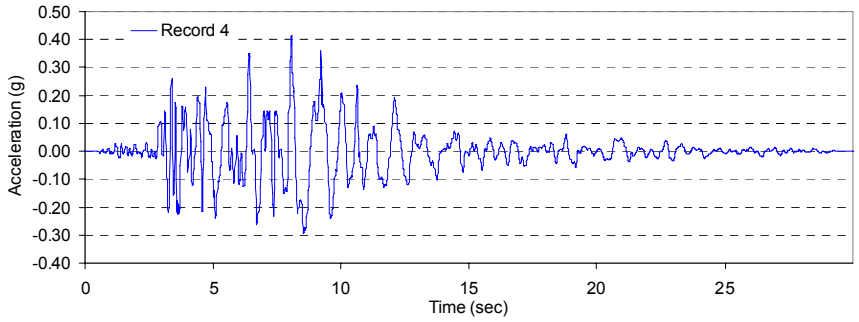

(c) Northridge (Beverly Hills 14145 Mulhol), 1994

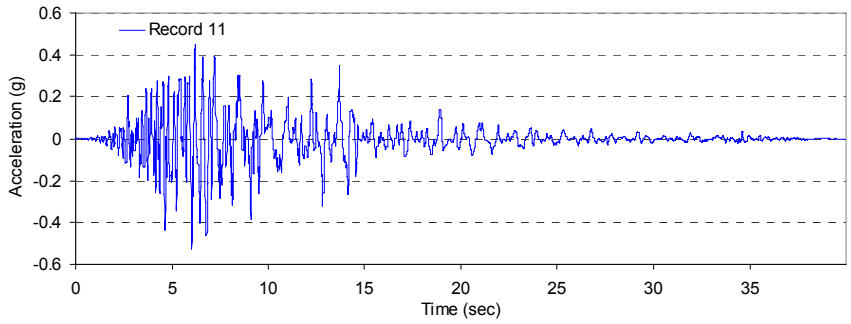

(d) Loma Prieta (Capitola), 1989

Figure 6.16 Ground Motions used for Generating Training Data

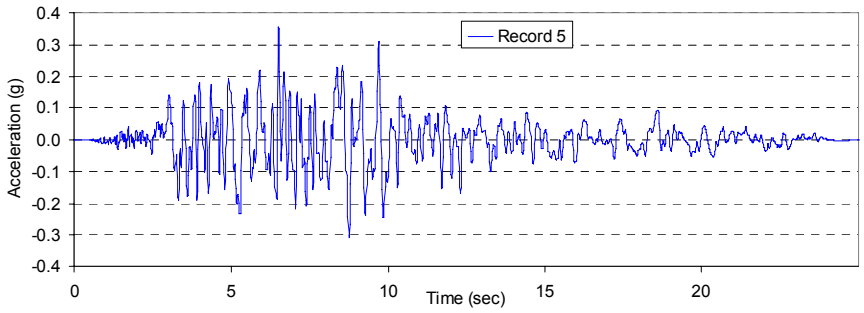

Figure 6.17 New Ground Motion used for Testing the Proposed Model

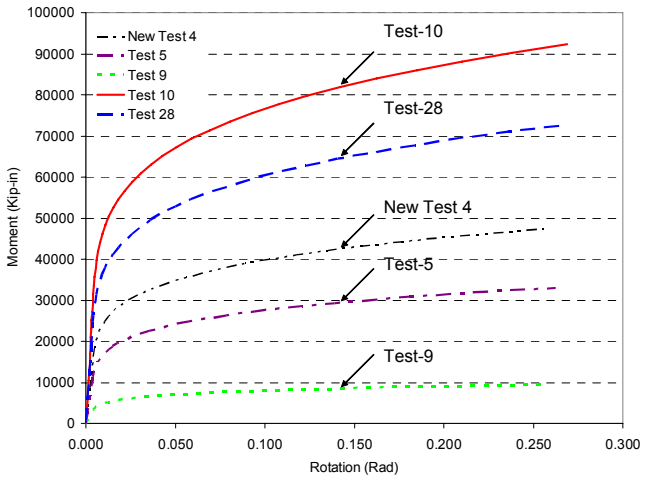

Figure 6.18 Selected Designs for Generation of Training Data

On the other hand, four sampled tests (Test-5, Test-9, Test-10 and Test-28) are selected to training the proposed model and Test-4 is chosen for testing the proposed model. Finally, the four tests and four ground motions are combined to make total 16 combinations. Training information of the proposed model is summarized in Table 6.4. Total number of training data is 84,744. The equation (6-11) expresses the trained GHNN based model.

$$M_n = \hat{\mathbf{M}}_{NN}\left(\left\{\theta_n, \theta_{n-1}, M_{n-1}, \xi_{\theta,n}, \Delta\eta_{\theta,n}, G(D,t,f)\right\} : \left\{9-50-50-1\right\}\right) \qquad (6\text{-}11)$$

After training the model, testing of the trained model is carried out with a new combination of test 4 and ground motion record 5.

Table 6.4 Training Information for Earthquake Loading

	Number of Epochs used in Training	NN Architecture	Average Error in Training
NN based Model	16,000	{9-50-50-1}	2.10×10^{-7}

After training the proposed model, it is tested with totally new situation whereby Test-4 and Record 5 are selected. The responses of the GHNN based inelastic hysteretic model to new set of design variables and a new ground motion are illustrated in time and frequency domain as illustrated in Figure 6.19 and Figure 6.20, respectively.

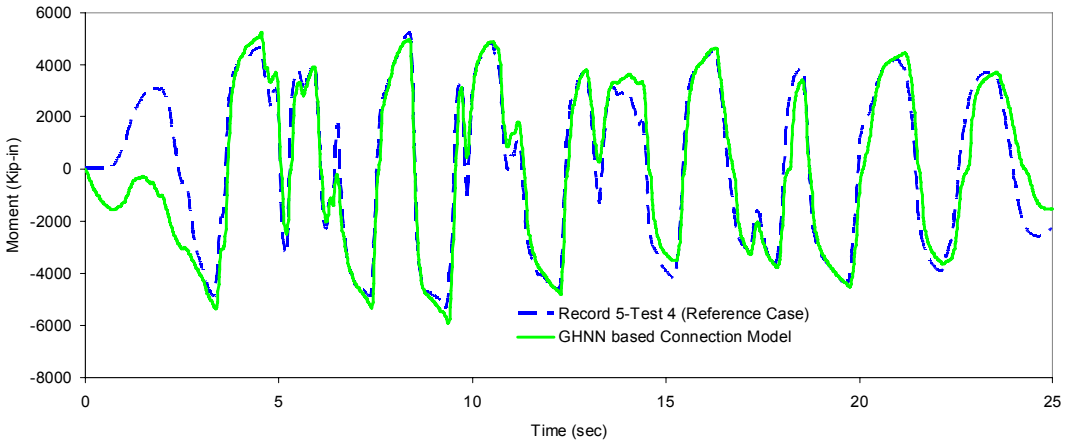

Figure 6.19 Time History of Predicted Moment by GHNN based Inelastic Hysteretic Model

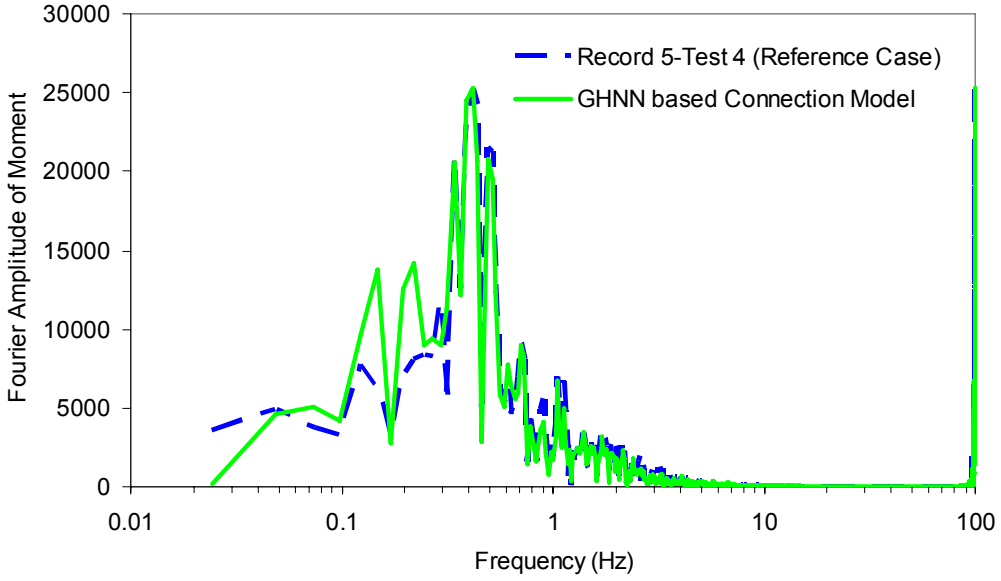

Figure 6.20 Comparison between Reference Case and GHNN based Model in Frequency Domain

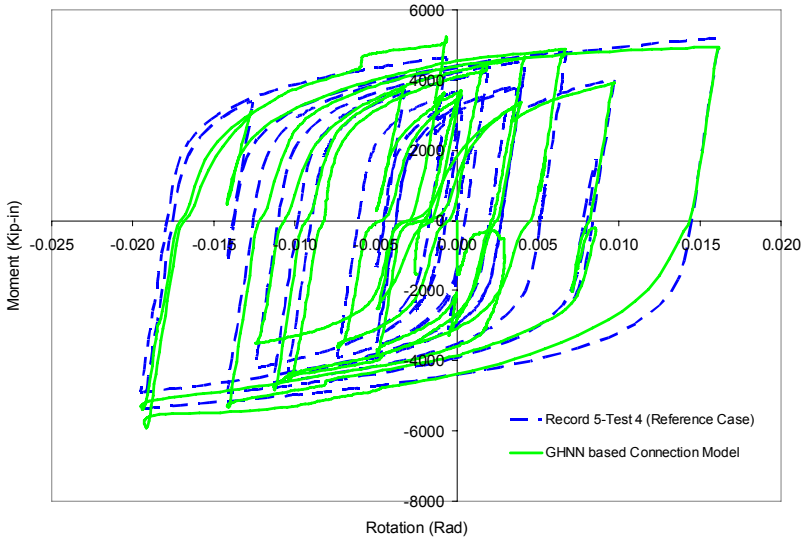

Figure 6.21 Comparison of Moment-Rotation Hysteresis between the Reference Case and GHNN based Model

The GHNN based inelastic hysteretic model is also shown to be reasonably responsive to the new combination of the design and ground motion in moment-rotation hysteresis curve as shown in Figure 6.21.

6.4.2 Top-and-Seat-Angle with Double Web Angle Connection

In this example, the verification of the GHNN based model is carried out with real experimental data with TSADW connections. Steel Connection Data Bank (SCDB) program provides the past testing data of various connection types (Chen and Toma 1994). Five test data are obtained from SCDB program; four of them are for training the model and one of them for testing the model. They were all tested in the U.S. in 1985 (Azizinamini and Radziminski 1989). The top- and seat-angles and web-angles are all assembled with high strength bolts.

Table 6.5 Test Cases on Top-and-Seat-Angle with Double Web Angle Connection

Test ID	Beam	Column	Angles	Fasteners	Tested by
Test 6	W8x21	W12X58	Flange Angle: 6 x 4.0 x 5/16 x 6.0 Web Angle: 4 x 3.5 x 1/4 x 5.5	A325 3/4"D 13/16" Oversize holes	A.Azizinamini et al. (1985) U.S.A
Test 9	W8X21	W12X58	Flange Angle: 6 x 3.5 x 3/8 x 6.0 Web Angle: 4 x 3.5 x 1/4 x 5.5	A325 7/8"D 15/16" Oversize holes	A.Azizinamini et al. (1985) U.S.A
Test 14	W14X38	W12X96	Flange Angle: 6 x 4.0 x 3/8 x 8.0 Web Angle: 4 x 3.5 x 3/8 x 8.5	A325 3/4"D 13/16" Oversize holes	A.Azizinamini et al. (1985) U.S.A
Test 16	W14X38	W12X96	Flange Angle: 6 x 4.0 x 1/2 x 8.0 Web Angle: 4 x 3.5 x 1/4 x 8.5	A325 7/8"D 15/16" Oversize holes	A.Azizinamini et al. (1985) U.S.A
New Test	W14X38	W12X96	Flange Angle: 6 x 4.0 x 3/8 x 8.0 Web Angle: 4 x 3.5 x 1/4 x 8.5	A325 3/4"D 13/16" Oversize holes	A.Azizinamini et al. (1985) U.S.A

The geometrical properties of the five test cases are summarized in Table 6.5. The moment-rotation curves from the five test cases are illustrated in Figure 6.22.

6.4.2.1 Design Variables and Mechanical Parameters

The design variables determined for the TSADW connection type are shown in Table 6.6. For each test case, the ultimate connection moment (M_u) is calculated from the simple mechanics and mechanism as explained in section 6.3.1.1. Like in extended-end-plate connection, the cyclic behavior is assumed to show non-pinching moment-rotation relationship following the polynomial model in section 2.3.1.3. Then the plastic rotation is calculated from equation (6-7) using the polynomial model. As done in the extended-

end-plate connections, the yield moment is assumed to be 2/3 of the ultimate moment capacity and the initial rotation is also calculated by equation (6-9).

Table 6.6 Design Variables and Material Properties of Five Test Cases

Test ID	d (in)	t (in)	t_c (in)	l_a (in)	g (in)	Material (ksi)
Test 6	8.25	0.31	0.25	6.0	2.125	Fy=40.65 Fu=68.43
Test 9	8.25	0.38	0.25	6.0	1.5625	Fy=39.55 Fu=67.95
Test 14	14.13	0.38	0.38	8.0	2.125	Fy=40.65 Fu=68.43
Test 16	14.13	0.50	0.25	8.0	2.0625	Fy=40.65 Fu=67.95
New Test	14.13	0.38	0.25	8.0	2.125	Fy=40.65 Fu=68.43

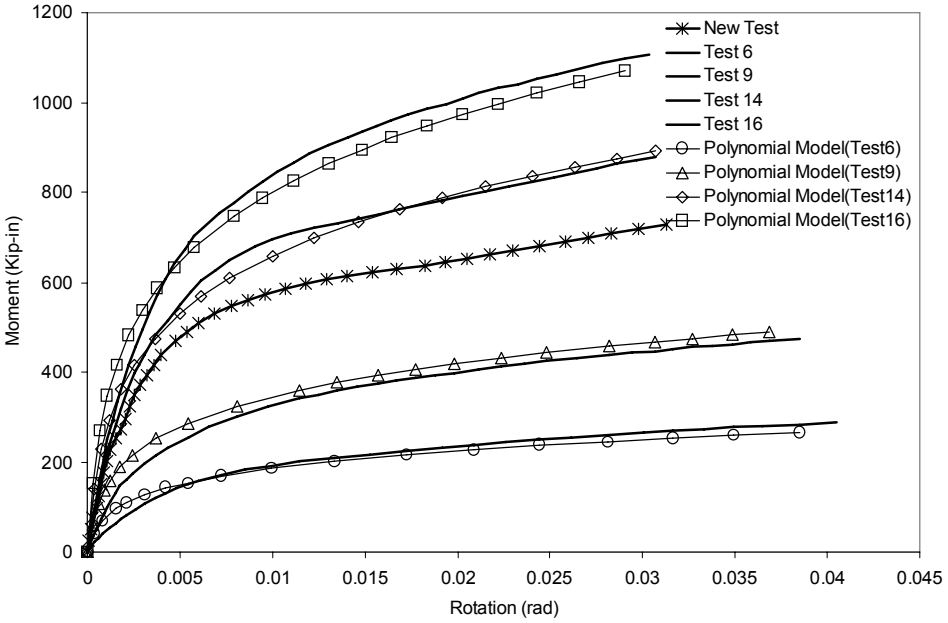

Figure 6.22 Moment-Rotation Curves from Experimental Results

Then the four mechanical parameters are calculated as shown in Table 6.7. As expected, the calculated rotational ductility is larger than the ones of the extended-end-plate connections.

Table 6.7 Mechanical Parameters for Test Cases

Test ID	K_i (kip-in/rad)	M_y(kip-in)	M_u(kip-in)	δ_θ
Test 6	128709.233	162.747	244.120	21.231
Test 9	239443.843	315.247	472.870	23.957
Test 14	456320.959	619.435	929.152	26.290
Test 16	555425.939	793.186	1189.779	30.751
New Test	385649.297	489.527	734.290	21.476

6.4.2.2 The Performance under Earthquake Loading

For earthquake ground motions, the same ground motions used in the extended-end-plate connections are used for training and testing the GHNN based model. To generate training data corresponding to each test case, nonlinear dynamic analysis is conducted with the finite element model illustrated in Figure 6.23. The finite element model consists of total 9 degrees of freedom, that is, 3 nodes and 3 DOF (dx, dy and rz) per node. Distributed mass is assumed for the beam-column element and lumped mass is at the top of the column.

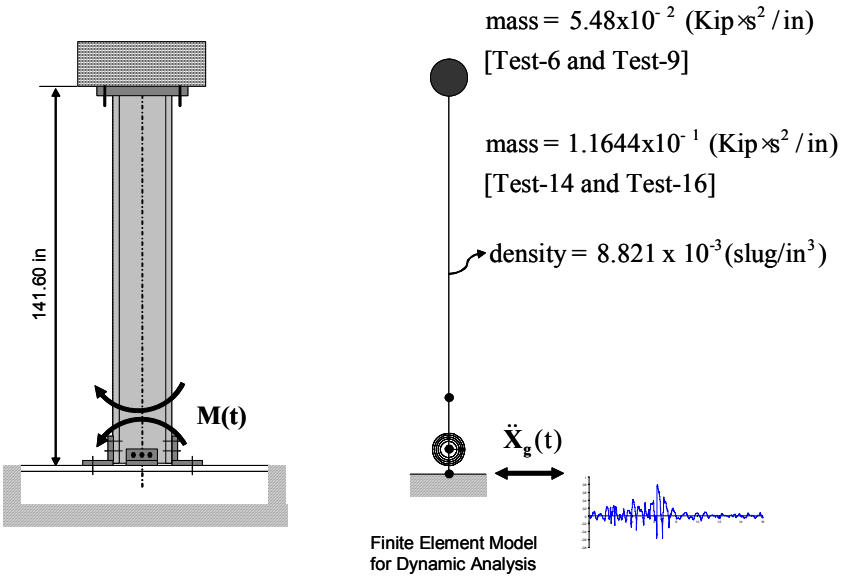

Figure 6.23 Dynamic Model of Column with TSADW connection

The natural periods of the first three modes of each test case are calculated as shown in Table 6.8. For the calculation, the rotational stiffness at the connection is assumed to be rigid.

Table 6.8 Natural Periods with Rigid Connection Assumption

Test ID	1st Mode (sec)	2nd Mode (sec)	3rd Mode (sec)
Test 6	0.9769	0.0418	0.0354
Test 9	0.9769	0.0418	0.0354
Test 14	0.7401	0.0533	0.0211
Test 16	0.7401	0.0533	0.0211
New Test	0.7401	0.0533	0.0211

From the four test cases and four ground motions, total 16 combinations are built to generate the training data. The moment-rotation hysteretic curves for the 16 combinations are illustrated in Figure 6.24. Because of different geometrical properties and ground motions, the hysteretic curves showed different paths from one another. The horizontal

displacement at the top also showed various time histories due to the variations. Then, the equation (6-12) describes the trained GHNN based model.

$$M_n = \hat{\mathbf{M}}_{NN}\left(\left\{\theta_n, \theta_{n-1}, M_{n-1}, \xi_{\theta,n}, \Delta\eta_{\theta,n}, G(d, t, t_c, l_a, g)\right\} : \left\{9-50-50-1\right\}\right) \qquad (6\text{-}12)$$

The training information is summarized in Table 6.9. The scale factor used in the training is 0.15 for all the inputs to the model.

Table 6.9 Training Information for Earthquake Loading

	Number of Epochs used in Training	NN Architecture	Average Error in Training
NN based Model	20,000	{9-50-50-1}	6.189×10^{-7}

For the purpose of verification, two new combinations of geometric properties and ground motion are used, which are new test/Record 4 and test14/new record.

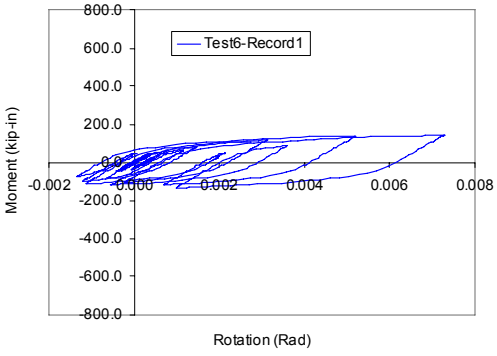

(a) Test 6-Record 1

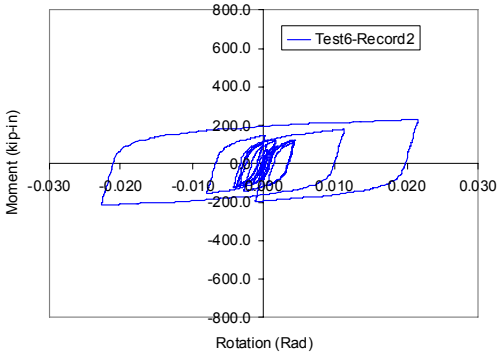

(b) Test 6-Record 2

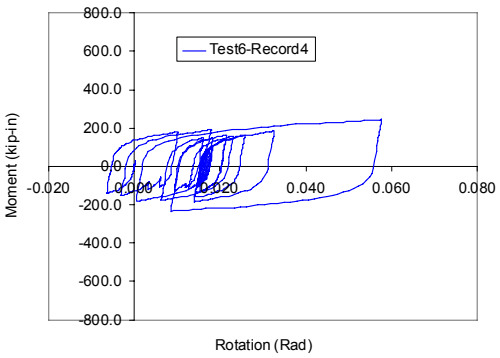

(c) Test 6-Record 4

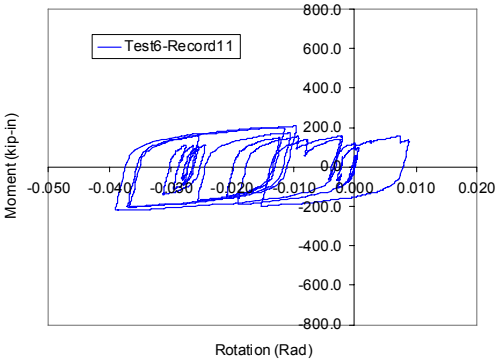

(d) Test 6-Record 11

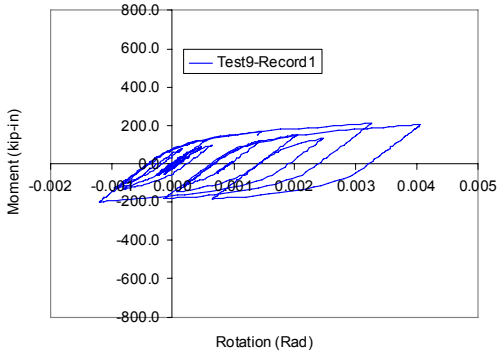

(e) Test 9-Record 1

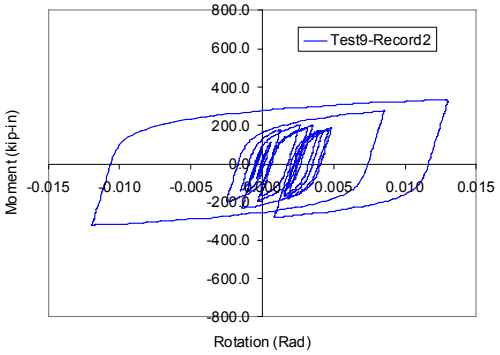

(f) Test 9-Record 2

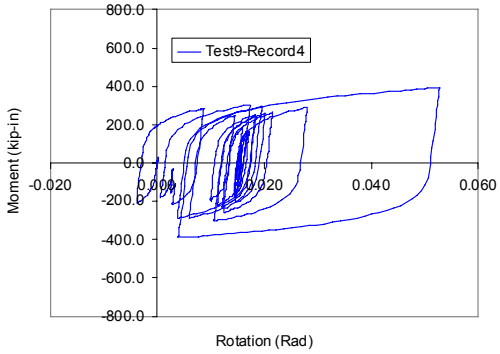

(g) Test 9-Record 4

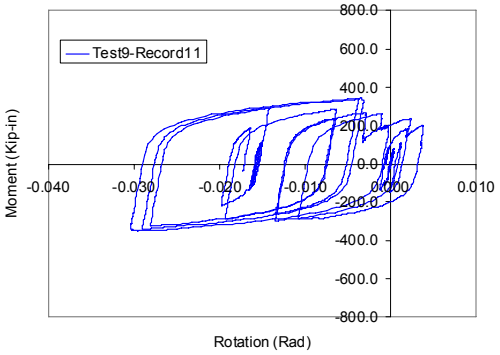

(h) Test 9-Record 11

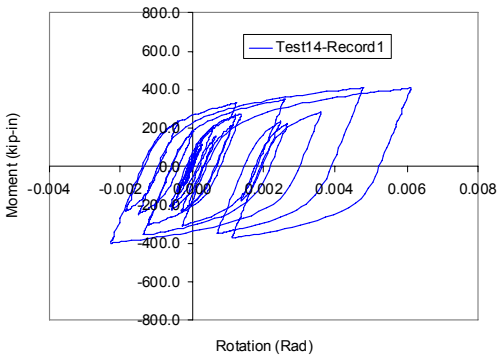

(i) Test 14-Record 1

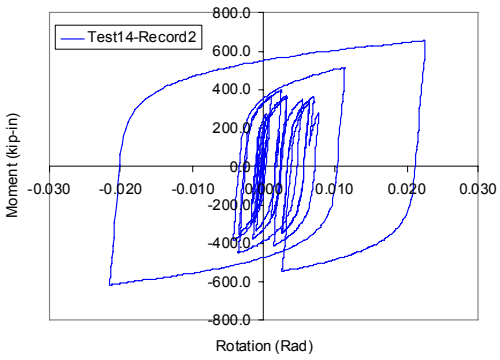

(j) Test 14-Record 2

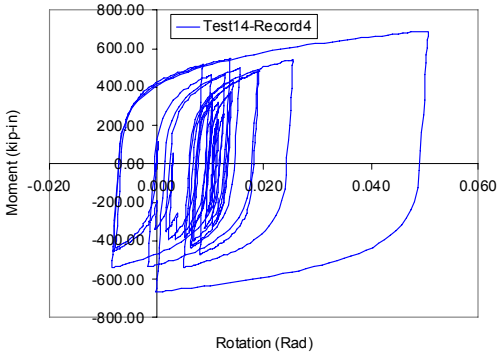

(k) Test 14-Record 4

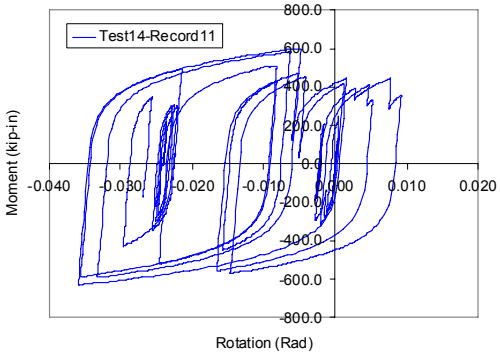

(l) Test 14-Record 11

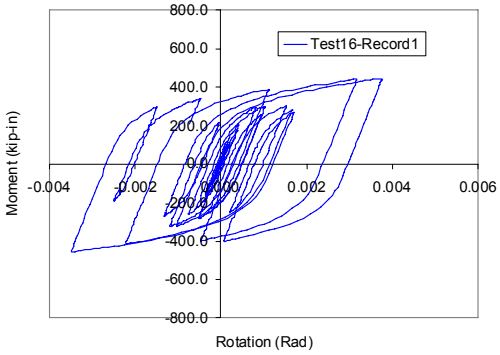

(m) Test 16-Record 1

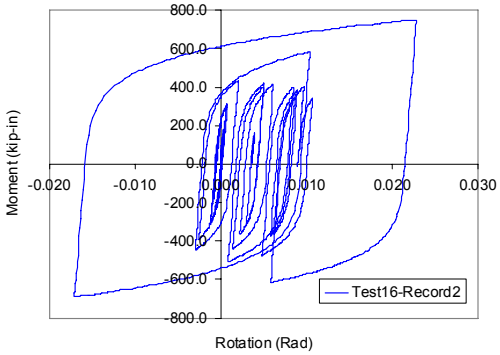

(n) Test 16-Record 2

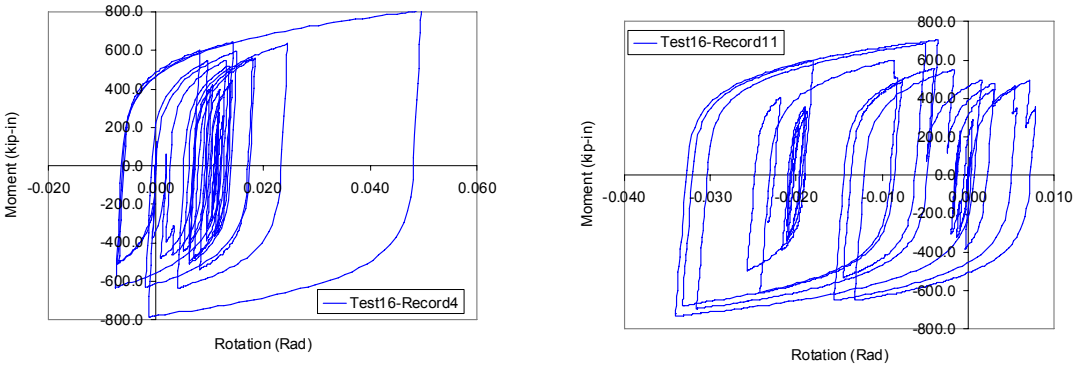

(o) Test 16-Record 4 (p) Test 16-Record 11

Figure 6.24 Moment-Rotation Hysteresis from 16 Combinations for Training GHNN based Model

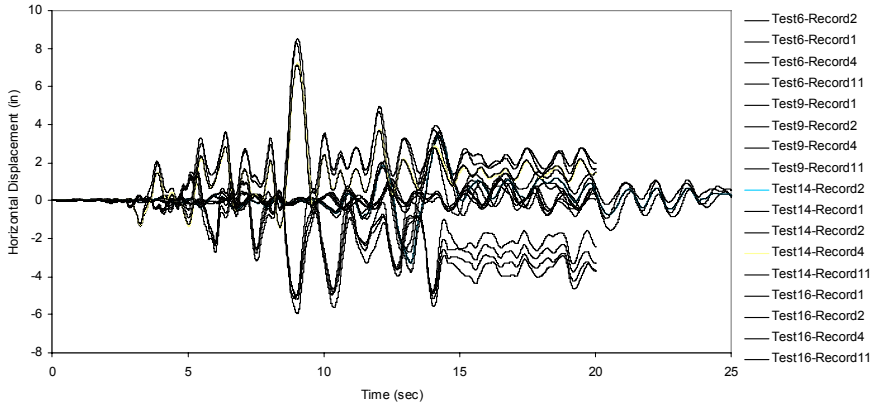

Figure 6.25 Time History of Horizontal Displacement at the Top

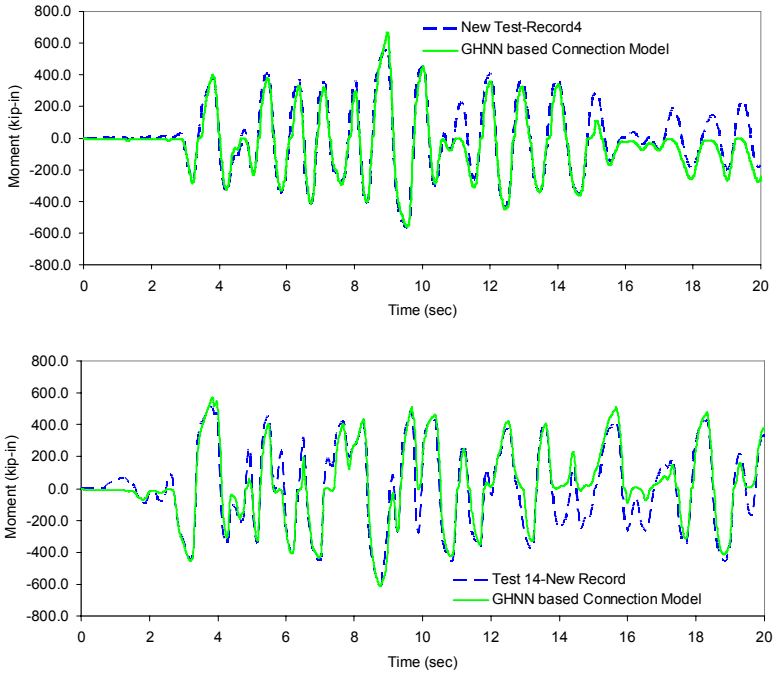

Figure 6.26 Time Histories of Predicted Moments by GHNN based Model

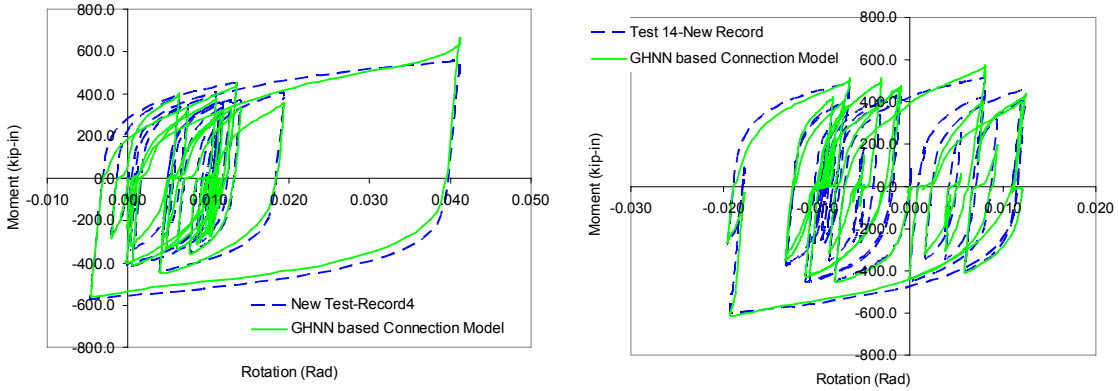

Figure 6.27 Moment-Rotation Hysteretic Curves of New test/Record 4 and Trained GHNN based Model

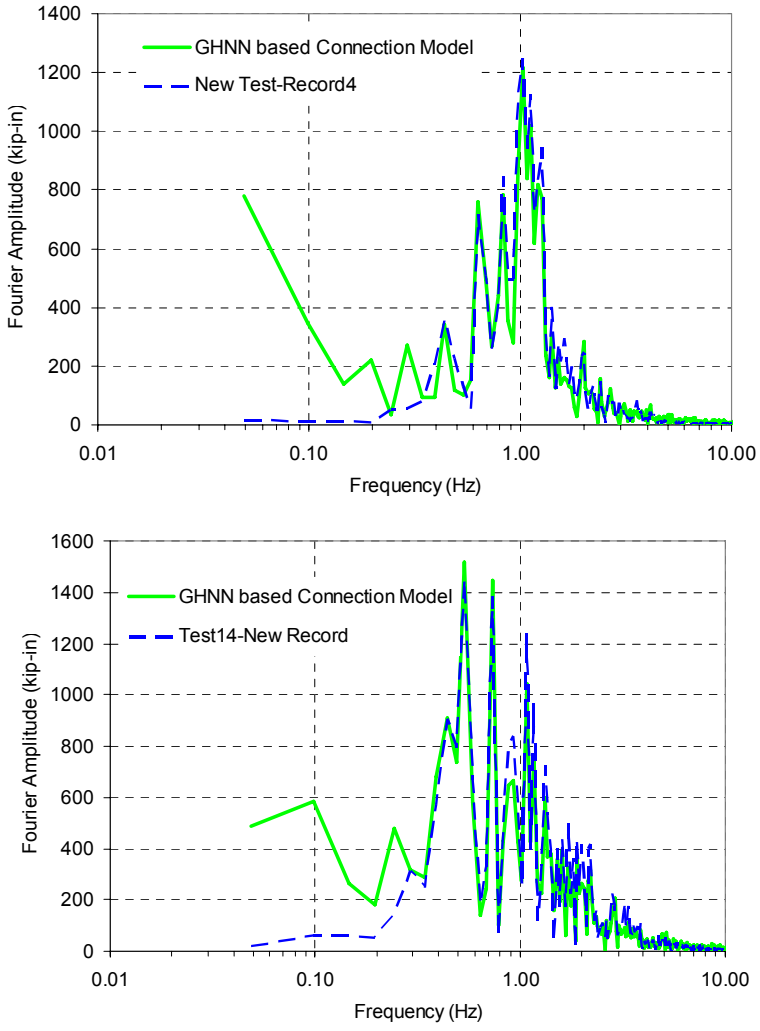

Figure 6.28 Fourier Amplitudes of Moment of GHNN based Model

Figure 6.26, Figure 6.27 and Figure 6.28 display moment predictions of the trained model at the connection subjected to new combinations of geometrical properties and earthquake records in time history, moment-rotation hysteretic curve and Fourier amplitude in frequency domain, respectively. It has been verified that the trained GHNN based model can give reasonable predictions of moment and responsive to variations in both geometrical parameters of connecting elements and earthquake records. The

proposed model opens up a new approach to design-based numerical model for hysteretic behavior of connections as following.

6.5 Further Applications of the Proposed Model

The trained GHNN based inelastic hysteretic model contains essential information on dynamic hysteretic behavior of connections. Because the model includes one prehistory point on moment-rotation curve, it has information on the path dependent connection behavior. Owing to the internal variables introduced in Chapter 3, the model can also learn dynamic evolutions in the moment and rotation space under earthquake loading conditions. Additionally, the model has a set of mechanical variables which stand for the load-carrying capacity of connections in the design point of view. This intensive information within connection weights of the model can open up many promising applications in many engineering problems. Moreover, the model can be easily implemented into nonlinear finite element analysis code for predicting the system response.

For modeling of the inelastic hysteretic behavior of connections, a set of libraries for many connection types can be constructed from available experimental results. The previous examples with two common connection types demonstrate part of this application. The self-learning simulation in Chapter 5 will be able to help generating necessary training data for the proposed model from structural tests. Since the proposed model requires design variables and it is responsive to the change in geometrical properties, the proposed model can be also used in design optimization based on inelastic hysteretic behavior. Furthermore, the GHNN based model can become a prototype model

that can be customized to any structural-geotechnical component beyond the application to beam-column connections.

6.6 Conclusions

Generalized hybrid neural network (GHNN) based inelastic hysteretic model has been suggested for modeling of beam-column connection behavior. The advantage of the model is that it accepts information from design variables through a separate physical principle based module and link the information to inelastic hysteretic model for reproducing the experimental data. Beyond simple reproduction of the experimental data, the model has been verified to be reasonably responsive to the changes in the design variables and ground motions.

For numerical examples, the model was verified with synthetic and experimental data on two common connection types; the extended-end-plate connection and top-and-seat-angle-with-double-web-angle connection. Beyond the application to beam-column connections, other promising applications were discussed.

CHAPTER 7 SUMMARY OF RESEARCH

7.1 Summary

In this report, a novel modeling approach to hysteretic behavior of beam-column connections has been proposed based on self-learning simulation and a generalized hysteretic model for connections has been suggested based on the proposed cyclic material model. To conduct development of the models and methodology, conventional modeling approaches were revisited and recommendations to improve accuracy and practicality were addressed.

For the application in earthquake engineering, a new neural network (NN) based cyclic material model has been proposed. Its distinct advantage is that it can learn and reproduce any complex hysteretic behavior of materials or structural members under earthquake loadings. Moreover, its numerical implementation is much easier than any other phenomenological model since it does not need to have interaction equations or plastic potential. The model has new internal variables as inputs to expedite learning of hysteretic behavior under earthquake loadings. The essential role of the variables is to provide a necessary condition for establishing a mathematical functional relationship between input and output values, which is one-to-one or many-to-one mapping. Performances of the model were verified with experimental data and simulated testing data. The proposed model was also shown to learn the cyclic plasticity behavior of metal in non-uniform state of multi-dimensional stresses.

For a nonlinear analysis considering inelastic behavior of connections, a nonlinear finite element code has been developed using three-dimensional beam-column element and plastic hinge approach for connections. Based on the Updated Lagrangian formulation, geometric nonlinearity was also implemented for large displacement analysis. The advantage of the NN based connection model was demonstrated with a series of numerical examples. The capabilities of the model in accuracy and generalization were demonstrated in a nonlinear dynamic analysis of a frame with semi-rigid connections under earthquake loading. Moreover, the proposed model was shown to reproduce behavior of a full three-dimensional finite element model under non-proportional cyclic loading conditions. Therefore, the accurate local behavior obtained from either advanced computational models or experimental data can be combined with simplified frame models. This approach opens up a new advanced simulation method for understanding actual effects of the nonlinear connection behavior on the global response.

To propose a new modeling approach of beam-column connections, a self-learning simulation framework has been developed. Its distinct advantage is that it can develop a set of NN based connection models using experimental measurements at control points over tested structures. In the framework, a dual nonlinear finite element analysis tool was equipped with the auto-progressive training algorithm. In particular, the algorithmic formulation of the NN based model for self-learning simulation has been investigated to suggest better formulation in terms of stability and accuracy. Based on the numerical test results, recommendations to improve performances of the self-learning simulation were suggested in the context of the algorithmic formulation relating to calculations of tangent

stiffness matrices and internal resisting forces. Both synthetic and experimental data were employed to verify the proposed modeling approach. It was shown that the NN based connection model obtained from self-learning simulations can reproduce realistic responses of frames with semi-rigid connections.

For practical applications of the model developed, it has been extended to a generalized hybrid NN (GHNN) based hysteretic model for beam-column connections. It consists of two modules; NN based module and physical principle based module. The physical principle based module associates design variables with mechanical parameters using simple mechanics for yield mechanisms and experimental observations. In the NN based module, the mechanical parameters are used as inputs. Eventually, it becomes a first-ever dynamic hysteretic model that can be physically responsive to changes in design variables and mechanical states in moment-rotation space. The performance of the model was validated with two common connection types (extended-end-plate connection and top-and-seat-angle-with-double-web-angle connection) using experimental data.

7.2 Concluding Remarks

Beam-column connections are regions that suffer from severe yielding, local buckling and tearing, etc as evidenced in damages from the past earthquakes. Classical plasticity theory can not deal with such complex hysteretic behaviors under earthquake loadings. Phenomenological models based on regression analysis with curve-fitting technique have inherent errors and limitations in dynamic representation of hysteretic behavior of connections. From the results of this research, it can be concluded that the NN based

cyclic material model is viable and promising for modeling of hysteretic behavior of materials both in uniform and non-uniform stress states. Moreover, the self-learning simulation methodology equipped with the proposed model provides an innovative method for completing modeling task of beam-column connections. The NN based connection model, as opposed to conventional models, does not need to introduce any idealization, assumption, and simplification in modeling of connections since it can directly learn its actual behavior from experimental data. The capability of the NN based approach is more than learning of the hysteretic behavior. Therefore, information flow from design variables through mechanical parameters was incorporated with the NN based model. Its generalized features clearly indicate its promising application in daily design process and open up further engineering applications.

The following conclusions can be drawn based on the results of these research investigations.

1. The new NN based cyclic material model has superior learning capability of hysteretic behavior as compared to conventional NN based material constitutive models whereby several recent states of stress-strain are introduced as inputs for capturing nonlinearities and path-dependency in the behavior of materials. Owing to the two internal variables observable in material testing, significant enhancement could be established in learning the hysteretic behavior.

2. The NN based connection modeling approach, as opposed to conventional modeling methods such as distributed inelasticity model and stress resultant-based lumped inelasticity model, open up a new analysis method which can incorporate actual behavior

of beam-column connections from experiments with nonlinear frame analysis. Not only can the hysteretic behavior under earthquake loading be represented by the proposed model but also the trained model can predict novel behavior that is not included in the training data.

3. The self-learning simulation framework can greatly simplify a modeling task from structural testing. Since NN is highly flexible and adaptable to new sets of experimental data, the NN based connection model and training data obtained from the self-learning simulation can be updated with novel experimental data available and reusable for further developments, respectively.

4. The GHNN based hysteretic model can be used in structural analysis for daily design purposes. A distinct advantage of GHNN based model is its predictive capability even with novel earthquake records and geometric properties as validated in this research. In particular, the training data obtained from the self-learning simulation can be used to develop the GHNN based model for each connection type.

7.3 Future Directions of Research

The modeling approaches developed in this report are fundamentally different from the conventional approaches. The developments of the NN based cyclic material model, self-learning simulation framework and the GHNN based hysteretic model open up potential applications in many complex engineering problems. For example, it can be applied to other engineering subjects such as bracing members, shape memory alloy applications,

highly engineered members with friction and damping, soil, and concrete material, etc within the same framework. The following are a list of the research directions that can be done in the near future.

1. In this research, beam-column element with the lumped inelasticity model at the connections was used for self-learning simulations. However, assumptions of the inelastic behavior at fixed locations could have inherent modeling error since inelastic deformations at the connection and any other high-stress region is actually distributed within a certain range. Moreover, experiments can also have uncertainties in construction quality, materials and measurements and so on. Therefore, the error can be explained in the context of uncertainties in both numerical modeling and experiments. Recognizing the source of errors, further research on self-learning simulation with refined numerical models would be in need, depending on the engineering subjects.

2. There could be different combinations of the trained NN based models that produce a same global response. For resolving this non-uniqueness problem, more refined model such as a component-based model could be suitable whereby the NN based model represents uni-axial inelastic hysteretic behavior of connecting components. Although there could be still modeling error related to yield/failure mechanisms in component level, they are not of our interest as long as accurate responses could be obtained in member and structural level.

3. Although the NN based cyclic material model was verified with a multi-dimensional problem, its performance in the self-learning simulation has not been verified since there are few experimental data from three-dimensional steel moment-resisting frames with

semi-rigid connections. However, if reliable test data are available, the verification can be readily conducted.

Since the proposed modeling approach can be used to solve inverse problems, its potential applications are far beyond the modeling of beam-column connections. It could have broad spectrum of applications such as nonlinear model updating, system identification, non-destructive testing, biomedical imaging and on-line hybrid simulation and testing. Detailed ideas on the potential applications need to be developed at the current stage.

REFERENCES

[1] ABAQUS/Standard, H. (2004). "A General Purpose Finite Element Code", Karlsson & Sorense, Inc: Hibbitt

[2] Abdalla, K. M. and Stavroulakis, G. E. A. (1995). "Backpropagation Neural Network Model for Semi-Rigid Joints", *Microcomputers in Engineering*, **10**, 77~87

[3] AISC, (2001). *Manual of Steel Construction-Load and Resistance Factor Design*,

[4] Albermani, F. G. A., Li, B., Zhu, K. and Kitipornchai, S. (1994). "Cyclic and Seismic Response of Flexibly Jointed Frames", *Engineering Structures*, **16**, 249-255

[5] Anderson, D., Hines, E. L., Arthur, S. J. and Eiap, E. L. (1997). "Application of Artificial Neural Networks to the Prediction of Minor Axis Steel Connections", *Computers & Structures*, **63**, 685-692

[6] Ang, K. M. and Morris, G. A. (1984). "Analysis of Three-Dimensional Frames with Flexible Beam-Column Connections", *Canadian Journal of Civil Engineering*, **11**, 245~254

[7] Azizinamini, A. and Radziminski, J. B. (1989). "Static and Cyclic Performance of Semirigid Steel Beam-to-Column Connections", *Journal of Structural Engineering-Asce*, **115**, 2979-2999

[8] Bahaari, M. R. and Sherbourne, A. N. (1996). "Three-Dimensional Simulation of Bolted Connections to Unstiffened Columns-2. Extended Endplate Connections", *Journal of Constructional Steel Research*, **40**, 189-223

[9] Bernuzzi, C., Zandonini, R. and Zanon, P. (1996). "Experimental Analysis and Modeling of Semi-Rigid Steel Joints under Cyclic Reversal Loading", *Journal of Constructional Steel Research*, **38**, 95-123

[10] Bodner, S. R. and Partom, Y. (1975). "Constitutive Equations for Elastic-Viscoplastic Strain Hardening Materials", *Trans ASME Journal of Applied Mechanics*, **42**, 385~389

[11] Bursi, O. S. and Jaspart, J. P. (1998). "Basic Issues in the Finite Element Simulation of Extended End Plate Connections", *Computers & Structures*, **69**, 361-382

[12] Chaboche, J. L. (1989). "Constitutive Equations for Cyclic Plasticity and Cyclic Viscoplasticity", *International Journal of Plasticity*, **5**, 247~302

[13] Chan, C. L. and Chui, P. P. T., (2000). *Nonlinear Static and Cyclic Analysis of Steel Frames with Semi-Rigid Connections*, Elsevier

[14] Chan, S. L. and Ho, G. W. M. (1994). "Nonlinear Vibration Analysis of Steel Frames with Semirigid Connections", *Journal of Structural Engineering-Asce*, **120**, 1075-1087

[15] Chen, W. F. and Toma, S., (1994). *Advanced Analysis of Steel Frames*, CRC Press

[16] Chopra, A. K., (2000). *Dynamics of Structures*, Prentice-Hall

[17] Christopoulos, C., Filiatrault, A. and Folz, B. (2002). "Seismic Response of Self-Centering Hysteretic Sdof Systems", *Earthquake Engineering & Structural Dynamics*, **31**, 1131-1150

[18] Cincotti, S., Marchesi, A. and Serri, A. (1998). "A Neural Network Model of Parametric Nonlinear Hysteretic Inductors", *IEEE transactions on Magenetics*, **34**, 3040~3043

[19] Citipitioglu, A. M., Haj-Ali, R. M. and White, D. W. (2002). "Refined 3d Finite Element Modeling of Partially-Restrained Connections Including Slip", *Journal of Constructional Steel Research*, **58**, 995~1013

[20] De Stefano, M., Deluca, A. and Astaneh Asl, A. (1994). "Modeling of Cyclic Moment-Rotation Response of Double-Angle Connections", *Journal of Structural Engineering-Asce*, **120**, 212-229

[21] Deng, C. G., Bursi, O. S. and Zandonini, R. (2000). "A Hysteretic Connection Element and Its Applications", *Computers & Structures*, **78**, 93-110

[22] Dhillon, B. S. and Abdelmajid, S. (1990). "Interactive Analysis and Design of Flexibly Connected Frames", *Computers & Structures*, **36**, 189-202

[23] Elnashai, A. S., Elghazouli, A. Y. and Denesh-Ashtiani, F. A. (1998). "Response of Semi-Rigid Steel Frames to Cyclic and Earthquake Loads", *Journal of Structural Engineering*, **124**, 857~867

[24] El-Tawil, S. and Deierlein, G. G. (1998). "Stress-Resultant Plasticity for Frame Structures", *Journal of Engineering Mechanics-Asce*, **124**, 1360-1370

[25] Faella, C., Piluso, V. and Rizzano, G., (2000). *Structural Steel Semi-Rigid Connections-Theory, Design and Software*, CRC Press LLC

[26] FEMA-355D, 2000. State of the Art Report on Connection Performance, *FEMA-355D*, *SAC Joint Venture*

[27] FEMA-355F, 2000. State of the Art Report on Performance Prediction and Evaluation of Steel Moment-Frame Buildings, *FEMA-355F*, *SAC Joint Venture*

[28] Frye, M. J. and Morris, G. A. (1975). "Analysis of Flexibly Connected Steel Frames", *Canadian Journal of Civil Engineering*, **2**, 280~291

[29] Furukawa, T. and Hoffman, M. (2004). "Accurate Cyclic Plastic Analysis Using a Neural Network Material Model", *Engineering Analysis with Boundary Elements*, **28**, 195~204

[30] Furukawa, T. and Yagawa, G. (1998). "Implicit Constitutive Modeling for Viscoplasticity Using Neural Networks", *International Journal for Numerical Methods in Engineering*, **43**, 195-219

[31] Ghaboussi, J., Garret, J. and Wu, X. (1991). "Knowledge-Based Modeling of Material Behavior with Neural Networks", *Journal of Engineering Mechanics, ASCE*, **117**, 132~153

[32] Ghaboussi, J., Pecknold, D. A., Zhang, M. F. and Haj-Ali, R. M. (1998a). "Autoprogressive Training of Neural Network Constitutive Models", *International Journal for Numerical Methods in Engineering*, **42**, 105-126

[33] Ghaboussi, J. and Sidarta, D. (1997). "New Method of Material Modeling Using Neural Networks", *In: 6th International Symposium on Numerical Models in Geomechanics*,

[34] Ghaboussi, J. and Sidarta, D. (1998b). "A New Nested Adaptive Neural Network for Modeling of Constitutive Behavior of Materials", *International Journal of Computer and Geotechnics*, **22**, 29~51

[35] Ghaboussi, J., Zhang, M., Wu, X. and Pecknold, D. A. (1997). "Nested Adaptive Neural Network: A New Architecture", *Proceeding, International Conference on Artificial Neural Networks in Engineering*, St. Louis, MO

[36] Goto, Y. and Chen, W. F. (1987). "2nd-Order Elastic Analysis for Frame Design", *Journal of Structural Engineering-Asce*, **113**, 1501-1519

[37] Green, A. E. and Naghdi, P. M. (1965). "A General Theory of an Elasto-Plastic Continuum", *Archive for rational mechanics and analysis*, **18**, 251~281

[38] Gupta, A. and Krawinkler, H., 1999. Seismic Demands for Performance Evaluation of Steel Moment Resisting Frame Structures, *Report No.132 Stanford University, The John A. Blume Earthquake Engineering Center*

[39] Hajjar, J. F. and Gourley, B. C. (1997). "A Cyclic Nonlinear Model for Concrete-Filled Tubes -1. Formulation", *Journal of Structural Engineering-Asce*, **123**, 736-744

[40] Hajjar, J. F., Gourley, B. C. and Olson, M. C. (1997). "A Cyclic Nonlinear Model for Concrete-Filled Tubes -2. Verification", *Journal of Structural Engineering-Asce*, **123**, 745-754

[41] Hashash, Y. M. A., Jung, S. and Ghaboussi, J. (2004). "Numerical Implementation of a Neural Network Based Material Model in Finite Element Analysis", *International Journal for Numerical Methods in Engineering*, **59**, 989~1005

[42] Hashash, Y. M. A., Marulanda, C., Ghaboussi, J. and Jung, S. (2003). "Systematic Update of a Deep Excavation Model Using Field Performance Data", *Computer and Geotechnics*, **30**, 477~488

[43] Hertz, J., Krogh, A. and Palmer, R. G., (1991). *Introduction to the Theory of Neural Computation*, Westview Press

[44] Hilber, H. M., Hughes, T. J. R. and Taylor., R. L. (1977). "Improved Numerical Dissipation for Time Integration Algorithms in Structural Dynamics", *Earthquake Engineering and Structural Dynamics*, **5**, 283-292

[45] Iman, R. L. and Conover, W. J. (1982). "A Distribution-Free Approach to Inducing Rank Correlation among Input Variables", *Communications in Statistics*, **B11**, 311~334

[46] Iwan, W. D. (1966). "A Distributed-Element Model for Hysteresis and Its Steady-State Dynamic Response", *Journal of Applied Mechanics*, **33**, 893~900

[47] Izzuddin, B. A. and Elnashai, A., 1989. Adaptic:A Program for Adaptive Large Displacement Inelastic Dynamic Analysis of Frames, *Engrg. Seismology and Earthquake Engrg. Rep. No. ESEE7/89*, *Imperial College, London*

[48] Jung, S. and Ghaboussi, J. (2006). "Neural Network Constitutive Model for Rate-Dependent Materials", *Computers & Structures*, **84**, 955-963

[49] Karsan, I. D. and Jirsa, J. O. (1969). "Behavior of Concrete under Compressive Loading", *Journal of Structural Division, ASCE*, **95**, 2543~2563

[50] Kishi, N. and Chen, W. F., 1986. Database of Steel Beam-to-Column Connections, *Structural Engineering Report, No. CE-STR-86-26*, *School of Civil Engineering, Purdue University*

[51] Kishi, N. and Chen, W. F. (1990). "Moment-Rotation Relations of Semirigid Connections with Angeles", *Journal of Structural Engineering-Asce*, **116**, 1813-1834

[52] Krawinkler, H. (1978). "Shear Design of Steel Frame Joints", *Engineering Journal, AISC*, **15**,

[53] Krawinkler, H., Bertero, V. V. and Popov, E. P., 1971. Inelastic Behavior of Steel Beam-to-Column Subassemblages, *Report EERC/71-7*, *University of California, Berkeley*

[54] Lefik, M. and Schrefler, B. A. (2003). "Artificial Neural Network as in Incremental Non-Linear Constitutive Model for a Finite Element Code", *Computer methods in applied mechanics and engineering*, **192**, 3265~3283

[55] Lemaitre, J. and Chaboche, J. L., (1990). *Mechanics of Solid Materials*, Cambridge University Press

[56] Lui, E. M. and Chen, W. F. (1986). "Analysis and Behavior of Flexibly-Jointed Frames", *Engineering Structures*, **8**, 107-118

[57] Madas, P. J. and Elnashai, A. S. (1992). "A Component-Based Model for Beam-Column Connections", *Tenth World Conference on Earthquake Engineering*, Madrid, Spain

[58] Mayergoyz, I. D., (1991). *Mathematical Models of Hysteresis*, Springer

[59] Nakashima, M., Suita, K., Morisako, K. and Maruoka, M. (1998). "Tests of Welded Beam-Column Subassemblies, I:Global Behavior", *Journal of Structural Engineering*, **124**, 1236~1244

[60] Orbison, J. G., McGuire, W. and Abel, J. F. (1982). "Yield Surface Applications in Non-Linear Steel Frame Analysis", *Computer Methods in Applied Mechanics and Engineering*, **33**, 557-573

[61] Ostrander, J. R., 1970. An Experimental Investigation of End-Plate Connections, Masters Report, University of Saskatchewan, Saskatoon, SK, Canada

[62] Palermo, D. and Vecchio, F. J. (2003). "Compression Field Modeling of Reinforced Concrete Subjected to Reversed Loading: Formulation", *ACI Structural Journal*, **100**, 616~625

[63] PEER, (2000), "Peer Strong Motion Database", http://peer.berkeley.edu/smcat/index.html, 2006, Regents of the University of California

[64] Plumier, A. (1994). "Behavior of Connections", *Journal of Constructional Steel Research*, **29**, 95-119

[65] Powell, G. H. and Chen, P. F. S. (1986). "3d Beam-Column Element with Generalized Plastic Hinges", *Journal of Engineering Mechanics-Asce*, **112**, 627-641

[66] Ramberg, W. and Osgood, W. R., 1943. Description of Stress-Strain Curves by Three Parameters, *Technical Report No. 992*, *National Advisory Committee for Aeronautics*

[67] Rassati, G. A., Leon, R. T. and Noe, S. (2004). "Component Modeling of Partially Restrained Composite Joints under Cyclic and Dynamic Loading", *Journal of Structural Engineering*, **130**, 343~351

[68] Richard, R. M. and Abbott, B. J. (1975). "Versatile Elastic-Plastic Stress-Strain Formula", *Journal of Engineering Mechanics, ASCE*, **101**, 511~515

[69] Riedmiller, M. and Braun, H. (1993). "A Direct Adaptive Method for Faster Back Propagation Learning: The Rprop Algorithm", *IEEE International Conference on Neural Networks*, Piscataway, NJ,USA

[70] Ristinmaa, M. (1999). "Thermodynamic Formulation of Plastic Work Hardening Materials", *Journal of Engineering Mechanics, ASCE*, **125**, 152~155

[71] SAC, (1995a), "Sac Steel Project: Test Summary No. 19", www.sacsteel.org/design/test-summaries.html, 2006, SAC

[72] SAC, (1995b), "Sac Steel Project: Test Summary No. 21", http://www.sacsteel.org/design/test-summaries.html, 2006, SAC

[73] SAC, (1999), "Sac Steel Project: Connection Database", http://www.sacsteel.org/connections/, 2006, SAC

[74] Sakla, S. S. S. (2004). "Neural Network Modeling of the Load-Carrying Capacity of Eccentrically-Loaded Single-Angle Struts", *Journal of Constructional Steel Research*, **60**, 965-987

[75] Sherbourne, A. N. and Bahaari, M. R. (1994). "3d Simulation of End-Plate Bolted Connections", *Journal of Structural Engineering-Asce*, **120**, 3122-3136

[76] Sherbourne, A. N. and Bahaari, M. R. (1996). "3d Simulation of Bolted Connections to Unstiffened Columns -1. T-Stub Connections", *Journal of Constructional Steel Research*, **40**, 169-187

[77] Shin, H. S. and Pande, G. N. (2000). "On Self-Learning Finite Element Codes Based on Monitored Response of Structures", *Computers and Geotechnics*, **27**, 161~178

[78] Shiratori, E. and Ikegami, K. (1968). "Experimental Study of the Subsequent Yield Surface by Using Cross-Shaped Specimens", *Journal of the Mechanics and Physics of Solids*, **16**, 373~394

[79] Sidarta, D. and Ghaboussi, J. (1998). "Constitutive Modeling of Geomaterials Materials from Non-Uniform Material Tests", *Computers and Geotechnics*, **22**, 53~71

[80] Simo, J. C. and Taylor, R. L. (1985). "Consistent Tangent Operators for Rate-Independent Elasto-Plasticity", *Computer Method in Applied Mechanics and Engineering*, **48**, 101~118

[81] Sinha, B. P., Gerstle, K. H. and Tulin, L. G. (1964). "Stress-Strain Relations for Concrete under Cyclic Loading", *ACI Structural Journal*, **61**, 195~211

[82] Stelmack, T. W., Marley, M. J. and Gerstle, K. H. (1986). "Analysis and Tests of Flexibly Connected Steel Frames", *Journal of Structural Engineering ASCE*, **112**, 1573~1588

[83] Stojadinovic, G., (1998), "Connection Database Test Id: Umsp3.1", http://www.sacsteel.org/connections/reports/SP3-1.pdf, Accessed in 2005, SAC Steel Project

[84] Takanashi, K., Elnashai, A. S., Ohi, K. and Elghazouli, A. Y., 1992. Experimental Behavior of Steel and Composite Frames under Cyclic and Dynamic Loading, *ESEE Research Report No.92-10*, *University of Tokyo and Imperial College*

[85] Takizawa, H. and Aoyama, H. (1976). "Biaxial Effects in Modeling Earthquake Response of Rc Structures", *Earthquake Engineering & Structural Dynamics*, **4**, 523~552

[86] Tong, Z., Tan, Y. and Zeng, X. (2005). "Modeling Hysteresis Using Hybrid Method of Continuous Transformation and Neural Networks", *Sensors and Actuators*, **119**, 254~262

[87] Wang, C. H. and Wen, Y. K. (2000). "Evaluation of Pre-Northridge Low-Rise Steel Buildings. I: Modeling", *Journal of Structural Engineering-Asce*, **126**, 1160-1168

[88] Weinand, K. (1992). "Sericon - Databank on Joints in Building Frames", *Proceedings of the 1st COST C1 Workshop*, Strasbourg

[89] Wen, Y. K. (1976). "Method for Random Vibration of Hysteretic Systems", *Journal of Engineering Mechanics, ASCE*, **102**, 249~263

[90] Wu, X., 1991. Neural Network-Based Material Modeling, Ph.D report, Department of Civil and Environmental Engineering, University of Illinois at Urbana-Champaign

[91] Xuanju, D. and Yonghong, T. (2005). "An Inner Product-Based Dynamic Neural Network Hysteresis Model for Piezoceramic Actuator", *Sensors and Actuators*, **121**, 535~542

[92] Yun, G. J., Ghaboussi, J. and Elnashai, A. S. (2006a). "Development of Neural Network Based Hysteretic Models for Steel Beam-Column Connections through Self-Learning Simulation", *Journal of Earthquake Engineering*, Accepted

[93] Yun, G. J., Ghaboussi, J. and Elnashai, A. S. (2006b). "A New Neural Network-Based Model for Hysteretic Behavior of Materials", *International Journal for Numerical Methods in Engineering*, Submitted

[94] Zhang, M., 1996. Neural Network Material Models Determined from Structural Tests, Ph.D report, Department of Civil and Environmental Engineering, University of Illinois at Urbana-Champaign

Appendix A Computer Codes for Neural Network based Connection Model

The neural network based connection model is written in MATLAB language (Ver 7.0). Although the codes shown in the Appendix are for one-dimensional problem, they can be extended to multi-dimensional cases with no restriction.

A.1 Calculation of Algorithmic Tangent Stiffness

```
% loop over each set of NN connection springs
   for ispNN=1:ntens(idNN):nspringNN_the_group(idNN)
      sp_label = NNSPRING_DATA(idNN).data(ispNN,1);
      dof = NNSPRING_DATA(idNN).data(ispNN,2);
      for inode=1:nnode
         nod = NNSPRING_DATA(idNN).data(ispNN,inode+2);
         for idofn=1:ndofn
            pos = (inode-1)*ndofn + idofn;
            ieq = IDArray(idofn,nod);
            if ieq <= 0
               continue;
            end
            U_current_sp(pos) = DEL_U_STEP(ieq) + U_n(ieq);
            U_prev_sp(pos) = U_n(ieq);
         end
      end
      % get input node values
      ipos = dof;
      jpos = ndofn + dof;
      inode(1) = U_current_sp(jpos) - U_current_sp(ipos);
      inode(2) = U_prev_sp(jpos) - U_prev_sp(ipos);
      % note that statv do not change when calculating tangent stiffness
      % matrix
      if istep==1
         inode(3) = 0.0;
      else
         inode(3) = IRF_SPRINGNN(sp_label,istep-1);
      end
      inode(4) = inode(3) * inode(1);     % inner product
      % preprocessing input node
      for i=1:ninp
```

```
    inode(i) = inode(i)/iscale(i);
end
% forward passing NN to get node_v
for i=1:ninp
    node_v(1,i) = inode(i);
end
for m=1:nlayer
    for i=1:NNstruct(idNN).NN_arch(m+1)
        node_h =0.0;
        for j=1:NNstruct(idNN).NN_arch(m)
            node_h = node_h + kweight_value(m+1,i,j)*node_v(m,j);
        end
        node_v(m+1,i) = tanh(sbeta*node_h);
    end
end

% copy the result to the output node
for i=1:nout
    onode(i) = node_v(nlayer+1,i);
end
% processing the output node
for i=1:nout
    onode(i) = onode(i) * oscale(i);
end

% calculate algorithmic tangent stiffness
for i = 1:ntens(idNN)
    for j = 1:ntens(idNN)
      ddsdde(i,j) = 0.0;
      for k = 1:NNstruct(idNN).NN_arch(3)
          sum = 0.0;
          for l = 1:NNstruct(idNN).NN_arch(2)
               sum = sum + (1.0-node_v(nlayer,k)^2.0) *
              kweight_value(nlayer,k,l)*(1.0-node_v(nlayer-
              1,l)^2.0)*(kweight_value(nlayer-1,l,j)+kweight_value(nlayer-
              1,l,j)*node_v(nlayer-2, ninp-(ntens(idNN)-j) ));
          end
          ddsdde(i,j) = ddsdde(i,j) + (1.0-node_v(nlayer+1,i)^2.0) *
          kweight_value(nlayer+1,i,k) * sum;
      end
      ddsdde(i,j)=ddsdde(i,j)*(sbeta^3.0)*oscale(i)/iscale(j);
    end
end

% transform the material stiffness matrix to global stiffness matrix
T = TransformMat(idNN,ispNN, ntens);
```

```
    temp = T'*ddsdde*T;  % expand to nevab x nevab size of global stiffness matrix to
be assembled to global system matrix
    estif_springNN(:,:,sp_label) = temp;
    clear temp;

    % initialization
    U_current_sp = zeros(nevab,1);
    U_prev_sp = zeros(nevab,1);

  end
```

A.2 Calculation of Internal Resisting Force

```
% loop over each set of NN connection springs
  for ispNN=1:ntens(idNN):nspringNN_the_group(idNN)
    sp_label = NNSPRING_DATA(idNN).data(ispNN,1);
    dof = NNSPRING_DATA(idNN).data(ispNN,2);
    for inode=1:nnode
      nod = NNSPRING_DATA(idNN).data(ispNN,inode+2);
      for idofn=1:ndofn
        pos = (inode-1)*ndofn + idofn;
        ieq = IDArray(idofn,nod);
        if ieq <= 0
          continue;
        end
        U_current_sp(pos) = DEL_U_STEP(ieq) + U_n(ieq);
        U_prev_sp(pos) = U_n(ieq);
      end
    end
    % get input node values
    ipos = dof;
    jpos = ndofn + dof;
    inode(1) = U_current_sp(jpos) - U_current_sp(ipos);
    inode(2) = U_prev_sp(jpos) - U_prev_sp(ipos);
    % note that statv do not change when calculating tangent stiffness
    % matrix
    if istep==1
      inode(3) = 0.0;
    else
      inode(3) = IRF_SPRINGNN(sp_label, istep-1);
    end
    inode(4) = inode(3) * inode(1);     % inner product

    % preprocessing input node
    for i=1:ninp
```

```
    inode(i) = inode(i)/iscale(i);
  end

  % forward passing NN to get node_v
  for i=1:ninp
    node_v(1,i) = inode(i);
  end
  for m=1:nlayer
    for i=1:NNstruct(idNN).NN_arch(m+1)
      node_h =0.0;
      for j=1:NNstruct(idNN).NN_arch(m)
        node_h = node_h + kweight_value(m+1,i,j)*node_v(m,j);
      end
      node_v(m+1,i) = tanh(sbeta*node_h);
    end
  end

  % copy the result to the output node
  onode(1) = node_v(nlayer+1,1);

  % processing the output node
  onode(1) = onode(1) * oscale(1);

  % store stress vector
  tmpI_e(jpos,sp_label) = onode(1);
  tmpI_e(ipos,sp_label) = -onode(1);

  % initialization
  U_current_sp = zeros(nevab,1);
  U_prev_sp = zeros(nevab,1);

end
```